π-EXCHANGE IN A PARTIAL WAVE ANALYSIS OF $\pi N \to N\pi\pi$

I. PARTIAL WAVE ANALYSIS INCLUDING π-EXCHANGE FOR $\pi N \to N\pi\pi$ IN THE CENTER OF MASS ENERGY RANGE 1.65 - 1.97 GeV

II. RESONANCE PARAMETER ANALYSES OF $\pi N \to \Delta\pi + \rho N + \epsilon N$

Thesis by

Daniel Edward Novoseller

In Partial Fulfillment of the Requirements for the Degree of Doctor of Philosophy

California Institute of Technology

Pasadena, California

1977

(Submitted May 19, 1977)

ACKNOWLEDGMENTS

It is a pleasure to thank Professor Geoffrey Fox for his guidance, criticism, insight and unwavering support of my work. I am indebted to the Berkeley-SLAC collaboration for allowing the use of their data tapes and programs, and to Dr. R. Longacre and Dr. D. Herndon for several illuminating discussions on the work of that collaboration. I have benefited from the kind help of Dr. M. Griss, Dr. S. K. Kauffmann, Dr. W. Kropac, R. Kennett, F. Nagy, Dr. P. Stevens and R. Waltzman in the computational aspects of this work. Suggestions on various aspects of this research by Dr. T. Curtright, Prof. D. Horn, Dr. S.K. Kauffmann and Prof. H. J. Melosh are appreciated. I gratefully acknowledge a fellowship from the National Science Foundation, and additional financial support from the U.S. Atomic Energy Commission and the United States Energy Research and Development Administration.

My understanding of physics has been enhanced by discussions with Dr. T. Curtright, Dr. G. Ghandour, Dr. S. Goldstein, Dr. C. Hill, Dr. D. Jackson, E. McGaffigan, Prof. H. J. Melosh, Dr. F. Barnes, Dr. R. Wang and C. Zachos.

I deeply appreciate the support of my family. Last but not least I thank my wife, Karen, and our son, Michael, who made it all worthwhile.

ABSTRACT

I. Partial Wave Analysis Including π-Exchange for $\pi N \to N\pi\pi$ in the center of mass Energy Range 1.65 - 1.97 GeV

We study the inelastic scattering processes $\pi N \to N\pi\pi$ from c.m. energies 1.65 - 1.97 GeV using an isobar model. The effect of including a non-zero high partial wave contribution on the determination of low partial wave scattering amplitudes is analysed in detail. The proper formulation of a high partial wave input due to the π-exchange process $\pi N \to \rho N$ is presented. The major improvements due to including the π-exchange high partial wave input in the analysis of low energy $\pi N \to N\pi\pi$ scattering are found to be the elimination of the overall phase ambiguity in the scattering matrix, and improvement in the representation of the angular scattering distribution by the fit parameterization, for c.m. energies above 1.8 GeV.

The previous major isobar model analysis of these reactions at these energies is found to have serious deficiencies, as well as having many areas of agreement with our analysis.

ABSTRACT

II. Resonance Parameter Analyses of $\pi N \rightarrow \Delta\pi + \rho N + \epsilon N$

Couplings of πN resonances with masses between 1.65 and 1.97 GeV/c^2 to $\Delta\pi$ and ρN channels are determined using the scattering matrix elements resulting from inelastic partial wave analyses of $\pi N \rightarrow N\pi\pi$. The inelastic amplitudes were derived using an isobar model with a π-exchange based high partial wave input. These couplings are compared to those derived from an analysis of $\pi N \rightarrow N\pi\pi$ without a high partial wave input. Evidence for coupling of the ρN channel to the P31(1910) resonance is found.

TABLE OF CONTENTS

ACKNOWLEDGMENTS ii

ABSTRACTS iii

TABLE OF CONTENTS v

PART I - Partial Wave Analysis

Introduction 1

I. Notation 12

II. The Isobar Model Formalism 16

III. The π-exchange Input for High Partial Waves 27

A. Motivation 27

B. The π-exchange amplitude 31

IV. The Final State Factor 36

V. Selection Criteria and Properties of the π-exchange Input 43

VI. The Analysis Procedures 54

A. The Likelihood Method 54

B. Errors in the Maximum Likelihood Method 57

C. The Calculational Procedures 58

D. The Penal Function and our Method 61

VII. Results 65

A. Total Cross Section 65

B. Partial Wave Cross Sections 66

C. Single Variable Distributions 71

D. T- matrix elements 74

VIII. Conclusions 77

References 81

Footnotes 87

Figure Captions 88

Tables 92

Figures 95

PART II - Resonance Parameter Analyses 127

Introduction 128

I. Determination of Resonance Couplings for D15, F15, P33, F35 and F37 135

II. The P31 wave: Resonant or Non-resonant 142

References 144

Figure Captions 146

Table 147

Figures 148

Appendices 151

1. π-exchange Differential cross sections 152

2. Angular Distributions for All Fits 171

3. T-matrix Elements for LBL-SLAC and π-fits 199

4. Table of T-matrix Elements for π-fit 214

To Karen

Part I

Partial Wave Analysis Including π-Exchange for $\pi N \to N\pi\pi$ in the center of mass Energy Range 1.65 - 1.97 GeV

Introduction

The study of strong hadronic interactions has not yet reached the stage of being a totally predictive science. At low energies (- of order of the mass of the particles interacting -), we believe we know how to classify and predict the existence and sometimes the masses and couplings of particles and resonances[Ro74]. But our fundamental knowledge of low energy interactions is very poor. We have not learned anything fundamental about the interaction Hamiltonian applicable to scattering processes beyond such general properties as P, C and T invariance, SU_2 (isospin) symmetry, Lorentz invariance, momentum conservation, analyticity and unitarity. Thus we are still forced in the study of low energy scattering to try to establish a parameterization of scattering amplitudes. In the elastic scattering case, e.g., $\pi^- p \to \pi^- p$, we try to write the most general form of the scattering amplitude and then impose our set of fundamental properties. Combining the symmetries above, we can express the scattering amplitude for a given energy in terms of a function of one variable - the scattering angle in the center of mass frame, $\cos\theta$. Due to the finite range of the strong interactions, we can estimate the largest angular momentum that can be excited in an interaction as $L_{max} \sim p \times R$. Angular momenta greater than L_{max} can be shown to contribute much less to the scattering. So we can expand the (complex) scattering amplitude in terms of Legendre polynomials

$$T(\cos\theta) = \sum_{L=0}^{\infty} (2L+1) c_L P_L(\cos\theta)$$

and use the finiteness of L_{max} to approximate

$$T(\cos\theta) \approx \sum_{L=0}^{L_{max}} (2L+1) c_L P_L(\cos\theta) \quad .$$

Thus our set of general principles has enabled us to describe the scattering amplitude in terms of a finite number of parameters, the "c_L" 's, which are functions only of the total center of mass energy, and not of $\cos\theta$.

Ignoring the complications due to internal symmetries and spin, one can express the constraint of unitarity as

$$|1+2ic_L| \leq 1$$

A useful parameterization of these expansion parameters turns out to be

$$c_L = \frac{\eta e^{2i\delta} - 1}{2i}$$

with η, δ the real "inelasticity" and "phase shift" parameters. In the general scattering process, δ and η carry labels corresponding to all the conserved quantum numbers (e.g., J, L, S, I, ...).

An important property of the phase shifts is that rapid variation of a phase shift with energy can be shown (under generally accepted assumptions) to be related to the presence of resonances.

The study of low energy phase shifts from hadronic collisions has discovered many partial waves (i.e., values of J, L, I, ...) that exhibit rapidly varying phase shifts. These are defined as resonances. The πN resonance for L, I, J = 1, 3/2, 3/2 at c.m. energy = 1.238 GeV (the "Δ") is a famous example of a resonance determined in this manner. The postulated symmetry with respect to isospin (SU_2) of the strong interactions apparent for the proton-neutron isodoublet could be tested in various multiplets. The mass degeneracy of all members of the Δ-resonance mentioned above presented a test of this symmetry in an isospin 3/2 multiplet.

Further phase shift analyses were performed - in πN, $\bar{K}N$ elastic and inelastic processes. The resonances found inspired the suggestion of additional conserved quantum members (hypercharge)[Ge56] and particle multiplet symmetries (SU_3)[Ge61,Ne61]. Amazingly enough the multiplet structure of low multiplicity multiplets of SU_3 ($\underset{\sim}{1}$, $\underset{\sim}{8}$, $\underset{\sim}{10}$) could be used to classify all resonances determined from phase shift analyses. The multiplets were not degenerate (as

compared to the degenerate isospin multiplets), but the existence of resonances could be classified (and even predicted), and schemes for classifying the mass differences between members of SU_3 multiplets were devised.

The successful extension of SU_2 (isospin) to SU_3 encouraged speculation on further extensions. An attempt to combine SU_3 and spin (another SU_2 distinct from isospin) led to consideration of SU_6[Gu64,Sa64]. This symmetry classified states in larger multiplets - $\underset{\sim}{1}$, $\underset{\sim}{35}$, $\underset{\sim}{56}$, $\underset{\sim}{70}$. Again the multiplet structure was consistent with the known resonances. The quark constituent model[Ge64,Zw64] was developed, which gave a nice representation of the observed SU_6 multiplet structure.

These classification schemes, however, only enabled the grouping of particles with related masses and mass splittings, i.e., the symmetry properties of states. Once this program was completed, an attempt was made to study the symmetry properties of interactions. An early attempt was to make SU_6 a symmetry of decay amplitudes (3 point functions). But SU_6 symmetry implies that the spin SU_2 is a conserved quantum number. In terms of the quark constituents, this implies conservation of quark spin. This was quickly discredited, since the strong decays $\Delta \to N\pi$ and $\rho \to \pi\pi$ involve quark spin transitions of $3/2 \to 1/2 + 0$ and $1 \to 0 + 0$ respectively. Quark spin is not conserved, and SU_6 is not a good symmetry for decay amplitudes.

Eventually a new symmetry, SU_{6W}, was devised[Li65,Li73,Ro74] which conserves W-spin instead of quark spin. This symmetry was designed to involve generators that commute with boosts along a specified axis. Since 2-body decays are collinear, a symmetry that respects linear boosts is a possible decay symmetry. (Spin is not a good quantum number for moving particles.) This classification symmetry interchanges the role of the π and the helicity zero ρ. The π is classified in the $\vec{W} = 1$ multiplet with the helicity = ± 1 ρ meson.

The helicity = 0 ρ meson is placed in the $\vec{W} = 0$ multiplet. This SU_{6W} symmetry (and modifications[Me74a]) allows the classification of 3-point functions, i.e., of couplings. It allows the determination of $\Delta \to N\pi, N\rho, \Delta\pi$ and $N^* \to N\pi$, $N\rho, \Delta\pi$ couplings, as well as predicting relations between these couplings.

Thus, we have a candidate symmetry, SU_{6W}, which can relate couplings of resonances to the $N\pi$ channel to the couplings to $N\rho$ and/or $\pi\Delta$ channels. It would be useful to test these predictions for couplings of resonances to channels <u>other</u> than πN (where most analyses are done due to the availability of π-beams and nucleon targets).

The study of $2 \to 3$ body scattering provides the hope of learning these couplings. In the $\pi N \to N\pi\pi$ case, the $N\pi\pi$ state is assumed[De66,He75a] to be primarily a 2-body state combined with a decay, e.g.,

$$\pi N \to \Delta\pi \quad (\Delta \to N\pi) \qquad \text{or} \qquad \pi N \to \rho N \quad (\rho \to \pi\pi)$$

Thus, there is a good chance of studying the coupling of resonances to unstable final states ($\Delta\pi$, ρN) by studying $2 \to 3$ scattering.

A further possibility is to study resonances that couple only weakly to the πN channel, i.e., highly inelastic resonances. If the coupling of such a resonance is called $g^{Res}_{\pi N}$, $g^{Res}_{\pi\Delta}$ or $g^{Res}_{\rho N}$ for coupling to πN, $\pi\Delta$ and ρN, then trying to observe the resonance in elastic $\pi N \to Res \to \pi N$ would involve a scattering amplitude like $(g^{Res}_{\pi N})^2$, while studying it in $\pi N \to Res \to \pi\Delta$ would involve $g^{Res}_{\pi N} g^{Res}_{\pi\Delta}$. If $g^{Res}_{\pi N} << g^{Res}_{\pi\Delta}$, then our chance of studying the resonance is enhanced by looking at final states other than πN, e.g., by looking at $\pi\pi N$, presumably dominated by the stronger coupled $\pi\Delta$ and ρN states.

The ultimate goals in studying $\pi N \to N\pi\pi$ using a model wherein the final state is considered as a 2-body unstable state are therefore:

a) study of 3-point couplings

b) observation of resonances which couple only weakly to the standard (πN) channel.

The analysis[He75b,Ro75] on which our own study is based in fact claimed besides satisfactorily fitting the $\pi N \to N\pi\pi$ scattering data, that

a) Many couplings were measured, and magnitudes and signs of known resonances to previously poorly studied $\pi\Delta$ and ρN states were determined[Ca75,Lo75]. These were successfully compared to the predictions of SU_{6W} symmetry[Fa73,Fa74,Gi74].

b) Observation of a new resonance ($D_{13}(1700)$) which fits well into the quark model classification scheme[Da69], and which couples strongly to the $\pi\Delta$ and ρN states, but was not seen in $\pi N \to \pi N$ scattering.

c) Furthermore, the approximation that $\pi\pi N \approx \rho N + \pi\Delta$ + other 2-body states ($\rho N \to \pi\pi$, $\pi\Delta \to N\pi$) was found to give a reasonable fit to the experimental distributions, so that the very difficult study of 3-body states could be ignored.

These are major successes of their analysis. These successes are strong motivation for further work.

Our analysis is an extension of the study of Herndon et al.[He75b]. Our modification is to add to the truncated partial wave expansion

$$T \sim \sum_{L=0}^{L_{max}} c_L P_L(\cos\theta)$$

an additional contribution for $L > L_{max}$ based on theoretical information about these waves. These high partial waves are given by the longest range (lightest mass exchange) force, the exchange of a single pion.

The importance of π-exchange in particle physics is an old subject. At low energies, π-exchange has been long recognized as important in nucleon-nucleon scattering[Yu35]. Phase shift analyses[Cz59,Ma59,Ma64] of this process always

include a π-exchange contribution for the high partial waves. Even the smaller multi-pion exchange contributions are included in the analysis of pp scattering.

More recently, the importance of the 2π exchange ($\pi\pi$ cut) has been used to bound the high partial wave part of elastic meson-baryon scattering (where single π-exchange does not occur)[Gr73]. The contribution of the high partial wave part of π-exchange in high energy inelastic processes is also well studied[Fe62b,Fo71,Ja65,Ma76]. Particularly well studied[Fe62b,Ja65] are the contributions from π-exchange to $\pi N \to \pi\pi N$, $pp \to pp\pi^o$ and $pn\pi^+$, and $\gamma p \to p\pi^+\pi^-$. The science of absorbing the low partial waves (which typically violate unitarity) has been formulated[Fo71,Ja65] and successfully applied to these high energy inelastic processes.

The importance of π-exchange in high energy $\pi N \to \rho N$ scattering is, in fact, the classic textbook example[Ga66,Ja65] of the single particle exchange mechanism. This fact emphasizes the necessity of including the effect of π-exchange in any low energy analysis of $\pi N \to \rho N$ (or $\pi N \to \pi\pi N$ with the ρ as a $\pi\pi$ isobar).

In our analysis, we have redone the analysis of Herndon et al.[He75b] including the π-exchange high partial wave input. We have studied the stability of the LBL-SLAC[He74,He75b,Ro75] solution, and find that some waves are not affected by the inclusion of π-exchange, while others are significantly affected. We also find that at the higher energies, the angular distributions resulting from the π-fit (including the π-exchange high partial wave input) are a more accurate representation of the experimental distributions than those of the LBL-SLAC solution. We learn that at certain energies, we are able to identify the important high partial waves due to π-exchange. The resultant high partial wave π-exchange input succeeds in fixing the overall phase of the scatter-amplitude. This is much more satisfying than the LBL-SLAC approach of using the K-matrix representation to fix the phase.

On the negative side, we have learned that violations of partial wave unitarity are significant in many waves. Any unjustified theoretical input to "hold down" this violation is thus to be considered with skepticism. Many of the details of the LBL-SLAC[He75b] results are, in fact, caused by the inclusion of such an input in their analysis.

Furthermore, the invariant mass distributions indicate a need for including the effect of $\pi N^*(1688)$ or $\pi N^*(1670)$ production at the higher energies. Our model presently is limited to $\pi\Delta(1236)$, ρN and εN production.

Our analysis was severely limited due to fiscal constraints. Due to cost, we were unable to include the proper production barriers. Nor could we do a search through parameter space for a "new" solution or add new waves, but had to be satisfied with studying the effect of our π-exchange input as a <u>perturbation</u> on the LBL-SLAC[He75b] solution. Finally, we did not attempt to incorporate proper unitarity in the invariant subenergies, since the method to do this is unknown.

In more detail, this work describes an analysis of the reactions

$$\begin{aligned} \pi^- p &\to n\pi^-\pi^+ \\ \pi^- p &\to p\pi^-\pi^o \\ \pi^+ p &\to p\pi^+\pi^o \end{aligned} \qquad (1)$$

from center of mass energies W = 1.63 - 1.99 GeV.

In a $2 \to 2$ scattering process $a + b \to c + d$, the standard approach is to parameterize the helicity amplitude in terms of its low partial waves

$$T_{\mu_a\mu_b,\mu_c\mu_d}(W,\cos\theta) = \sum_J A^J_{\mu_a\mu_b\mu_c\mu_d}(W)\, d^J_{\mu_c-\mu_d,\ \mu_a-\mu_b}(\cos\theta)$$

The $\cos\theta$ independent parameters, $A^J_{\mu_a\mu_b\mu_c\mu_d}(W)$, are related to the scattering phase shift parameters by

$$A^J_{\mu_a\mu_b\mu_c\mu_d}(W) = \sum_{LL'SS'} \begin{pmatrix} S_a & S_b & S \\ \mu_a & -\mu_b & \mu_a-\mu_b \end{pmatrix} \begin{pmatrix} S_c & S_d & S' \\ \mu_c & -\mu_d & \mu_c-\mu_d \end{pmatrix}$$

$$\times \begin{pmatrix} L & S & J \\ o & \mu_a-\mu_b & \mu_a-\mu_b \end{pmatrix} \begin{pmatrix} L' & S' & J \\ o & \mu_c-\mu_d & \mu_c-\mu_d \end{pmatrix} A^J_{LL'SS'}(W)$$

One can study s-channel resonances of spin J which couple to the a+b and c+d systems by studying the energy dependence of the amplitudes $A^J_{LL'SS'}(W)$. (For elastic processes, $A^J_{LL'SS'}(W)$ are often parameterized by the inelasticity and phase shift $\left(\frac{\eta^J_{LL'SS'} e^{2i\delta^J_{LL'SS'}} - 1}{2i}\right)$. In fact, $A^J_{LL'SS'}$ measures the product

$$g_{R_J ab}\ g_{R_J cd}$$

where $g_{R_J \alpha\beta}$ is the coupling of the spin J resonance to particles α and β when W is near the mass of the resonance.

For a $2 \to 3$ body scattering process, there is no model independent method for "quantizing" all the variable dependence. In the general case, the $2 \to 3$ process can be parameterized by 3 angles, 2 invariant subenergies, and the overall c.m.s. energy:

$$T_{a\ b \to c\ d\ e}(W, w_{cd}, w_{de}, \alpha, \beta, \gamma) = \sum_J \mathcal{D}^J(\alpha,\beta,\gamma)\ A^J(W, w_{cd}, w_{de})$$

Thus, an energy independent analysis of these amplitudes gives information about subenergy dependent functions, not the constants of the $2 \to 2$ body process. There is no known model independent parameterization of these functions in terms of a small number of constant parameters. The standard procedure[De66, Do76, He75a, He75b] is to resort to a model. The model used to describe the processes in Equation (1) is motivated by the Dalitz plot analysis result[He75b] that much of the cross section lies in bands identifiable with $\pi\Delta(1236)$ and

ρN final states. This observation inspires the hope that the $2 \to 3$ scattering amplitude can be represented as a sum of isobar production and decay amplitudes:

$$\begin{aligned} T(\pi N \to N\pi\pi) \approx\ & T(\pi N \to \pi\Delta)D(\Delta \to \pi p) \\ & +T(\pi N \to \rho N)D(\rho \to \pi\pi) \\ & +T(\pi N \to \varepsilon N)D(\varepsilon \to \pi\pi) \end{aligned} \tag{2}$$

where ε is the S-wave $\pi\pi$ scattering enhancement, and where, e.g., $T(\pi N \to \pi\Delta)$ represents the production of a 2-body $\pi\Delta$ intermediate state, and $D(\Delta \to \pi p)$ represents the decay of the Δ isobar into $\pi + p$, the other two particles in the final state. The decay amplitudes, D, are known functions, while the production amplitudes $T(\pi N \to \pi\Delta, \rho N, \varepsilon N)$ are functions of the center of mass scattering angle and are expanded in partial waves.

Thus, the analysis of $\pi N \to N\pi\pi$ has been transformed to the study of the low partial waves for

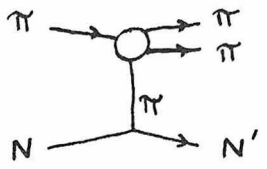
$$\begin{aligned} &\pi N \to \pi\Delta \\ &\pi N \to \rho N \\ &\pi N \to \varepsilon N \end{aligned} \tag{3}$$

The results hoped for are <u>not</u> a better understanding of the 3-body system "$\pi\pi N$". Rather, the results of the analysis are an understanding of the 2-body final states in Equation (3), and how they couple to low spin resonances. Any "pure" 3-body interaction, i.e., an interaction that <u>cannot</u> be described as a 2-body state decaying, is ignored and assumed negligible.

In the standard analysis[He75b,Do76] the high partial waves ($J > 7/2$) are ignored. Our contribution to the analysis is to add a non-zero high partial wave input to Equation (2). Our input is given by using the high partial wave part of a π-exchange process:

$$\text{High P.W.}[T_{\pi}(\pi N \to (\pi\pi)N') \times D(\ (\pi\pi) \to \pi+\pi\ )$$

i.e., the production and decay of a $\pi\pi$ isobar, where $T_{\pi}(\pi N \to (\pi\pi)N')$ is given by the π-exchange diagram



In detail, Equation (2) becomes

$$\begin{aligned} T(\pi N \to N\pi\pi) \approx\ & T(\pi N \to \pi\Delta)D(\Delta \to \pi p) \\ & + T(\pi N \to \rho N)D(\rho \to \pi\pi) \\ & + T(\pi N \to \varepsilon N)D(\varepsilon \to \pi\pi) \end{aligned}$$

$$\begin{aligned} + \text{ High Partial Wave } \Big[& T_{\pi\text{-exchange}}(\pi N \to \rho N) \times D(\rho \to \pi\pi) \\ & + T_{\pi\text{-exchange}}(\pi N \to \varepsilon N) \times D(\varepsilon \to \pi\pi) \\ & + T_{\pi\text{-exchange}}(\pi N \to (\pi\pi)^{I=2}_{\ell=0}\ N) \times D\left((\pi\pi)^{I=2}_{\ell=0} \to \pi\pi\right)\Big] \end{aligned} \qquad (4)$$

Our goal is to study the modifications to the results of Herndon et al.[He75b] for the $2 \to 2$ inelastic amplitudes caused by the inclusion of this high partial wave input. The stability, or lack of stability, of the amplitudes under inclusion of this input is some measure of the reliability of the LBL-SLAC[He75b] results.

This work is organized as follows: In Section I, we describe our notation and coordinate systems. In Section II, we review the Berkeley-SLAC isobar formalism[He75a]. In Section III, we motivate the π-exchange term, and present the appropriate amplitude. In Section IV, we present the $\pi\pi$ and πN amplitudes used as final state interaction factors. In Section V, we calculate properties of the π-exchange term, and describe our selection of which

π-exchange partial waves to include in our fit. Section VI details the fitting technique. Section VII presents our results quantifying our conclusions on the importance of the π-exchange high partial wave input.

I. Notation

In this section, we define our notation for the $2 \to 3$ process. We pattern our discussion after Herndon, Söding and Cashmore[He75a] (hereafter called HSC). We first recall the generalized isobar notation of HSC. Then we describe our π-π isobar notation for describing the π-exchange contribution.

The process being considered is

$$a + b \to 1 + 2 + 3 \tag{I-1}$$

where a is the beam particle, b is the target, and 1, 2, 3 are the three final state particles. In our case, $a = \pi_{beam}$, $b = p_{target}$, $1 = N_{final}$, $2 = \pi_{same\ charge\ as\ beam}$, $3 = \pi_{other\ charge}$. Since the three reactions being analyzed are

$$\begin{aligned} &\pi^- p \to n\pi^-\pi^+ \\ &\pi^- p \to p\pi^-\pi^o \\ &\pi^+ p \to p\pi^+\pi^o \end{aligned} \tag{I-1a}$$

this identification of same charge pions is well defined.

We let j, k, ℓ be any cyclic permutation of 1, 2, 3. The label j will be used to denote properties of the diparticle "kℓ" as well as properties of the particle "j".

We now list the variables in the process (I-1), as illustrated in Figure 1.

(a) $W = \sqrt{s}$ = total center-of-mass energy

J = total angular momentum

(b) $p_a\ p_b\ Q_j\ Q_k\ Q_\ell$ = c.m.s. 4-momenta

(c) $\sigma_a\ \sigma_b\ \sigma_j\ \sigma_k\ \sigma_\ell$ = spins

(d) $\mu_a\ \mu_b\ \mu_j\ \mu_k\ \mu_\ell$ = c.m.s. helicities

(e) $w_j \equiv w_{k\ell}$ = diparticle mass

(f) $j_j\ \lambda_j$ = spin and c.m.s. helicity of diparticle

(g) L S = orbital and spin angular momenta of incident ("a+b") system

(h) $L_j\ S_j$ = orbital and spin angular momenta of final 2-body system containing particle "j" and diparticle "kℓ"

(i) $q_k\ q_\ell$ = 4-momenta of the decay particles in the diparticle rest frame

(j) $\nu_k\ \nu_\ell$ = helicities of the decay particles in the diparticle rest frame

(k) $\ell_j\ s_j$ = orbital and spin angular momenta of the decay particles in the diparticle rest frame

(l) $I^a\ I^b\ I^j\ I^k\ I^\ell\ I^{(k\ell)}$ = isospins of particles a, b, j, k, ℓ, and of diparticle "kℓ"

(m) $\tau^a\ \tau^b\ \tau^j\ \tau^k\ \tau^\ell\ \tau^{(k\ell)}$ = 3rd component of isospin of particles a, b, j, k, ℓ and diparticle "kℓ"

(n) I τ = total isospin and its 3rd component

Angular momenta are coupled as follows:

$$\vec{S} = \vec{\sigma}_a + \vec{\sigma}_b$$

$$\vec{J} = \vec{L} + \vec{S}$$

$$\vec{s}_j = \vec{\sigma}_k + \vec{\sigma}_\ell$$

$$\vec{j}_j = \vec{\ell}_j + \vec{s}_j$$

$$\vec{S}_j = \vec{\sigma}_j + \vec{j}_j$$

$$\vec{J} = \vec{L}_j + \vec{S}_j$$

Note that parity conservation implies

$$P_a P_b (-)^L = P_j P_k P_\ell (-)^{L_j + \ell_j}$$

where P_i is the parity of the i^{th} particle.

We will use the shorthand notation μ to represent the set $(\mu_a\ \mu_b\ \mu_j\ \mu_k\ \mu_\ell)$ of all five c.m.s. helicities, and the letter "n" to indicate the set of quantities

$$(J;\ L\ S;\ L_j\ S_j;\ j_j\ \ell_j\ s_j;\ j)$$

where the final j emphasizes the grouping of final state particles into the particle "j" and the diparticle system "kℓ".

The helicity formalism and phase conventions of Jacob and Wick[Ja59], henceforth called JW, are used.

We define the three body relativistically invariant phase space as

$$d\rho = \frac{d^3\vec{Q}_j}{2E_j}\,\frac{d^3\vec{Q}_k}{2E_k}\,\frac{d^3\vec{Q}_\ell}{2E_\ell}\,\delta^4(Q_j+Q_k+Q_\ell-p_a-p_b) \tag{I-2}$$

where

$$Q_i = (E_i,\ \vec{Q}_i) \qquad i = j,\ k,\ \ell$$

$$p_i = (E_i,\ \vec{p}_i) \qquad i = a,\ b$$

The transition matrix element, M, is defined as

$$M_\mu = \langle \text{out} \mid T \mid \text{in} \rangle \tag{I-3}$$

where μ includes all helicity labels, and

$$\langle \text{out} \mid S \mid \text{in} \rangle = \delta_{\text{out,in}} + i\delta^4(P_{\text{out}}-P_{\text{in}})\langle \text{out} \mid T \mid \text{in} \rangle \tag{I-4}$$

The differential cross section is then

$$d\sigma = \frac{\pi^2}{F}\,\frac{1}{(2\sigma_a+1)(2\sigma_b+1)}\,\sum_\mu |M_\mu|^2 d\rho \tag{I-5}$$

where $F = |\vec{p}_a|W$.

Next, we define our coordinate systems. Our center of mass system has the three final state particles in the $\hat{x}$-$\hat{z}$ plane. We define $\hat{z} \parallel \vec{Q}_j$, i.e. $\hat{z}$ antiparallel to the diparticle. $\hat{y}$ is given by the cyclic cross product, $\vec{Q}_j \times \vec{Q}_k$, and $\hat{x} = \hat{y} \times \hat{z}$. The c.m.s. angles, with respect to these axes, are called

$$\Theta_i, \Phi_i \qquad i = a, b, j, k, \ell$$

We define our diparticle rest frame to be given by boosting the c.m.s. along the $-\hat{z}$ axis. The direction of $\hat{z}$ remains the same as in the c.m.s., i.e., parallel to the "j" particle. $\hat{x}$ and $\hat{y}$ are unaffected by the boost. The angles in this frame will be called

$$\tilde{\theta}_i^{(k\ell)} \quad \tilde{\phi}_i^{(k\ell)} \qquad i = k, \ell$$

for the angles describing the momentum of particle i in this frame.

Note that HSC call our angles $\tilde{\theta}_i$ $\tilde{\phi}_i$ by the names θ_i ϕ_i (with no "tilde").

Finally, we observe that the density of final states, Equation (I-2), may be manipulated[He75b,Be65] to give

$$d\rho = \frac{1}{8} dE_k dE_\ell d^3\Omega \tag{I-6}$$

$$= \frac{1}{8} q_1 \frac{Q_1}{W} dw_1 d\cos\tilde{\theta}_2^{(23)} d^3\Omega \tag{I-7}$$

where Ω are the Euler angles for the orientation of the final three-particle state relative to the initial system. Another expression ideally suited to a single isobar process is

$$d\rho = \frac{\pi Q_j q_j}{4W} dw_j d\cos\Theta_a d\cos\tilde{\theta}_k^{(k\ell)} d\tilde{\phi}_k^{(k\ell)} \tag{I-8}$$

An azimuthal angle has been integrated over in this expression. The variables in this representation will be used in our single variable distributions in Section VII.

II. The Isobar Model Formalism

Here we summarize the isobar model formalism as formulated by HSC[He75a] and used by Herndon et al.[He75b] as well as in our analysis.

We first note that there is an extensive literature on properly formulating an isobar model. We note in particular the works of Namyslowski et al.[Na67] who describe the formalism in some detail, Goradia and Lasinski[Go75,Go77] who consider corrections to the formalism in great detail, and Hansen et al.[Ha74] who give a very clear presentation of the assumptions involved (given for the 3-meson system).

The naïve approach is to write the helicity amplitude

$$f_\mu \equiv \langle \vec{Q}_j \mu_j \vec{Q}_k \mu_k \vec{Q}_\ell \mu_\ell | T | \vec{p}_a \mu_a \vec{p}_b \mu_b \rangle \approx f_\mu^j + f_\mu^k + f_\mu^\ell \qquad \text{(II-1)}$$

i.e., as a sum of contributions from a j-, k-, and ℓ- type diparticle. (Recall that j- diparticle is equivalent to a (kℓ)- diparticle.) In detail, (HSC[He75a] Equations 43-45 and 48)

$$f_\mu^j = \sum_{\substack{JLS \\ L_j S_j}} \frac{W}{\pi^{p_a Q_j q_k}} \left(\frac{w_j}{\pi}\right)^{1/2} \sqrt{(2L+1)(2L_j+1)(2\ell_j+1)}$$

$$j_j \ell_j s_j \times \begin{pmatrix} \sigma_a & -\sigma_b & S \\ \mu_a & -\mu_b & \mu_a - \mu_b \end{pmatrix} \begin{pmatrix} L & S & J \\ o & \mu_a - \mu_b & \mu_a - \mu_b \end{pmatrix}$$

$$\times \sum_{\lambda_j} \begin{pmatrix} \sigma_j & j_j & S_j \\ \mu_j & -\lambda_j & \mu_j - \lambda_j \end{pmatrix} \begin{pmatrix} L_j & S_j & J \\ o & \mu_j - \lambda_j & \mu_j - \lambda_j \end{pmatrix} \mathcal{D}^J_{\mu_j - \lambda_j,\ \mu_a - \mu_b}(\alpha_j, \beta_j, \gamma_j)$$

$$\times \sum_{\nu_k \nu_\ell} \begin{pmatrix} \sigma_k & \sigma_\ell & s_j \\ \nu_k & -\nu_\ell & \nu_k - \nu_\ell \end{pmatrix} \begin{pmatrix} \ell_j & s_j & j_j \\ o & \nu_k - \nu_\ell & \nu_k - \nu_\ell \end{pmatrix} d^{j_j}_{-\lambda_j, \nu_k - \nu_\ell}(\theta_k^{(k\ell)})$$

$$(-)^{\sigma_\ell - \nu_\ell} d^{\sigma_k}_{\nu_k \mu_k}(\theta_j^k)\, d^{\sigma_\ell}_{\nu_\ell \mu_\ell}(-\theta_j^\ell)$$

$$\times \hat{T}^j_{JLSL_j S_j j_j \ell_j s_j}(W, w_j) \qquad \text{(II-2)}$$

In this equation, we use the rotation matrices and Clebsch-Gordan coefficients of Rose[Ro57]. The various angles are (see References He75b, Wi62, and especially No76, Section D2) the Wigner angles θ_j^k and θ_j^ℓ which relate the helicity state of a particle at rest to the state of a moving particle, and the Euler angles between the initial and final states, α_j, β_j, γ_j, where

$$\mathcal{D}^J_{\mu_j - \lambda_j, \mu_a - \mu_b}(\alpha_j, \beta_j, \gamma_j) = \sum_M \mathcal{D}^J_{\mu_j - \lambda_j, M}(\Phi_j, -\Theta_j, -\Phi_j)\, \mathcal{D}^J_{M, \mu_a - \mu_b}(\Phi_a, \Theta_a, -\Phi_a) \qquad \text{(II-3)}$$

Explicit forms for these angles are given in Equations 26-29 and 47-51 of Reference (No76). (Reference (No76) is a manual describing the Triangle 2 system, LBL-SLAC's[He75b] program for calculating the f^j_μ functions.)

Note that the formulae in Reference (He75a) for the angles θ_j^k, θ_j^ℓ in Equation (II-2) are incorrect. The formulae actually used by LBL-SLAC in their analysis[He75b] were the correct equations. See Reference (No76) for more details.

The physics behind the decomposition (II-2) is straightforward. In formulae,

i.e., T^j separates into a $2 \to 2$ body production operator T_p^j times a 1-body decay operator T_d^j. The helicity amplitude for the 2-2 process is evaluated in the c.m.s. and decomposed into partial waves (which generates $\mathcal{D}^J(\alpha\ \beta\ \gamma)$) and into LS states (which generates the Clebsch-Gordan coefficients in Equation (II-2)). The decay amplitude is evaluated by boosting to the isobar rest frame (which generates the $d^{\sigma_k}(\theta_j^k)$ and $d^{\sigma_\ell}(\theta_j^\ell)$) and then decomposed into $\ell_j\ s_j$ states (generating more Clebsch-Gordan coefficients).

Next, we recall our notation:

$$n \longleftrightarrow (J;\ LS;\ L_jS_j;\ j_j\ell_js_j;\ j) \tag{II-4}$$

Then Equation (II-2) may be written

$$f_\mu^j = \sum_{n_{\text{fixed } j}} g_\mu^n\ T_n\ (W,\ w_j) \tag{II-5}$$

and g_μ^n is known. Furthermore, we may sum over diparticle types to get

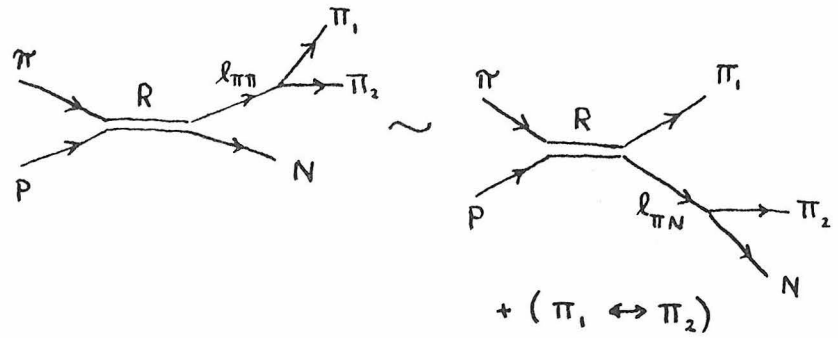
$$f_\mu = \sum_n g_\mu^n\ T_n\ (W,\ w_j) \tag{II-6}$$

At this point, we note that we have made two major assumptions[Ha74] of the model:

(1) We truncate the sum over J. This is the standard approximation in low energy partial wave analysis.

(2) We truncate the sum over ℓ_j. It is assumed that the high ℓ_j waves are "dual" to the low ℓ_k and ℓ_ℓ waves.

For example, the contribution due to high values of $\ell_{\pi N}$, which is omitted, is assumed to be taken up by the low values of $\ell_{\pi\pi}$ (i.e., $\ell_{\pi\pi} = 0$ and 1, the ε- and ρ- contributions). This is just a statement of duality[Do67] of the processes



where high $\ell_{\pi\pi}$ in the direct channel

$$R\bar{N} \rightarrow \pi_1\pi_2$$

correspond to small $\ell_{\pi N}$ in the exchange channel

$$R\bar{\pi}_1 \rightarrow \pi_2 N.$$

It is also expected that there is not much overlap in performing the integral $\int(d\sigma/d\rho)\, d\rho$ between the ℓ_j, ℓ_k and ℓ_ℓ waves, since there is no overlap in the cross section between low ℓ_j and high ℓ_j waves. As we discuss later, rescattering corrections due to unitarity make this "duality"-based hope a false expectation, causing an inherent weakness of the model. (Note that if the ℓ_j, ℓ_k and ℓ_ℓ summations went to infinity, then (II-6) would be replaced by

$$\sum_n g_\mu^n T_n = 3\, f_\mu,$$

i.e., (II-6) would cause triple counting.)

Next we introduce the isospin dependence of $T_n(W, w_j)$. Also, we extract barrier factors

$$B_L(Q)$$

where at threshold

$$B_L(Q) \sim Q^{L+\frac{1}{2}}$$

Then the actual form is

$$T_n(W,w_j) = \frac{1}{4W} B_L(p_a)\, B_{L_j}(Q_j) \times \frac{1}{\sqrt{4w_j}} \frac{1}{B_{\ell_j}(q_k)} \frac{\eta_j^{I(k\ell)} e^{2i\delta_j^{I(k\ell)}} - 1}{2i} \times \sum_I \begin{pmatrix} I^a & I^b & I \\ \tau^a & \tau^b & \tau \end{pmatrix} \begin{pmatrix} I^{(k\ell)} & I^j & I \\ \tau^{(k\ell)} & \tau^j & \tau \end{pmatrix} \times \begin{pmatrix} I^k & I^\ell & I^{(k\ell)} \\ \tau^k & \tau^\ell & \tau^{(k\ell)} \end{pmatrix} {}^{Jj_jII^{(k\ell)}}_{\tau LSL_jS_j}(W) \tag{II-7}$$

We use the values of Herndon et al.[He75b,No76]:

$$B_L(p_a) = p_a^{1/2} \tag{II-8a}$$

$$B_{L_j}(Q_j) = Q_j^{L_j + 1/2} \tag{II-8b}$$

$$B_{\ell_j}(q_k) = q_k^{\ell_j + 1/2} \tag{II-8c}$$

HSC[He75a] now advocate a more detailed form of the barrier factors (Reference (He75a), Footnote 17 and Reference He75b, section IIIe). The $B_L(p_a)$ barrier used was incorrect as it should have at least a $p_a^{L+1/2}$ dependence but this amounted to only a change in normalization at each energy, since p_a depends only on the fixed energy, W, and not on any subenergies. The

other barriers should have suppression factors to prevent anomalous behavior at large Q. Von Hippel and Quigg[Hi72] advocate the use of Blatt-Weisskopf[Bl52] barrier factors. This was not done by Herndon et al.[He75b] due to an inadvertent mistake. We did not incorporate the favored barriers due to the expense of the computer calculations.

Equation (II-7) contains the most controversial assumption alluded to earlier in this section - the simple factorization of w_j dependence. It is claimed[Aa73,Gu73] that this form violates proper subenergy dependence dictated by unitarity and analyticity. A study of this effect is in progress[Aa76]. We will discuss this correction later in this section.

The parameters η_j and δ_j correspond to the inelasticity and phase shifts for the elastic scattering $k + \ell \to k + \ell$. The form used is detailed in Section IV.

Combining Equation (II-5 and 7), we write

$$f_\mu^j = \sum_{nII(k\ell)} C_\mu^{nII(k\ell)} \tau^{nII(k\ell)}(W) \qquad \text{(II-9)}$$

where

$$C_\mu^{nII(k\ell)} = \frac{W}{\pi}\left(\frac{w_j}{\pi p_a Q_j q_k}\right)^{1/2} \sqrt{(2L+1)(2L_j+1)(2\ell_j+1)}$$

$$\times \begin{pmatrix} \sigma_a & \sigma_b & S \\ \mu_a & -\mu_b & \mu_a - \mu_b \end{pmatrix} \begin{pmatrix} L & S & J \\ o & \mu_a - \mu_b & \mu_a - \mu_b \end{pmatrix} \frac{p_a^{1/2} Q_j^{L_j+1/2}}{4W\sqrt{4w_j}\, q_k^{\ell_j+1/2}}$$

$$\times \frac{\eta_j^{I(k\ell)} e^{2i\delta_j^{I(k\ell)}} - 1}{2i} \begin{pmatrix} I^a & I^b & I \\ \tau^a & \tau^b & \tau \end{pmatrix} \begin{pmatrix} I^{(k\ell)} & I^j & I \\ \tau^{(k\ell)} & \tau^j & \tau \end{pmatrix}$$

$$\times \begin{pmatrix} I^k & I^\ell & I^{(k\ell)} \\ \tau^k & \tau^\ell & \tau^{(k\ell)} \end{pmatrix} \sum_{\lambda_j} \begin{pmatrix} \sigma_j & j_j & S_j \\ \mu_j & -\lambda_j & \mu_j - \lambda_j \end{pmatrix} \begin{pmatrix} L_j & S_j & J \\ o & \mu_j - \lambda_j & \mu_j - \lambda_j \end{pmatrix}$$

$$\times \mathcal{D}^J_{\mu_j - \lambda_j, \mu_a - \mu_b}(\alpha_j, \beta_j, \gamma_j) \sum_{\nu_k \nu_1} \begin{pmatrix} \sigma_k & \sigma_\ell & s_j \\ \nu_k & -\nu_\ell & \nu_k - \nu_\ell \end{pmatrix} \begin{pmatrix} \ell_j & s_j & j_j \\ o & \nu_k - \nu_\ell & \nu_k - \nu_\ell \end{pmatrix}$$

$$\times (-)^{\sigma_\ell - \nu_\ell} d^{\sigma_k}_{\nu_k \mu_k}(\theta^k_j) \, d^{\sigma_\ell}_{\nu_\ell \mu_\ell}(-\theta^\ell_j) \, d^{j_j}_{-\lambda_j, \nu_k - \nu_\ell}(\theta^{(k\ell)}_k) \qquad \text{(II-10)}$$

Herndon et al.[He75b] allow $J \leq 7/2$ and $L, L_j \leq 3$. This allows "n I $I^{(k\ell)}$" for three isobars ($\Delta_{\pi N}$, $\rho_{\pi\pi}$, and $\varepsilon_{\pi\pi}$) to take on 60 values. An expression of this sort may be written for each charge channel in Equation (I-1a). For charge channel α, we will sometimes call

$$C^{nII^{(k\ell)}}_{\alpha,\mu}\left(W, w_j, \Theta_\pi, \Phi_\pi, \tilde{\theta}^{(k\ell)}_\pi\right) = \vec{C}_{\alpha,\mu}(\vec{\omega}) \qquad \text{(II-11)}$$

The complex parameters $\tau^{nII^{(k\ell)}}$ we sometimes call $\vec{\tau}$, and sometimes refer to as the real parameters $\vec{A}$ (e.g., $\tau_1 = A_1 + iA_2$). The forms

$$\sum_{nII^{(k\ell)}} C^{nII^{(k\ell)}}_{\alpha,\mu} \, \tau^{nII^{(k\ell)}}$$

$$\vec{C}_{\alpha,\mu} \cdot \vec{\tau}$$

$$\vec{C}_{\alpha,\mu} \cdot \vec{A}$$

are all meant to be representations of Equation (II-9) for charge channel α.

Finally, we discuss the subenergy dependence problem mentioned earlier. Consider a two channel 2-body (time reversal invariant) S-matrix

$$\begin{pmatrix} S_{11} & S_{12} \\ S_{12} & S_{22} \end{pmatrix} \quad .$$

Unitarity requires

$$|S_{11}|^2 + |S_{12}|^2 = 1 = |S_{22}|^2 + |S_{12}|^2$$

$$S_{11}^* \, S_{12} + S_{12}^* \, S_{22} = 0$$

Thus, if we parameterize

$$S_{11} = \eta e^{2i\delta_1}$$

$$S_{22} = \eta e^{2i\delta_2}$$

then

$$S_{12} = \sqrt{1 - \eta^2} \; e^{2i\delta_{12}}$$

$$\delta_{12} = \frac{1}{2} \left(\delta_1 + \delta_2 \pm (2n+1)\pi\right)$$

Thus, rapid phase variation in the final state elastic channels (1→1 and 2→2) is manifest in the inelastic process 1 → 2. This effect is often called the Watson Theorem[Wa54,Fe62a]. An example of its application is in the photoproduction [Me74b] process

$$\gamma p \to \pi^+ n$$

where it is expected that

$$\delta_{\gamma p \to \gamma p} \sim 0$$

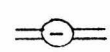
$$\delta_{\gamma p \to \pi N} \sim \frac{1}{2} \delta_{\pi N \to \pi N} + \pi/2$$

(An alternative way to say this is that the phase of the $\gamma p \to \pi N$ T-matrix is equal to that of the $\pi N \to \pi N$ T-matrix.) If we represent the S-matrix by

$$S_{ij} = \delta_{ij} + iT_{ij}$$

and use the "bubble" notation(Ed66)

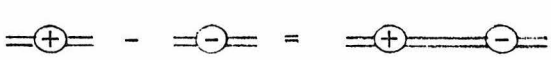
$i<j|T|i> \equiv$ 

$i<j|T^{+}|i> \equiv$ 

then the unitarity relation

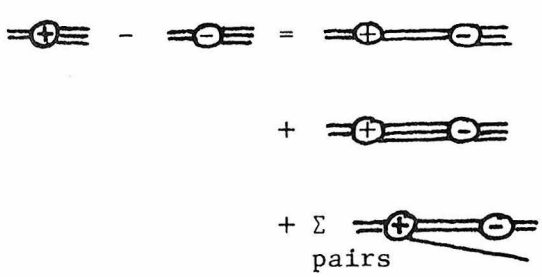
$$S\,S^{+} = 1$$

becomes

 (II-12)

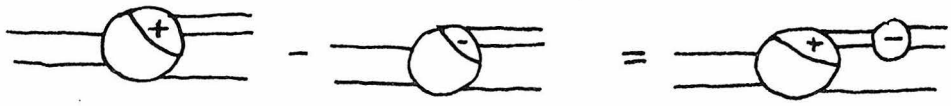
Thus, we see pictorially that the discontinuity of the 2-2 scattering amplitude (the left hand side of Equation (II-12)) has the phase variation of the initial and final state elastic scattering. Note that the more general understanding of + or - in the bubbles is to note that they tell us to evaluate the matrix element above or below the physical cut in the complex c.m.s. energy plane.

For a $2 \to 3$ scattering process, unitarity implies



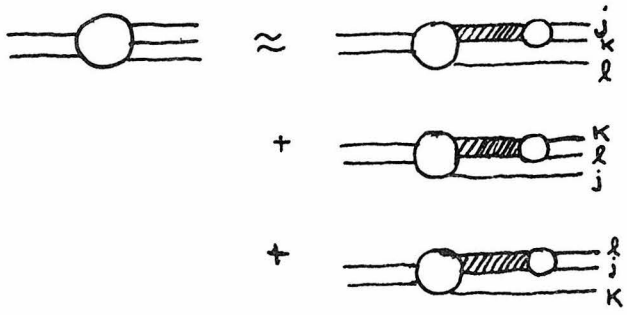
Here, we again see that the scattering matrix element gets the phase variation of each pair of final state particles.

We can consider discontinuities in the invariant subenergies w_{kl} as well as in the c.m.s. energy. The + and - in our bubbles now refer to position relative to the cut in the complex subenergy plane. The standard procedure[Ed66,O165,Go74] is to postulate a discontinuity relation for normal thresholds in the subenergy



(II-13)

The isobar model, however, assumes the structure



(II-14)

each term of which separately has the rescattering structure of Equation (II-13). The sum of terms, i.e., the whole isobar amplitude, does not.

In particular, for $\pi N \to \pi\pi N$, the "$\pi\pi$" isobar term does not have any "πN" rescattering dictated by Equation (II-13). It has been claimed [Aa73,Gu73] that the absence of such structure in isobar model analyses might affect the validity of the resultant phase shifts. Aaron and Amado[Aa73] claim, furthermore, that incorporating additional subenergy dependence into the τ-parameters of Equation (II-7), e.g.,

$$\tau^j(W) \to \tau_1^j(W) + \tau_2^j(W)\ q_j$$

enables the isobar model to satisfy these unitarity corrections.

This approach has, in turn, been criticized[Ai75,Ai77] for getting the correct subenergy discontinuity at the expense of destroying analyticity by inducing spurious singularities. To insure analyticity requires using dispersion relations to derive the full amplitude from the suggested discontinuity. Schematically, our isobar model (see Equation (II-6,7)) assumes

$$f_\mu \approx \sum_{\text{isobars}} g_j(W,w_j)\tau_j(W)$$

where g_j contains the normal barrier and final state interaction factors, while the corrected approach has

$$\tau_j(W) \to \tau_j(W,w_j)$$

with

$$\tau_j(W,w_j) = \tau_j(W) + \int_{\substack{\text{physical}\\ \text{cut}}} \frac{dw^2}{w^2-w_j^2-i\varepsilon}\ q_j(w^2) \int d\cos\tilde{\theta}_k^{(k\ell)}\ [g_k\tau_k+g_\ell\tau_\ell]$$

An amplitude structure of this form is being used by Aaron et al.[Aa76] in their study of $\pi N \to N\pi\pi$.

III. The π-exchange Input for High Partial Waves

A. Motivation

The standard approach in phase shift analysis is briefly described as follows:

A scattering matrix element expressed in terms of the scattering angle, θ, may be expanded in terms of Legendre polynomials:

$$f(\theta) = \sum_{L=0}^{\infty} (2L+1)\, A_L\, P_L(\cos\theta) \qquad \text{(III-1)}$$

It is assumed that only a few values of L are important, so we attempt to find the parameters A_L, L = 0 ... L_{MAX} such that

$$f^{theory}(\theta) = \sum_{L=0}^{L_{MAX}} (2L+1)\, A_L\, P_L(\cos\theta) \qquad \text{(III-2)}$$

best describes the experimental f(θ) (or its modulus).

The value of L_{MAX} chosen is motivated by two criteria:

1) Make the problem tractable: In Reference (He75b), it is noted that L,L' $\leq$ 3 and J $\leq$ 7/2 gives 60 partial waves. (Each additional unit of L, L', J adds 22 partial waves - 2 "εN" waves, 12 "ρN" waves and 8 "πΔ" waves.) These waves are listed in Table 1.

2) Heuristic arguments: For an interaction of range "R", the maximum angular momentum that can be excited is

$$L_{MAX} \sim P \times R$$

where R is the maximum impact parameter or the "range of interaction". For the exchange of a scalar particle, we find

$$A_L \sim \int \frac{d\cos\theta P_L(\cos\theta)}{y-\cos\theta} \sim Q_L(y) \qquad \text{(III-3)}$$

where the amplitude for the process

$$A + B \rightarrow C + D$$

is given by

$$f \sim \frac{1}{t-m^2_{exchange}} \sim \frac{1}{y-\cos\theta}$$

and

$$y = \frac{2E_A E_C - M_A^2 - M_C^2 + m^2_{exchange}}{2P_A P_C}$$

For large values of $L^{(Ch66)}$, the Legendre function of the second kind is approximately:

$$Q_L(y) \sim \frac{1}{\sqrt{L}} e^{-(L+1/2)\ln(y+\sqrt{y^2-1})} \qquad \text{(III-4)}$$

Thus, a "small" wave has

$$(L+1/2)\ln(y+\sqrt{y^2-1}) \sim 1$$

and the "Range" of interaction is

$$R \approx \frac{L_{MAX}}{P} \approx \frac{1}{P \ln(y+\sqrt{y^2-1})} \qquad \text{(III-5)}$$

For elastic scattering,

$$y = 1 + \frac{m^2_{exchange}}{2p^2}$$

and for $m^2_{exchange}/2p^2 << 1$,

$$\ln(y+\sqrt{y^2-1}) \approx \frac{m_{exchange}}{p}$$

Thus, the range is

$$R \approx \frac{1}{m_{exchange}} \qquad \text{(III-6)}$$

as we would naively have guessed for a Yukawa force.

For the case of interest, we consider our lowest and highest energies, assuming $(\pi\pi)$-exchange for $\pi N \to \pi\Delta$ and π-exchange for $\pi N \to \rho N$:

	W=1.65 GeV	W=1.97 GeV
$P_{\pi N}$	.55 GeV/c	.754 GeV/c
$P_{\pi\Delta}$	.34 GeV/c	.586 GeV/c
$P_{\rho N}$	0	.49 GeV/c
$L_{MAX} \sim \sqrt{P_{\pi N} P_{\pi\Delta}}/2m_\pi$	1.5	2.4
$L_{MAX} \sim \sqrt{P_{\pi N} P_{\rho N}}/m_\pi$	0	4.3

(The effective mass for the $\pi\pi$ threshold is actually much larger than $2m_\pi$ (Gr73) due to the weak $\pi\pi$ scattering at threshold. Thus, our estimate of L_{MAX}, in this case, is an overestimate.) We assume that the maximum value of L that will be excited in the process "in → out" is:

$$L_{MAX} \sim \sqrt{P_{in} P_{out}}\ R$$

This comes from Equation (III-5) for inelastic scattering at high energy in the forward direction assuming no complications due to spin. In our case, these complications exist so we can only hope to develop estimates for L_{MAX} from this analysis. For example, one might estimate that $L_{MAX} \approx 4$ may be excited at our highest energies in $\pi N \to \rho N$. In the final analysis,

however, the "proper" value of L_{MAX} to use must be determined empirically, for example, by looking at the moments of the decay angular distributions or by seeing how many waves are needed to adequately represent the differential cross sections.

In any case, the sum over partial waves to be fit is cut off. A common approach is to set the high partial wave contribution to zero. However, there are good reasons to believe that a better value of the high partial wave contribution may exist. Empirically, attempts to fit the $d\sigma/d\cos\theta_\pi$ distributions with low partial waves fail at the higher energies of the range fit. This failure is discussed in detail in Section VII. The high partial waves of low mass exchanges have sharp peaks at $\cos\theta \approx 1$, where the fits fail, due to the pole term

$$\frac{1}{t-m_{exch}^2} \sim \frac{1}{y-\cos\theta}$$

with $y \approx 1$. Also, the estimate

$$L_{MAX} \sim \sqrt{P_{\pi N} P_{\rho N}}/m_\pi \sim \text{"4.3"} \qquad \text{(III-7)}$$

at W = 1.97 GeV indicates that using L, L' $\leq$ 3, J $\leq$ 7/2 is very close to naive estimates of waves that ought to be included. Thus, a truncation of the partial wave series at L, L' = 3 might be ignoring significant contributions to the scattering. In fact, if a theory for high partial waves is known, an estimate of the importance of these high waves can be made by comparing their cross section contribution to the experimental cross section. (As we see later, our high partial wave input significantly affects the fit when

$$\frac{\sigma^{\text{High Partial Waves}}}{\sigma^{\text{Experiment}}} \sim 10\%) \ .$$

Some theory for these waves, at least in the $\pi N \to \rho N$ channel, might be better than setting them to zero.

The exact type of input to use in our analysis was suggested long ago[Fo72a,Ca73], the high partial wave part of π-exchange. Note that an additional bonus accrues from including a theoretical input - the fixing of the phase. Recall that a phase shift analysis which fits to differential cross sections cannot fix an overall energy-dependent phase, since if a solution T is found by fitting to $d\sigma \sim |T|^2$, then $Te^{i\theta}$ is just as valid a solution. But if we are fitting to $d\sigma \sim |T + T_\pi|^2$, then the phase of T is no longer free. Thus, there are two features of the π-exchange input that are of interest

1) possibility for improved fit to $d\sigma/d\cos\theta$ by including the expected $L \gtrsim 4$ waves.

2) removing the overall phase ambiguity from fitting to $|T|^2$ while parameterizing T.

B. The π-exchange amplitude

Next, we present the amplitude for $\pi N \to (\pi\pi)N$ via π-exchange. The amplitude for an elementary particle pion exchange was calculated according to the rules in Gasiorowicz[Ga66]. Using these rules, $\pi N \to \rho N \to \pi\pi N$ was calculated. The result was then extended to other isobars.

We note that no form factors or other modifying factors (eg., absorption or Regge residues) are used. This approach is motivated by three factors

1) It is not clear that a favored modification is more appropriate than the unmodified Born term. The high partial waves are thought to be unaffected by such modifications, and the transition (J, L, L' ~ 4) partial waves are not uniquely determined by any well-based theory.

2) The Born term automatically satisfies proper analyticity and $\pi\pi$ sub-energy unitarity conditions.

3) The Born term can be easily decomposed into partial waves for subtraction of the low partial waves.

The π-exchange amplitude for $\pi^- p \to n\pi^-\pi^+$ is

$$\mathcal{M}^{\pi\text{-exchange}}_{\mu_p\mu_n} = -\frac{i4g_{Np\pi}}{(2\pi)^{5/2}} \sqrt{(E_p+M_p)(E_n+M_n)} \quad \frac{w_{\pi\pi}}{[q_1\, q(t=m^2_{\pi\text{-exch}})]^{1/2}}$$

$$\times \sum_{\ell_{\pi\pi}\lambda} (2\ell_{\pi\pi}+1)\, d^{\ell_{\pi\pi}}_{-\lambda 0}(\tilde{\theta}^{(\pi\pi)}_{\pi})\, e^{-i\Phi_\pi(\mu_p+\mu_n-\lambda)}$$

$$\times \left\{\frac{p_\pi}{q(t=m^2_{\pi\text{-exch}})}\right\}^{\ell_{\pi\pi}} T_{\ell_{\pi\pi}}(w_{\pi\pi}) \left(\frac{2\mu_p p_p}{E_p+M_p} - \frac{2\mu_n Q_n}{E_n+M_n}\right)$$

$$\times \frac{d^{1/2}_{\mu_n-\mu_p}(\Theta_\pi)}{t-m^2_\pi} \left[f_{\ell_{\pi\pi}\lambda} d^{\ell_{\pi\pi}}_{-\lambda 0}(\Theta_\pi) + g_{\ell_{\pi\pi}\lambda}\right] \qquad \text{(III-8)}$$

where the subscripts π, p, n refer to the initial pion, initial proton and final neutron, and

$g_{np\pi}$ = $np\pi$ coupling = $-\sqrt{2}G$

G = $pp\pi^o$ coupling = $\sqrt{4\pi(14.64)}$

$q(t)$ = momentum of the exchanged pion in the $\pi\pi$ rest frame as a function of t

$t = (Q_n - p_p)^2$, the square of the momentum transferred at the nucleon vertex

$$f_{\ell_{\pi\pi}\lambda} = \begin{cases} (W-E_n)/w_{\pi\pi} & \ell_{\pi\pi} = 1 \quad \lambda = 0 \\ 1 & \ell_{\pi\pi} = 0 \text{ or } \ell_{\pi\pi} = 1, \ \lambda = \pm 1 \end{cases}$$

$$g_{\ell_{\pi\pi}\lambda} = \begin{cases} E_\pi Q_n / w_{\pi\pi} & \ell_{\pi\pi} = 1 \quad \lambda = 0 \\ 0 & \ell_{\pi\pi} = 0 \text{ or } \ell_{\pi\pi} = 1, \ \lambda = \pm 1 \end{cases}$$

The $\pi\pi$ scattering amplitude $T_{\ell_{\pi\pi}}(w_{\pi\pi})$ has had its $\cos\Theta_\pi$ dependence factored out. In the Born approximation for a ρ-isobar

$$T_{\ell_{\pi\pi}=1} = \frac{f^2_{\rho\pi\pi}}{6\pi w_{\pi\pi}} \quad \frac{(q(t=m^2_{\pi\text{-exch}})q_1)^{3/2}}{(m_\rho - i\Gamma_\rho/2)^2 - w^2_{\pi\pi}} \qquad \text{(III-9)}$$

where[Eb71,Pi73]

$$f^2_{\rho\pi\pi/4\pi} = 2.13$$

which corresponds to a width $\Gamma_\rho = 2/3(p^3/m^2_p)(f^2/4\pi) = 112$ MeV. (See Section IV for more details of this parameterization.) As defined in Equation (III-9), $T_{\ell_{\pi\pi}}$ is normalized to

$$\sigma^{\pi^-\pi^+\to\pi^-\pi^+} = \frac{4\pi}{k^2_\pi} \sum_{\ell_{\pi\pi}} (2\ell_{\pi\pi}+1) \left| T_{\ell_{\pi\pi}} \right|^2 \qquad \text{(III-10)}$$

This implies that $\mathcal{M}_{\mu_p\mu_n}$ in Equation (III-8) is normalized as in Equation (I-5).

We postpone to the next section our description of explicit forms for $T_{\ell_{\pi\pi}}$.

The expression Equation (III-8) is valid for $\pi^- p \to n\pi^-\pi^+$. For other charge channels, we use the convention, that $T_{\ell_{\pi\pi}} = C^{I_{\pi\pi}}_{\ell_{\pi\pi}} T^{I_{\pi\pi}}_{\ell_{\pi\pi}}$, where C^I_ℓ is a product of Clebsch Gordan coefficients. Note that for the case above, $C^I_\ell \equiv 1$. We tabulate below the product of two factors: $C^{I_{\pi\pi}}_{\ell_{\pi\pi}}$, and the ratio between $g_{N_{final}p\pi_{initial}}$ and G (also a Clebsch Gordan coefficient)

Charge Channel	$I_{\pi\pi}=0$ $\ell_{\pi\pi}=0$	$I_{\pi\pi}=1$ $\ell_{\pi\pi}=1$	$I_{\pi\pi}=2$ $\ell_{\pi\pi}=0$
$\pi^- p \to n\pi^-\pi^+$	$-\sqrt{2}/3$	$-\sqrt{2}$	$-\sqrt{2}/6$
$\pi^- p \to p\pi^-\pi^o$	0	1	1/2
$\pi^+ p \to p\pi^+\pi^o$	0	1	1/2

We did not use the entire π-exchange Born term of Equation (III-8). The low partial waves were subtracted out according to the following formula

$$\mathcal{M}^{\text{high p.w.}}_{\mu_p\mu_n}(W, w_{\pi\pi}, \tilde{\theta}^{(\pi\pi)}_\pi, \Theta_\pi, \Phi_\pi)$$

$$= \mathcal{M}_{\mu_p\mu_n}(W, w_{\pi\pi}, \tilde{\theta}^{(\pi\pi)}_\pi, \Theta_\pi, \Phi_\pi)$$

$$- \sum_J (J+\tfrac{1}{2}) d^J_{\mu_n-\lambda,-\mu_p}(\Theta_\pi) \sum_{LL'S'} c^{\mu_p\mu_n\lambda}_{LL'S'} \qquad \text{(III-11)}$$

$$\times \sum_{\alpha\beta\gamma} c^{\alpha\beta\gamma}_{LL'S'} \int d\cos\psi \; d^J_{\beta-\gamma,-\alpha}(\psi) \mathcal{M}_{\alpha\beta}(W, w_{\pi\pi}, \tilde{\theta}^{(\pi\pi)}_\pi, \Theta_\pi, \Phi_\pi)$$

where

$$C^{\mu_p \mu_n \lambda}_{LL'S'} = \sqrt{\frac{(2L+1)(2L'+1)}{(2J+1)^2}} \begin{pmatrix} L & 1/2 & J \\ 0 & -\mu_p & -\mu_p \end{pmatrix} \begin{pmatrix} L' & S' & J \\ 0 & \mu_n - \lambda & \mu_n - \lambda \end{pmatrix} \begin{pmatrix} 1/2 & \ell_{\pi\pi} & S' \\ \mu_n & -\lambda & \mu_n - \lambda \end{pmatrix}$$

(III-12)

L', S' = orbital and spin angular momenta of the n-($\pi\pi$) system

and the decomposition (III-10) is done separately for each $\ell_{\pi\pi}$ and λ. Those waves that are to be removed are thus included in the sum over J, L, L', S' in Equation (III-11). The selection of waves to be removed from the π-exchange amplitude to give our high partial wave input is discussed in detail in Section V.

IV. The final state factor

In this section we describe the $\pi\pi$ and πN amplitudes used by Herndon et al.[He75b]:

$$\frac{\eta_j e^{2i\delta_j} - 1}{2i} \tag{IV-1}$$

as in Equation (II-7), and our own corresponding $\pi\pi$ amplitudes (which we use only in the high partial wave input):

$$T^{I_{\pi\pi}}_{\ell_{\pi\pi}} \tag{IV-2}$$

as in Equation (III-8) and the discussion following. Both of the forms for the two particle scattering amplitudes have the same normalization, as given for the $\pi\pi$ case in Equation (III-10). As discussed by HSC[He75a] either a Breit Wigner form (in terms of resonance mass and width) or a phase shift form (in terms of elastic phase shifts and inelasticities) is appropriate for these scattering amplitudes. We use the phase shift representation, as it is more appropriate for scattering in channels such as the $\ell_{\pi\pi}=0$ channels which are not clearly dominated by a resonance ($I_{\pi\pi}=0$) or are not at all resonant ($I_{\pi\pi}=2$). For the resonant ρ-channel ($\ell_{\pi\pi}=1$) and the resonant Δ-channel ($\ell_{\pi N}=1$), the two forms are equally appropriate. For example, we present in figure 2 a comparison of a Breit Wigner resonant form and our phase shift representation for the ρ-isobar channel.

For the πN isobar, Herndon et al.[He75b,He72] used a table look-up from a compilation[He70] of πN phase shifts. We use these same low partial wave parameterizations of Herndon et al.[He75b,He72] in Equation (IV-1).

For the ρ-isobar we use the Herndon[He75b,He72] form in both Equation (IV-1) and Equation (IV-2):

$$T = \frac{1}{\cot\delta_\ell^I - i} \tag{IV-3}$$

where the parameterization of Morgan and Shaw[Mo70] is used

$$\cot\delta_P^1 = \frac{(m_\pi^2 - .1536q_1^2)(m_\pi^2 + .028q_1^2)\sqrt{m_\pi^2+q_1^2}}{.035\ m_\pi^2 q_1^3} \tag{IV-4}$$

In Figure 2, we present the phase shift of this parameterization, as well as that of a Breit Wigner

$$T_{BW} = \frac{m_\rho \Gamma}{-m_{\pi\pi}^2 + (m_\rho - i\Gamma/2)^2} \tag{IV-5}$$

with

$$\Gamma = \frac{2}{3m_{\pi\pi}} \quad \frac{f_{\rho\pi\pi}^2}{4\pi} \quad \frac{q_1^3}{m_\rho}$$

$$m_\rho = .77 \text{ GeV}$$

$$f^2_{\rho\pi\pi}/4\pi = 2.13$$

Both parameterizations have inelasticity $\eta^1_P = 1$. Also plotted are $\pi\pi$ phase shifts from the recent Protopopescu et al.[Pr73] and CERN-Munich[Oc73,Hy73] analyses. (The low energy limit of this parameterization corresponds to a scattering length $a^1_P = .035/m_\pi$, as compared to the Weinberg[We66,Ma76] linear current algebra model value of $a^1_P = .030/m_\pi$.)

For the $I_{\pi\pi} = 0$, $\ell_{\pi\pi} = 0$ isobar (the "ε"), we deviate from Herndon's[He72] parameterization. Herndon and the LBL-SLAC collaboration used

$$\cot\delta^0_S = \frac{2(.9-w_{\pi\pi})}{.74} \qquad w_{\pi\pi} > .66 \text{ GeV}$$

$$\cot\delta^0_S = \frac{w_{\pi\pi}}{q_1}\left(\frac{1}{.32} - 109.5\, q_1^2 + 1114.0\, q_1^4\right) \qquad w_{\pi\pi} < .4 \text{ GeV} \tag{IV-6}$$

and a table look up (from a hand drawn interpolation of the above forms) for $.4 < w_{\pi\pi} < .66$. This parameterization corresponds to a scattering length of $a^0_S = .16/m_\pi$, nearly the Weinberg[We66,Ma76] value of $.157/m_\pi$. It has inelasticity $\eta^0_S = 1$.

Since we use the LBL-SLAC[He75b] low partial wave data tapes, we use their $I_{\pi\pi}=\ell_{\pi\pi}=0$ and $I_{\pi\pi}=\ell_{\pi\pi}=1$ parameterizations for these waves. For the high partial wave π-exchange Born term, we use Protopopescu's "case 1" fit

(reference Pr73, Table VI) with linear interpolation between the values of δ_S^0 and η_S^0 tabulated for $.625 < w_{\pi\pi} < 1.15$ GeV. For $w_{\pi\pi} < .55$ GeV, we use the parameterization of Basdevant et al., (reference (Ba74), Equation B.6):

$$e^{2i\delta_S^0} = R(z, z_\varepsilon)\, R(z, z_{S^*})\, R(z, z_S^0) \qquad \text{(IV-7)}$$

$$\times\, C(\alpha_S^0, \beta_S^0, z)$$

where

$$R(x,y) = \frac{(x-y^*)(x+y)}{(x-y)(x+y^*)} \qquad \text{(IV-8a)}$$

$$C(a,b,x) = \frac{i+x}{i-x}\,\frac{i-ax}{i+ax}\,\frac{i-bx^3}{i+bx^3} \qquad \text{(IV-8b)}$$

$$z = \{p - \sqrt{p^2-1}\}^{1/2}$$

$$p = \cos 32.6^0 + \frac{(1.92)^2}{2(q/m_\pi)^2}$$

and their BKLY 2 fit parameters

$$z_\varepsilon = .67 - .282i$$

$$z_{S^*} = .928 - .074i$$

$$z_S^0 = 1.18 + 1.25i$$

$$\alpha_S^0 = .933$$

$$\beta_S^0 = -.339$$

For $.625 > w_{\pi\pi} > .55$, we interpolate between the Basdevant value at $w_{\pi\pi} = .55$ and the Protopopescu value at .625 GeV.

In Figure 3, we present the phase shifts and inelasticity parameters for the LBL-SLAC parameterization and for the high partial wave π-exchange parameterization described above. For comparison, we present also the data values of Protopopescu[Pr73] and the CERN-Munich[Oc73] collaboration. (The BKLY 2 parameterization of Basdevant et al.[Ba74] introduces a pole for the ε-meson at $w_{\pi\pi} = .439 - \frac{1}{2} .671\ i$ GeV and a zero in T_S^0 below threshold, corresponding to the zero required by the low energy expansion

$$\text{Re } T_S^0 \approx \frac{w_{\pi\pi}}{2q} \left(a_S^0 + b_S^0 q^2 \right)$$

This parameterization has a scattering length

$$a_S^0 = .169/m_\pi \quad .)$$

For the high partial wave π-exchange term, we included an $I_{\pi\pi} = 2$, $\ell_{\pi\pi} = 0$ contribution. For this input, we used the parameterization of Basdevant[Ba74]

$$S_S^2(z_2) = R(z_2, e^{i\theta_1}) R(z_2, e^{i\theta_2}) R(z_3, z_S^2) \times C(\alpha_S^2, \beta_S^2, z_2) \tag{IV-9}$$

where R and C are as defined in Equation (IV-8), and

$$z_2 = \frac{w_{\pi\pi}/2 - m_\pi}{q_1}$$

$$\theta_1 = -62°$$
$$\theta_2 = 1°$$
$$\alpha_S^2 = 1.06$$
$$\beta_S^2 = -.884$$
$$z_S^2 = .069 + 1.06i$$

These correspond to a scattering length of $a_S^2 = -.044/m_\pi$ = Re T_S^2 x $\frac{2q_1}{w_{\pi\pi}}$. This parameterization and various data (Ba70,Ba72,La71,Co73,Du73,Ho74,Lo74,Pr74) are presented in Figure 4. The Weinberg value, $-.045/m_\pi$, is again nearly realized.

We note that the low energy $\ell_{\pi\pi} = 0$, $I_{\pi\pi} = 0$ is not well understood. We chose the BKLY 2 parameterization with the Weinberg (We66,Ma76) scattering length because

a) Guidance by naive theoretical predictions is better than no guidance at all. Basdevant (Ba74) provided parameterizations consistent with higher and lower a_S^0. But the experimental situation is not clear enough to be a valid discriminant. (See the excellent review by Martin et al. (Ma76) for a comprehensive discussion.)

b) Pennington and Protopopescu (Pe73) point out that taking the low energy phase shifts of Protopopescu et al. (Pr73) seriously forces $a_S^0 = (.15 \pm .07)/m_\pi$, so at least our larger $w_{\pi\pi}$ phase shifts are not naively inconsistent with this scattering length.

We note that the $I_{\pi\pi} = 2$ contribution is not very large. It causes, at worst, 15% variations in the $\pi\pi$ S-wave contribution to the $\pi^- p \to n\pi^-\pi^+$

cross section. (Its contribution to the total cross section in $\pi^{\pm}p \to p\pi^{\pm}\pi^{o}$ is even smaller, since there is no $I_{\pi\pi} = 0$ term with which to interfere.)

Finally, we note that the q_1 threshold behavior of the cross section is correctly given by (Equations I-8, II-2, II-7, II-8c)

$$\frac{1}{q_1}\left|\frac{T^{I_{\pi\pi}}_{\ell_{\pi\pi}}}{q_1^{\ell_{\pi\pi}+1/2}}\right|^2 \cdot q_1 \sim q_1^{2\ell_{\pi\pi}+1}$$

V. Selection criteria and properties of the π-exchange input

In Eq.(III-8) we presented the π-exchange matrix element which we expanded in the ππ angular momentum basis:

$$\mathcal{M}_{\mu_p\mu_n}(W,w_{\pi\pi},\tilde{\theta}_\pi^{(\pi\pi)},\Theta_\pi,\Phi_\pi) = \sum_{\ell_{\pi\pi}\lambda} (2\ell_{\pi\pi}+1)\, d^{\ell_{\pi\pi}}_{-\lambda\,0}(\tilde{\theta}_\pi^{(\pi\pi)})\, e^{-i\Phi_\pi(\mu_p+\mu_n-\lambda)}\, M^{\ell_{\pi\pi}}_{\mu_p\mu_n\lambda}(W,w_{\pi\pi},\Theta_\pi) \quad . \tag{V-1}$$

Then the cross section, defined by Eq. (I-5), can be equivalently represented by

$$d\sigma = \frac{1}{2}\frac{\pi^2}{F} \sum_{\substack{\ell_{\pi\pi}\lambda \\ \mu_p\mu_n}} (2\ell_{\pi\pi}+1)\, \left|M^{\ell_{\pi\pi}}_{\mu_p\mu_n\lambda}\right|^2 \frac{\pi^2 Q_1 q_1}{W}\, dw_{\pi\pi} d\cos\Theta_\pi \tag{V-2}$$

where we have used

$$\frac{1}{(2\sigma_a+1)\,(2\sigma_b+1)} = \frac{1}{2} \quad . \tag{V-3}$$

We next expand in terms of partial waves

$$M^{\ell_{\pi\pi}}_{\mu_p\mu_n\lambda}(W,w_{\pi\pi},\Theta_\pi) = \sum_J \frac{(2J+1)}{2}\, d^J_{\mu_n-\lambda,\,-\mu_p}(\Theta_\pi)\, A^{J\,\ell_{\pi\pi}}_{\mu_p\mu_n\lambda}(W,w_{\pi\pi}) \tag{V-4}$$

in terms of which the differential cross section is

$$\frac{d\sigma}{dw_{\pi\pi}} = \frac{1}{2}\frac{\pi^2}{F} \sum_{\substack{\ell_{\pi\pi}J \\ \mu_p\mu_n\lambda}} (2\ell_{\pi\pi}+1) \left(\frac{\pi^2 Q_1 q_1}{W}\right) \left(\frac{2J+1}{2}\right) \left| A^{J\,\ell_{\pi\pi}}_{\mu_p\mu_n\lambda} \right|^2 \quad . \tag{V-5}$$

We then expand in an L-S basis

$$A^{J\,\ell_{\pi\pi}}_{\mu_p\mu_n\lambda} = \sum_{L\,L'\,S'} c^{\mu_p\mu_n\lambda}_{LL'S'}\, A^{J\,\ell_{\pi\pi}}_{LL'S'}(W,w_{\pi\pi}) \tag{V-6}$$

with $c^{\mu_p\mu_n\lambda}_{LL'S'}$ defined in Eq. (III-12). These partial wave amplitudes

have the normalization

$$\frac{d\sigma}{dw_{\pi\pi}} = \frac{1}{2}\frac{\pi^2}{F}\left(\frac{\pi^2 Q_1 q_1}{W}\right)\sum_{\substack{\ell_{\pi\pi} J \\ LL'S'}}(2\ell_{\pi\pi}+1)\left(\frac{2J+1}{2}\right)\left|A^{J\ell_{\pi\pi}}_{LL'S'}\right|^2 . \qquad \text{(V-7)}$$

If we define the magnitude of the phase space averaged T-matrix element by

$$\left|T^{J\ell_{\pi\pi}}_{LL'S'}\right| \equiv \left\{\frac{\int dw_{\pi\pi}\left(\frac{\pi^4 Q_1 q_1}{2WF}\right)(2\ell_{\pi\pi}+1)\left(\frac{2J+1}{2}\right)\left|A^{J\ell_{\pi\pi}}_{LL'S'}\right|^2}{\frac{4\pi}{p_\pi^2}\left(\frac{2J+1}{2}\right)}\right\}^{\frac{1}{2}} \qquad \text{(V-8)}$$

then the cross section becomes

$$\sigma = \frac{4\pi}{p_\pi^2}\sum_{\substack{\ell_{\pi\pi} J \\ LL'S'}}\left(\frac{2J+1}{2}\right)\left|T^{J\ell_{\pi\pi}}_{LL'S'}\right|^2 . \qquad \text{(V-9)}$$

Note that this formalism is for $\pi^- + p \longrightarrow n + \pi^- + \pi^+$. These "charge channel" T-matrix elements can be decomposed into isospin matrix elements, thus defining the quantities

$$T^{J\ I\ \ell_{\pi\pi}\ I_{\pi\pi}}_{L\ L'\ S'} .$$

For the ρ-isobar, we find that in terms of the $\pi^- p \longrightarrow n\pi^-\pi^+$ T-matrix elements,

$$T^{J\ I=1/2\ \ell_{\pi\pi}=1\ I_{\pi\pi}=1}_{L\ L'\ S'} = \sqrt{2}\ T^{J\ \ell_{\pi\pi}=1}_{LL'S'} \qquad \text{(V-10)}$$

and

$$T^{J\ I=3/2\ \ell_{\pi\pi}=1\ I_{\pi\pi}=1}_{L\ L'\ S'} = -\frac{1}{2}\ T^{J\ I=1/2\ \ell_{\pi\pi}=1\ I_{\pi\pi}=1}_{L\ L'\ S'} . \qquad \text{(V-11)}$$

(Eq. (V-11) is a general property of isospin 1 exchange mechanisms[Re70].)

The $T^{J\ I\ \ell_{\pi\pi}\ I_{\pi\pi}}_{L\ L'\ S'}$ are unitarity bounded by

$$\left| T^{J\ I\ \ell_{\pi\pi}\ I_{\pi\pi}}_{L\ L'\ S'} \right| \leq \frac{1}{2} \quad . \tag{V-12}$$

The tests which we describe next were all performed for the ρ-isobar ($\ell_{\pi\pi} = I_{\pi\pi} = 1$).

Properties of the low partial wave amplitudes

For each value of J, there are (at most) six partial waves. We label these waves in a manner similar to that of Herndon et al.[He75b]

$$\rho_{(2S')}{}^{L\ L'\ (2I)\ (2J)} \quad .$$

Then for I=1/2, the waves for each J fall into six classes:

α: ρ_1 [SS11,PP13,DD15,FF17,...] <---> [α_1,α_3,α_5,α_7,...]

β: ρ_1 [PP11,DD13,FF15,GG17,...] <---> [β_1,β_3,β_5,β_7,...]

γ: ρ_3 [PP13,DD15,FF17,...] <---> [γ_3,γ_5,γ_7,...]

δ: ρ_3 [PP11,DD13,FF15,GG17,...] <---> [δ_1,δ_3,δ_5,δ_7,...]

ε: ρ_3 [SD11,PF13,DG15,...] <---> [ε_1,ε_3,ε_5,...]

ϕ: ρ_3 [DS13,FP15,GD17,...] <---> [ϕ_3,ϕ_5,ϕ_7,...]

The I=3/2 waves are related by Eq. (V-11). In the energy range of interest in this analysis, 1.63 GeV $\leq$ W $\leq$ 1.99 GeV, there are definite patterns for the relative sizes of these waves. For J=3/2, 5/2 and 7/2 ρ-production,

$$\phi_i >> \gamma_i >> \beta_i \sim \alpha_i \sim \delta_i >> \varepsilon_i \qquad i=3,5,7 \tag{V-13a}$$

a pattern set primarily by the $Q_1^{L'}$ threshold factor,

while for J=1/2,

$$\alpha_1 \sim \delta_1 >> \varepsilon_1 >> \beta_1 \quad . \tag{V-13b}$$

It is claimed by Herndon et al. (ref. He75b, section IV.H) that their analysis is not sensitive to any wave whose strength,

$$\left| \begin{matrix} J & I & \ell_{\pi\pi} & I_{\pi\pi} \\ T & & & \\ L & L' & S' & \end{matrix} \right|$$

is much less than 0.1. From this we conclude that we should not attempt to learn anything from including any <u>single</u> π-exchange wave with strength smaller than 0.1. In our energy range, waves that satisfy $|T| \geq 0.1$ are listed in Table 2. From this we see that 17 out of the 42 waves considered are not small. See figure 5 for plots of the I=1/2 waves vs. c.m. energy. (Recall that $T^{I=3/2} = -\frac{1}{2} T^{I=1/2}$.) Since the higher partial waves are those most likely to have physical importance (since they will not be cancelled by contributions from more massive particle exchange mechanisms), we can classify the waves in terms of their relative importance as:

Most important: (J=7/2 or L+L' $\geq$ 5)

ρ_3 GD17. We included the effect of this wave by including it in our π-exchange input term. (We also included ρ_3 GD37 in the π-exchange input, in the amount given by Eq. (V-11).)

Next important: (J=5/2 or L+L' $\geq$ 3)

ρ_3 FP15 and ρ_3 FP35. These waves were fit by both Herndon et al.[He75b] and by us.

ρ_3 DD15, ρ_3 DD13 and ρ_1 DD13. These waves are not included in either the LBL-SLAC analysis or in our work.

So the approach of looking at high J or L+L' waves with $|T| > 0.1$ suggests that the ρ_3 GD17 wave of π-exchange must be included in our parameterization of the scattering amplitude. We therefore incorporated this wave as part of the π-exchange input. We also learn that the ρ_3 FP15 and ρ_3 FP35 waves of π-exchange should be included. These waves were included as fit parameters.

Finally we find that the ρ_3 DD15, ρ_3 DD13 and ρ_1 DD13 waves should be included. We did not include them as fit parameters, since inclusion of new parameters diminishes the value of our study of the stability of the LBL-SLAC[He75b] solution under π-exchange. The fact that they are the second level of corrections (- presumably the ρ_3 GD17 wave is the most important π-exchange correction -) made their inclusion in the parameterization of the T-matrix less pressing. (Also, adding these new waves as fit parameters required computer program modifications that we were glad to avoid.) We also did not add these waves as part of the π-exchange input, since these waves would have interfered with the "fit" waves in the total cross section. By not adding these waves, the total cross section becomes

$$\sigma_{Total} = \sigma_{fit} + \sigma_{\pi\text{-input}}$$

i.e. there is no cross term between the fit cross section and our final form of the π-exchange high partial wave input. Including the DD15 and DD13 waves in the π-input would have generated an interference term. To incorporate this effect would have required a large increase in the cost of our computer calculations. In particular, the 'KREBS DECKS' discussed in section VI.C. would have had to be recalculated. Again

the fact that these waves are the second level of corrections encouraged us to omit their effect.

Note that if we consider the partial wave cross sections:

$$\sigma^{\,J\ I\ \ell_{\pi\pi}\ I_{\pi\pi}}_{\,L\ L'\ S'} = .389\ \frac{1}{2}\ \frac{4\pi}{p_\pi^2}\ (2J+1)\ \left|\ T^{\,J\ I\ \ell_{\pi\pi}\ I_{\pi\pi}}_{\,L\ L'\ S'}\ \right|^2$$

then we might develop criteria for selecting important waves that enhance the importance of higher J waves, due to the (2J+1) factor in the cross section. Analysis of this quantity is considered in Ref. Aa76. We feel that since the stated sensitivity[He75b] is to $|T|<0.1$, then it is $|T|$ that should be considered when evaluating which waves are most important.

In conclusion, our analysis has told us that the π-exchange amplitude has important contributions to the $\pi N \to \rho N$ scattering process in the ρ_3 GD17 wave, and also somewhat important contributions in the ρ_3FP15, ρ_3 FP35, ρ_3 DD15, ρ_3 DD13 and ρ_1 DD13 waves. We included the most important effect in the π-exchange input. We included the effects of the L=3 scattering in the fit amplitude. The suggested D-wave corrections were ignored due to the difficulty of incorporating these waves, and to the second order nature of their corrections.

Effect of a form factor

We then multiplied the π-exchange amplitude by a form factor

$$e^{3(t-m_\pi^2)}$$

which approximates a Regge residue function[Fo73], in order to diminish the strength of the very low π-exchange partial waves. (As is apparent

from figure 5, many low partial waves from the π-exchange Born term violate the unitarity bound, which in its weakest form says $|T| \leq 1/2$. At high energy, this Regge damping empirically agrees with π-exchange dominated cross sections. At W=1.89 GeV, we find that

(1) The ρ_3GD17 wave that we include in our π-exchange input is modified by only $\sim$ 20%. Thus we are encouraged that the unmodified Born term gives a reasonable evaluation of this wave. The other members of the series of 'ϕ' waves that we found to be important, the ρ_3FP15 and ρ_3FP35 waves, are modified by 45% by the form factor. Thus evaluating the size of these waves from the unmodified Born term might be somewhat unreliable.

(2) The ρ_3DD15 wave, which belongs to the 'γ' series, is modified by 63% by the form factor. Clearly inclusion of this wave as an unmodified π-exchange input would be unreliable. The next member of the 'γ' series, the ρ_3FF17, suffers a 33% modification, and thus while smaller than its D-wave partner, might be more reliably estimated from a π-exchange calculation, and included as being a correct, though possibly not critically important, part of the total amplitude.

(3) The 'β' series (for J=3/2,5/2 and 7/2) were practically unaffected by the form factor. These waves are, however, small enough that they can be completely ignored in terms of their contribution from the π-exchange mechanism.

(4) All the corrections mentioned above tended to diminish the magnitude of the amplitude. Thus a 33% correction means that the

magnitude of the form factor modified amplitude is 67% of the magnitude of the unmodified amplitude.

(5) The two larger D-waves discussed previously as possible second level corrections were strongly modified by the form factor. The ρ_3DD15 (γ_5) suffered a 63% reduction, while the ρ_3DD13 (δ_3) was reduced 78%. Only the smallest of these waves, the ρ_1DD13 (β_3) was unaffected by the form factor, as mentioned in (3) above.

We conclude that our decision to include as a pure π-exchange input only the ρ_3GD17 and GD37 waves, from the set of all the low J waves, is a very reasonable approach.

Naïve effect due to higher mass exchanges

Next we performed a simple test of the corrections one might expect from including higher mass exchanges. We calculated the π-exchange Born diagram assuming the mass of the exchanged pion was 0.77 GeV. We evaluated the partial waves for $w_{\pi\pi}$=0.77 GeV and W=1.89 GeV. The corrections to the ρ_3GD17 (ϕ_7), ρ_3FP15 (ϕ_5), ρ_3FF17 (γ_7) and ρ_3DD15 (γ_5) waves were 10%, 20%, 15% and 33% of the result for the same W and $w_{\pi\pi}$, but for the mass of the exchanged pion = 0.13957 GeV. Thus our series of preferred correcting waves, the ϕ and γ series, are not severely affected by the inclusion of higher mass spin=0 isospin=1 exchanges. In fact the effect on our most favored wave, the ρ_3GD17, is a rather minimal correction from this effect.

The final form

The conclusion of these various analyses is that the ρ_3GD17 is an

important wave. Since we do not fit it, we include it in the π-exchange high partial wave input. For J=7/2, it is the only large π-exchange wave at the energies we are considering.(It is also true that its fellow member of the ϕ series of waves, the ρ_3FP15, is the largest J=5/2 wave.) In fact, the ϕ_7 wave contributes more to the π-exchange cross section than all the higher partial waves combined (in our energy range). As to the inclusion of other waves from the π-exchange diagram in the π-exchange input, we decided to:

(1) include in our π-exchange input term all waves with $J \geq 9/2$. The ρ_3 HF19,.... waves, i.e. the ϕ series, should dominate the contribution from each value of J.

(2) include all the waves with L=4. This includes the β_7 and δ_7 waves, but not the ε_5 wave (which has L'=4, but L=2).

(3) exclude all waves with both $L \leq 3$ and $J \leq 7/2$. As previously discussed, the only waves in this set that are large and which we might have considered including are the ρ_3FF17, ρ_3FF37, ρ_3DD15, ρ_3DD35, ρ_3FP15, ρ_3FP35 and the J=3/2,L=2 waves. Of these waves, the ρ_3FF37, ρ_3FP15, ρ_3FP35 are included as fit waves, while the ρ_3DD15, ρ_3DD35, ρ_3 DD13 and ρ_3DD33 are severely affected by our form factor (and hence our estimate of their importance is not incontestable). The other waves, i.e. the ρ_3FF17 and ρ_1DD13, are both much smaller than our favored ρ_3GD17 wave, and to include them would have caused a great increase in computer time. So they were not included. One advantage of the $L \geq 4$ or $J \geq 9/2$ ('logical or') criterion is

that these waves will not interfere with the 'fit' waves ($L \leq 3$ 'logical and' $J \leq 7/2$)in the calculation of the cross section, thus avoiding significant computer calculations.

These wave selection criteria were used both for the ρ-isobar and for the $\ell_{\pi\pi} = 0$ ($I_{\pi\pi} = 0$ and 2) isobar partial waves.

Properties of the π-exchange high partial wave input

We present in figures 6 and 7 the differential cross sections $d\sigma/d\cos\Theta_{\pi}$ and $d\sigma/dw_{\pi\pi}$ at our lowest and highest energies[f1] calculated from our π-exchange high partial wave input. In figure 8 we show the total cross section from the π-exchange input. All curves are for the charge channel $\pi^- p \to n\pi^-\pi^+$. (For $\pi^{\pm} p \to p\pi^{\pm}\pi^o$ the contribution of the ρ-isobar is multiplied by 1/2, the I=0 by 0, and the I=2 contribution by 4.5.) The following features should be observed:

(1) There is a very sharp peak at $\cos\Theta_{\pi} = -1.0$, i.e. at $t-m_{\pi}^2$ near 0. The sharpness of the peak has been enhanced by our removal of the low partial waves.

(2) The I=2 contribution is very small (and could probably have been ignored).

(3) Even below ρN threshold (1.7 GeV) the contribution of the ρ-isobar to the cross section far exceeds that of the $\ell_{\pi\pi}$=0 isobar (in the energy range being considered).

(4) The ρ-resonance shape is not in its full glory at the lowest energy. (It is not fully excited until $\sim$ 1.8 GeV.)

(5) The ρ_3GD17 wave contributes over half of the total π-exchange high partial wave input cross section, with the percentage decreasing

from more than 70% at the lower energies to slightly over half at the high energy end of our range of interest.

(6) By comparing figures 8 and 9, we see that the π-exchange input contributes a fraction of the total inelastic cross section that grows with energy. For $\pi^- p \to n\pi^- \pi^+$, the ratio of $\sigma^{\pi\text{-input}}/\sigma^{\text{experiment}}$ is 1% at W=1.65 GeV, 10% at W=1.81 GeV and 30% at W=1.97 GeV. For $\pi^- p \to p\pi^- \pi^o$ the percentages are 0.8%, 10% and 25%. For $\pi^+ p \to p\pi^+ \pi^o$ the percentages are 0.5%, 3% and 11% at the same three energies.

VI. The analysis procedure

A. The Likelihood method

The computational problem we face is to find the best values for a set of parameters, $\{A_i\}$ (- which we will denote by $\vec{A}$, and which are the real and imaginary parts of $\tau^{J\ j_j\ I\ I^{(k\ell)}}_{L\ S\ L_j\ S_j}(W)$ of Eq. (II-7)). Experimental information is available for

$$q_\alpha(\vec{\omega}_n,\vec{A}) = \sum_{\text{helicities}} \left| \vec{c}_{\alpha,\text{helicities}}(\vec{\omega}_n) \cdot \vec{A} + \vec{b}_{\alpha,\text{helicities}}(\vec{\omega}_n) \right|^2$$

$$Q_\alpha(\vec{A}) = \left(\frac{1}{N^\alpha_{MC}} \sum_{n=1}^{N^\alpha_{MC}} q_\alpha(\vec{\omega}_n,\vec{A}) \right) \int \text{phase space} \qquad \text{(VI-1)}$$

where $\vec{\omega}_n$ are the kinematic variables (-subenergies and angles -) for the n^{th} event, α is the charge channel (e.g. $\pi^\pm + p \text{ ---> } p + \pi^\pm + \pi^o$), N^α_{MC} is the total number of Monte Carlo events for charge channel α (generated from the phase space distribution in Eq. (I-8)), $\vec{c}_{\alpha,\text{helicites}}(\vec{\omega})$ given in Eq. (II-11) and $\vec{b}_{\alpha,\text{helicities}}(\vec{\omega})$ are known functions of the variables, $\vec{\omega}$. In our calculations, $\vec{b}_{\alpha,\text{helicities}}(\vec{\omega})$ represents the high partial wave part of the elementary π-exchange Born term, Eq. (III-11). (In previous analyses[He75b,Do76], $\vec{b}_{\alpha,\text{helicities}}(\vec{\omega})$ was set equal to zero.) Thus $q_\alpha(\vec{\omega}_n,\vec{A})$ is the differential cross section for the charge channel, α, evaluated for the n^{th} event described by the kinematic variables, $\vec{\omega}_n$. $Q_\alpha(\vec{A})$ is the predicted total cross section for charge channel, α . The parameters $\vec{A}$ depend only on the total center of mass energy, W.

An estimate of the parameters, $\vec{A}$, is given by maximizing the Generalized Likelihood Function[So64,Fo72b]

$$\mathcal{L}(\vec{A}) = \prod_{\alpha} \left(\left\{ \prod_{n=1}^{N_\alpha} \frac{q_\alpha(\vec{\omega}_n,\vec{A})}{Q_\alpha(\vec{A})} \right\} \frac{\{\hat{N}_\alpha(\vec{A})\}^{N_\alpha}}{(N_\alpha)!} \; e^{-\hat{N}_\alpha(\vec{A})} \right)$$

where $\hat{N}_\alpha(\vec{A})$ is the number of events predicted by our parameters, $\vec{A}$, given a Poisson distribution of events. In fact,

$$\hat{N}_\alpha(\vec{A}) = \frac{Q_\alpha(\vec{A})}{\sigma_\alpha} \; N_\alpha$$

where σ_α is the experimental total cross section and N_α the number of experimental events for charge channel, α . Thus

$$\mathcal{L}(\vec{A}) = \prod_{\alpha} \left(\frac{1}{(N_\alpha)!} \left\{ \frac{N_\alpha}{\sigma_\alpha} \right\}^{N_\alpha} e^{-\frac{N_\alpha}{\sigma_\alpha} Q_\alpha(\vec{A})} \prod_{n=1}^{N_\alpha} q_\alpha(\vec{\omega}_n,\vec{A}) \right) \qquad \text{(VI-2)}$$

The average of the logarithm of the Generalized Likelihood Function is a more useful object to compute, since it is linearly related to the common χ^2 function, and thus its derivatives are trivially related to those of χ^2. Ignoring $\vec{A}$ - independent constants, we define

$$\begin{aligned} \mathcal{F}(\vec{A}) &\equiv \frac{1}{\sum_\alpha N_\alpha} \ln \mathcal{L}(\vec{A}) \quad + \vec{A} \text{ - independent term} \\ &\equiv \frac{1}{\sum_\alpha N_\alpha} \sum_\alpha \left\{ \sum_{n=1}^{N_\alpha} \ln q_\alpha(\vec{\omega}_n,\vec{A}) - \frac{N_\alpha}{\sigma_\alpha} Q_\alpha(\vec{A}) \right\}. \end{aligned} \qquad \text{(VI-3)}$$

The fitting technique which we use to maximize $\mathcal{F}(\vec{A})$ uses the first and second derivatives

$$\frac{d\mathcal{F}(\vec{A})}{dA_j} = \frac{1}{\sum_\alpha N_\alpha} \sum_\alpha \left(\sum_{n=1}^{N_\alpha} \frac{dq_\alpha(\vec{\omega}_n,\vec{A})/dA_j}{q_\alpha(\vec{\omega}_n,\vec{A})} - \frac{N_\alpha}{Q_\alpha} \frac{dQ_\alpha(\vec{A})}{dA_j} \right)$$

$$\frac{d^2\mathcal{F}(\vec{A})}{dA_j dA_k} = \frac{1}{\sum_\alpha N_\alpha} \sum_\alpha \{ \mathcal{S}_1 + \mathcal{S}_2 + \mathcal{S}_3 \}$$

where

$$\mathcal{J}_1 = -\sum_{n=1}^{N_\alpha} \frac{d\,\ell n\, q_\alpha(\vec{\omega}_n,\vec{A})}{dA_j} \frac{d\,\ell n\, q_\alpha(\vec{\omega}_n,\vec{A})}{dA_k}$$

$$\mathcal{J}_2 = \sum_{n=1}^{N_\alpha} \frac{1}{q_\alpha(\vec{\omega}_n,\vec{A})} \frac{d^2 q_\alpha(\vec{\omega}_n,\vec{A})}{dA_j dA_k}$$

$$\mathcal{J}_3 = -\frac{N_\alpha}{\sigma_\alpha} \frac{d^2 Q_\alpha(\vec{A})}{dA_j dA_k}$$

Near a solution, $Q_\alpha(\vec{A}) \approx \sigma_\alpha$, and the Central Limit Theorem implies (Fo72a)

$$< \mathcal{J}_2 + \mathcal{J}_3 > \approx 0$$

Also, it may be seen that

$$< \mathcal{J}_1 > \approx N_\alpha$$

$$\sqrt{< \{ \mathcal{J}_2 + \mathcal{J}_3 \}^2 >} \approx \sqrt{N_\alpha}$$

Therefore in the large N_α limit, the terms $\mathcal{J}_2 + \mathcal{J}_3$ contribute to $\mathcal{F}(\vec{A})$ only $\sim \sqrt{N_\alpha}$ (via their dispersion), while the dominant term, $\mathcal{J}_1$, contributes $\sim N_\alpha$. Thus we neglect the last two terms of the second derivative of $\mathcal{F}$, and define

$$M_{jk}(\vec{A}) \equiv -\frac{1}{\sum_\alpha N_\alpha} \sum_\alpha \sum_{n=1}^{N_\alpha} \left\{ \frac{1}{q_\alpha(\vec{\omega}_n,\vec{A})} \right\}^2 \frac{dq_\alpha(\vec{\omega}_n,\vec{A})}{dA_j} \frac{dq_\alpha(\vec{\omega}_n,\vec{A})}{dA_k} \tag{VI-4}$$

with

$$\frac{d^2 \mathcal{F}(\vec{A})}{dA_j dA_k} \approx M_{jk}(\vec{A}) \tag{VI-5}$$

for large N_α. We use this approximation to the second derivative of the average log likelihood function. We note that our approximant has the calculational convenience that it does not involve second derivatives of $q_\alpha(\vec{\omega}_n,\vec{A})$ or $Q_\alpha(\vec{A})$. The use of M_{jk} in problems of this type is a standard approximation (Fo72b,Mi71).

B. Errors in the Maximum Likelihood method

Let us call

$$N \equiv \sum_\alpha N_\alpha$$

so that

$$\mathcal{L}(\vec{A}) = \text{constant } e^{N\mathcal{F}(\vec{A})} .$$

Now $\mathcal{L}(\vec{A})$ is the conditional probability for the set of experimental results

$$\{ \vec{\omega}_1, \ldots \vec{\omega}_n , \sigma_1, \ldots \sigma_N \}$$

given the parameters, $\vec{A}$. In the limit of large N, $\mathcal{L}(\vec{A})$ is Gaussian distributed in $\vec{A}$ (Fo72b,So64). The most probable value of the parameters, $\vec{A}^*$, given the experimental data $\{\vec{\omega}_1,\ldots\sigma_N\}$ may be shown to be given by

$$\left.\frac{d\mathcal{F}(\vec{A})}{dA_i}\right|_{\vec{A}=\vec{A}^*} = 0 \qquad \text{(VI-6)}$$

and the dispersion of the Gaussian is

$$\sigma_{ij} = \left[N \frac{d^2\mathcal{F}(\vec{A})}{dA_i dA_j} \right]^{-1} \Bigg|_{\vec{A}=\vec{A}^*} .$$

We will instead use

$$\sigma_{ij} \approx \frac{1}{N}(\overleftrightarrow{M}^{-1})_{ij} \Big|_{\vec{A}=\vec{A}^*} \qquad \text{(VI-7)}$$

where M_{ij} is defined in Eq. (VI-5). The error in the determination of a parameter, A_i, is then defined as

$$\delta A_i \equiv \sqrt{\sigma_{ii}} \qquad \text{(VI-8)}$$

(Another estimate of the error is

$$\delta A_i \geq 1/\sqrt{(\sigma^{-1})_{ii}} \quad . \qquad \text{(VI-9)}$$

The difference between this error and the correct value, given by Eq. (VI-8), gives an estimate of correlations in the error matrix. The errors we quote will be the statistically correct ones from Eq. (VI-8).) The correlations of errors in these parameter determinations are discussed in Miller's these[Mi71]. We note here that our two estimates (eqs. (VI-8) and (VI-9)) coincide in the absense of correlations. Empirically the two values are often very close at the higher energies of our analysis.

C. The calculational procedures

In this analysis we used the data described and previously used by Herndon et al.[He75b]. We analysed those data with c.m. energies satisfying $1.63 \leq W \leq 1.99$ GeV. We used the LBL-SLAC[He75b] Triangle 2[No76] data tapes with their coefficient functions $c^n_{\alpha,\mu}$ (defined in Eq. (II-10)) as our source of experimental events. These data tapes combine data in 40 Mev bins, with central energies 1.65, 1.69, 1.73, 1.77, 1.81, 1.85, 1.89, 1.93 and 1.97 GeV. This binning was found[He75b] to be necessary to provide sufficient statistics in order to give a reliable determination of the scattering matrix elements. The number of events varies between 7500 to 21,000 per energy bin.

We added the π-exchange information to each event on these data tapes.

The calculation of the cross section by Herndon et al.[He75b] proceeded by generating N_{MC} Monte Carlo events uniformly distributed in phase space (Eq. (I-2)), and then storing the matrix

$$R^{\alpha}_{ij} \equiv \frac{1}{N_{MC}} \sum_{\text{events},\mu} c^{i}_{\alpha,\mu} \, c^{j\,*}_{\alpha,\mu} \quad . \qquad \text{(VI-10)}$$

This provides for easy calculation of

$$\frac{1}{N_{MC}} \sum_{\substack{\text{Monte} \\ \text{Carlo} \\ \text{events}}} \sum_{\mu} \left| \vec{c}_{\alpha\mu}(\vec{\omega}) \cdot \vec{A} \right|^2 = \sum_{i,j} A^{i} \, R^{\alpha}_{ij} \, A^{j}$$

which is proportional to the predicted cross section for the channel, α. The R^{α}_{ij} were stored and called "KREBS DECKS" by Herndon et al.[He75b] Typically, N_{MC} was 9000 for each 10 MeV bin.

We note that our π-exchange input will not interfere with the low partial wave representation of the cross section, since waves with different values of "L" do not interfere. Thus

$$Q_{\alpha}(\vec{A}) \equiv \sigma_{\alpha}(\vec{A},\pi) = \sigma_{\alpha}(\pi) + \text{constant } A^{i} R^{\alpha}_{ij} A^{j} \qquad \text{(VI-11)}$$

where we use the repeated index convention. But $\mathcal{F}(\vec{A})$ depends linearly on $Q(\vec{A})$ (- see Eq. (VI-3)), so the additive constant $\sigma_{\alpha}(\pi)$ can be dropped in our evaluation of the average log likelihood function. Thus the LBL-SLAC "KREBS DECKS" did not have to be changed, and $Q(\vec{A})$ alone was used in the evaluation of $\mathcal{F}(\vec{A})$.

The translation from LBL-SLAC[He75b,He74] tabulated T-matrix elements to the τ -parameters in the fit is given by

$$\tau_n = T_n \sqrt{\frac{\frac{(2I+1)}{3}(2J+1)\,\frac{1}{2}\,\frac{4\pi}{p_\pi^2}\,0.389}{\sum R^\alpha_{ii} \int d\rho}} \qquad \text{(VI-12)}$$

(Recall that τ_n represents $A_{2n-1} + i\,A_{2n}$.) The cross section is then given by

$$Q_\alpha(\vec{A}) = \sigma_\alpha(\pi) + 0.389\,\frac{1}{2}\,\frac{\pi^2}{F}\,A^i\,R^\alpha_{ij}\,A^j \int d\rho$$

where the phase space integral $\int d\rho$ was calculated for each bin's central energy, and the event probabilities are

$$q_\alpha(\vec{\omega}_n,\vec{A}) = \sum_\mu \left| \sum_i c^i_{\alpha,\mu}(\vec{\omega}_n)\,A_i + b^i_{\alpha,\mu}(\vec{\omega}_n) \right|^2$$

where $c^i_{\alpha,\mu}$ is given in Eq. (II-11) and $b_{\alpha,\mu}$ is the π-exchange input.

The values of σ_α used in Eq. (VI-3) were obtained by taking points from a curve drawn through plots of tabulated values[Br72,Fl70,Ch73] for these cross sections. See Fig. 9 for the data and for these curves.

The general maximization procedure involves taking an estimate of the parameters, $\vec{A}(0)$, and finding a better estimate, $\vec{A}(1)$, by using the "stepping" algorithm

$$\vec{A}(1) \equiv \vec{A}(0) - \frac{1}{2}\,\overleftrightarrow{M}^{-1}\,\frac{d\mathcal{J}}{d\vec{A}} \qquad . \qquad \text{(VI-13)}$$

In the eigenvalue method[Fo68], $\overleftrightarrow{M}$ is diagonalized, and its eigenvalues are grouped according to size. Then the largest eigenvalues are used in Eq. (VI-13), and only the corresponding combinations of components of $\vec{A}$, i.e. the eigenvectors of $\overleftrightarrow{M}$, are improved by the stepping algorithm. Then the next largest eigenvalues are used to improve $\vec{A}$. The procedure

continues until all eigenvalues have been used. In terms of the structure of $\mathcal{F}(\vec{A})$ in parameter space, large eigenvalues of $\overleftrightarrow{M}$ correspond to regions of $\mathcal{F}$ with large curvature, i.e. with well determined minima, while small eigenvalues correspond to nearly flat structure, i.e. regions with poorly determined minima. So variation of small eigenvalues is not expected to increase the likelihood very much. This method is thus not sensitive to poorly determined parameters. In fact, poorly determined eigenvectors of $\overleftrightarrow{M}$ can be completely ignored (i.e. not improved). The eigenvalue method is formulated in the computer program FFFWNPF[Fo68]. This program includes many niceties which we need not discuss here.

We note that our code is an improvement of that of LBL-SLAC in that each iteration took around 1/3 the time of their iteration.

A fitting procedure was defined as complete when the change in $\mathcal{F}(\vec{A})$ was $\leqslant 10^{-6}$. The number of iterations needed to achieve this accuracy varied between 15 and 60.

D. The Penal function and our method

Previous analyses[He75b,Do76] have used "Penalty functions" to discriminate against solutions that violate partial wave unitarity. The prescription used is to add to $\mathcal{F}(A)$

$$\delta\mathcal{F} = -\frac{1}{N} \sum_{I,J,L} \alpha_{IJL} \left[\frac{\sigma^{IJL} - \sigma^{IJL}_{EPSA}}{\delta\sigma^{IJL}_{EPSA}} \right]^2 \theta(\sigma^{IJL} - \sigma^{IJL}_{EPSA}) \qquad \text{(VI-14)}$$

where σ^{IJL} are the values of the partial wave cross sections predicted

by the parameters, A_I, and σ^{IJL}_{EPSA} and $\delta\sigma^{IJL}_{EPSA}$ are the inelastic partial wave cross sections and their errors (from elastic phase shift analysis). N is equal to the total number of experimental events, as in Eq. (VI-3).

There are three problems with this approach:

1) It is arbitrary.

2) It is not smooth. (The term added to the log likelihood function has a discontinuous derivative.)

3) The α_{IJL} of LBL-SLAC[(He75b)] are not documented.

We did not use a Penalty function! We therefore followed the following procedure at each energy:

A) We refit the LBL-SLAC[(He75b,He74)] solution <u>without</u> the π-exchange high partial wave input and <u>without</u> the Penalty function. The resultant solution is called the "No Penal" solution.

B) We then refit the "No Penal" solution including our π-exchange input. The result is our "π-solution".

Thus our approach has been to <u>study the stability of the LBL-SLAC solution without the Penalty function and with the inclusion of a π -exchange high partial wave input</u>.

The "No Penal" fit was performed using the eigenvalue method, holding the smallest eigenvector of $\overleftrightarrow{M}$ fixed. (Since the π -exchange input was neglected, and therefore

$$\mathcal{F} \sim \sum \ell_n \left| \vec{c} \cdot \vec{A} \right|^2$$

there is an overall phase freedom, i.e.

$$\mathcal{F}(A_i) = \mathcal{F}(e^{i\lambda} A_i)$$

for any real phase, λ , which corresponds to a poorly determined eigenvector of $\overleftrightarrow{M}$ (Mi71). By holding this eigenvector fixed, senseless variation along this direction in $\vec{A}$ - space (along which $\mathcal{F}(\vec{A})$ doesn't vary) is avoided.)

As a test of our fitting procedure, we included a Penalty function and refit with no π-exchange input at W = 1.89 GeV. (We had available a set of the α_{IJL} in Eq. (VI-14) which LBL-SLAC used at this energy.) We found that our fitting procedure, i.e. holding the smallest eigenector fixed, did not change the LBL-SLAC solution from which we started in this test.

We note that by not varying the smallest eigenvalue to arrive at our "No Penal" solution, we guaranteed that this solution had the same overall phase as the LBL-SLAC solution(He75b).

In both the No Penal and the π -fits, we included the F35 and F37 (L-2I-2J) waves at 1.65 and 1.69 GeV. This is in contrast to Herndon et al.(He75b) who felt that these waves were small enough to ignore at these energies in determining the LBL-SLAC solution.

As a preview of our discussion of our results, we see in Fig. 10 the comparison of the inelastic partial wave cross sections predicted from each fit, compared to the constraints imposed by the various elastic phase shift analyses(Pa74,A172,Ay73) on these inelastic partial wave cross sections. We find that the Penalty function used in the LBL-SLAC analysis(He75b) diminished the unitarity violation of the D13 and D33 waves, forced the F15, S31 and F35 waves against the

unitarity bound, besides generally damping fluctuations of the P11 and P13 waves with energy.

The reasonable, though pessimistic, conclusion from this is that we should not rely on any result gotten from waves strongly affected by the penalty function. The least reliable systems are the D33 and F35 (above 1.8 GeV).

Note that the input values of the inelastic cross sections used by Herndon et al.[He75b] were not available except at W=1.89 GeV. We used our own values in our "No Penal" and "π" fits, as described in section VI.C. above, and as presented in Fig. 9. At W=1.89 GeV we had available the LBL-SLAC α_{IJL} Penal parameters of Eq. (VI-14), enabling us to check our fitting procedure against their results, as we have already discussed.

The histograms described in the next section comparing our solutions to the data were prepared using the same Monte Carlo tapes used in creating the "KREBS DECKS" (- see Eq. (VI-10)), except that the π -exchange input was added to these tapes in order to be able to include this effect in our histogram calculations.

VII. Results

A. Total cross sections

We first observe that both the "No Penal" and π -fits reproduce the input total inelastic cross sections for reactions (I-1a) quite well. The comparison is presented in Fig. 11. The LBL-SLAC fit[He75b] is also very close. Due to the fact that we did not use the same input cross sections as did they, it would have been very surprising had they agreed exactly with our values.

Our fits do make predictions for the reactions

$$\pi^- + p \longrightarrow n + \pi^o + \pi^o$$

$$\pi^+ + p \longrightarrow n + \pi^+ + \pi^+$$

which are not fit! The π-fit seems somewhat better at the higher energies for the $\pi^- + p \longrightarrow n + \pi^o + \pi^o$ reaction, though data are very sparse. As noted by Herndon et al.[He75b], the $\pi^+ + p \longrightarrow n + \pi^+ + \pi^+$ cross section is not accurately reproduced. They argue that Clebsch-Gordan coefficients enhance the contribution of N^*($I=\frac{1}{2}$) isobars in this channel. In particular, they argue that the primary missing waves are

$$\pi N^*(1520)_{D13} \quad \text{DP35}$$

$$\pi N^*(1688)_{F15} \quad \text{DS35}$$

$$\pi N^*(1470)_{P11} \quad \text{PP31}$$

where the subscript on the N^* indicates in which πN partial wave it resonates. (Using this notation, the $\pi\Delta$ would become $\pi\Delta(1236)_{P33}$.)

B. Partial wave cross sections

In Fig. 10 we present the partial wave cross sections, $\sigma^{L\ (2I)\ (2J)}$ resulting from the three fits (-LBL-SLAC, No Penal, and π -fit). The limits imposed by the CERN[A172] and Saclay[Ay73] elastic phase shift analyses are also presented.

I= 1/2:

The P11 cross section is poorly handled by the π-fit. The rapid oscillations with c.m. energy, W, should convince the reader that the smoothness found by Herndon et al.[He75b] is unstable under the inclusion of the π-exchange high partial wave input. Actually the resonance contribution to this wave contributes significantly to the $N\eta$, ΛK and ΣK final states[Pa76]. So saturation of partial wave unitarity should not have been expected.

The S11 cross section is smooth with energy, and reasonably well behaved until the two highest energy bins, where $N^*_{I=\frac{1}{2}}$ isobar production might well be coming into play.

The P13 cross section is severely suppressed in the π-fit. Even more so than in the P11 case, we believe this should dampen our enthusiasm for the LBL-SLAC[He75b] solution. The claim that Herndon et al.[He75b] have observed the P13(1700) should be reconsidered.

The D13 cross section violates unitarity even in the LBL-SLAC fit, with its Penal function for unitarity violation. The violation of unitarity by this wave should cast any results above 1.77 GeV into serious doubt.

The D15 cross section is expected[Pa76,Pa72] to saturate unitarity

near the $N^*(1670)$ resonance. The results of our fits give 70-80% saturation. The suppression at higher energies might be due to $N^*_{I=\frac{1}{2}}$ isobar production, for example in the $N^*(1520)$ DP15 or $N^*(1688)$ DS15 waves.

The F15 cross section saturates unitarity until $W \approx 1.75$ GeV, as might be expected by studying the decay channels of the $N^*(1688)$[Pa76,Pa72]. The LBL-SLAC[He75b] conclusion that unitarity is saturated throughout the energy range under consideration is presumably due to compensation by the fit for "Penal function" suppression of unitarity violation in other waves.

The F17 cross section was omitted in all fits.

I= 3/2:

The I=3/2 waves are much better behaved as a function of c.m. energy. There are three classes of behavior:

1. cross sections similar in all fits. This includes P31, S31, P33 and F37 waves.
2. cross sections severely suppressed by LBL-SLAC to diminish unitarity violations. The D33 cross section is the example of this behavior.
3. cross sections that are enhanced by the LBL-SLAC fit relative to the No Penal fit and π-fit to take up the slack in cross section left by class 2 above. The F35 waves fit in to this classification.

We now discuss the waves in more detail.

Herndon et al.[He75b] explain the suppression of the P31 by the omission of $N^*(1470)$ isobar contributions, for example in the $\pi N^*(1470)$ PP31 partial wave. One could similarly claim possible large contributions by $\pi N^*(1520 \text{ or } 1535)$ in a PS31 wave.

The F37 cross section saturates unitarity until approximately 1.89 GeV. Since this is very near to an energy at which this wave resonates, 1.93 GeV[Pa74,Pa76], this suggests a strong coupling of this resonance to another state whose production is just being allowed at this energy. The isobar state possibility with lowest final state orbital angular momentum, L_j (and hence the smallest barrier suppression factor $(Q_j)^{L_j}$,) is the $\pi N^*(1688)$ FP37 wave. (The ΣK cross section is known[Pa76] to contribute only about one percent. ΣK is the lowest mass two-body source for F37 cross section other than the πN, $\pi\Delta$, πN^* and ρN states.)

The P33 cross section also deviates from unitarity saturation at approximately 1.89 GeV. Again we note the possible relevance of $\pi N^*(1688)$ PP33, and we note the possible additional importance of $\pi N^*(1670)$ PS33.

The errors in the S31 elastic phase shift results are large enough that all three inelastic solutions could be consistent with unitarity saturation throughout. We should not expect to learn too much by studying the details of saturation of the unitarity bound for this wave.

The D33 cross section severely violates unitarity above 1.77 GeV. Near the D33(1720) effect[He75b], however, the fits are in accord. The agreement between the No Penal and π-fits at higher energies suggests that saturation of unitarity by the LBL-SLAC[He75b] solution is an artifact of the Penal function.

The F35 cross section has a behavior opposite to that of the D33 wave. The LBL-SLAC solution saturates unitarity throughout the energy

range. This presumably is due to the Penalty function, which attempts to share the unitarity violation of the D33 with other waves. The No Penal and π-fits have an F35 cross section far below the unitarity bound. It is perhaps better to claim ignorance of this cross section[Pa72] rather than to accept the LBL-SLAC[He75b] unitarity saturating results for the $\Delta(1890)_{F35}$ resonance[Pa76]. Note also that a naïve extrapolation of the F35 cross section implies that it should not have been ignored at 1.65 and 1.69 GeV. The extrapolated value of $\sigma_{F35} \sim 1$ mb. at 1.69 GeV is comparable to the S11, P13 and P31 contributions, though the associated T-matrix element is smaller due to the $\sqrt{2J+1}$ factor.

If we take seriously the non-saturation of unitarity in the F35 cross section above 1.8 GeV, then we might try to ascribe this missing cross section to the presence of $\pi N^*(1520)$ FS35 production. The lack of agreement between the fits clearly indicates a need for further study.

The D35 cross section was omitted in all fits. Herndon et al.[He75b] suggest that N^* isobar production might make up the entire cross section for this wave.

So our conclusions from studying the partial wave cross sections are that the waves fall into four classes:

(A) waves consistently determined by all three methods. These are the S11, D13 (W<1.75 GeV), D15, F15 (W<1.75 GeV), S31, P31, P33, F35 (W<1.8 GeV) and F37 waves.

(B) waves that are significantly affected by the Penal function used by Herndon et al. to enforce unitarity. These are the D13 (W>1.75 GeV),

F15 (W>1.8 GeV), D33 and F35 (W>1.8 GeV) waves.

(C) waves not to be trusted due to inconsistencies between the solutions. The P11 and P13 waves fall into this class.

(D) waves omitted from the fitting procedure because Herndon et al.[He75b] found them to be unimportant. All the D35 and F17 waves fall into this class.

Next we recall that in Longacre's K-matrix analysis[Lo73, Lo75] of the resonant content of the LBL-SLAC amplitudes[He75b], he used the F15(1688) and the D15(1670) resonances to fix the overall phase in the 1.65 GeV $\leq$ W $\leq$ 1.81 GeV region, and the F35(1890) and F37(1930) to fix the overall phase for 1.73 GeV $\leq$ W $\leq$ 1.97 GeV. We observe that the D15, F15 and F37 partial wave cross sections are not disturbed by the π -exchange input or by the Penal function. However both unitarity corrections and the π-input caused considerable change in the F35 partial wave cross sections for W > 1.75 GeV. There is room here for possible errors in the resultant analyses of resonance couplings[Lo75, Ca75] and of resonance classification[Fa73b] for the F35 wave.

Finally we note that our claims for possible $N^*(1688)$ production will be supported in our discussion of invariant mass distributions in the following section.

C. Single variable distributions

Next we study the single variable distributions. For each variable that we study, we present a set of four histograms: the data, and the ratio of each of the three fits to the data, normalized to an average of 1. The ideal fit would thus have these last three histograms (which we call LBLSLAC/Data, No Penal/Data and π/Data in the histograms) form horizontal lines with unit intercept. Errors presented in the histograms are statistical (though in the fit results these errors are overestimated due to correlations in the histogram normalization procedure).

The variables that we use are those in Eq. (I-8) which are suitable for studying the effect of a new input in a single isobar (in our case the π -exchange input in the ($\pi\pi$) isobar).

Invariant mass distributions: $d\sigma/dw_{\pi\pi}$

The $w_{\pi\pi}$ distributions are not well represented by any of the fits. Apparently when the "ρ" is being excited fully, it is well fit, but the rest of the $w_{\pi\pi}$ distribution is not. Sample distributions are presented in Fig. 12. We conclude from these distributions that the $w_{\pi\pi}$ dependence used in the parameterization of the T-matrix is wrong. Perhaps more elaborate angular momentum barriers (see Eq. (II-6)) would resolve this deficiency.

Invariant mass distributions: $d\sigma/dw_{N\pi}$

In Fig. 13 we present various invariant mass distributions at W=1.97 GeV. We see that there is strong evidence for a $w_{N\pi} \sim 1.7$ GeV enhancement in the data of $\pi^{\pm} + p \longrightarrow p + \pi^{\pm} + \pi^{o}$. These effects

correspond to slight dips in the goodness of fit at 1.7 GeV. The fits therefore compensate for this scattering enhancement through an increase in ρ and ε production. Perhaps the deterioration of the fit at the highest energies is a manifestation of this compensation mechanism.

The primary lesson is clear - there is significant $N^*(1688)$ or $N^*(1670)$ production at our highest energies. The assumption that the πN isobar of the $\pi\pi N$ final state is saturated by $\Delta(1236)$ is not valid at the higher energies. A study of the moments of the angular distributions of the $w_{N\pi}$=1.7 GeV data might be useful in identifying possible contributions to the P33 and F37 partial wave cross sections. (In fact the data for $\pi^+ + p \longrightarrow p + \pi^+ + \pi^o$ show strong scattering at $w_{N\pi} \approx 1.7$ GeV even at W = 1.89 GeV, i.e. in the $1.87 \leq W \leq 1.91$ GeV energy bin.)

c.m. angle distributions: $d\sigma/d\cos\Theta_\pi$

These angular distributions present a real success of the π-fit. In Fig. 14 we present these results[f2]. For $\pi^- + p \longrightarrow n + \pi^- + \pi^+$ and $\pi^+ + p \longrightarrow p + \pi^+ + \pi^o$ the LBL-SLAC and No Penal fits fail to adequately represent the distribution of the data at $\cos\Theta_\pi \sim -1$ for $W \gtrsim 1.8$ GeV, while the π-fits are a good representation of the data throughout the W range. For $\pi^- + p \longrightarrow p + \pi^- + \pi^o$, with its forward dip, this situation is not true. All fits fail to give a good representation of the $\cos\Theta_\pi$ behavior in this channel near $\cos\Theta_\pi = -1$. The explanation for this effect is not known.

Decay distributions in the isobar rest frame:

There are some minor improvements observed in other distributions.

For example, the π-fit is better than the No Penal fit in $dN/d\tilde{\phi}_{\pi^-}^{(\pi\pi)}$ in $\pi^- + p \text{ ---> } n + \pi^- + \pi^+$ at W = 1.89 GeV. However there is no improvement that is systematic (in its energy dependence).

Comments

Because of the rather poor representation of the invariant mass distributions by all fits, improvement of the $\cos\Theta_\pi$ distribution must be isolated. In particular, if we look at another distribution $d\sigma/dx$ where $x=x(w_{\pi\pi},w_{\pi N},\Theta_\pi)$, then the improvement we might expect to see due to the improvement in the $\cos\Theta_\pi$ representation by the π-fit might have been lost in the general degradation of the representation by the $w_{\pi\pi}$ and $w_{\pi N}$ dependence of the x-variable. Thus it was necessary to know the variable (- in this case $\cos\Theta_\pi$ -) to study in order to see improvement in the fit due to a specific input (- in this case the π-exchange high partial wave input). Until our representation of the invariant mass distributions improves we will have this problem, that we must know ab initio the best variable to study to see improvements due to a new input.

D. T-matrix elements

As indicated in section VII-C, only above 1.77 GeV do we observe any improvement in the angular distribution from the inclusion of the π-exchange input. Further tests were performed to find at what energies the π-exchange input with its precisely defined sign fixes the overall phase of the T-matrix. The procedure was to change the sign of the π-exchange term and re-fit. For $W \leq 1.77$ GeV (i.e. for our lowest four energy bins), the fit parameters move around the Argand plot, but do not precisely change sign. At W=1.81 GeV, the fit parameters change sign to compensate for the sign change of the π-exchange input. Thus we conclude that the phase determined by the π-exchange input is not reliable until 1.81 GeV. With this caveat in mind, we present the more interesting[f3] T-matrix elements of the LBL-SLAC solution[He75b,He74] with their overall phase determined by a complicated K-matrix analysis[Lo73,Lo75], and the π-solution with phases determined by the phase of the π-exchange input. These results are given in Fig. 15. We note the following features:

(1) D15 and F15 waves: Below 1.77 GeV (, 'D' in the figures), the π-fit differs from the LBL-SLAC fit. But at higher energies, the fits give similar results. This is a manifestation of the poor phase determination by the π-exchange input below 1.77 GeV. If any waves should have been well determined below 1.8 GeV, these resonant channels should have been. We caution that the phases at the higher energies in the LBL-SLAC have to be considered

less than completely reliable, due to their dependence on phases determined from the F35 waves, which we have seen (in section VII.B.) are controversial.

(2) P13 wave: The rather smooth variation above 1.8 GeV in the LBL-SLAC solution[He75b] has been replaced in the π-solution by a rapidly varying circle of small diameter for energies $\geq$ 1.81 GeV. Herndon et al.[He75b] interpret the LBL-SLAC solution as indicating a strongly coupled resonance at 1.7 GeV. Our π-solution could be consistent with an N^* resonance at somewhat above 1.8 GeV. However the magnitude of the coupling has been strongly attenuated relative to that of the LBL-SLAC results.

(3) F35 wave: It is very hard to see the very broad F35(1890) without doing serious resonance parameter analysis. We note that the rotation, and even suppression in magnitude, of the $\rho_3 N$ FP35 wave between the LBL-SLAC and π-solutions is another indication of the weaker nature of this coupling and of this wave being unstable under the inclusion of the π-exchange input.

(4) F37 wave: Between 1.81 and 1.93 GeV there is very good agreement between both fits. This indicates the possibility for reliable resonance parameter determination in this wave. The anomalous behavior of the 1.97 GeV point in the π-fit is not understood. It perhaps indicates the need for

   a. more low partial waves to be fit

   b. less of the π-exchange input.

The fact that the F37 waves are nearly all real in all fits near

resonance is also a puzzle. In the absence of background, one would expect the scattering matrix element to be imaginary at resonance. A nearly real T-matrix element indicates a strong background, which is not physically reasonable for a high partial wave relatively close to threshold. Perhaps the $\pi N^*(1688)$ FP37 effect suggested in section VII.B. is the important missing factor here.

(5) We observe that the energy dependence of the LBL-SLAC solution is much smoother than that of the π-solution. Herndon et al.(He75b) found many solutions at each energy above 1.65 GeV, and used energy continuity as a means of selecting between alternative solutions. The jaggedness of the π-solution indicates that this smoothness criterion is not stable under the inclusion of the π-exchange high partial wave input.

VIII. Conclusions

Our study of $\pi N \rightarrow N\pi\pi$ has led us to formulate the ideal analysis (unhampered by fiscal constraints). This analysis should

(a) include all $\pi\Delta$, ρN, εN low partial waves. Herndon et al.[He75b] removed many waves that they felt were unimportant. This closing off of allowed channels might be the cause of the unitarity violation that we have found. Suppressing allowed waves forces other waves to bulge beyond the unitarity bound. (Recall that of the 60 waves that met the initial fitting criteria, only 28 were kept in the final solution.)

(b) include the effects of various $\pi N^*_{I=\frac{1}{2}}$ isobar contributions. Such states are definitely present at the higher energies. Ignoring their contribution in the fitting process presumably causes aberrations in the $\pi N \rightarrow \rho N$ results at these energies.

(c) include proper barrier factors for the isobar production amplitude.

(d) include the π-exchange input for the high partial waves. This addition is the major contribution of our analysis.

(e) incorporate subenergy unitarity. (Unfortunately, the theoretical formulation of this correction is not yet complete.)

(f) include the effect of I=2 $\pi\pi$ scattering.

(g) include corrections due to electromagnetic mass differences (e.g. $m(\pi^+) \neq m(\pi^o)$) whenever these differences occur.

Only (a) and (b) require additional data. We estimate that a factor of 20 more data will allow the determination of most waves at twice the accuracy of our present determination of a subset of the waves.

One could then classify the waves as rapidly varying with energy (resonant) or slowly varying with energy (background) in each energy bin. By then binning the data in smaller energy bins, and fixing the background waves at their values from the large bin fitting, one can determine the variation of the resonant waves with energy between the smaller bins.

Since resonance parameters are the output of primary theoretical interest, perhaps performing an energy dependent analysis to resonant amplitude forms would be a successful approach, smoothing out the fluctuations in phase shifts with energy due to poor statistics at some energies.

Our analysis pursued only (d) above - the incorporation of π-exchange as a high partial wave input. We review our results.

By analysing the structure of the low partial waves of the π-exchange Born term contribution to $\pi N \rightarrow \rho N$, we have found a reasonable π-exchange input for the high partial waves of $\pi N \rightarrow N\pi\pi$. The effect of this input can be separated into three regions:

(1) Below 1.77 GeV, the angular distributions $d\sigma/d\cos\Theta_\pi$ need no improvement, and are not improved by including the π-exchange input. Below this energy, our π-exchange input does not fix the overall phase of the T-matrix.

(2) At 1.97 GeV there is a hint of peculiar behavior in the T-matrix elements in F37. Perhaps more of the π-exchange amplitude must be removed from the high partial wave input, and more of the higher angular momentum waves fit.

(3) Between 1.81 and 1.93 GeV, the π-input has significantly improved the $d\sigma/d\cos\Theta_\pi$ distribution. The overall phase is apparently well determined by the π-exchange input.

Furthermore, we observe the following features:

(1) The F35 contribution at 1.65 and 1.69 GeV should not be ignored (as it was by Herndon et al.[He75b]). Also the behavior of the F35 waves at the higher energies differs between the fits. Therefore use of these waves to fix the overall phase of the T-matrix at high energies[Lo73,Lo75] should be reexamined.

(2) The poor representation of the invariant mass distributions by all fits makes it necessary to know exactly where improvement in single particle distributions is expected due to a new input. An improvement in these mass distributions is imperative. Perhaps better barrier factors than Eqs. (II-8), or better incorporation of subenergy unitarity[Go77] will be the key to getting better mass distributions from future fits. These ideas are being incorporated in an analysis now in progress[Aa76] which will perform a new search for partial wave solutions.

(3) The Penal function unitarity 'fix' of the LBL-SLAC[He75b] fit severely modifies the D13, F15, D33 and F35 waves. This behavior must be better understood. The need for the Penal fix is very unsatisfying.

(4) Possible important contributions to the πN invariant mass distributions and to the saturation of partial wave unitarity may be the

isobar waves

πN^* (1470) PP31

πN^* (1520) PS31, DP15, FS35

πN^* (1535) PS31

πN^* (1670) PS33

πN^* (1688) PP33, DS15, FP37

The N^*(1670 or 1688) contributions are especially favored by the $w_{N\pi}$ distributions.

We conclude that some of the resonance information derived from the LBL-SLAC[He75b] analysis for $W \gtrsim 1.8$ GeV should be reconsidered. Furthermore, the use of couplings of the F35 resonance derived from the LBL-SLAC solution to provide evidence for further SU_6 representations[Fa73b] is premature.

References

Aa73 R. Aaron and R.D. Amado, Phys. Rev. Lett. 31 (1973)1157.

Aa76 R. Aaron et al., NUB #2306 (Northeastern University report, 1976).

Ai75 I.J.R. Aitchison and R.J.A. Golding, Phys. Letters 59B (1975) 288.

Ai77 I.J.R. Aitchison, Jour. Phys. G: Nucl. Physics 3 (1977) 121.

Al72 S. Almehed and C. Lovelace, Nucl. Phys. B40 (1972)157 and CERN-TH-1408 (-unpublished CERN tables).

Ay73 R. Ayed and P. Bareyre, paper presented at second International Conference on Elementary Particles, Aix-en-Provence, 1973 (unpublished), and 1973 Phase Shifts (unpublished Saclay tables).

Ba70 J.P.Baton et al., Phys. Letters 33B (1970) 528. Tables of this solution are in Refs. Ba72 and La 71.

Ba72 J.P. Baton et al., in Meson Resonances and Related Electromagnetic Phenomena, ed. R.H. Dalitz and A.Zichichi, (Editrice Compositori, Bologna, 1972).

Ba74 J.L. Basdevant, C.D. Froggart and J.L. Petersen, Nucl.Phys. B72 (1974)413.

Be65 S. Berman and M. Jacob, Phys. Rev. 139 (1965) B1023.

Bl52 J. Blatt and V.F. Weisskopf, Theoretical Nuclear Physics (Wiley, New York, 1952) especially page 361.

Br72 E. Bracci et al., CERN-HERA report 72-1, (CERN,1972).

Ca73 R. Cashmore, lecture in Baryon Resonances-73 (Purdue University Press, Indiana, 1973) ed. E.C. Fowler, p. 53, especially section C.

Ca75 R. Cashmore et al., Nucl. Phys. B92 (1975) 37.

Ch66 G.F. Chew, The Analytic S-Matrix (Benjamin, New York, 1966) especially sections 6.1-6.2.

Ch73 D.M. Chew et al., LBL-53 (Particle Data Group compilation, Lawrence Berkeley Laboratory, 1973).

Co73 D. Cohen et al., Phys. Rev. D7 (1973) 661. We thank Dr. Ferbel for sending us a table of these phase shifts.

Cz59 P. Cziffra et al., Phys. Rev. 144 (1959) 880.

Da69 R. H. Dalitz, in πN Scattering, ed. G. L. Shaw and D. Y. Wong (Wiley- Interscience, New York, 1969)p. 189.

De66 B. Deler and G. Valladas, Nuovo Cimento 45A (1966) 559.

Do67 R. Dolen, D. Horn, C. Schmid, Phys. Rev. Letters 19 (1967) 402 and Phys. Rev. 166 (1968) 1768.

Do76 J. Dolbeau et al., Nucl. Phys. B108 (1976) 365. This work will sometimes be called the Saclay analysis.

Du73 N. B. Durusoy et al., Phys. Letters 45B (1973) 517. We thank Dr. Durusoy for sending us a table of these phase shifts. We plot the DP-OPE fit with constrained inelasticity, η_S^2.

Eb71 G. Ebel et al., Nucl. Phys. B33 (1971) 317, sec. 6.3.

Ed66 R.J. Eden et al., The Analytic S-Matrix, (Cambridge University Press, Cambridge, 1966)pp. 188-194 and pp. 232ff.

Fa73 D. Faiman and J.L. Rosner, Phys. Letters 45B (1973) 357.

Fa73b D. Faiman, J.L. Rosner and J. Weyers, Nucl. Phys. B57 (1973) 45.

Fa74 D. Faiman, Nucl. Phys. B77 (1974) 443.

Fe62a B.T. Feld, CERN Yellow Report 62-14 (1962), Chapter 7 has a lucid exposition of the Watson final state interaction theorem.

Fe62b E. Ferrari and F. Selleri, Suppl. Nuovo Cimento 24 (1962) 452 gives a review of π-exchange in inelastic processes.

Fl70 E. Flaminio et al., CERN-HERA reports 70-5 and 70-7, (CERN, 1970).

Fo68 G.C. Fox, "Fee-Foe-Fum's Well Nigh Perfect Fit", computer program and Caltech report, unpublished (1968)

Fo71 G.C. Fox, π-exchange, talk at Argonne Workshop on Meson Spectroscopy (August, 1971) Caltech report CALT-68-335.

Fo72a G.C. Fox, private communication (1972).

Fo72b G.C. Fox, Lectures on Statistics, unpublished lecture notes, (1972) section D5.

Fo73 G.C. Fox, private communication (1973).

Ga66 S. Gasiorowicz, Elementary Particle Physics (Wiley, New York, 1966).

Ge56 M. Gell-Mann, Suppl. Nuovo Cimento, Series X, 4 (1956) 848.

Ge61 M. Gell-Mann, CTSL-20 (1961), (Caltech Report, 1961).

Ge64 M. Gell-Mann, Phys. Letters 8 (1964) 214.

Gi74 F.J. Gilman, M. Kugler, and S. Meshkov, Phys. Rev. D9 (1974) 715.

Go74 Y. Goradia, T. Lasinski, M. Tabak and G. Smadja, Unitarity and the Isobar Model (Lawrence Berkeley Laboratory report, unpublished, 1974)

Go75 Y. Goradia, LBL-3628 (Lawrence Berkeley Laboratory report, 1975)

Go77 Y. Goradia and T. Lasinski, Phys. Rev. D15 (1977) 220.

Gr73 M. L. Griss and G. C. Fox, Phys. Rev. D7 (1973) 74.

Gu64 F. Gürsey and L. Radicati, Phys. Rev. Letters 13 (1964) 173.

Gu73 G. Gustafson, Nucl. Phys. B63 (1973) 325.

Ha74 J.D. Hansen et al., Nucl. Phys. B81 (1974) 403.

He70 D. Herndon et al., UCRL-20030πN (Particle Data Group compilation, Lawrence Berkeley Laboratory, 1970).

He72 D.J. Herndon, thesis, LBL-544 (Lawrence Berkeley Laboratory report, 1972).

He74 D.J. Herndon et al., Supplement to SLAC-PUB-1108, Revised. (SLAC report, 1974, appendix to He75b).

He75a D. Herndon, P. Söding, R. Cashmore, Phys. Rev. D11 (1975) 3165. This work will sometimes be referred to as HSC.

He75b D. Herndon et al., Phys. Rev. D11 (1975) 3183. This work will sometimes be referred to as the LBL-SLAC analysis. See also He74 and Ro75.

Hi72 F.von Hippel and C. Quigg, Phys. Rev. D5 (1972) 624.

Ho74 W. Hoogland et al., Nucl. Phys. B69 (1974) 266, table 1. We present results of their methods A and B.

Hy73 B. Hyams et al., Nucl. Phys. B64 (1973) 134.

Ja59 M. Jacob and G.C. Wick, Ann. Phys. (N.Y.)7(1959) 404. This work will be called JW. The "particle 2" convention of these authors is used throughout.

Ja65 J.D. Jackson, Rev. Mod. Phys. 37 (1965) 484.

La71 G. Laurens, thesis, report #CEA-N-1497 (Saclay, 1971) table XI. We thank Drs. Baton and Laurens for sending us this report.

Li65 H. Lipkin and S. Meshkov, Phys. Rev. Letters 14 (1965) 670.

Li73 H. Lipkin, Phys. Reports 8C (1973) 173.

Lo73 R. Longacre, thesis, LBL-948 (Lawrence Berkeley Laboratory report, 1973).

Lo74 M.J. Losty et al., Nucl. Phys. B69 (1974) 185, table 5.

Lo75 R. Longacre et al, Phys. Letters 55B (1975) 415.

Ma59 M.H. MacGregor, M.J. Moravcsik and H.P. Stapp, Phys. Rev. 116 (1959) 1248.

Ma64 M.H. MacGregor, R.A. Arndt and A.A. Dubow, Phys. Rev. 155 (1964) B628.

Ma76 B.R. Martin, D. Morgan and G. Shaw, Pion-Pion Interactions in Particle Physics (Academic Press, New York, 1976).

Me74a H.J. Melosh, Phys. Rev. D9 (1974) 1095.

Me74b W.J. Metcalf and R.L. Walker, Nucl. Phys. B76 (1974) 253.

Mi71 L.R. Miller, thesis, LBL-38 (Lawrence Berkeley Laboratory report, 1971).

Mo70 D. Morgan and G. Shaw, Phys. Rev. D2 (1970) 520.

Na67 J.M. Namyslowski, M.S.K. Razmi, and R.G. Roberts, Phys. Rev. 157 (1967) 1328.

Ne61 Y. Ne'eman, Nucl. Physics 26 (1961) 222.

No76 D. Novoseller, Manual for TRIANGLE 2, CALT-68-572 (California Institute of Technology report, 1976).

Oc73 W. Ochs, thesis (Munich, 1973), energy independent solution, table 5. This solution is plotted in reference Hy73.

Ol65 D.I. Olive, Nuovo Cimento 37 (1965) 1422, section 2.3 and references therein.

Pa72 Particle Data Group, Phys. Letters B39 (1972)1. This com-

pilation is the last pre-LBL-SLAC analysis.

Pa74 Particle Data Group, Partial-Wave tape #11085 (Lawrence Berkeley Laboratory, 1974). See also ref. He70. The two solutions used are the CERN (see ref. A172) and Saclay 1973 (see ref. Ay73) solutions.

Pa76 Particle Data Group, Rev. Mod. Phys. 48(1976) 51.

Pe73 M.R. Pennington and S.D. Protopopescu, in π-π Scattering 1973, ed. P.K. Williams and V. Hagopian, AIP conference proceedings #13.

Pi73 H. Pilkuhn et al., Nucl. Phys. B65 (1973) 460, sec. 3.8.

Pr73 S. D. Protopopescu et al., Phys. Rev D7 (1973) 1279, table VI.

Pr74 J.R. Prukop et al., Phys. Rev D10 (1974) 2055, fig. 10b. We thank K. Novoseller for digitizing this graph. We plot only their $\beta\Delta^2$ parametrization.

Re70 C. Rebbi and R. Slansky, Rev. Mod. Phys. 42 (1970) 68.

Ro57 M.E. Rose, Elementary Theory of Angular Momentum, (Wiley, New York, 1957).

Ro74 J. Rosner, Phys. Reports 11C (1974) 189.

Ro75 A. H. Rosenfeld et al., Phys. Letters 55B (1975) 486.

Sa64 B. Sakita, Phys. Rev. 136 (1964) B1756.

So64 F.T. Solmitz, Ann. Rev. Nucl. Sci. 14 (1964) 375.

Wa54 K.M. Watson, Phys. Rev. 95 (1954) 228.

We66 S. Weinberg, Phys. Rev. Lett. 17 (1966) 616.

Wi62 G.C. Wick, Ann. Phys. (N.Y.) 18 (1962) 65.

Yu35 H. Yukawa, Proc. Phys. Math. Soc. Jap. 17 (1935) 48.

Zw64 G. Zweig, CERN Reports TH-401 and TH-412 (CERN, 1964).

Footnotes

(f1) See Appendix 1 for the $d\sigma/ d\cos\Theta_{\pi}$ and $d\sigma /dw_{\pi\pi}$ distributions at all energies.

(f2) See Appendix 2 for the $dN/d\cos\Theta_{\pi}$ fit results at all energies and for all channels.

(f3) See Appendix 3 for a complete set of Argand diagrams of T-matrix elements comparing the LBL-SLAC and π-fits. See Appendix 4 for tables of our π-fit amplitudes.

Figure Captions

Figure 1: Notation for the reaction $a+b \to j+k+\ell$ (figure as in Herndon et al.[He75b].

(a) Quantities in the center of mass frame.

(b) Quantities in the diparticle rest frame.

Figure 2: $\pi\pi$ phase shifts and inelasticities for the ρ-channel ($\ell_{\pi\pi}=I_{\pi\pi}=1$). The curves are the input form for our analysis and a similar Breit-Wigner parameterization for comparison. Experimental phase shifts are from Protopopescu[Pr73] and Ochs[Oc73]. Both parameterizations have $\eta_P^{I=1} = 1$.

Figure 3: $\pi\pi$ phase shifts and inelasticities for the ε-channel ($\ell_{\pi\pi}=I_{\pi\pi}=0$). Curves are the input forms for the π-exchange input and for the LBL-SLAC parameterization. Experimental phase shifts are from Protopopescu[Pr73] and Ochs[Oc73].

Figure 4: $\pi\pi$ phase shifts for the $\ell_{\pi\pi}=0$, $I_{\pi\pi}=2$ channel. The curve is the input form for the π-exchange input. Data are from Refs. Ba70, Ba72, La71, Co73, Du73, Ho74, Lo74, Pr74. Our parameterization has $\eta_S^{I=2} = 1$.

Figure 5: Low partial wave amplitudes in the L-S representation for the π-exchange input. Most of these waves were removed from the π-exchange input term. Notation for waves is described in section V. All waves with $J \leq 7/2$ and L, $L' \leq 4$ are presented. The

largest waves are in a), with smaller waves presented in an expanded scale in b) and c). Waves of sizes appropriate for two plots are presented in both plots.

Figure 6: $d\sigma/d\cos\Theta_\pi$ vs. $\cos\Theta_\pi$ for the π-exchange input at W=1.65 GeV and W=1.97 GeV. The calculation was for the contribution of the various isobars to the $\pi^- p \longrightarrow n \pi^- \pi^+$ channel. For this channel

$$\frac{d\sigma^{(\text{all isobars})}}{d\cos\Theta_\pi} = \frac{d\sigma^{(\rho)}}{d\cos\Theta_\pi} + \frac{d\sigma^{(I=0+2)}}{d\cos\Theta_\pi} \quad .$$

For the $\pi^\pm p \longrightarrow p \pi^\pm \pi^0$ channels,

$$\frac{d\sigma^{(\text{all isobars})}}{d\cos\Theta_\pi} = \frac{1}{2}\frac{d\sigma^{(\rho)}}{d\cos\Theta_\pi} + \frac{9}{2}\frac{d\sigma^{(I=2)}}{d\cos\Theta_\pi} \quad .$$

Figure 7: $d\sigma/dw_{\pi\pi}$ vs. $w_{\pi\pi}$ for the π-exchange input at W=1.65 GeV and W=1.97 GeV. See caption to Fig. 6 for specialization to specific charge channels.

Figure 8: σ for the π-exchange input. See caption to Fig. 6 for specialization to specific charge channels.

Figure 9: Experimental Data from "Data tables" (refs. Br72, Ch73, F&70) for the $\pi p \to N\pi\pi$ cross sections. The curves are representations of hand drawn curves through the data, from which the values of cross sections used in the fit were taken. These points are called "π-fit input". The data values called "Brody", "Williamson" and "Chavanon", are from the

same tables. These points, however, are from the groups whose events were used in our fit and so are specially indicated on our plots. Note that the channels $\pi^-p\to n\pi^0\pi^0$ and $\pi^+p\to n\pi^+\pi^+$ were not fit. These figures are included for use in the comparison made in Fig. 11.

Figure 10: The inelastic partial wave cross sections, σ^{LIJ} (actually $\sigma^{L\ (2I)\ (2J)}$) for the LBL-SLAC, No Penal and π-solutions. Also given are the upper bounds on σ^{LIJ} from the CERN (Aℓ72) and Saclay (Ay73) Elastic Phase Shift Analyses, as presented in Reference (Pa74).

Figure 11: Comparison of the predictions for $\sigma(\pi p\to N\pi\pi)$ by the three fits (-LBL-SLAC, No Penal and π-solutions) to the curves determined in Fig. 9.

Figure 12: A set of distributions $dN/dw_{\pi\pi}$ vs. $w_{\pi\pi}$ comparing the three fits to the data. A good fit would present a straight line in a plot of Fit/Data.

Figure 13: $dN/dw_{N\pi}$ vs. $w_{N\pi}$ at 1.97 GeV. These distributions tell us that there is additional structure at $w_{N\pi}$=1.7 GeV, perhaps due to production of an $N^*(1688)$ isobar.

Figure 14: $dN/d\cos\Theta_\pi$ vs. $\cos\Theta_\pi$ for W= 1.65, 1.81 and 1.97 GeV for $\pi^-p\to n\pi^-\pi^+$. A good fit would present a straight line in a plot of Fit/Data. The comparison of all three fits to the data is displayed. The contribution in the first bin ($-0.975\geqslant\cos\Theta_\pi\geqslant-1$) just for the π-exchange high partial wave input would be 7.4, 33.0 and 254.0 for the three energies.

Figure 15: Argand diagrams for the more interesting T-matrix parameters comparing the results of the LBL-SLAC[He75b] and π-fits. The letters A,B,C,D,E,F,G,H,I correspond to the c.m. energies W=1.65,1.69,1.73,1.77,1.81, 1.85,1.89,1.93 and 1.97 GeV. Note that the overall phase of the π-fit is not well determined below 1.8 GeV, i.e. for points A,B,C and D, though the relative phases of the different waves are determined by the fit at all energies.

Table 1: List of all Δ, ρ, ε low partial waves that satisfy $J \leq 7/2$, $L \leq 3$, $L_j \leq 3$. The waves that are boxed were used by LBL-SLAC[He75b] and by us in our fits. Waves indicated by "π" are those waves that π-exchange tells us might be important. For comparison, waves indicated by "*" are those that Saclay[Do76] felt should be included for $W \leq 1.73$ GeV. (Notation is $[L\ L_j\ (2I)\ (2J)]_{S_j}$ and S_j is included only if omission could cause confusion, i.e., for the ρ-isobar.)

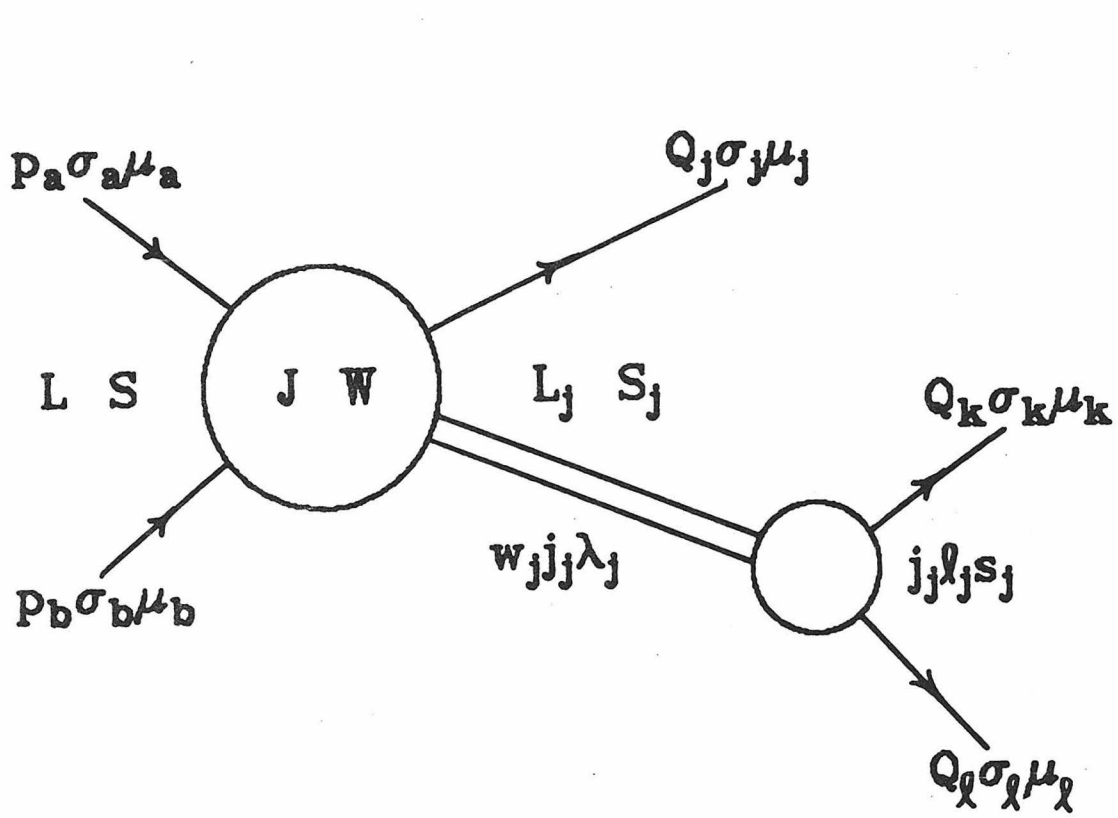
Isobar	J=1/2	J=3/2	J=5/2	J=7/2
Δ	* **SD11**	* PP13	* **DD15**	* FF17
	* **SD31**	* **PP33**	* DD35	* **FF37**
	* **PP11**	PF13	* **FP15**	
	* **PP31**	* PF33	* FP35	
		* **DS13**	* **FF15**	
		* **DS33**	* **FF35**	
		* **DD13**		
		* **DD33**		
ρ	* $(SD11)_{3/2}$	* $(PP13)_{3/2}$	π* $(DD15)_{3/2}$	$(FF17)_{3/2}$
	* $(SD31)_{3/2}$	* $(PP33)_{3/2}$	* $(DD35)_{3/2}$	**$(FF37)_{3/2}$**
	* $(PP11)_{3/2}$	$(PF13)_{3/2}$	π* **$(FP15)_{3/2}$**	
	* $(PP31)_{3/2}$	$(PF33)_{3/2}$	π **$(FP35)_{3/2}$**	
		* **$(DS13)_{3/2}$**	* $(FF15)_{3/2}$	
		* **$(DS33)_{3/2}$**	$(FF35)_{3/2}$	
		π $(DD13)_{3/2}$		
		$(DD33)_{3/2}$		
	* **$(SS11)_{1/2}$**	* **$(PP13)_{1/2}$**	$(DD15)_{1/2}$	$(FF17)_{1/2}$
	* **$(SS31)_{1/2}$**	* $(PP33)_{1/2}$	$(DD35)_{1/2}$	$(FF37)_{1/2}$
	* **$(PP11)_{1/2}$**	π $(DD13)_{1/2}$	$(FF15)_{1/2}$	
	$(PP31)_{1/2}$	$(DD33)_{1/2}$	* $(FF35)_{1/2}$	

Table 1 (continued)

Isobar	J=1/2	J=3/2	J=5/2
ε	* [SP11]	* PD13	* DF15
	* [PS11]	* [DP13]	* [FD15]

Table 2: The π-exchange low partial waves for $\pi N \to \pi NN$ through a ρ-isobar that satisfy $|T| \gtrsim .1$. Waves are listed in decreasing size at W = 2.0 GeV and in different columns for different values of J. Waves considered important are boxed. The "class" notation of Section V is also presented.

J=1/2	J=3/2	J=5/2	J=7/2
ρ_1 SS11 (α)			
ρ_3 PP11 (δ)			
	ρ_3 DS13 (ϕ)		
ρ_1 SS31 (α)			
	ρ_3 DS33 (ϕ)		
ρ_3 PP31 (δ)			
	ρ_3 PP13 (γ)		
		$\boxed{\rho_3 \text{ FP15 } (\phi)}$	
ρ_3 SD11 (ε)			
	ρ_3 PP33 (γ)		
			$\boxed{\rho_3 \text{ GD17 } (\phi)}$
		$\boxed{\rho_3 \text{ FP35 } (\phi)}$	
ρ_3 SD31 (ε)			
		$\boxed{\rho_3 \text{ DD15 } (\gamma)}$	
	$\boxed{\rho_3 \text{ DD13 } (\delta)}$		
ρ_1 PP11 (β)			
	$\boxed{\rho_1 \text{ DD13 } (\beta)}$		


$p_a\sigma_a\mu_a$
$Q_j\sigma_j\mu_j$
L S
J W
L_j S_j
$Q_k\sigma_k\mu_k$
$w_j j_j \lambda_j$
$j_j \ell_j s_j$
$p_b\sigma_b\mu_b$
$Q_\ell\sigma_\ell\mu_\ell$
(a)

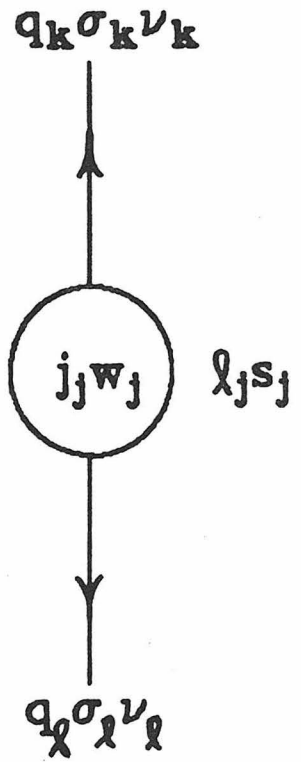

$q_k\sigma_k\nu_k$
$j_j w_j$
$\ell_j s_j$
$q_\ell\sigma_\ell\nu_\ell$
(b)

Fig. 1

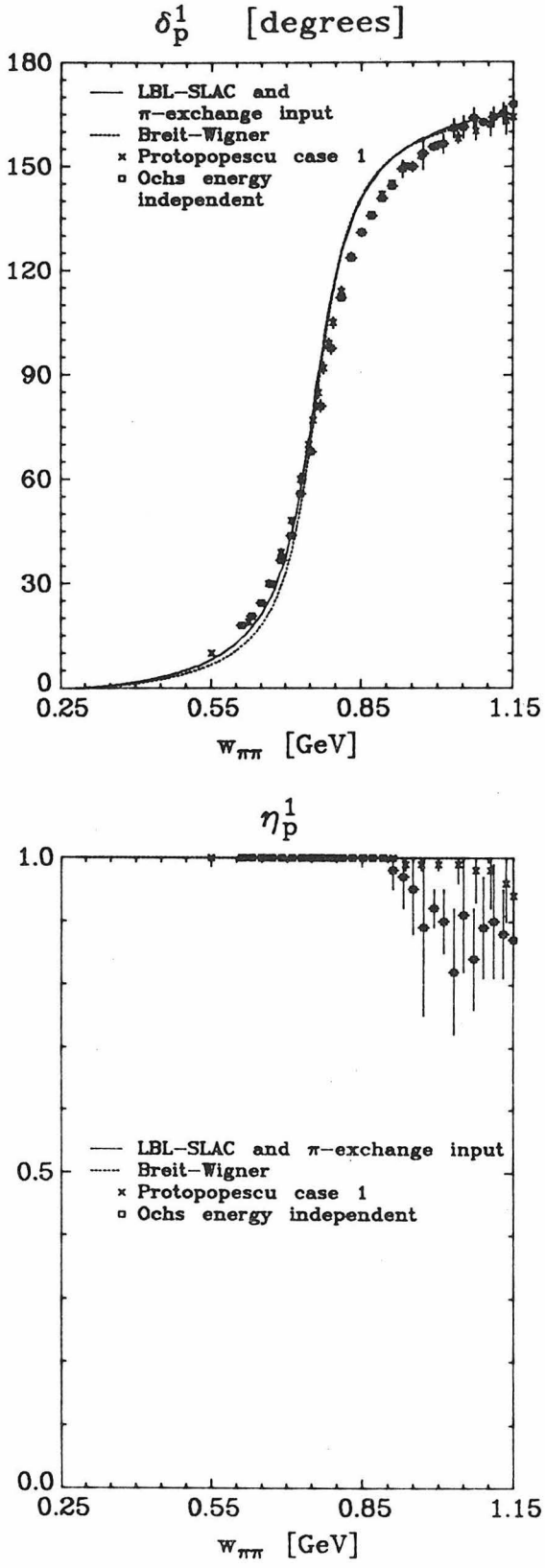
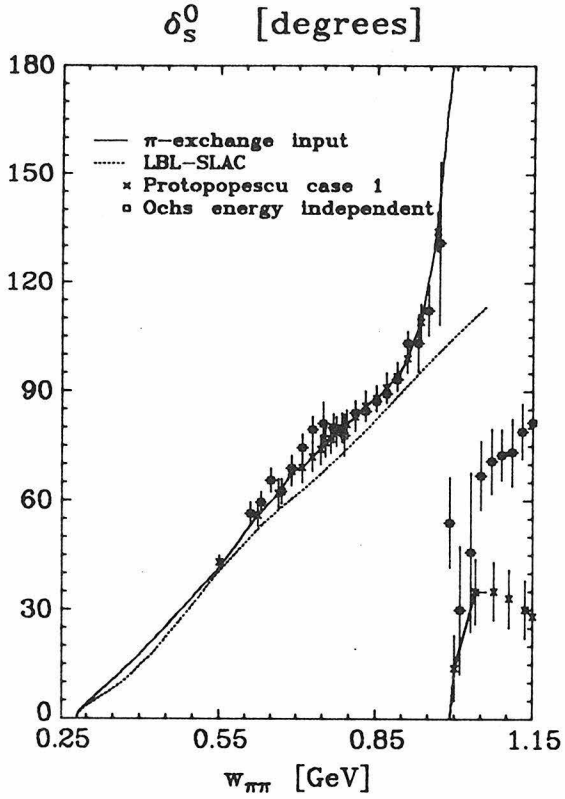

δ_p^1 [degrees]
180
150
120
90
60
30
0
LBL–SLAC and
π–exchange input
Breit–Wigner
Protopopescu case 1
Ochs energy
independent
0.25
0.55
0.85
1.15
$w_{\pi\pi}$ [GeV]
η_p^1
1.0
0.5
0.0
LBL–SLAC and π–exchange input
Breit–Wigner
Protopopescu case 1
Ochs energy independent
0.25
0.55
0.85
1.15
$w_{\pi\pi}$ [GeV]

Fig. 2


δ_s^0 [degrees]
180
150
120
90
60
30
0
0.25
0.55
0.85
1.15
$w_{\pi\pi}$ [GeV]
π−exchange input
LBL−SLAC
Protopopescu case 1
Ochs energy independent

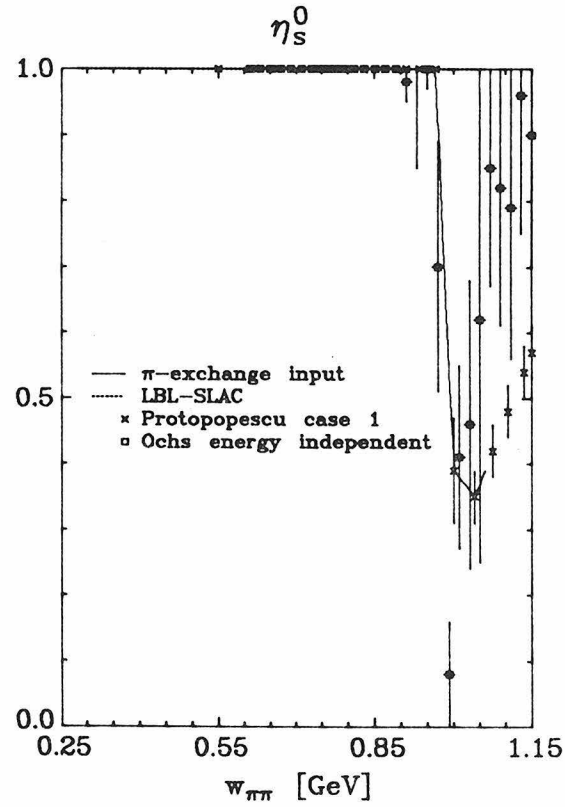

η_s^0
1.0
0.5
0.0
0.25
0.55
0.85
1.15
$w_{\pi\pi}$ [GeV]
π−exchange input
LBL−SLAC
Protopopescu case 1
Ochs energy independent

Fig. 3

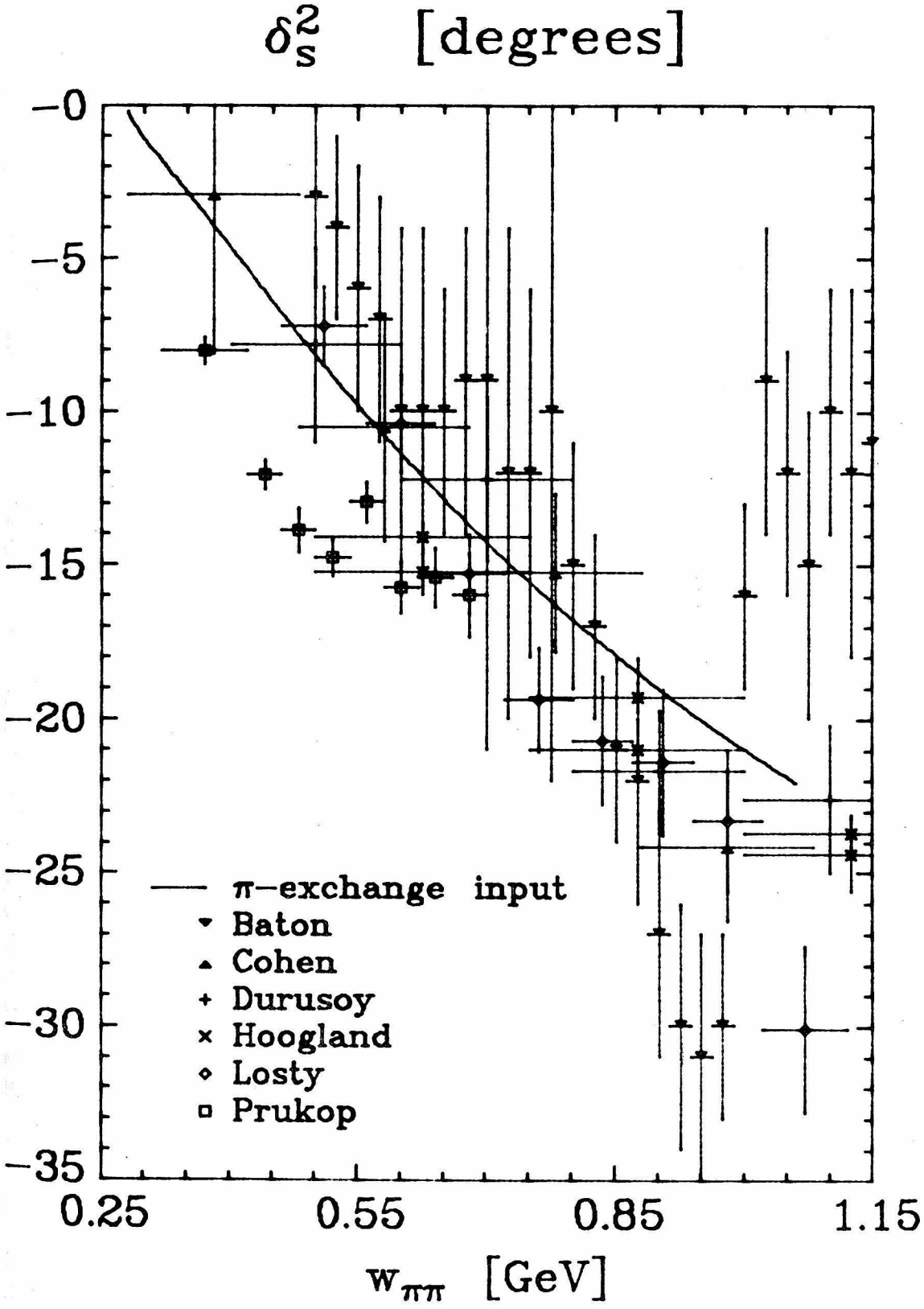

δ_s^2 [degrees]
-0
-5
-10
-15
-20
-25
-30
-35
0.25
0.55
0.85
1.15
$W_{\pi\pi}$ [GeV]
π-exchange input
Baton
Cohen
Durusoy
Hoogland
Losty
Prukop

Fig. 4

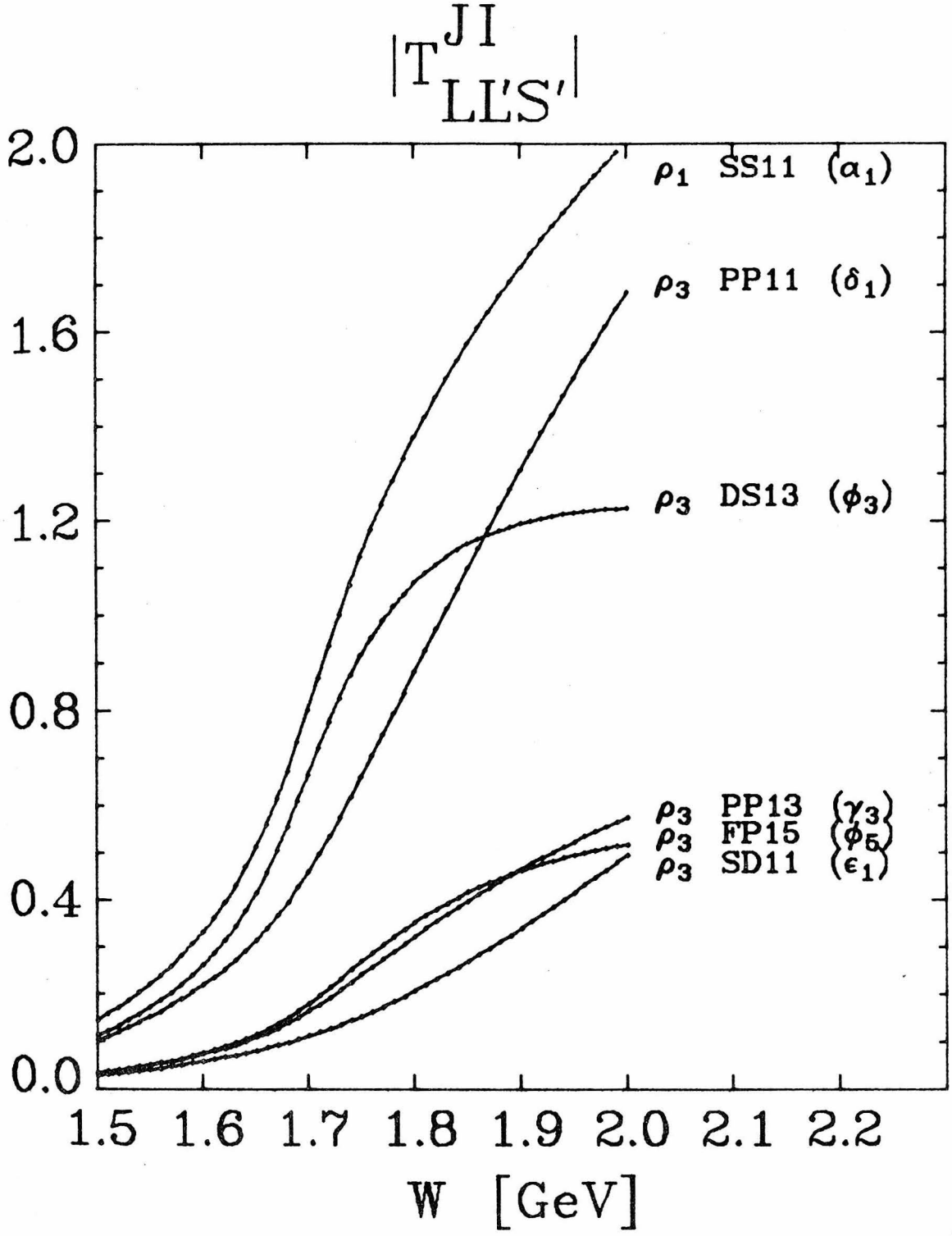

$|T^{JI}_{LL'S'}|$
2.0
1.6
1.2
0.8
0.4
0.0
1.5 1.6 1.7 1.8 1.9 2.0 2.1 2.2
W [GeV]
ρ_1 SS11 (α_1)
ρ_3 PP11 (δ_1)
ρ_3 DS13 (ϕ_3)
ρ_3 PP13 (γ_3)
ρ_3 FP15 (ϕ_5)
ρ_3 SD11 (ϵ_1)

Fig. 5a

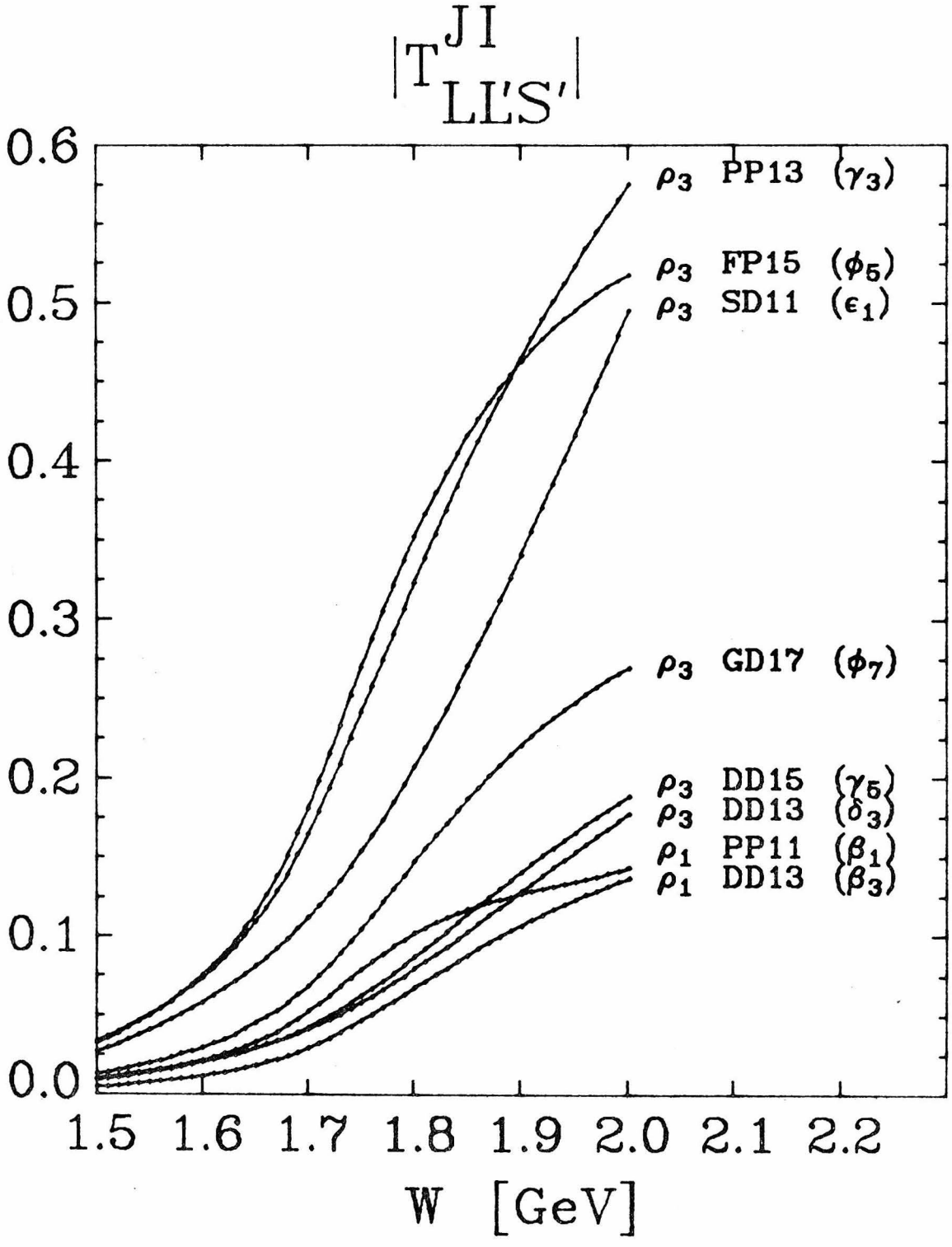

$|T^{JI}_{LL'S'}|$
0.6
0.5
0.4
0.3
0.2
0.1
0.0
1.5 1.6 1.7 1.8 1.9 2.0 2.1 2.2
W [GeV]
ρ_3 PP13 (γ_3)
ρ_3 FP15 (ϕ_5)
ρ_3 SD11 (ϵ_1)
ρ_3 GD17 (ϕ_7)
ρ_3 DD15 (γ_5)
ρ_3 DD13 (δ_3)
ρ_1 PP11 (β_1)
ρ_1 DD13 (β_3)

Fig. 5b

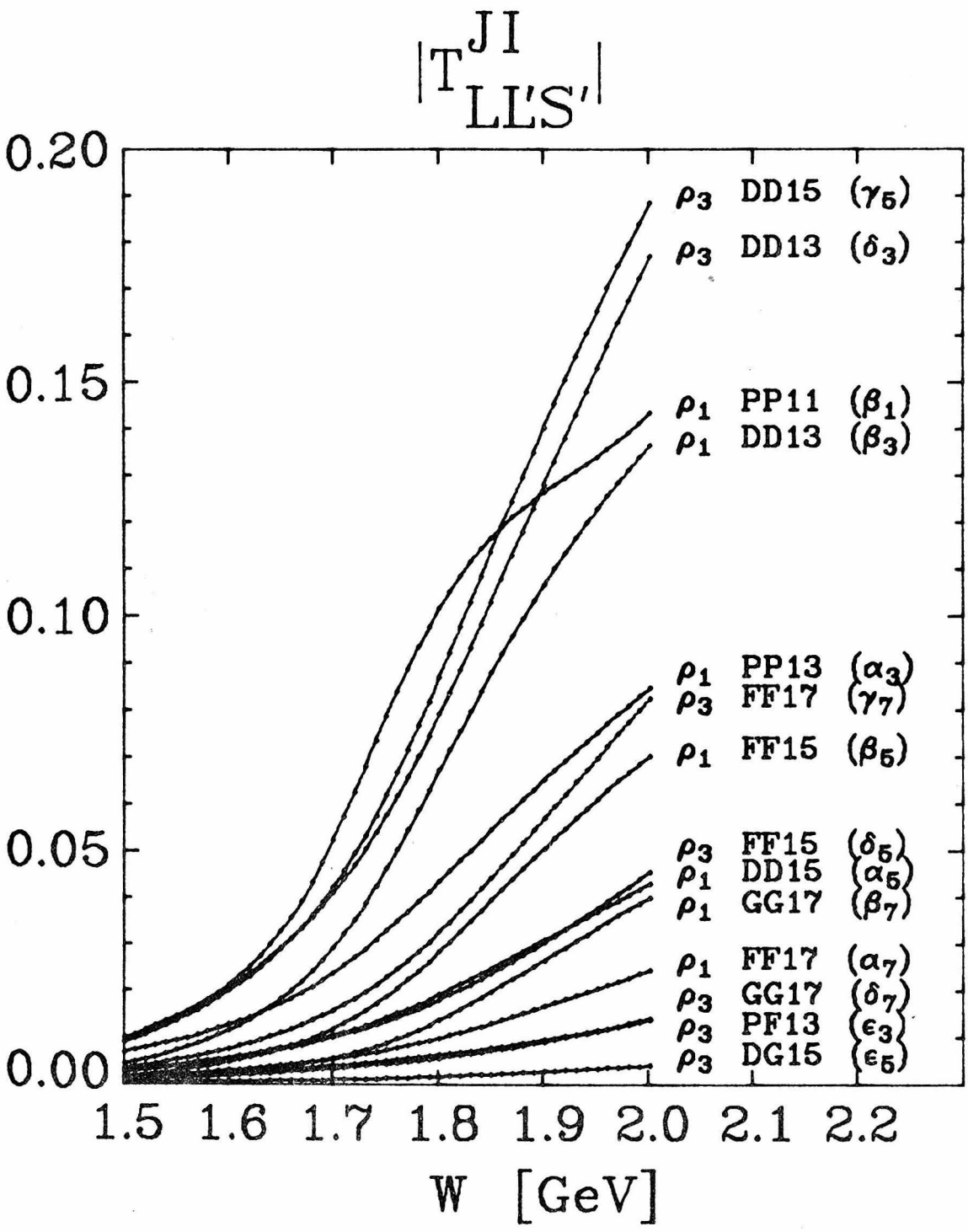

$|T^{JI}_{LL'S'}|$
0.20
0.15
0.10
0.05
0.00
1.5 1.6 1.7 1.8 1.9 2.0 2.1 2.2
W [GeV]
ρ_3 DD15 (γ_5)
ρ_3 DD13 (δ_3)
ρ_1 PP11 (β_1)
ρ_1 DD13 (β_3)
ρ_1 PP13 (α_3)
ρ_3 FF17 (γ_7)
ρ_1 FF15 (β_5)
ρ_3 FF15 (δ_5)
ρ_1 DD15 (α_5)
ρ_1 GG17 (β_7)
ρ_1 FF17 (α_7)
ρ_3 GG17 (δ_7)
ρ_3 PF13 (ϵ_3)
ρ_3 DG15 (ϵ_5)

Fig. 5c

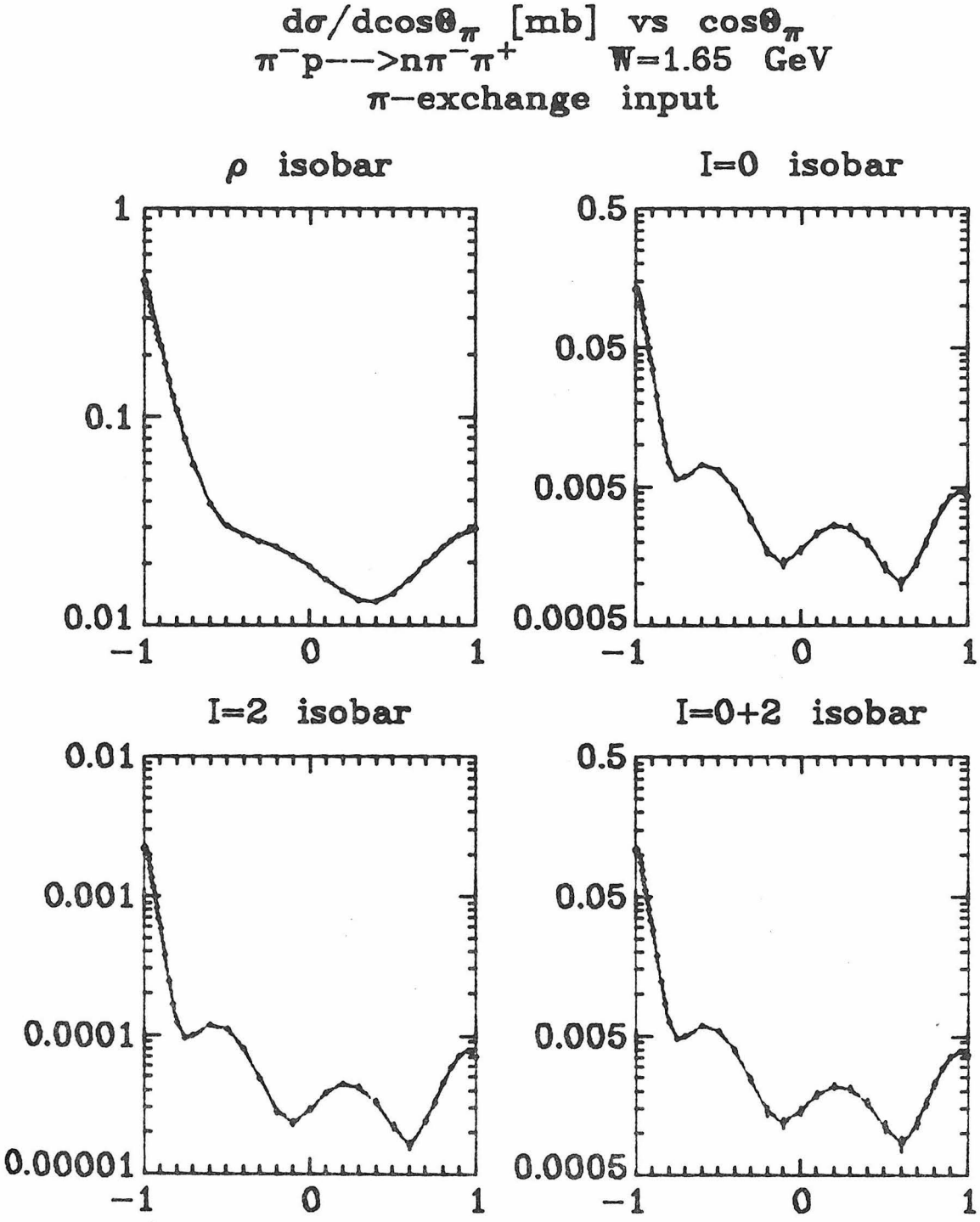

dσ/dcosθ_π [mb] vs cosθ_π
π⁻p--->nπ⁻π⁺ W=1.65 GeV
π-exchange input
ρ isobar
I=0 isobar
I=2 isobar
I=0+2 isobar
1
0.1
0.01
0.5
0.05
0.005
0.0005
0.001
0.0001
0.00001
-1
0
1

Fig. 6a

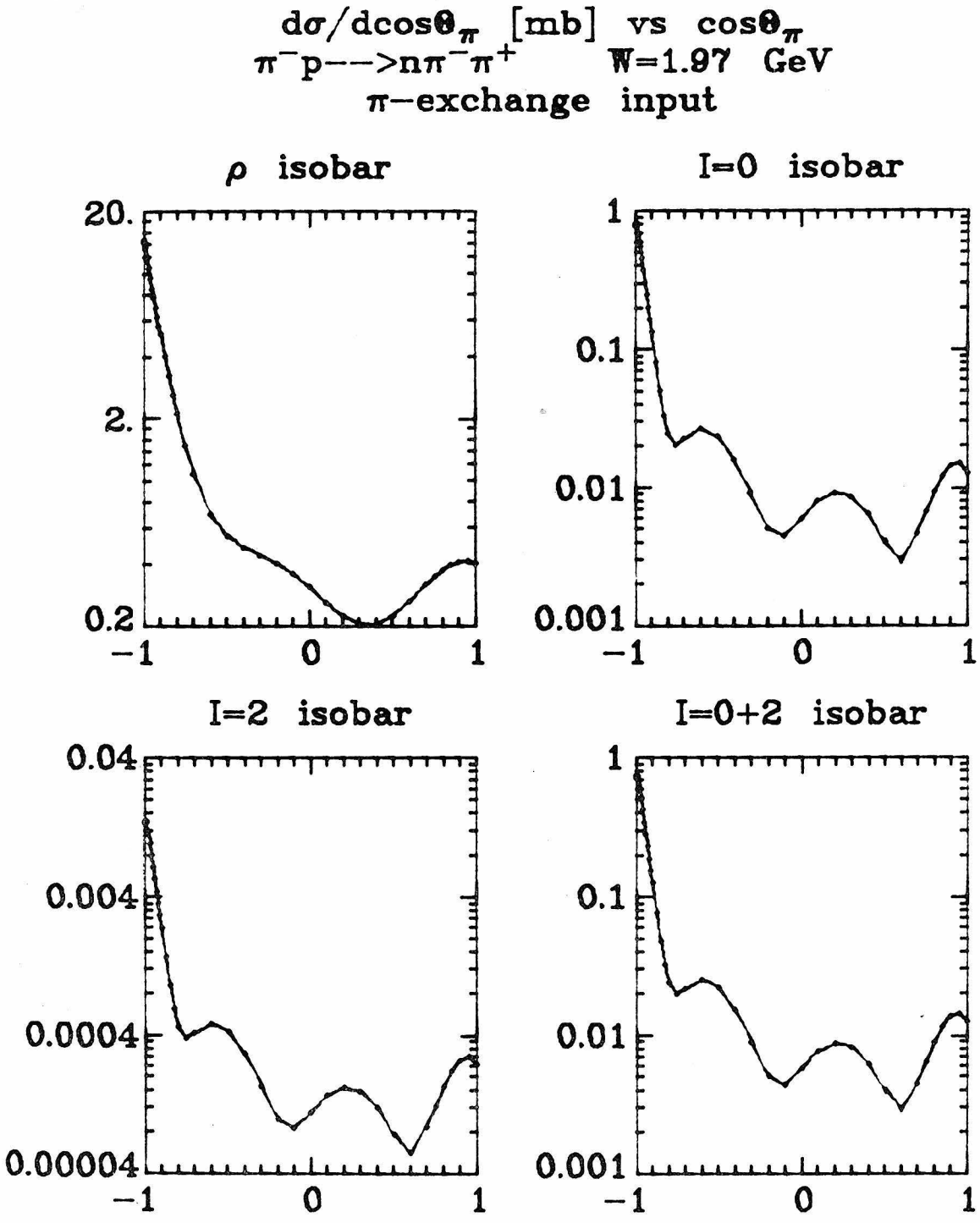

dσ/dcosθ_π [mb] vs cosθ_π
π⁻p-->nπ⁻π⁺ W=1.97 GeV
π-exchange input
ρ isobar
I=0 isobar
I=2 isobar
I=0+2 isobar
20.
2.
0.2
1
0.1
0.01
0.001
0.04
0.004
0.0004
0.00004
-1
0
1

Fig. 6b

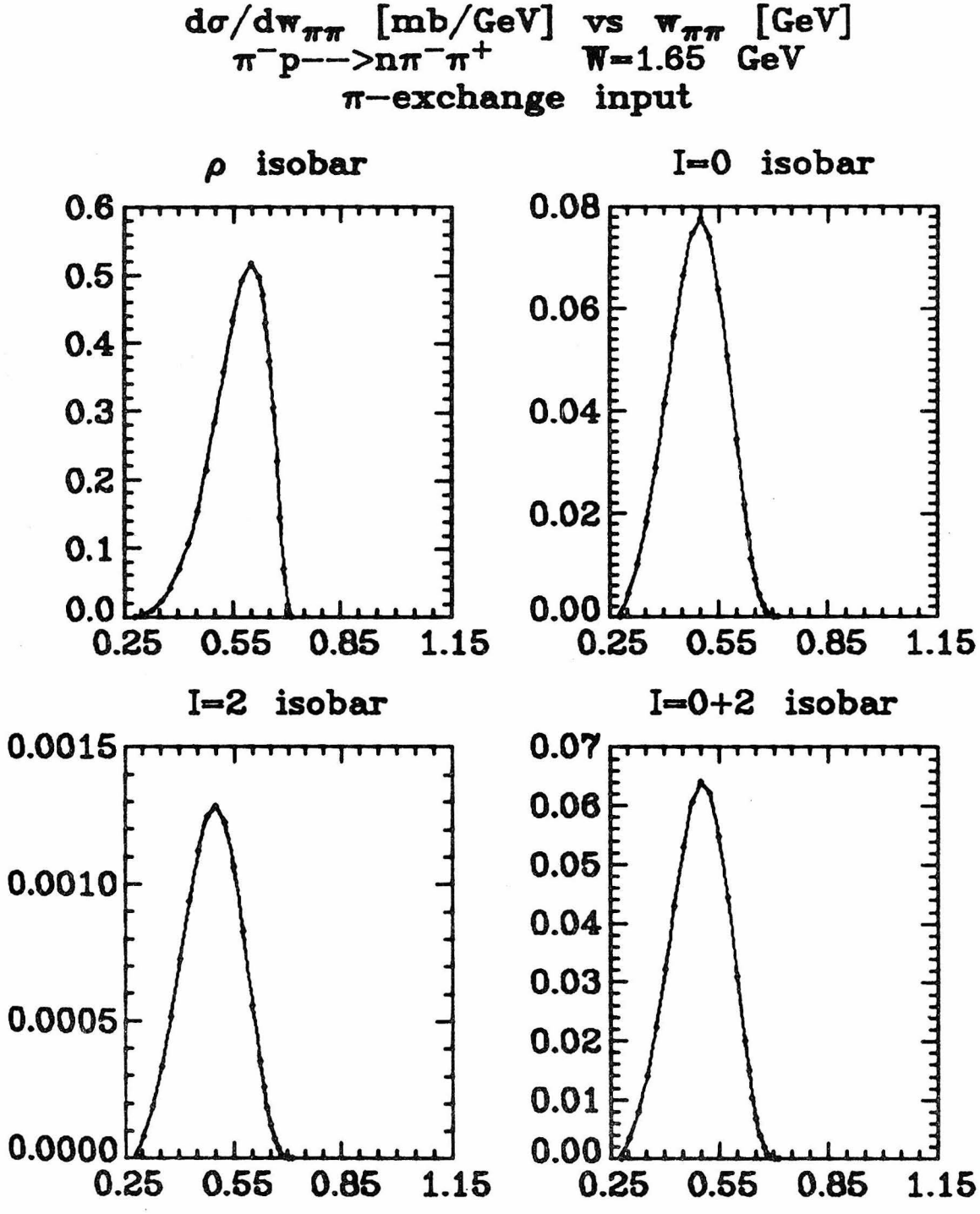

dσ/dw_ππ [mb/GeV] vs w_ππ [GeV]
π⁻p−−>nπ⁻π⁺ W=1.65 GeV
π−exchange input
ρ isobar
I=0 isobar
I=2 isobar
I=0+2 isobar
0.6
0.5
0.4
0.3
0.2
0.1
0.0
0.08
0.06
0.04
0.02
0.00
0.0015
0.0010
0.0005
0.0000
0.07
0.06
0.05
0.04
0.03
0.02
0.01
0.00
0.25 0.55 0.85 1.15

Fig. 7a

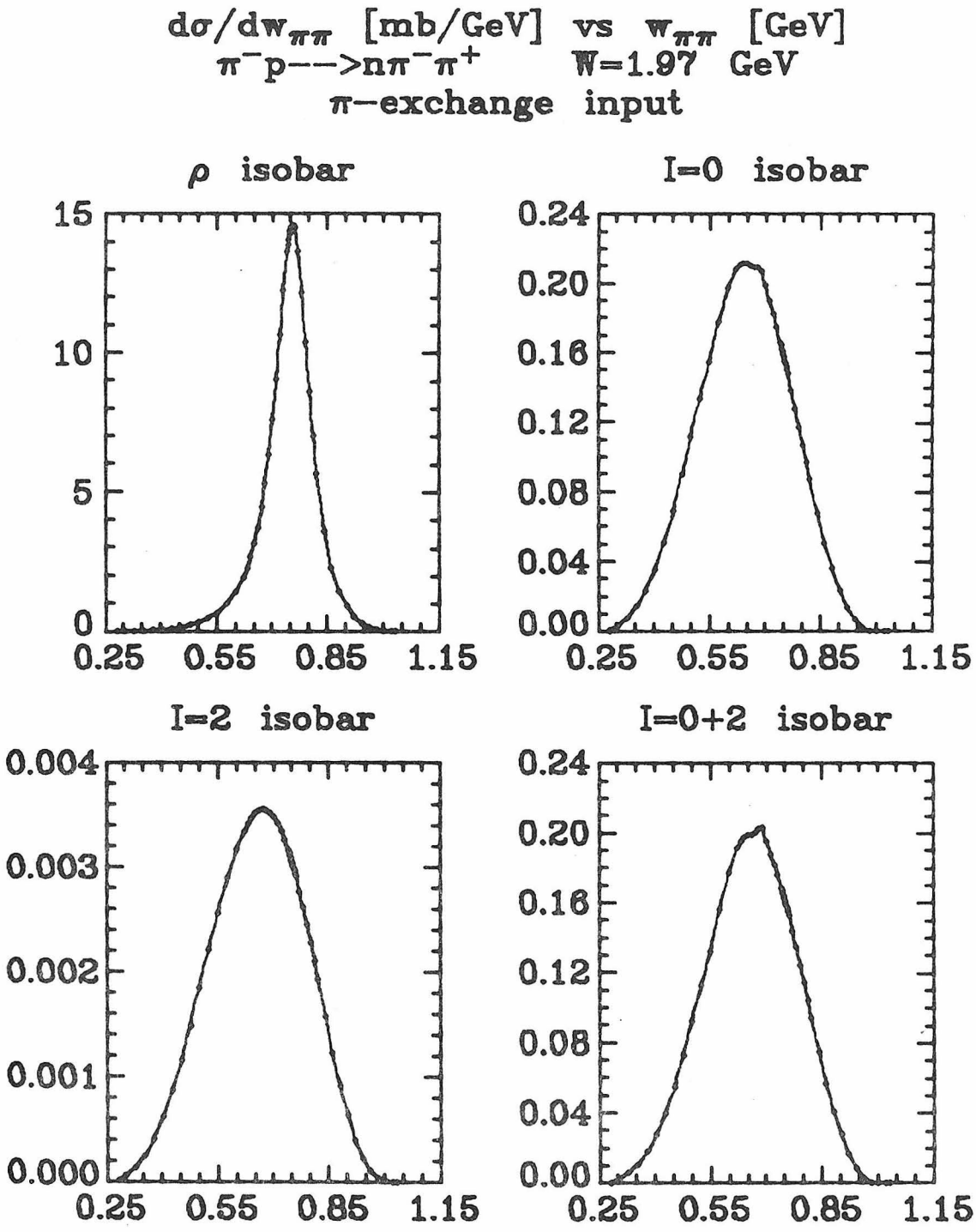

dσ/dw_ππ [mb/GeV] vs w_ππ [GeV]
π⁻p--->nπ⁻π⁺ W=1.97 GeV
π-exchange input
ρ isobar
I=0 isobar
I=2 isobar
I=0+2 isobar
15
10
5
0
0.24
0.20
0.16
0.12
0.08
0.04
0.00
0.004
0.003
0.002
0.001
0.000
0.25
0.55
0.85
1.15

Fig. 7b

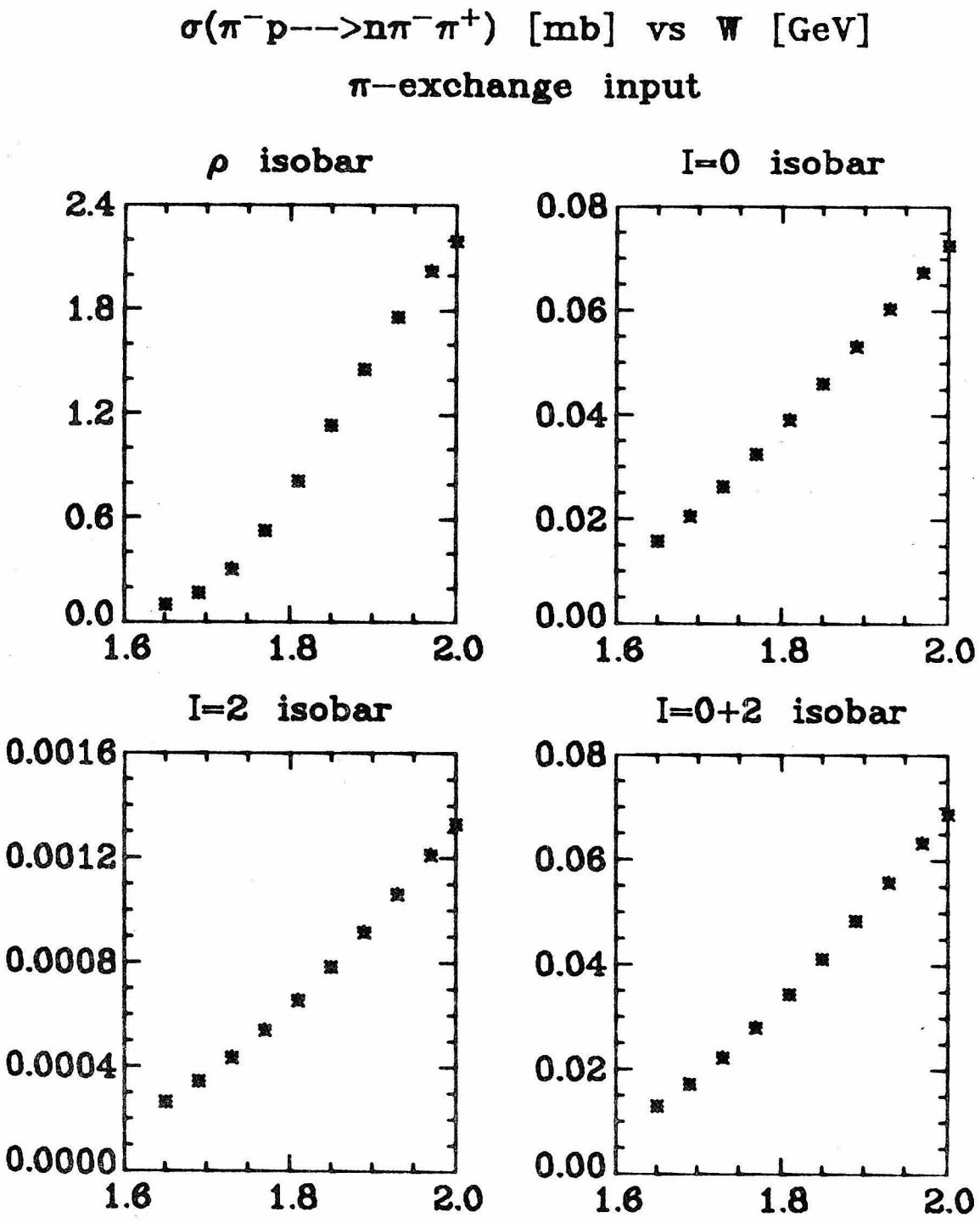

σ(π⁻p--->nπ⁻π⁺) [mb] vs W [GeV]
π-exchange input
ρ isobar
I=0 isobar
I=2 isobar
I=0+2 isobar
2.4
1.8
1.2
0.6
0.0
0.08
0.06
0.04
0.02
0.00
0.0016
0.0012
0.0008
0.0004
0.0000
1.6
1.8
2.0

Fig. 8

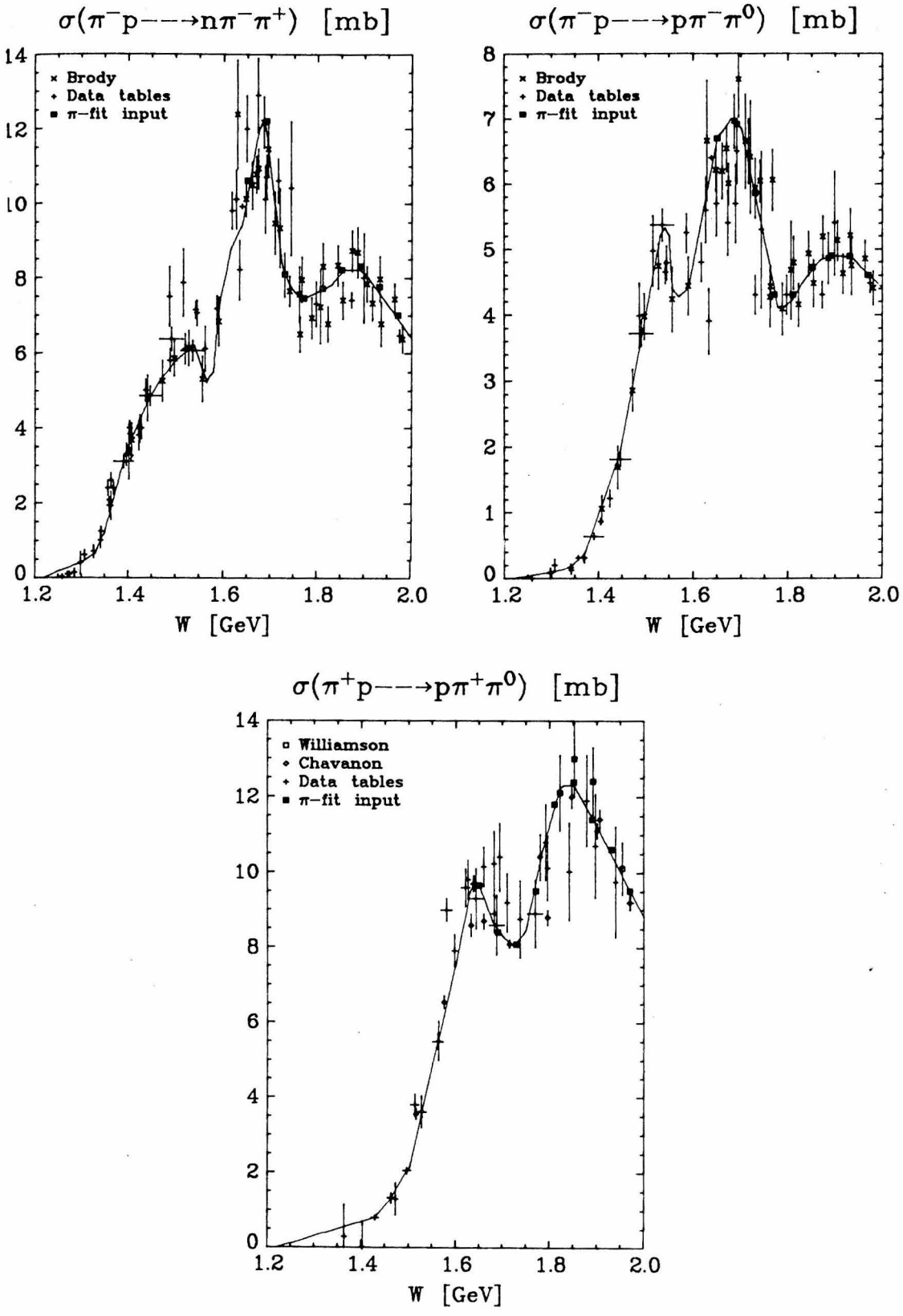

σ(π⁻p→nπ⁻π⁺) [mb]
× Brody
+ Data tables
■ π–fit input
W [GeV]
σ(π⁻p→pπ⁻π⁰) [mb]
× Brody
+ Data tables
■ π–fit input
W [GeV]
σ(π⁺p→pπ⁺π⁰) [mb]
□ Williamson
◇ Chavanon
+ Data tables
■ π–fit input
W [GeV]

Fig. 9a

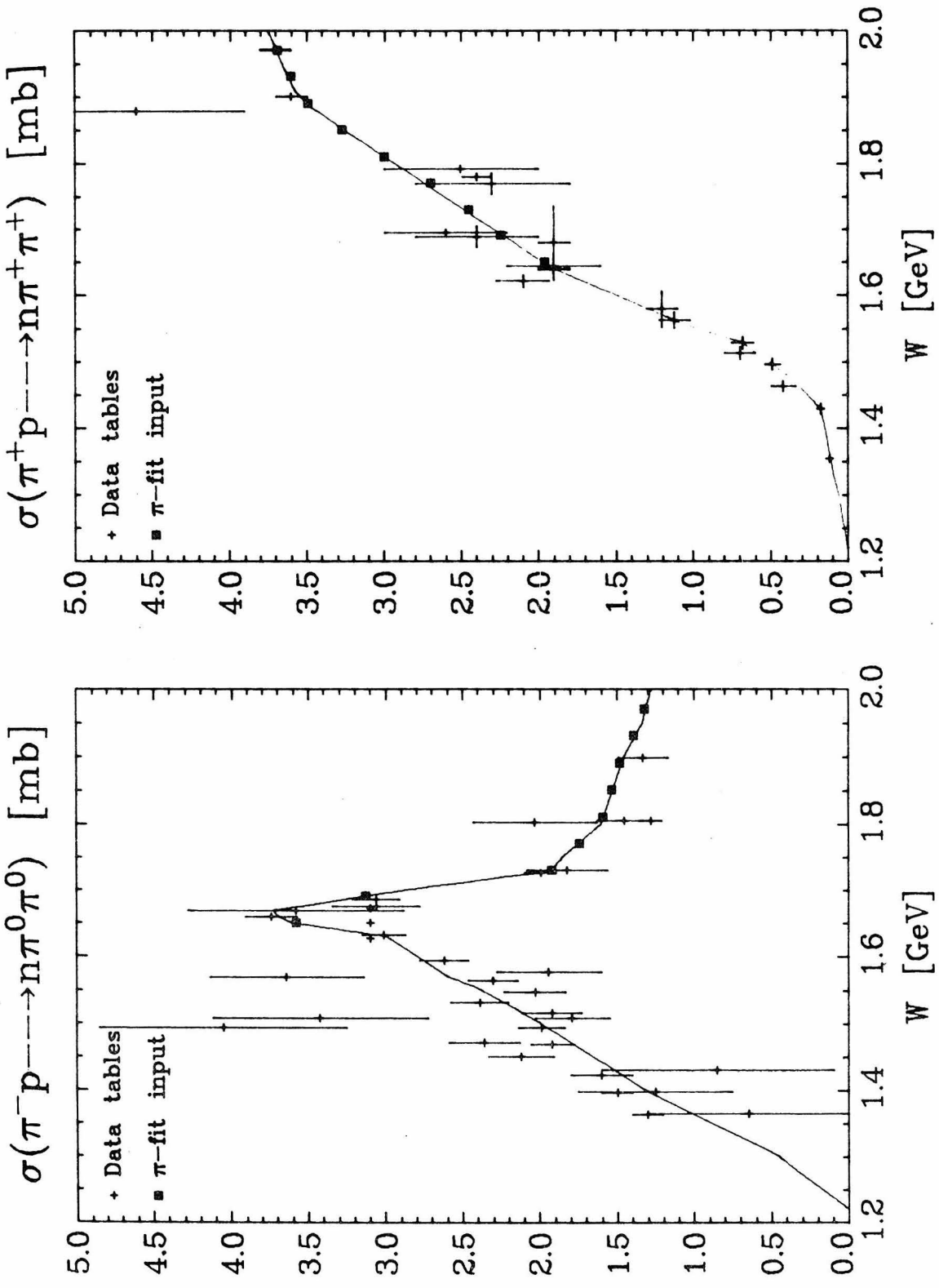

$\sigma(\pi^- p \to n\pi^0\pi^0)$ [mb]
+ Data tables
■ π-fit input
W [GeV]
$\sigma(\pi^+ p \to n\pi^+\pi^+)$ [mb]
+ Data tables
■ π-fit input
W [GeV]

Fig. 9b

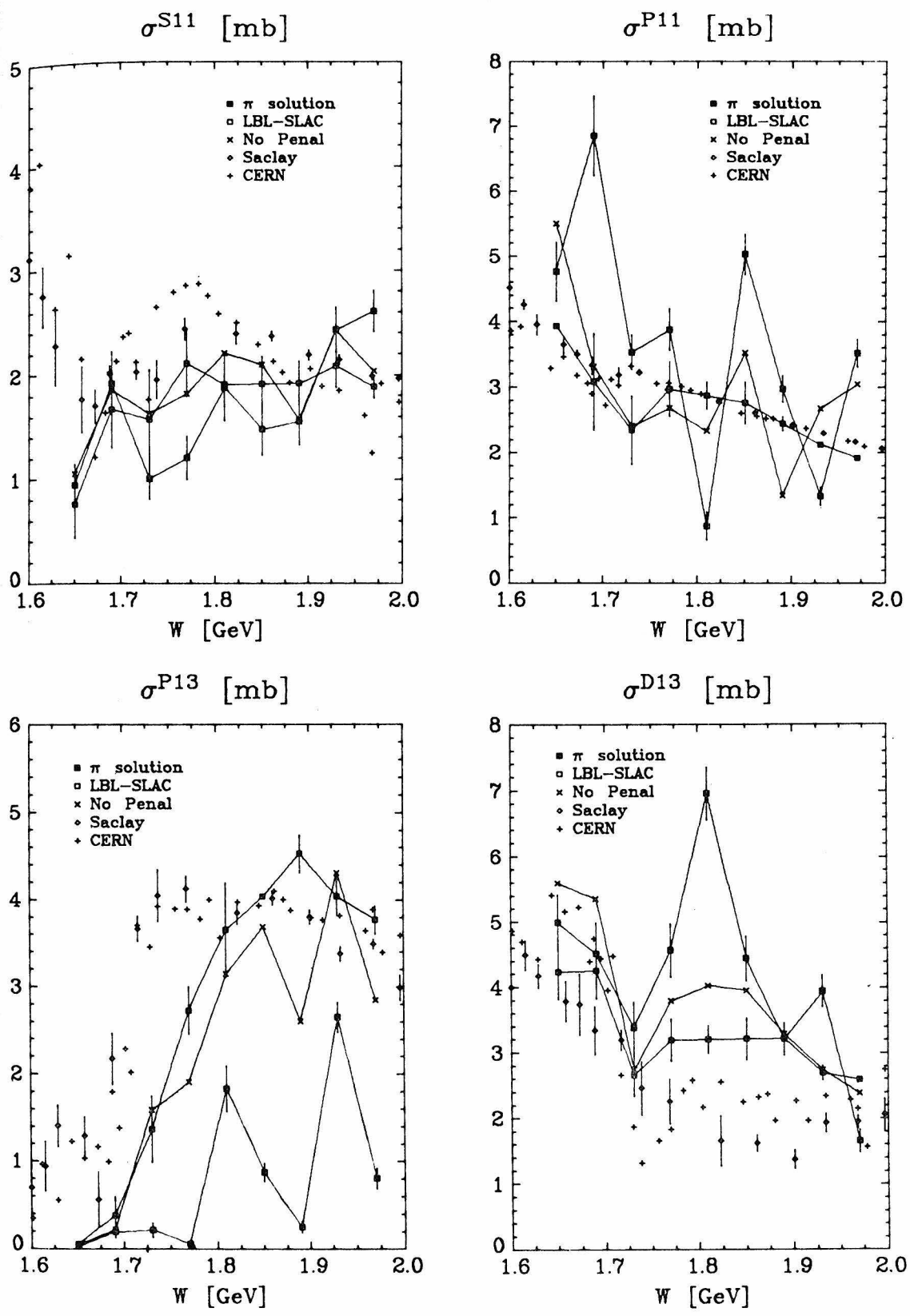

σ^{S11} [mb]
σ^{P11} [mb]
σ^{P13} [mb]
σ^{D13} [mb]
π solution
LBL-SLAC
No Penal
Saclay
CERN
W [GeV]

Fig. 10a

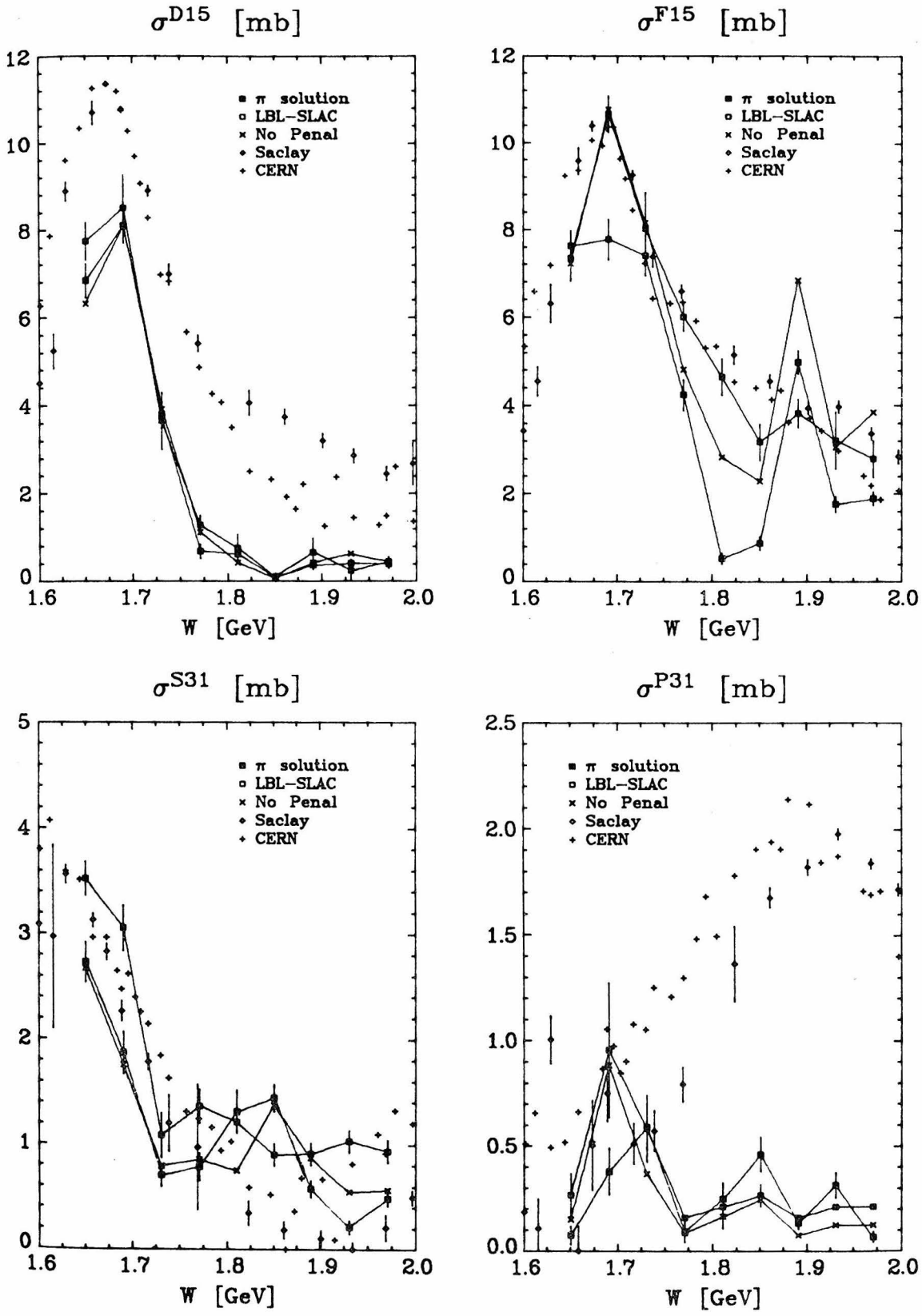

σ^D15 [mb]
σ^F15 [mb]
σ^S31 [mb]
σ^P31 [mb]
π solution
LBL–SLAC
No Penal
Saclay
CERN
W [GeV]

Fig. 10b

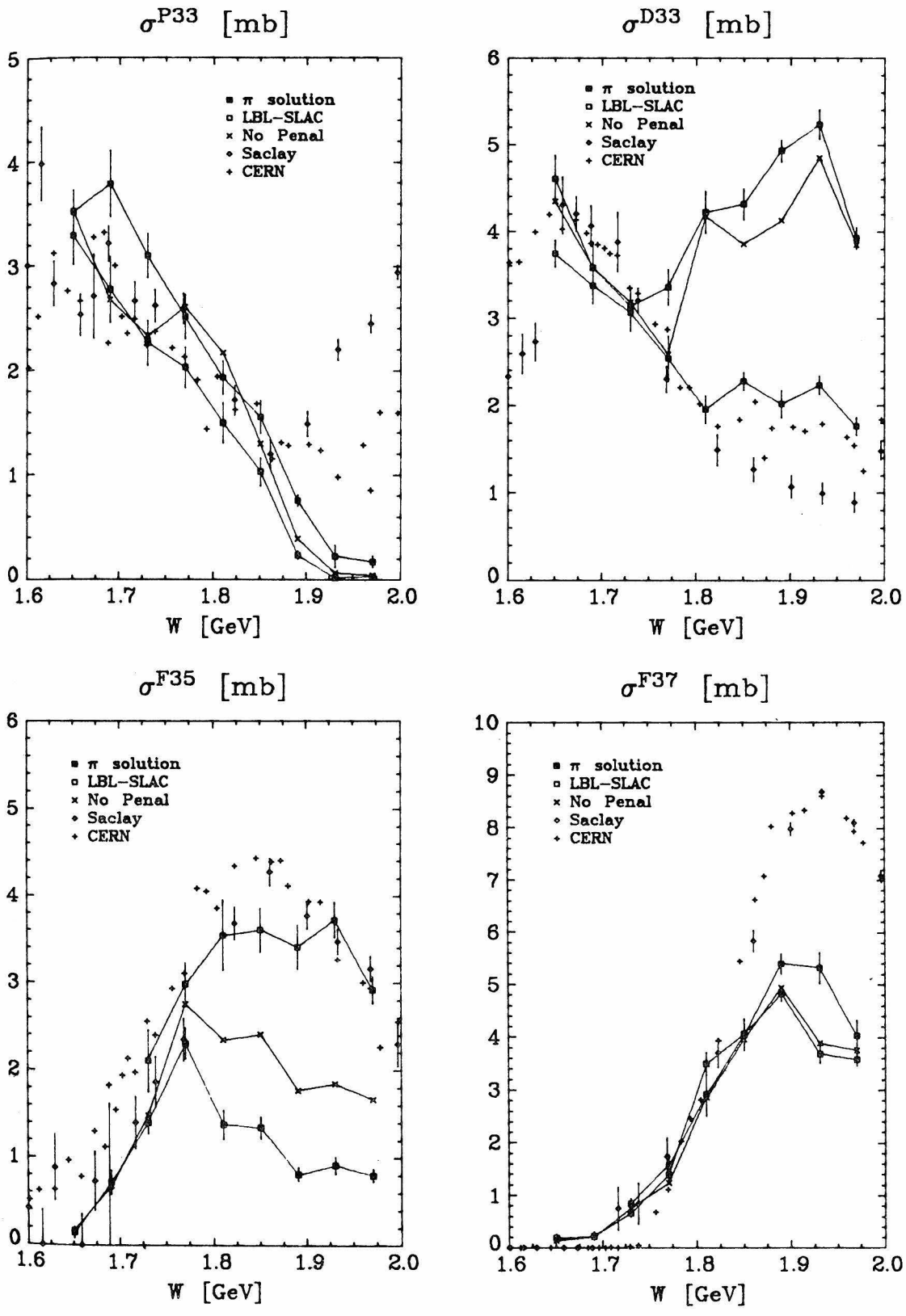

σ^{P33} [mb]
σ^{D33} [mb]
σ^{F35} [mb]
σ^{F37} [mb]
π solution
LBL-SLAC
No Penal
Saclay
CERN
W [GeV]

Fig. 10c

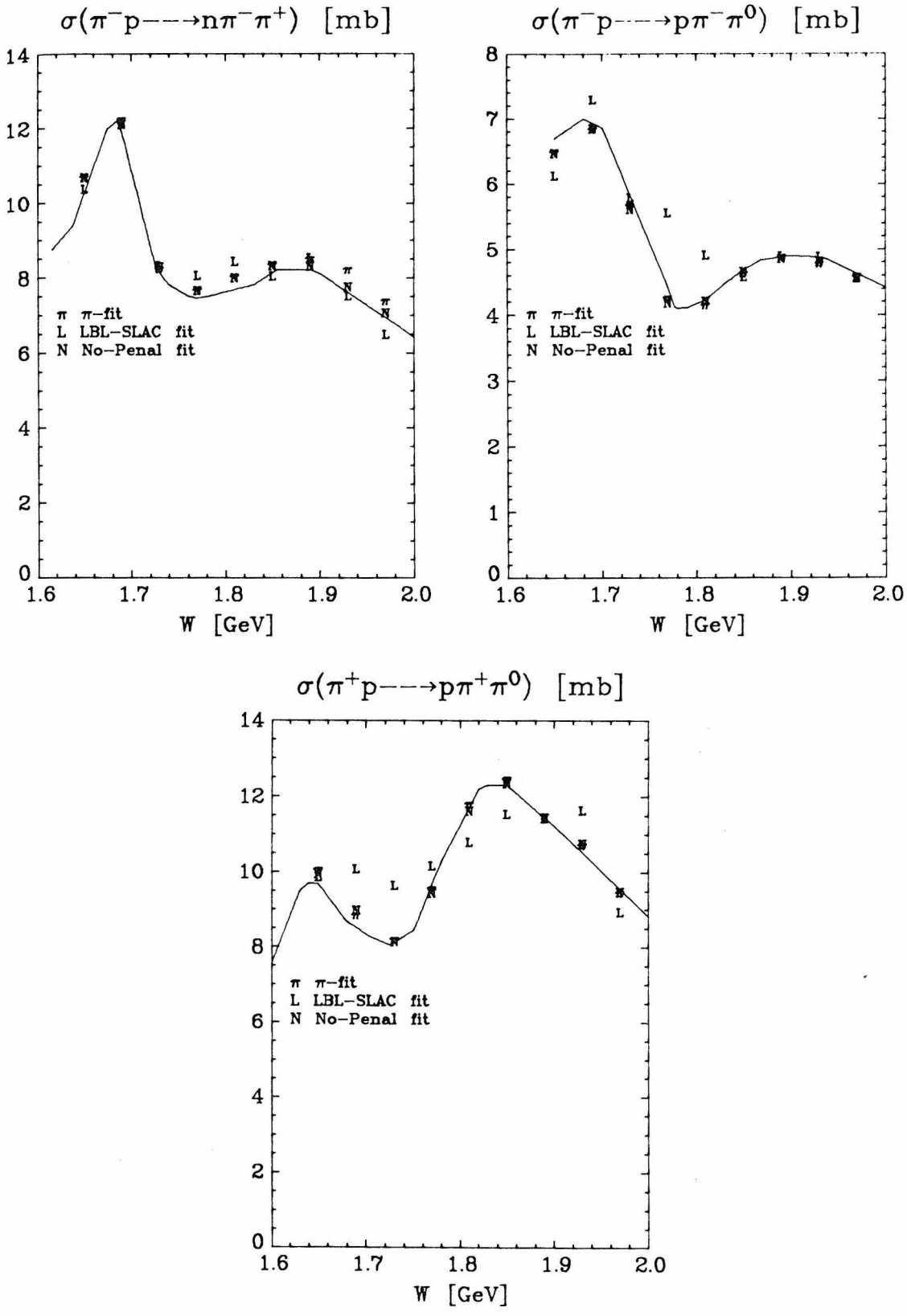

σ(π⁻p→nπ⁻π⁺) [mb]
π π−fit
L LBL−SLAC fit
N No−Penal fit
W [GeV]
σ(π⁻p→pπ⁻π⁰) [mb]
π π−fit
L LBL−SLAC fit
N No−Penal fit
W [GeV]
σ(π⁺p→pπ⁺π⁰) [mb]
π π−fit
L LBL−SLAC fit
N No−Penal fit
W [GeV]

Fig. 11a

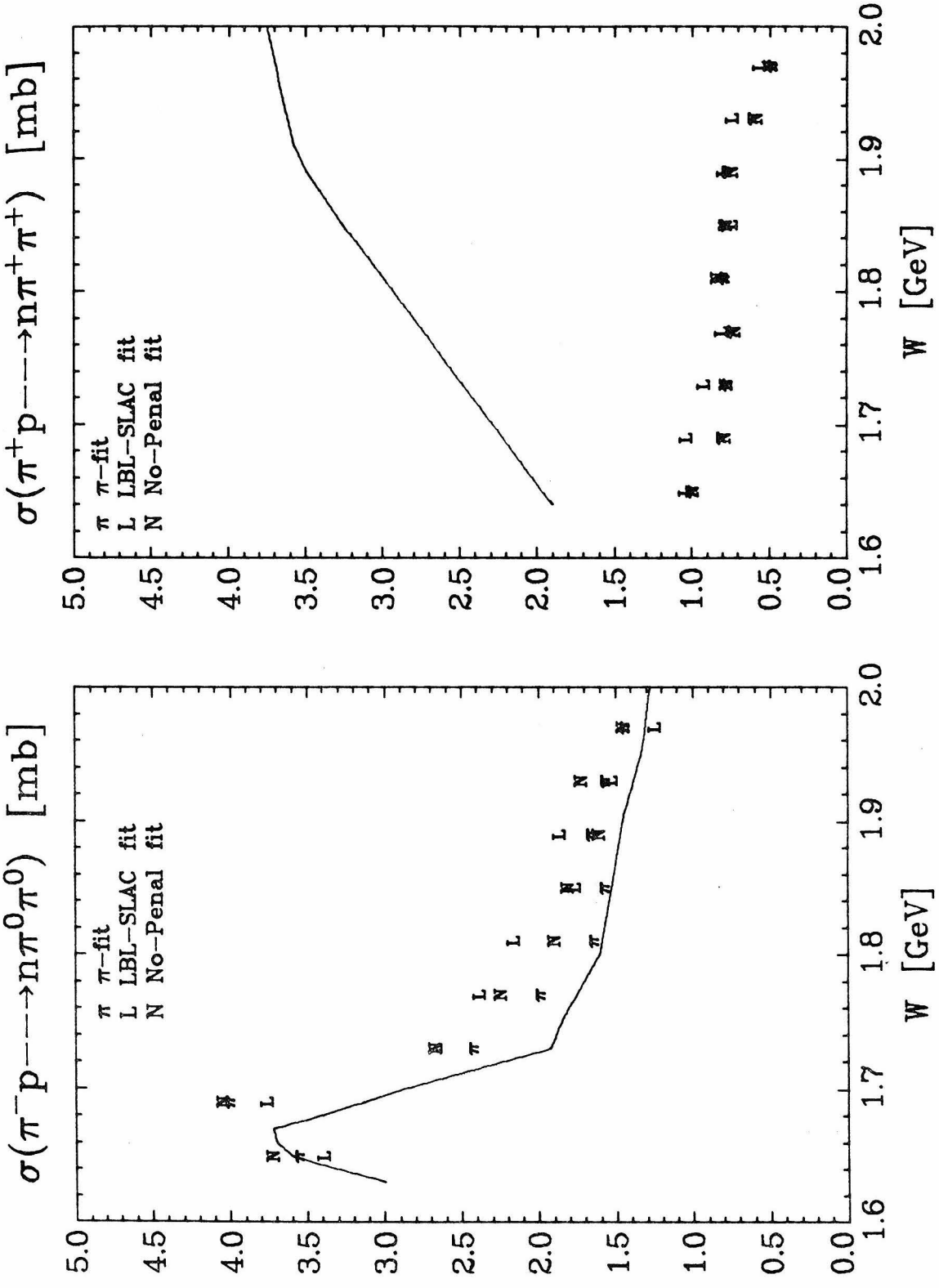

$\sigma(\pi^- p \longrightarrow n\pi^0\pi^0)$ [mb]
$\sigma(\pi^+ p \longrightarrow n\pi^+\pi^+)$ [mb]
π π−fit
L LBL−SLAC fit
N No−Penal fit
W [GeV]
1.6
1.7
1.8
1.9
2.0
0.0
0.5
1.0
1.5
2.0
2.5
3.0
3.5
4.0
4.5
5.0

Fig. 11b

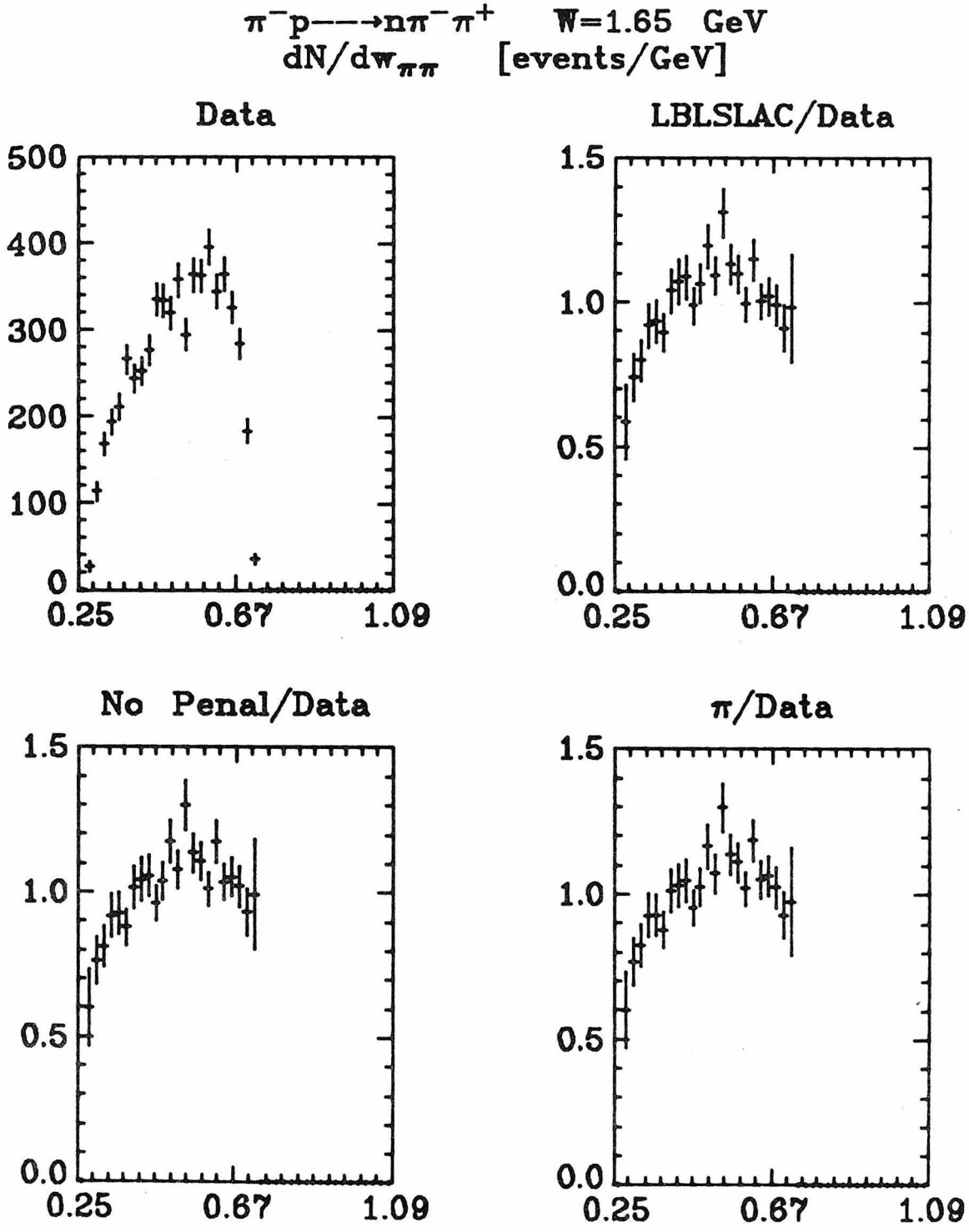

$\pi^- p \longrightarrow n\pi^-\pi^+$ W=1.65 GeV
$dN/dw_{\pi\pi}$ [events/GeV]
Data
LBLSLAC/Data
No Penal/Data
π/Data
500
400
300
200
100
0
1.5
1.0
0.5
0.0
0.25
0.67
1.09

Fig. 12a

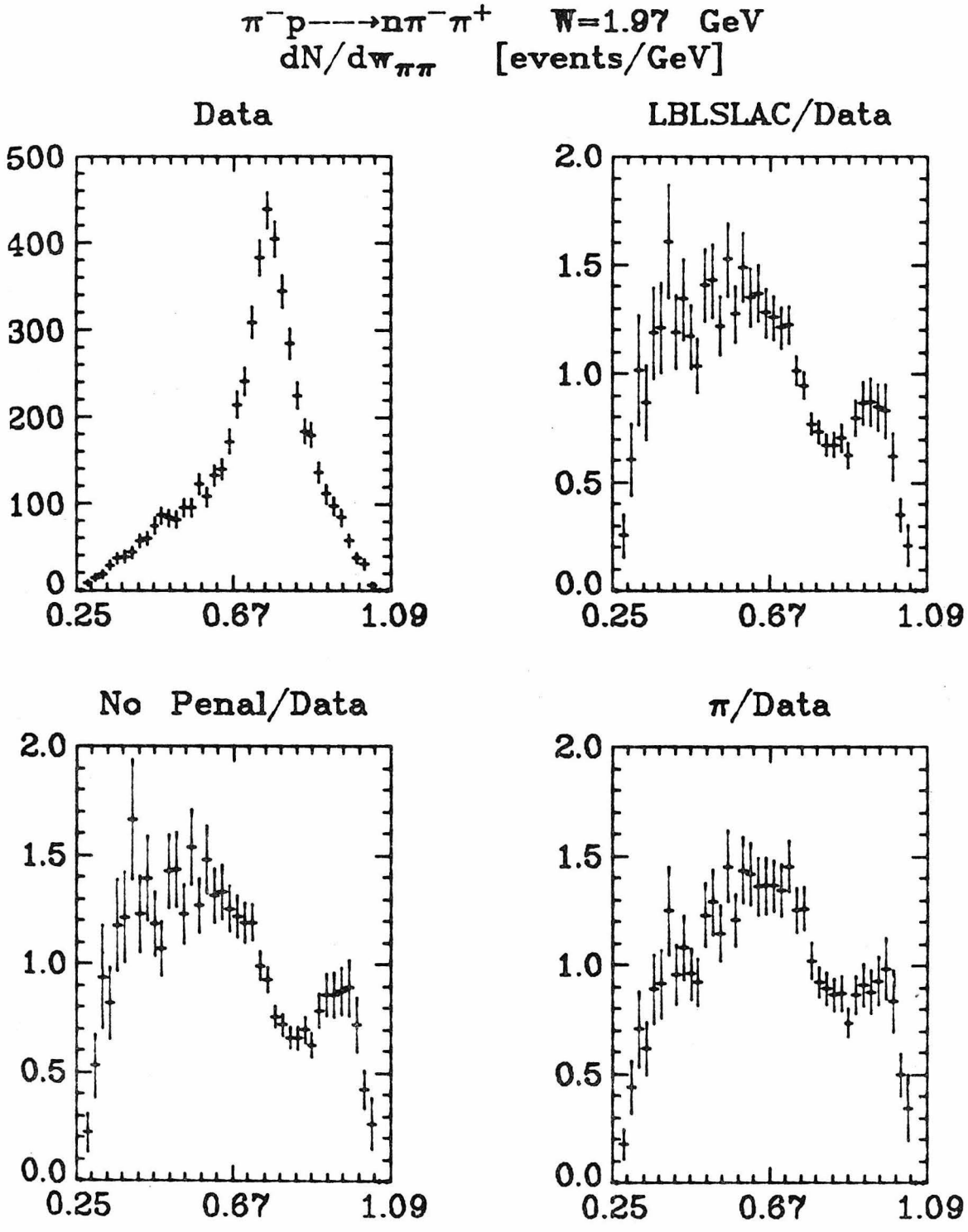

$\pi^- p \longrightarrow n\pi^-\pi^+$ W=1.97 GeV
$dN/dw_{\pi\pi}$ [events/GeV]
Data
LBLSLAC/Data
No Penal/Data
π/Data
500
400
300
200
100
0
2.0
1.5
1.0
0.5
0.0
0.25
0.67
1.09

Fig. 12b

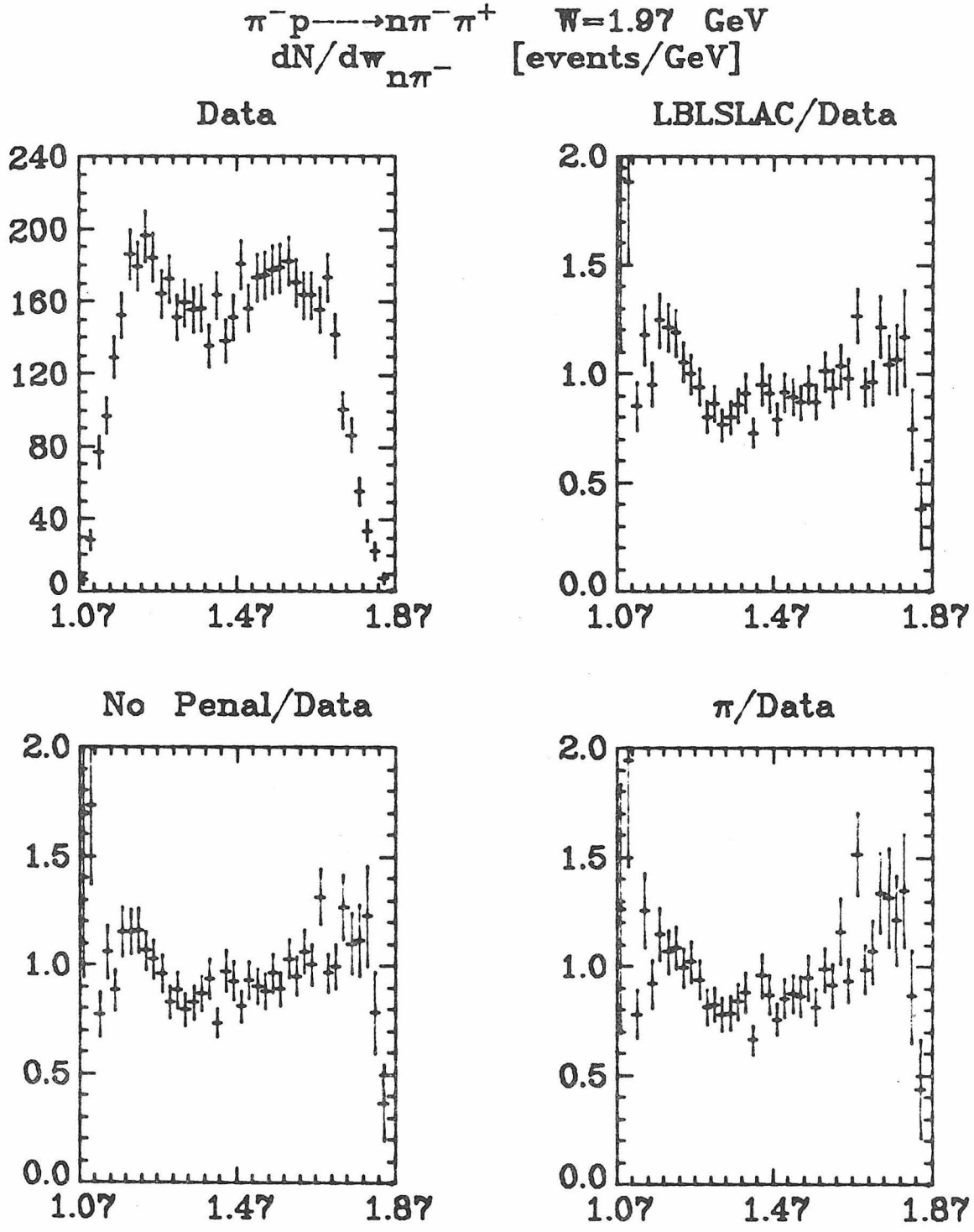

$\pi^- p \longrightarrow n\pi^-\pi^+$ W=1.97 GeV
$dN/dw_{n\pi^-}$ [events/GeV]
Data
LBLSLAC/Data
No Penal/Data
π/Data
240
200
160
120
80
40
0
2.0
1.5
1.0
0.5
0.0
1.07
1.47
1.87

Fig. 13a

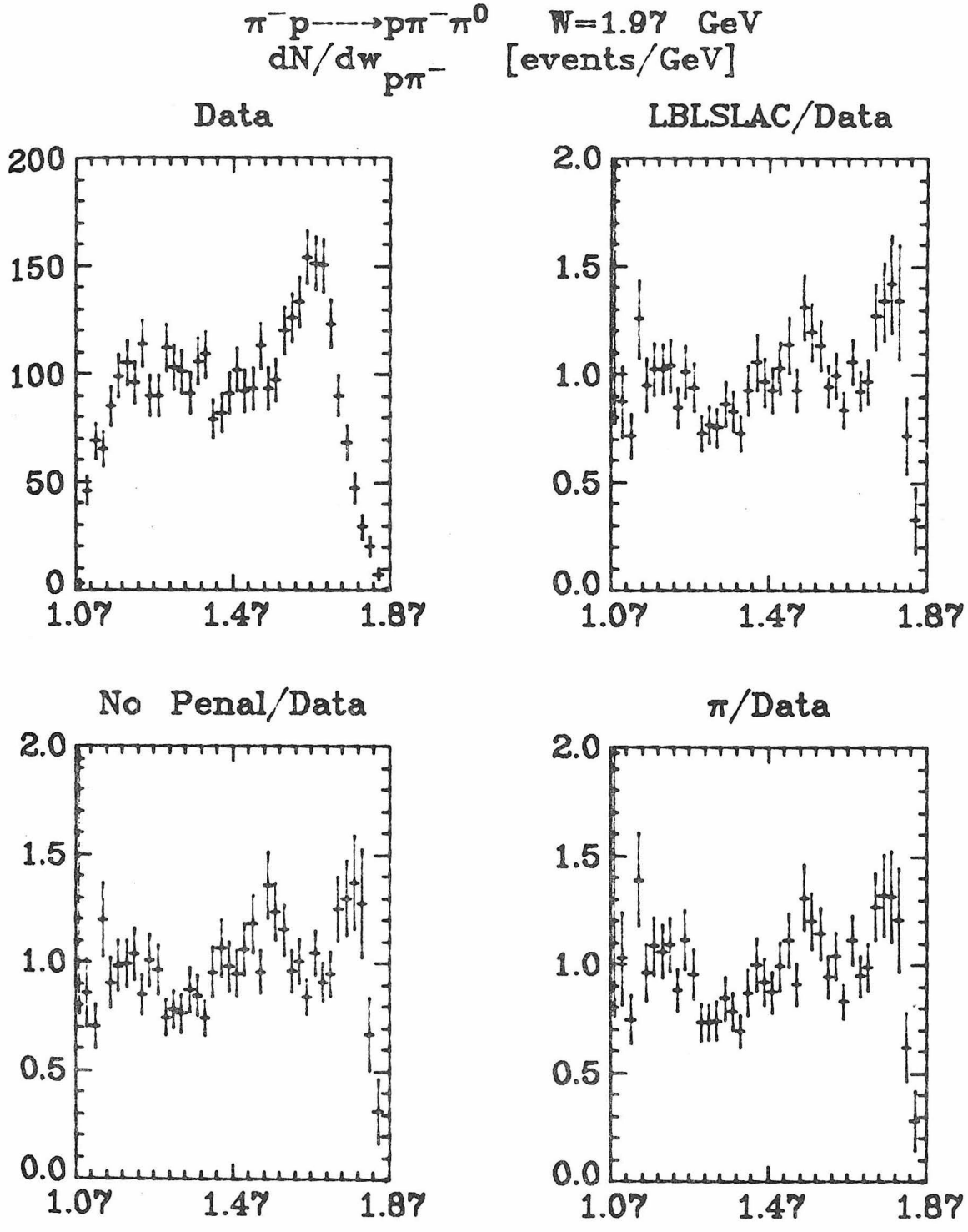

$\pi^- p \longrightarrow p\pi^- \pi^0$ W=1.97 GeV
$dN/dw_{p\pi^-}$ [events/GeV]
Data
LBLSLAC/Data
No Penal/Data
π/Data
200
150
100
50
0
2.0
1.5
1.0
0.5
0.0
1.07
1.47
1.87

Fig. 13b

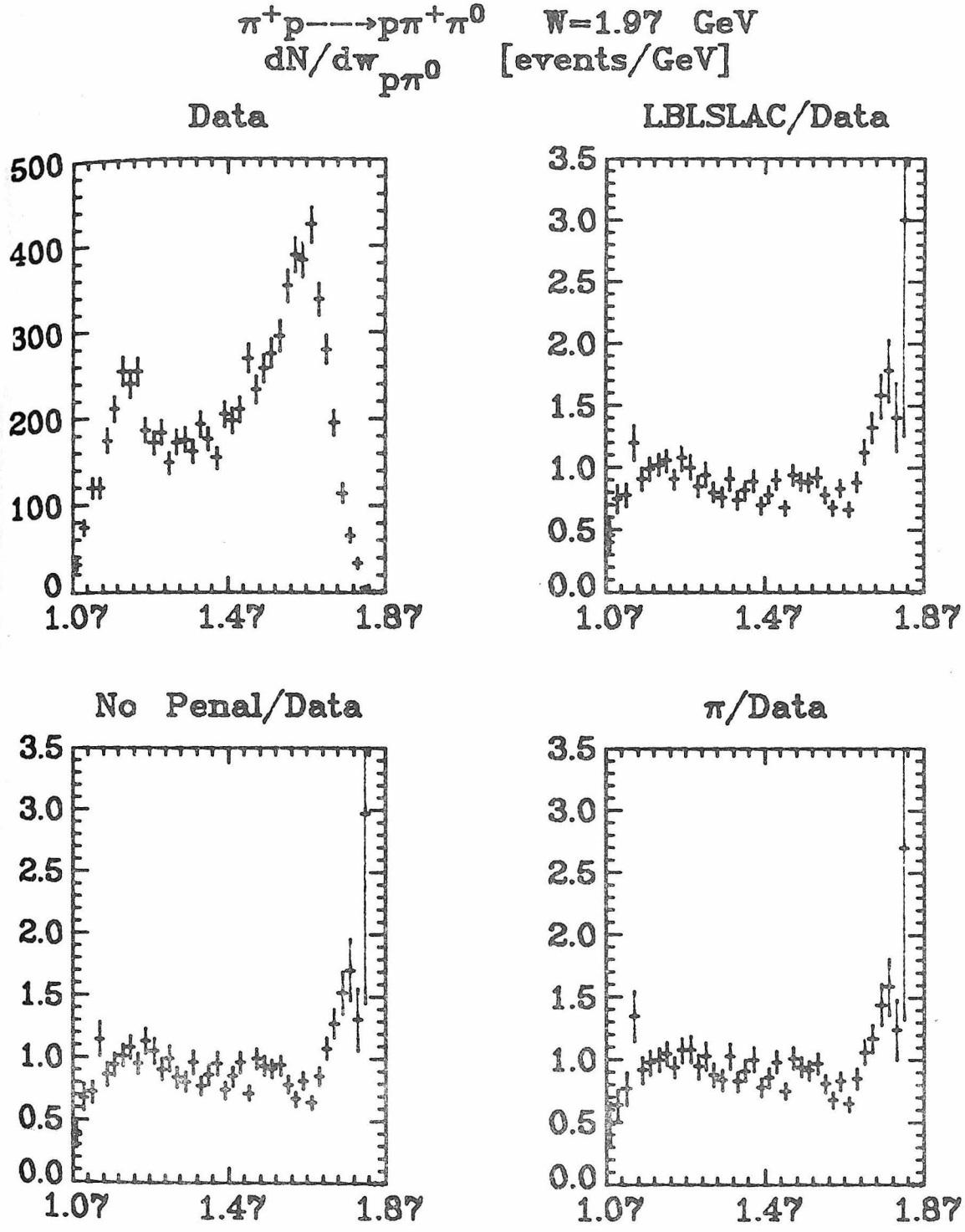

$\pi^+p \longrightarrow p\pi^+\pi^0$ W=1.97 GeV
$dN/dw_{p\pi^0}$ [events/GeV]
Data
LBLSLAC/Data
No Penal/Data
π/Data
500
400
300
200
100
0
3.5
3.0
2.5
2.0
1.5
1.0
0.5
0.0
1.07
1.47
1.87

Fig. 13c

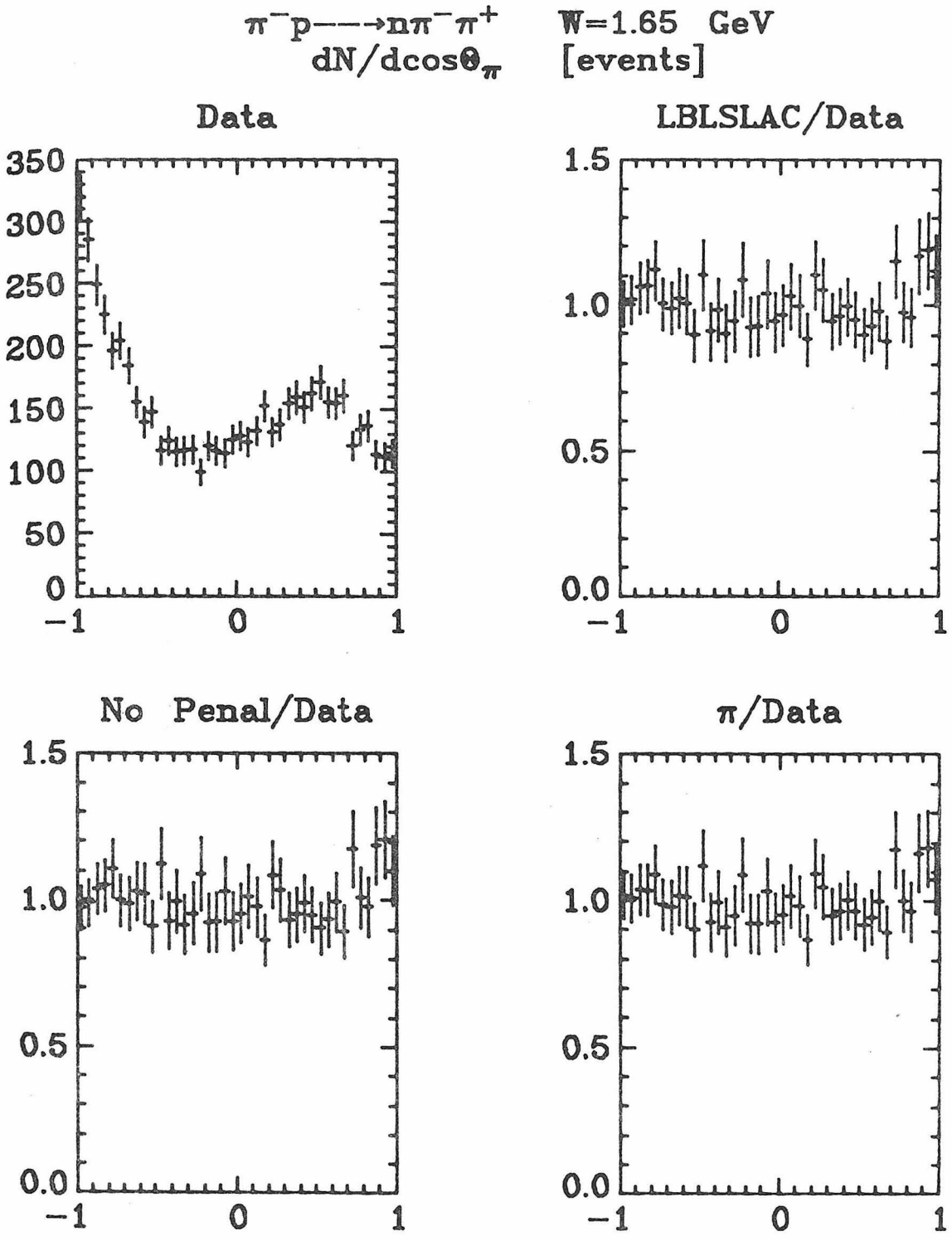

$\pi^- p \longrightarrow n\pi^-\pi^+$
$dN/d\cos\Theta_\pi$
W=1.65 GeV
[events]
Data
LBLSLAC/Data
No Penal/Data
π/Data
350
300
250
200
150
100
50
0
1.5
1.0
0.5
0.0
−1
0
1

Fig. 14a

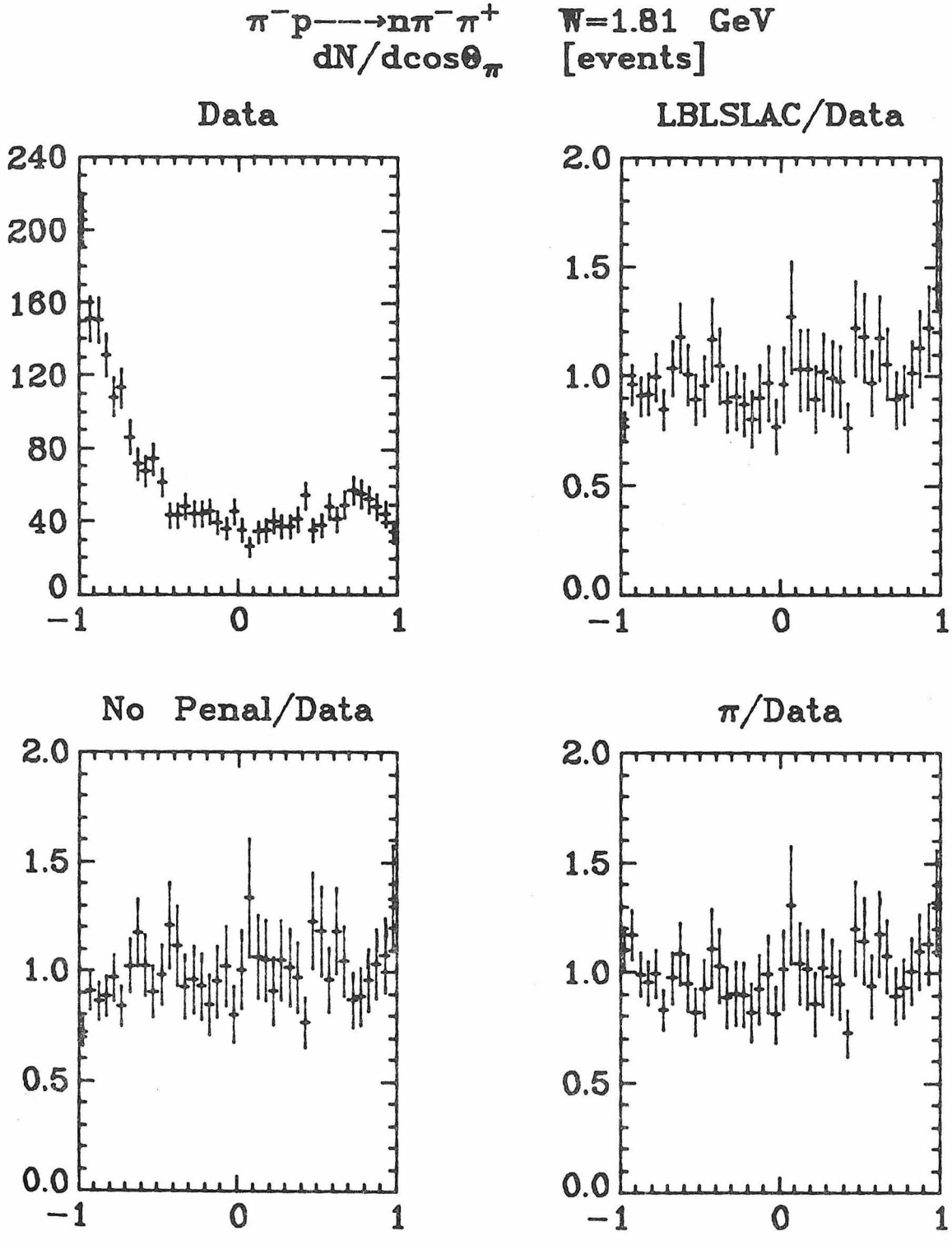

$\pi^- p \longrightarrow n\pi^-\pi^+$
W=1.81 GeV
$dN/d\cos\Theta_\pi$
[events]
Data
LBLSLAC/Data
No Penal/Data
π/Data
240
200
160
120
80
40
0
2.0
1.5
1.0
0.5
0.0
−1
0
1

Fig. 14b

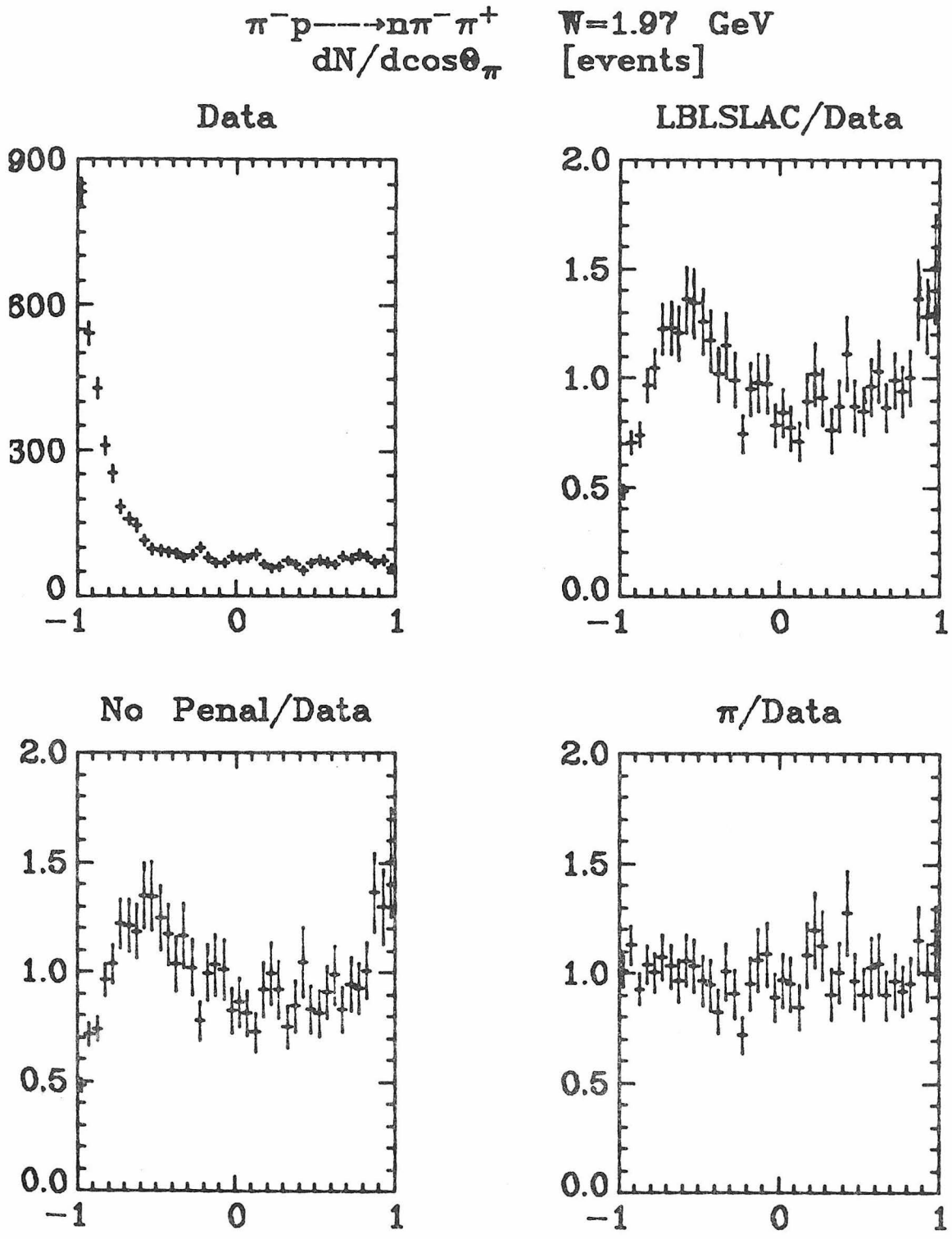
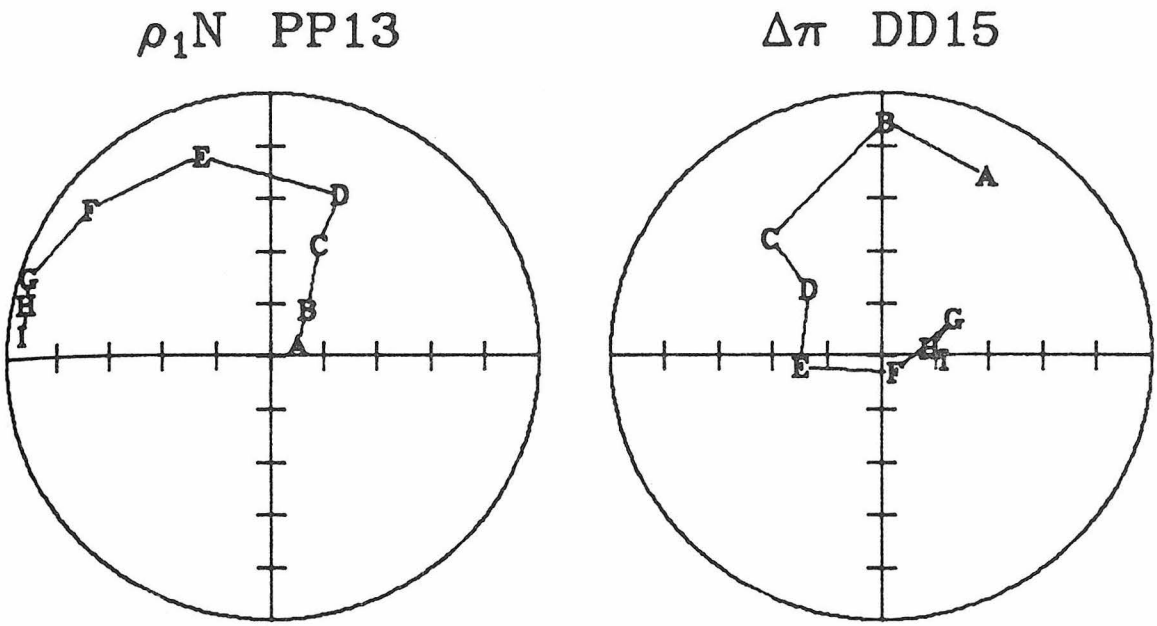

$\pi^- p \longrightarrow n\pi^-\pi^+$
W=1.97 GeV
$dN/d\cos\theta_\pi$
[events]
Data
LBLSLAC/Data
No Penal/Data
π/Data
900
600
300
0
2.0
1.5
1.0
0.5
0.0
−1
0
1

Fig. 14c



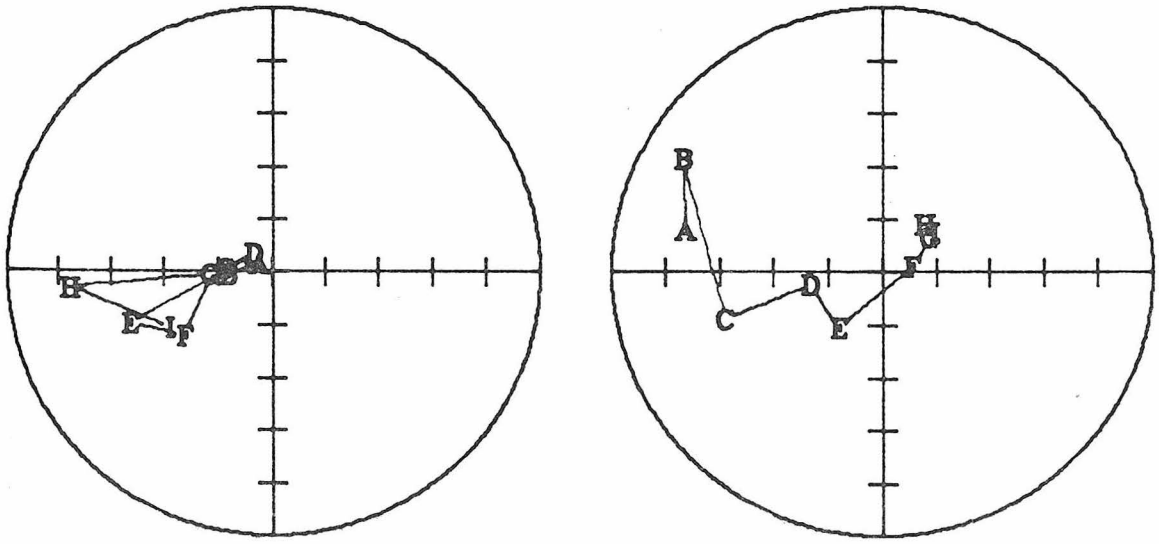


Fig. 15a

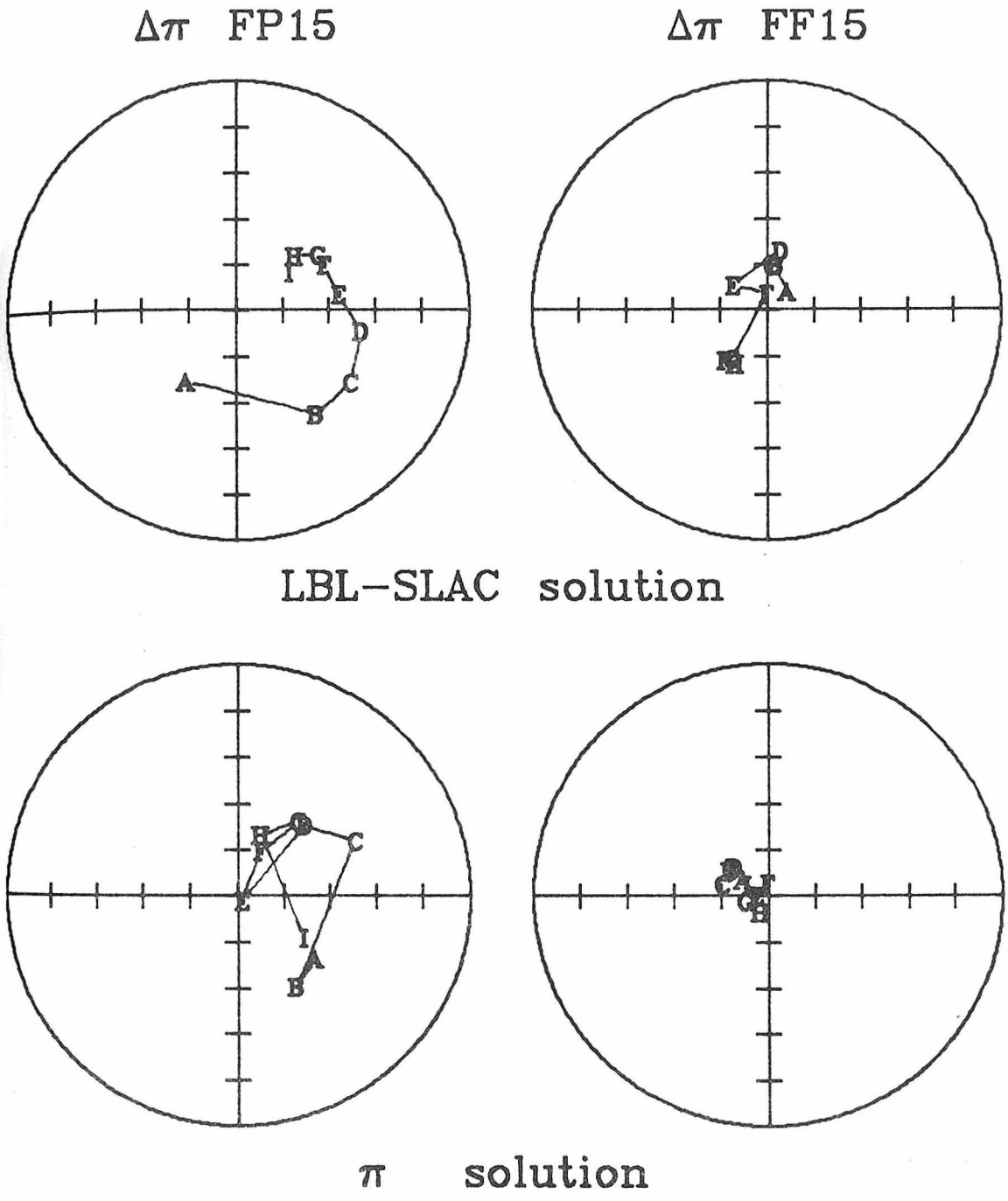


Fig. 15b

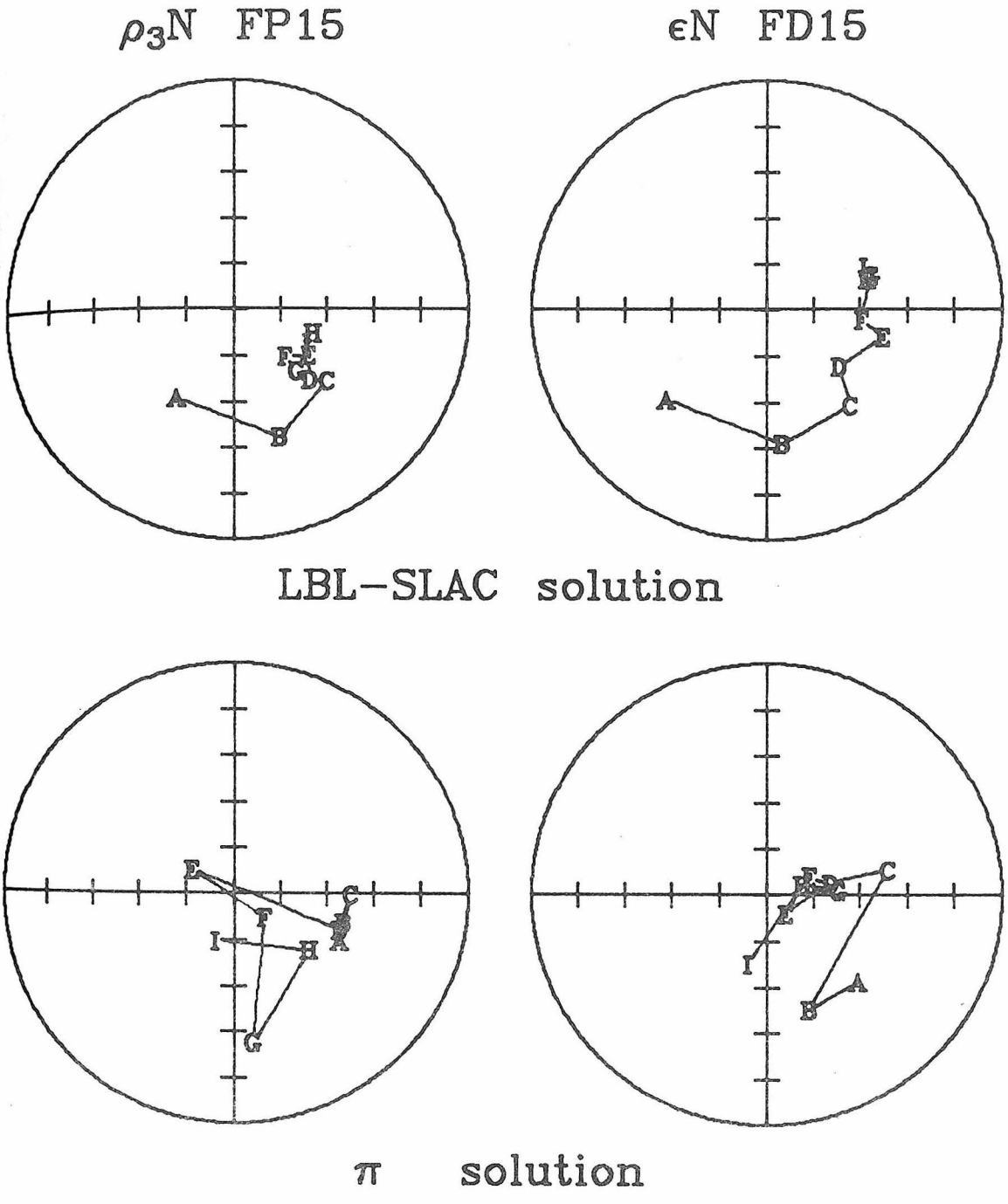


Fig. 15c

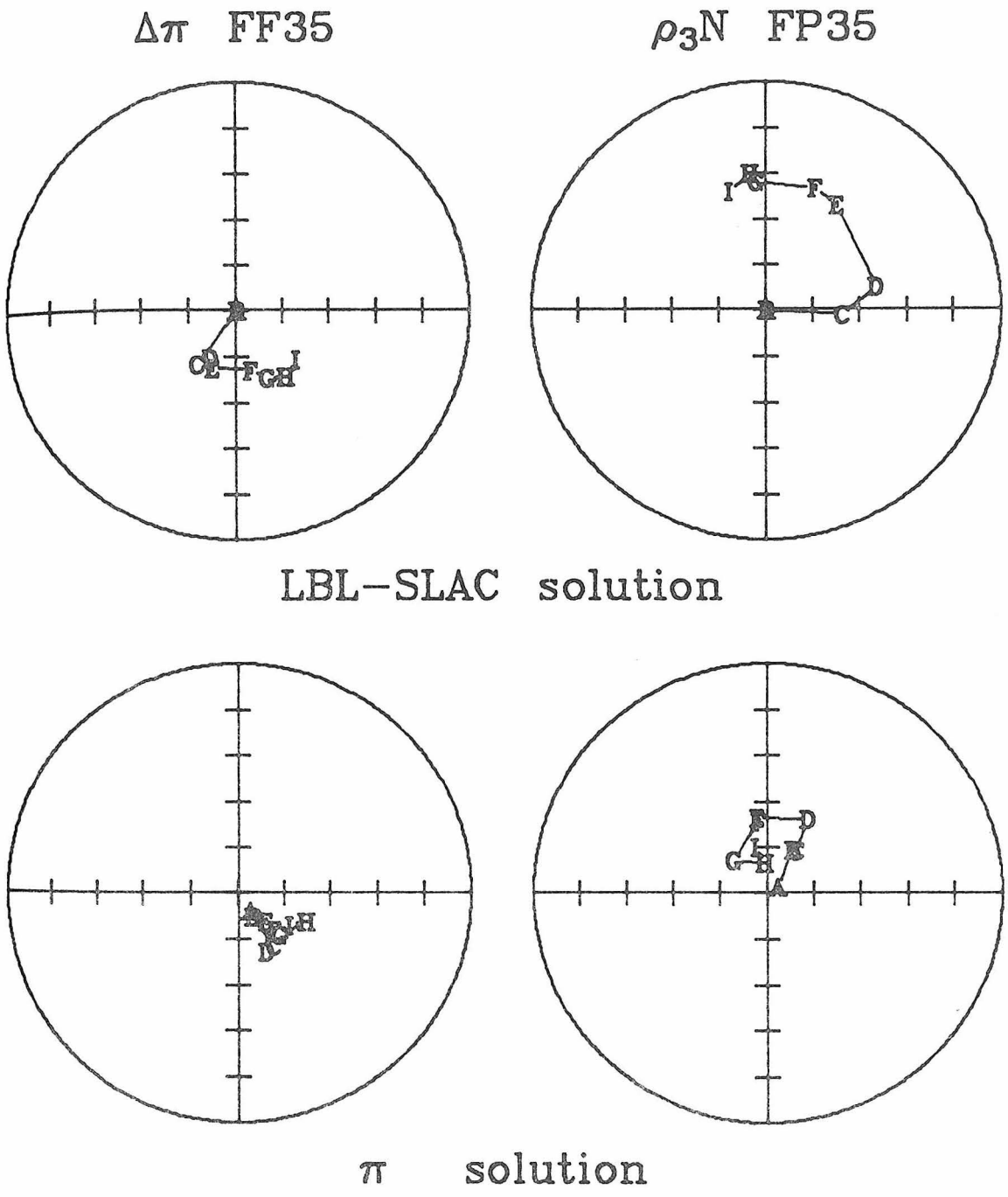


Fig. 15d

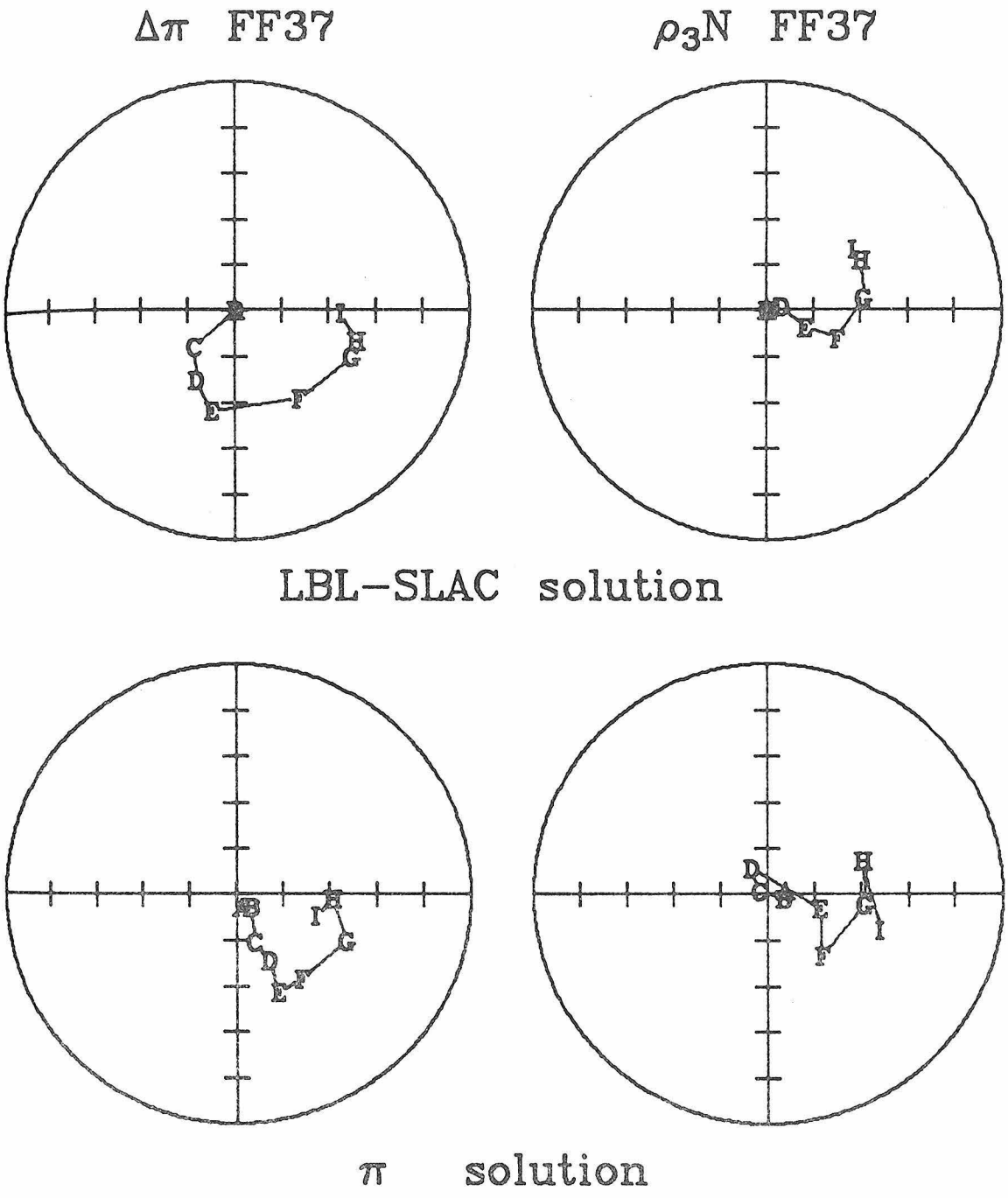


Fig. 15e

Part II

Resonance Parameter Analyses of $\pi N \to \Delta\pi + \rho N + \varepsilon N$

Introduction

In the first part of this thesis[1] an analysis of the reactions

$$\begin{aligned} \pi^- + p &\longrightarrow n + \pi^- + \pi^+ \\ \pi^- + p &\longrightarrow p + \pi^- + \pi^0 \\ \pi^- + p &\longrightarrow p + \pi^+ + \pi^0 \end{aligned} \qquad (1)$$

from c.m. energies 1.65 to 1.97 GeV is described. That analysis used data compiled by Herndon et al.[2] in their analysis of the same reactions. The analysis of Herndon et al., which we will call the LBL-SLAC analysis, assumed that the production amplitude, e.g. for the reaction $\pi^- + p \longrightarrow n + \pi^- + \pi^+$, is given by

$$\begin{aligned} T^{\text{LBL-SLAC}} = & \frac{1}{\sqrt{2}} P(\pi^- + p \longrightarrow \Delta^- + \pi^+)\, D(\Delta^- \longrightarrow n + \pi^-) \\ & + \frac{1}{\sqrt{2}} P(\pi^- + p \longrightarrow \Delta^+ + \pi^-)\, D(\Delta^+ \longrightarrow n + \pi^+) \\ & + P(\pi^- + p \longrightarrow \rho^0 + n)\, D(\rho^0 \longrightarrow \pi^- + \pi^+) \\ & + P(\pi^- + p \longrightarrow \varepsilon + n)\, D(\varepsilon \longrightarrow \pi^- + \pi^+) \end{aligned} \qquad (2)$$

i.e. by the sum of contributions of various sequential isobar production and isobar decay processes. The π - analysis described earlier[1] added a high partial wave input, giving

$$T^{\pi\text{-analysis}} = T^{\text{LBL-SLAC}} + T^{\text{high partial waves from } \pi\text{-exchange}} \qquad (3)$$

The production amplitudes, P(a + b ---> c + d), are the basic unknowns, though certain dependences (-e.g. threshold dependence on the momentum in the channel -) were inserted as multiplicative factors. The decay

amplitudes, D(c ---> e + f), are known functions. For example, up to (known) threshold behavior, the ρ-isobar decay is given by

$$D(\rho^0 \text{---}> \pi^- + \pi^+) \propto \frac{e^{2i\delta^{I=1,\ell=1}} - 1}{2i}$$

i.e. by the $\pi\pi$ scattering in the $I_{\pi\pi}=\ell_{\pi\pi} = 1$ channel. The π-exchange term in Eqn. (3) had its low partial waves removed. It was included as a correction to the standard[2] assumption that the high partial waves may be ignored. (The form of the various terms in Eqns. (2) and (3) is discussed in more detail in references 1,3 and 4.)

Using each form, Eqns. (2) and (3), best values of the scattering parameters were found[1,2]. These parameters are conveniently expressed in terms of complex partial wave amplitudes

$$T^{\text{S' isobar}}_{\text{L L' I J}}$$

which are bounded by unitarity by

$$\sum_{\text{isobar},L',S'} \left| T^{\text{S' isobar}}_{\text{L L' I J}} \right|^2 = \frac{1}{4} - \frac{1}{4} \left| S^{\text{elastic}}_{\text{L I J}} \right|^2$$

where I and J are the isospin and total angular momentum of the partial wave, L is the orbital angular momentum of the initial (πN) state, and L' and S' are the orbital and spin angular momenta of the final 2-body ($\pi\Delta$, ρN, εN) state. (For the elastic S-matrix, πN---> πN, the initial and final orbital angular momenta are the same, and the spin angular momentum is $\frac{1}{2}$.)

We will represent these partial waves with a more economical notation, whose use is best illustrated by two examples:

$$\Delta(\text{FP15}) \quad \text{<---->} \quad T \begin{matrix} \frac{3}{2} & \Delta \\ 3\ 1\ \frac{1}{2}\ \frac{5}{2} & \end{matrix}$$

$$\rho_3(\text{FP35}) \quad \text{<---->} \quad T \begin{matrix} \frac{3}{2} & \rho \\ 3\ 1\ \frac{3}{2}\ \frac{5}{2} & \end{matrix}$$

The new notation corresponds to

$$\text{Isobar}_{2S'}\ (\ L\ L'\ 2I\ 2J\ ).$$

For the $\Delta\pi$ and ϵN states, the final spin is fixed at $S' = \frac{3}{2}$ and $S' = \frac{1}{2}$ respectively. Thus the $2S'$ subscript is unnecessary and is omitted. For the ρN state, both $S' = \frac{1}{2}$ and $S' = \frac{3}{2}$ are possible, so the spin label is necessary, and is included.

The two sets of parameters which we study are the LBL-SLAC solution described in references 2 and 5, and the π- solution described in reference 1. The actual T-matrix elements for the LBL-SLAC solution are documented in reference 6, while those for the π-solution are given in reference 7.

Resonance parameters were first derived from the LBL-SLAC solution in references 8 and 9. These authors used several methods to extract their resonance parameters. We emphasize that the extraction of resonance parameters is not easy, since the T-matrix elements of the solutions (- both LBL-SLAC and π-solutions -) are <u>not smooth</u> in their energy dependence, while all known resonance parameterizations are smoothly dependent on energy. This absence of smoothness is easily seen by perusing the Argand diagrams for the various waves. (See, e.g., reference 7.) The need for "optical inspection" and physical intuition

in evaluating the results of the fits is thus a property of the two inelastic phase shift solutions used as input to the resonance parameter fits.

Longacre et al.[8,9] used three methods to extract resonance parameters from the LBL-SLAC solution. These are:

I. Eyeball fits using elastic phase shift analysis results[10] for the values of the resonant masses and widths.

II. Eyeball fits to a K-matrix fit to the elastic-inelastic system.

III. Search for poles in the T-matrix derived from the K-matrix fit to the elastic inelastic system.

Our method of resonance parameter extraction involves fitting to a Breit-Wigner form with appropriate centrifugal barrier factors.

In our comparisons to the work of Longacre et al.[8,9], we have compared to their method I. Methods II and III tend to alter the values of the resonant mass and width from the elastic phase shift analysis results[10,11]. We believe that as much input as possible should be used from the elastic phase shift analyses, since the reliability of these analyses is much better than our inelastic analyses. (Their data sets are smaller, but more selective. They also have $\frac{1}{3}$ as many relevant waves, and an exact formalism, rather than the isobar model formalism.) We therefore take the resonant mass and width from the elastic analysis, where they can be reliably determined, and determine only the inelastic coupling from the inelastic phase shift solutions.

Longacre et al.[8,9] point out that their method III is very attractive in that it is independent of the T-matrix parameterization.

However, given the present state of the inelastic phase shift solutions, we feel that any method which places such strong emphasis on the inelastic solutions as do methods II and III of Longacre et al.[8,9] is not very reliable.

Method I of Longacre et al.[8,9] is simple, but it ignores the energy dependence in the speed (dT/dW) of the resonant loop.

Therefore, until the inelastic solutions improve to the reliability of the elastic phase shift solutions, we believe that our method, i.e. fitting to a resonant parameterization of the T-matrix with resonant mass and width fixed by the elastic phase shift results, is the best method to use to extract couplings of resonances to inelastic channels.

We conclude our introductory remarks with some warnings about the LBL-SLAC solution. This solution is the result of two analyses. First the experimental data were fit to a form as in Eqn. (2). The resultant solution was a set of T-matrix elements for each energy, W :

$$T^{\,S'\ \text{isobar}}_{L\ L'\ I\ J}(W) \quad .$$

However the solution is invariant under multiplication of each partial wave by the same, but energy dependent, phase, i.e.

$$e^{\,i\,\phi(W)}\, T^{\,S'\ \text{isobar}}_{L\ L'\ I\ J}(W)$$

is just as good a solution. The value of this phase at each energy was determined by Longacre[9] by performing a K-matrix analysis of the F15 and D15 waves (for $1.65 \leq W \leq 1.81$ GeV) and of the F35 and F37 waves (for $1.73 \leq W \leq 1.97$ GeV). These analyses fit the elastic and inelastic

channels jointly. Hence any smooth energy dependence of the T-matrix in these waves must be partially due to the smoothness of the elastic solution, rather than to the inelastic analysis alone.

The π -solution, on the other hand, did not have this phase ambiguity. Since the π -solution has been shown[1] to give a better representation of the differential cross section above W= 1.8 GeV, we must conclude that the greater smoothness (-circular shape-) of the LBL-SLAC solution for the D15,F15,F35 and F37 waves is misleading as a signature of a good fit. So the lack of ambiguity in extracting resonance parameters from the LBL-SLAC solution must be considered as at least partially due to this effect.

We describe in this work three analyses:

I. We determine the resonant couplings to the inelastic channels from the LBL-SLAC solution using a form

$$T = \text{Background} + \text{Breit-Wigner resonance} \quad (4)$$

We use the same resonant mass and total width as used by Longacre et al.[8] in their Method I. These values are from the Saclay elastic phase shift analysis[10]. We do this analysis for each major wave which resonates in our energy range ($1.65 \leq W \leq 1.97$ GeV), i.e. the D15,F15,P33,F35 and F37 waves. (The notation is L-2I-2J, where all values of L', S', and isobar type are studied for each L-2I-2J wave listed.) We compare our results to those of Longacre et al.[8]

II. We then perform the same analysis for the π -solution for those waves which resonate above 1.8 GeV. (As discussed in reference 1,

it is above this energy that the π-exchange high partial wave input fixes the overall phase of all the T-matrix elements.) The waves analysed are the P33, F35 and F37. We compare the resonant coupling parameters determined from the π -solution to those determined from the LBL-SLAC solution. We again caution that the phase of the F35 and F37 resonant behavior for the LBL-SLAC solution was determined by a K-matrix fit to the joint elastic-inelastic system. The fact that it is easier to extract resonance information for these waves from the LBL-SLAC solution is thus to a large extent put in! We then present our best estimates for the values of the resonant couplings.

III. Finally, we study the ρ_1(PP31) wave, where resonant activity is seen in the π-solution, but not in the LBL-SLAC solution.

In section I, we describe the form of the resonant amplitude used in our first two analyses. The results are tabulated and discussed. In section II we describe our study of the P31 wave.

I. Determination of resonance couplings for D15, F15, P33, F35 and F37

The form of the resonant T-matrix used in our fits is a constant (unitarity bounded) background plus a resonant term:

$$T_{i\,f} = \left(\tfrac{1}{2} \cos^2 A \; e^{i\phi} + e^{i\theta} \frac{\tfrac{1}{2} z \gamma_T}{m_r - W - \tfrac{1}{2} i \gamma_T \{b_i(W)\}^2} \right) \times b_i(W)\, b_f(W) \qquad (5)$$

where the four real parameters in the fit are

$$A \;,\; \phi \;,\; \theta \;,\; z$$

which are determined separately for each wave. The mass and total width of the resonance, m_r and γ_T, are given in Table I. The elastic width given in Table I may be used to find the inelastic width by

$$\gamma_{inel} = \frac{\gamma_T^2}{\gamma_{el}} \; z^2 \qquad (6)$$

Note that a commonly used variable is the branching ratio, which is

$$x_{el} = \gamma_{el} / \gamma_T$$

$$x_{inel} = \gamma_{inel} / \gamma_T$$

Thus our parameter, z, can be expressed as

$$z = \sqrt{x_{el} x_{inel}}$$

The only energy dependence (other than in the denominator of the Breit-Wigner resonant form) is in the centrifugal barriers. We use the normalized barrier

$$\{b(W)\}^2 = \frac{\beta(W)}{\beta(m_r)} \tag{7}$$

where the elastic channel has

$$\beta_{el}(W) = \frac{Q(W)}{4W} \; B_L\left(\frac{Q(W)}{M}\right) \tag{8}$$

and for the inelastic channel

$$\beta_{inel}(W) = \int dw^2 \, \frac{q}{4w} \left| \frac{\eta e^{2i\delta} - 1}{2iq^{\ell+\frac{1}{2}}} \right|^2 \frac{Q'(W,w)}{4W} \; B_{L'}\left(\frac{Q'(W,w)}{M}\right) \tag{9}$$

In these expressions, Q(W) is the c.m. momentum in the elastic channel, Q'(W,w) is the c.m. momentum of the inelastic two-body final state, q and w are the decay momentum and total energy of the isobar (Δ, ρ, ε) in the isobar's rest frame, and η and δ describe the isobar's final state interaction[1,2]. L,L' and ℓ are the orbital angular momenta of the initial (elastic) channel, the final (two-body) channel, and of the isobar decay products, respectively. B_L is the Blatt-Weisskopf barrier factor[12,13]

$$\begin{aligned} B_0(x) &= 1 \\ B_1(x) &= x^2 \; / \; (\; 1 + x^2 \;) \\ B_2(x) &= x^4 \; / \; (\; 9 + 3x^2 + x^4 \;) \\ B_3(x) &= x^6 \; / \; (\; 225 + 45x^2 + 6x^4 + x^6 \;) \; . \end{aligned} \tag{10}$$

M is a constant, taken as 0.2 GeV. This corresponds to an interaction range of 1 fermi. This value of M is suggested by the Saclay elastic phase shift analysis[10]. Eqn. (9) is the appropriate form for the inelastic barrier[9], since (except for the value of M) it has the

same W and w dependence as the form used to extract the LBL-SLAC and π-solution T-matrix elements. (These original analyses used $B_L(x) = x^{2L}$, i.e. they essentially had M = ∞ instead of M = 0.2 GeV in determining their T-matrix elements.) The form of Eqn. (9) may be understood[9] as averaging the production barrier factor over the allowed values of the isobar's production mass.

For each wave, we have 9 'data' points, i.e. 9 values of T, corresponding to c.m. energies W = 1.65,1.69,1.73,1.77,1.81,1.85,1.89, 1.93 and 1.97 GeV. (These data are presented in references 1,2 and 7.) In order to emphasize those points near the resonant energy, we modify the errors by

$$\delta T(W) \longrightarrow \left| \frac{m_r - W - i\gamma_T/2}{-i\gamma_T/2} \right| \delta T(W) \qquad (11)$$

We also choose to fit only a few points near resonance, and not the full set of 9 points. This allows us to reasonably ignore energy dependence in the parameters A,ϕ,θ and z. (This restriction also lessens the importance of the barrier factors.) Most of our fits use only 3 to 5 data points. The number of degrees of freedom was $2N_{data} - N_{parameters}$ which is thus usually between 2 and 6.

The results tabulated in Table I are selected from many fits as most pleasing (optically and by χ^2). The statistical errors are

$$\delta\theta_{stat} \sim 5 - 10 \text{ degrees}$$

$$\delta z_{stat} \sim 0.04$$

The following facts should be noted:

A. The "coupling sign" used by Longacre et al.[8] is the sign of $\cos\theta$, when that sign is well determined (i.e. θ not near 90^{o}). We thus conclude that our re-analysis of the LBL-SLAC solution agrees with the analysis of Longacre et al.[8] whenever θ is far enough from 90^{o} to give meaning to the sign of the coupling.

B. The diameter of the resonance circle is $z=\sqrt{x_{el}x_{inel}}$. The agreement of our fit and that of Longacre et al.[8] in our analyses of the LBL-SLAC solution with respect to this magnitude is satisfying, though Longacre's fit[8] tends to diminish the strength of the F15 in a way not manifest in the data.

C. For the π -solution, the ρ_3(FP35) fit is not optically pleasing. While the phase of $\theta \sim 80^{o}$ from the fits is reasonable, the fits tend to enhance the size of the resonant circle (to a diameter of 0.2 rather than an optically pleasing diameter of about 0.1). The fit diameter of $\sqrt{x_{el}x_{inel}} = 0.2$ implies $\gamma_{inel} = 0.07$ GeV, while the optically pleasing diameter $\sqrt{x_{el}x_{inel}} = 0.02$ implies $\gamma_{inel} = 0.02$ GeV. Since the χ^2 are large in the fits to this wave, we do not enter a favored value into the π -solution column of Table I, but include both values of $\sqrt{x_{el}x_{inel}}$ in determining the allowed range of values of $\sqrt{x_{el}x_{inel}}$.

For Δ(FF37), the solution presented in Table I has a larger resonant circle than one might have expected by inspection of the T-matrix parameters. A value of $\sqrt{x_{el}x_{inel}} = 0.25$ (giving

γ_{inel} = 0.036 GeV) might be just as good optically, though its χ^2 is worse. (We also find that the W=1.97 GeV data point does not fit in well with the expected resonant circle. Possible deficiencies at this energy are discussed in more detail in reference 1. The same doubts about the W=1.97 GeV data point exist for the ρ_3(FF37) wave as well.)

For ρ_3(FF37), an estimate of the coupling from inspection of the T-parameters gives $\sqrt{x_{el}x_{inel}}$ = 0.27 (i.e. γ_{inel}= 0.042 GeV). This is somewhat smaller than the results of the χ^2 minimization technique whose results are given in Table I. Clearly the results of these fits for the π-solution cannot be exactly correct, since the sum of the partial widths for this wave is greater than the total width.

D. In comparing our fits to the two solutions (LBL-SLAC and π-), we find remarkable agreement in the phase of four waves. However the ρ_3(FP35) is 90^o out of phase between the two solutions. Most of the magnitudes differ (- see especially discussion above -), which suggests that a proper estimation of the errors involved is given by considering the range of values of $\sqrt{x_{el}x_{inel}}$, as tabulated in Table I. However the Δ(FF35) is considerably (-a factor of almost 3 in $\sqrt{x_{el}x_{inel}}$ -) less strongly coupled in the π -solution.

E. Note that both solutions share the puzzling 90^o rotation of the F37 waves. The naïve expectation would be that

$$T(W=m_r) = i\sqrt{x_{el}x_{inel}}$$

i.e. purely imaginary at resonance. Though the representation of Eqn. (5) encourages rotation of the amplitude at resonance to

$$T(W=m_r) = \tfrac{1}{2} \cos^2 A\, e^{i\phi} + e^{i\theta}\, i\sqrt{x_{el}x_{inel}}$$

the absense of practically all of the imaginary part of T at resonance requires a conspiracy of the parameters via a strong background contribution. The presence of a strong background is surprising for a high partial wave like the F37. For the ρ_3(FF37) case, the fit to the π-solution has

$$T_{background}(W=m_r) = -0.2 - 0.1\, i$$

$$T_{resonance}(W=m_r) = 0.4 + 0.2\, i$$

In reference 1 it was noted that the amplitude is predominantly real at resonance, and we suggested possible $N^*(1688)$ production mechanisms as disturbing the fit. In the language of Eqn. (5), we see that a strong background exists, and we again suggest that this background might be due to the production of N^* isobars which has been ignored in the original fits[1,2].

By comparing the results of the analyses for $\sqrt{x_{el}x_{inel}}$, we see that the discrepancies are large. The differences are even larger when γ_{inel} is derived, since $\gamma_{inel} \propto (\sqrt{x_{el}x_{inel}})^2$. The reasonableness of such large uncertainties in these parameters is immediately obvious when we inspect the Argand (or T-matrix element) plots from which they come[1,2,7]. The jagged nature of both LBL-SLAC and π -solutions requires large uncertainties when extracting parameters by smooth parameterizations, such as the parameterization of Eqn. (5). In using

any results from smoothly parameterizing these inelastic phase shift solutions, we suggest that the statistical errors ($\delta\sqrt{x_{el}x_{inel}} \sim 0.04$) should be used only as a lower limit. A more reasonable approach is to quote a range of allowed values of this coupling strength, as determined by the range of values from all fits to both inelastic phase shift solutions. We present in Table I this range of values. (We have included the results of methods II and III of Longacre et al.[8] in determining this range of values.)

II. The P31 wave: resonant or non-resonant

In this section we discuss the P31 waves. The Δ(PP31) does not exhibit resonant activity for either the LBL-SLAC or π-solution. The ρ_3(PP31) does not vary much above 1.77 GeV in the LBL-SLAC solution. However it does have variation with energy in the π-solution. The elastic phase shift analyses[12,13] cannot guide us with values for the resonant mass and widths for the P31, since the values vary between m_r= 1.9 GeV, γ_T= 0.2 GeV, γ_{el}= 0.067 GeV for the CERN analysis[13] and m_r= 1.786 GeV, γ_T= 0.222 GeV, γ_{el}= 0.036 GeV for the Saclay elastic phase shift analysis[12]. Our attempts to fit the π-solution with these values and Eqn.(5) were not very successful, as they resulted in large χ^2 and optically poor fits.

We therefore restrict ourselves to estimating $\sqrt{x_{el}x_{inel}}$ by measuring the diameter of a likely resonant circle, and giving a reasonable estimate of the resonant mass from the region of the loop with the fastest variation with energy. This estimate is given in figure 2b. We find that a resonant loop through the T-matrix elements with greatest energy variation gives $\sqrt{x_{el}x_{inel}} \sim 0.17$. Since the wave varies most between 1.81 and 1.85 GeV, we feel that a good estimate of the resonant mass is $m_r \sim$ 1.82 GeV. The appropriate rotation angle is $\theta \sim 0^o$, which gives a positive sign to the inelastic coupling. To convert to the baryon-first convention requires an additional $(-)^{L'}$ for ρ-isobars, i.e. an additional - sign. Thus the coupling is negative in the baryon-first sign convention. The sign predicted by $SU(6)_W$ is[14] + for the $\underset{\sim}{56}_{L=2}$ representation, and - for the $\underset{\sim}{70}_{L=0}$ representation. Our

analysis thus implies a classification or a coupling for the P31 that disagrees with the conventional ones[15]. (We caution, however, that different estimates of the mass of the resonance and the size and orientation of the resonance loop can be made. For example, a resonance mass of 1.78 GeV would not be in terrible conflict with figure 2b, and would have an orientation of $\theta \sim 90^{\circ}$, i.e. an ill-defined coupling sign.)

Finally, we caution that our resonant interpretation depends crucially on the 1.81 GeV point, which has

$$|T| = 0.075$$

This is not a large wave, and if all the errors conspired against us, the resonant effect could be easily eradicated.

References

1. D. Novoseller, thesis, part 1 (1977) and CALT-68-596 (California Institute of Technology report, 1977). The inelastic phase shift solution presented in these works will be referred to as the π - solution.
2. D. Herndon et al., Phys. Rev. D11 (1975) 3183. The inelastic phase shift analysis presented in this work will be referred to as the LBL-SLAC solution.
3. D. Novoseller, Manual for TRIANGLE 2, CALT-68-572 (California Institute of Technology report, 1976).
4. D. Herndon, P. Söding and R. Cashmore, Phys. Rev.D11 (1975) 3165.
5. A. Rosenfeld et al., Phys. Letters 55B (1975) 486.
6. D. Herndon et al., Supplement to SLAC-PUB-1108-revised. (Stanford Linear Accelerator Center report, unpublished supplement to reference 2, 1974).
7. D. Novoseller, thesis, appendix (1977).
8. R. Longacre et al., Phys. Letters 55B (1975) 415.
9. R. Longacre, thesis, LBL-948 (Lawrence Berkeley Laboratory report, 1973).
10. R. Ayed and P. Bareyre, paper presented at Second International Conference on Elementary Particles,(Aix-en-Provence, 1973, unpublished), and 1973 Phase Shifts (unpublished tables, Saclay).
11. S. Almehed and C. Lovelace, Nucl. Phys. B40 (1972) 157, and CERN-TH-1408 (unpublished tables, CERN, 1972).

12. J. Blatt and V. F. Weisskopf, Theoretical Nuclear Physics (Wiley, New York, 1952) especially page 361.

13. F. von Hippel and C. Quigg, Phys. Rev. D5 (1972) 624.

14. D. Faiman, Nucl. Phys. B77 (1974) 443 and Nucl. Phys. B109 (1976) 286.

15. J. Rosner, Phys. Reports 11C (1974) 189.

Figure Captions

1. T-matrix parameters for the Δ(PP33) wave from the π -solution. Presented are the data (labelled by F, G, H, I corresponding to c.m. energies 1.85, 1.89, 1.93 and 1.97 GeV respectively), and a sample fit (the solid curve, with energies at the points P, Q, R, S corresponding to those at the data points F, G, H, I respectively). The fit is further decomposed into the (essentially constant) background, labelled B, and the resonant contribution, again with points P, Q, R, S, but now connected by a dotted line. The resonant mass was taken as 1.90 GeV.

2. T-matrix parameters for the ρ_1(PP31) wave. The letters A, B, ... I correspond to the energies 1.65, 1.69, ... 1.97 GeV (at intervals of 0.04 GeV), with upper case letters corresponding to the non-resonant LBL-SLAC solution (figure 2a), and lower case letters to the π -solution (figure 2b). The errors in figure 2a are omitted for clarity of the figure, and are between 0.03 and 0.04. The lines connecting the various energies in figure 2a are included to guide the eye in searching for rapid variation with energy. The curve in figure 2b corresponds to the resonant circle described in section II of the text.

			Fits to LBL-SLAC solution[2]						Fits to π-solution[1]			Range of results
			Longacre et al.[8] Method I			This analysis			This analysis			
wave	m_r (GeV/c^2)	γ_T (GeV)	$\sqrt{x_{el}x_{inel}}$	γ_{inel} (GeV)	(γ_{el}) (GeV)	$\sqrt{x_{el}x_{inel}}$	θ (°)	γ_{inel} (GeV)	$\sqrt{x_{el}x_{inel}}$	θ (°)	γ_{inel} (GeV)	$\sqrt{x_{el}x_{inel}}$
Δ(DD15)	1.66	0.145	+0.45	0.072	0.059	0.5	- 18	0.087				
Δ(FP15)	1.68	0.125	-0.26	0.014	0.074	0.38	174	0.03				
Δ(FF15)	1.68	0.125	0	0	0.074	0.05	- 40	0				
ρ_3(FP15)	1.68	0.125	-0.27	0.015	0.074	0.34	-170	0.024				
ε(FD15)	1.68	0.125	-0.28	0.016	0.074	0.42	174	0.037				
Δ(PP33)	1.90	0.205	-0.36	0.140	0.039	0.3	-102	0.1	0.27	- 76	0.08	0.27-0.36
Δ(FF35)	1.87	0.255	-0.12	0.026	0.036	0.17	-160	0.05	0.06	-170	0.007	0.06-0.20
ρ_3(FP35)	1.87	0.255	+0.28	0.143	0.036	0.26	- 2	0.123	see discussion			0.11-0.33
Δ(FF37)	1.93	0.235	-0.25	0.036	0.096	0.21	- 70	0.025	0.38	- 62	0.083	0.21-0.38
ρ_3(FF37)	1.93	0.235	±0.18	0.019	0.096	0.24	- 50	0.033	0.43	- 63	0.106	0.18-0.43

Table I: Results of fits to resonance parameters, determined from LBL-SLAC[2,6] and π-solutions to πN inelastic scattering amplitudes. Note that the coupling signs are in the isobar model convention[4]. To convert to the baryon first convention, multiply Δ isobar amplitudes by $(-)^{I+\frac{1}{2}}$ and the ρ and ε isobar amplitudes by $(-)^{L'}$.

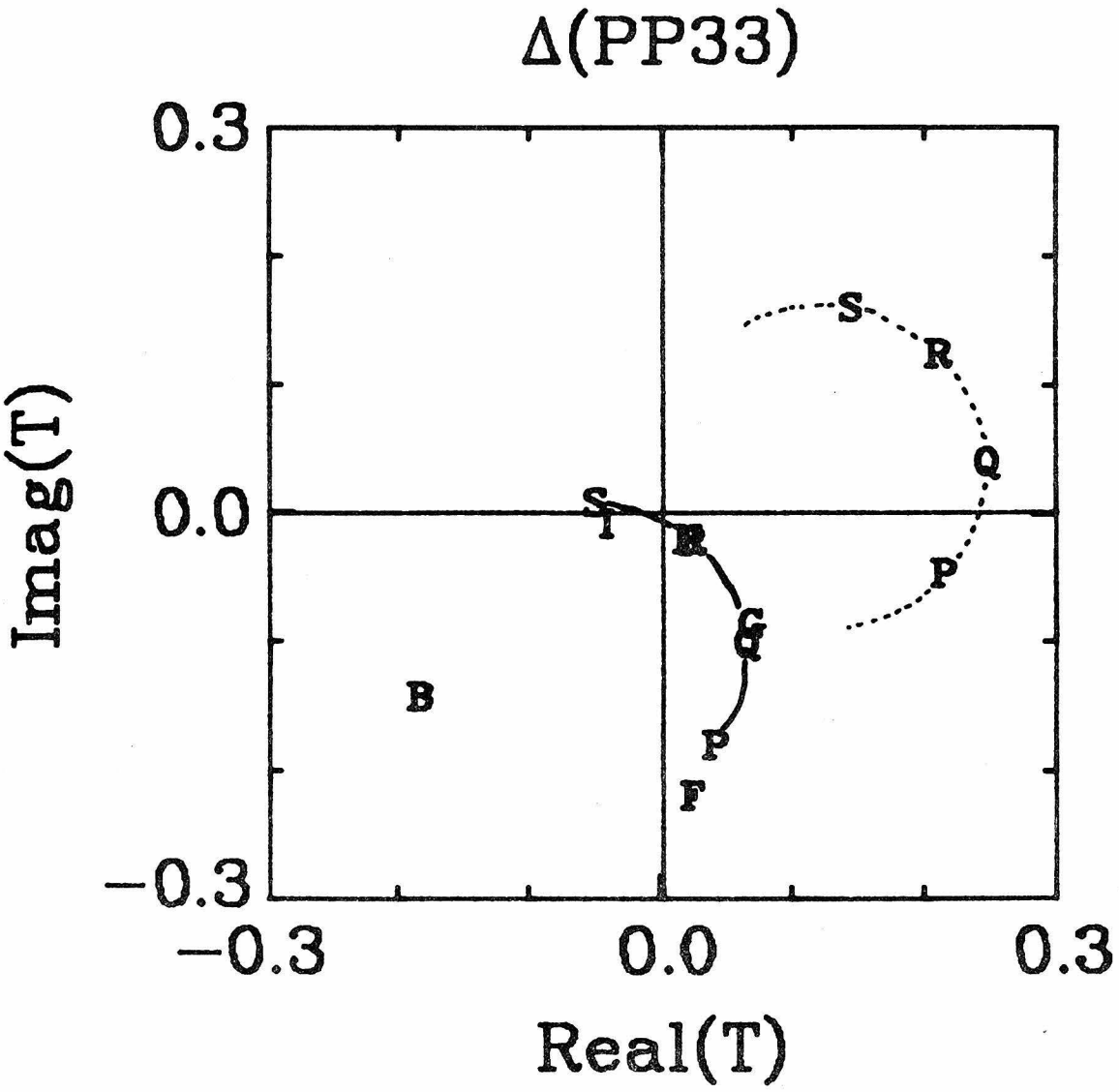


Fig. 1

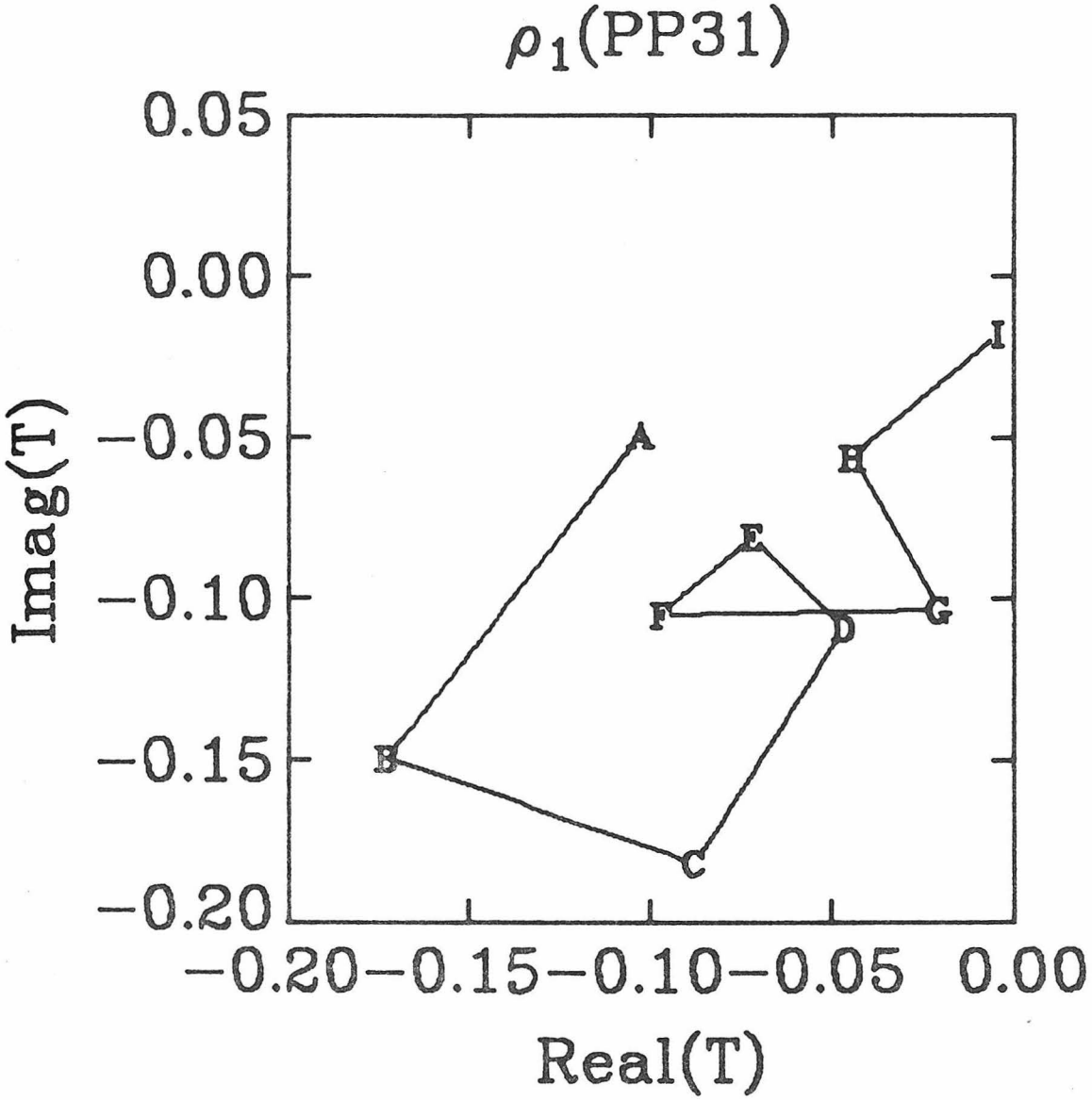

ρ_1(PP31)
0.05
0.00
−0.05
−0.10
−0.15
−0.20
Imag(T)
−0.20−0.15−0.10−0.05 0.00
Real(T)
A
B
C
D
E
F
G
H
I

Fig. 2a

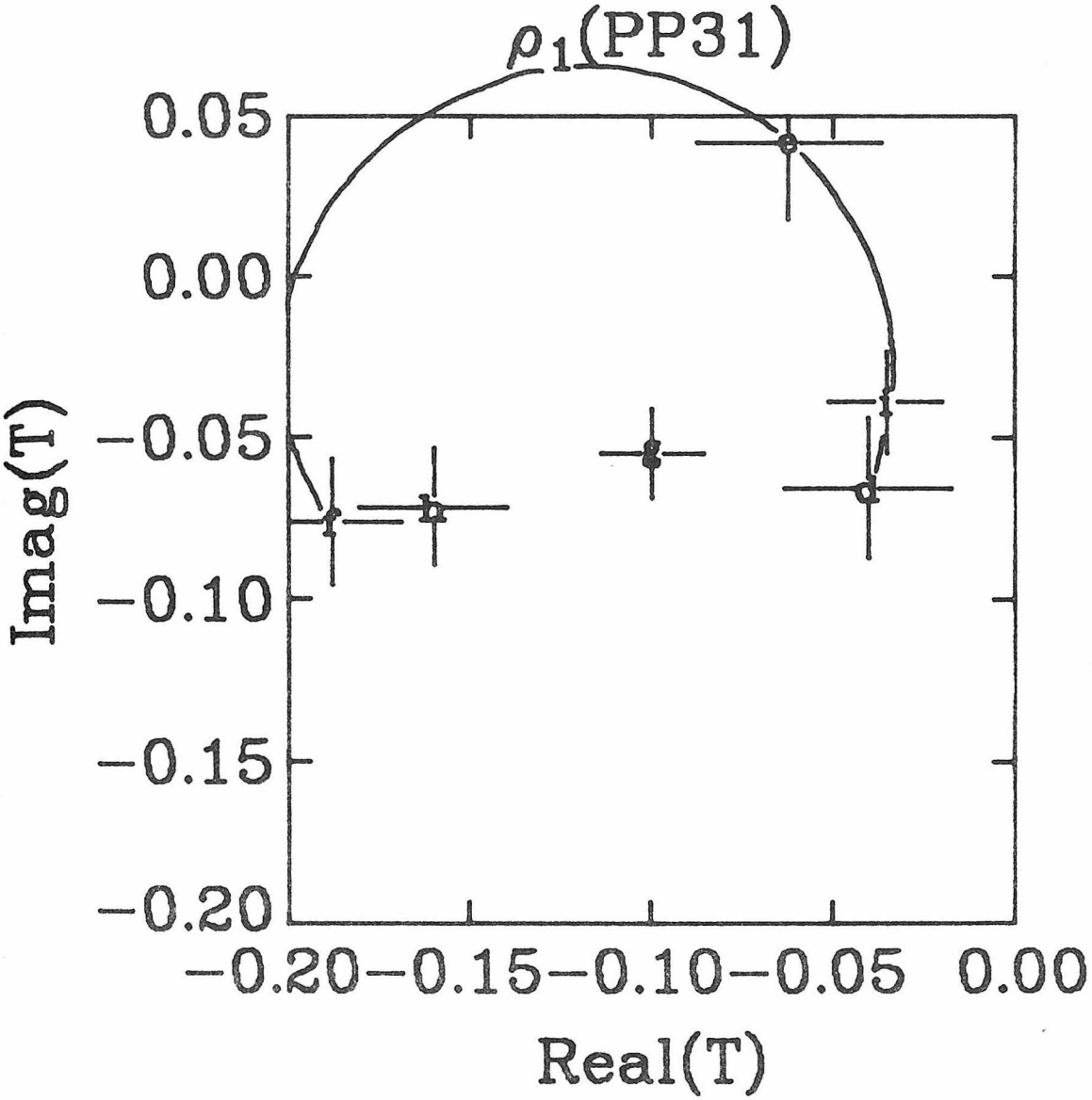

ρ_1(PP31)
0.05
0.00
−0.05
−0.10
−0.15
−0.20
Imag(T)
−0.20−0.15−0.10−0.05 0.00
Real(T)

Fig. 2b

APPENDICES

Appendix 1: $d\sigma/d\cos\Theta_\pi$ and $d\sigma/dw_{\pi\pi}$ distributions for the high partial wave π-exchange input in the $\pi^- p \to n\pi^-\pi^+$ channel. For this channel,

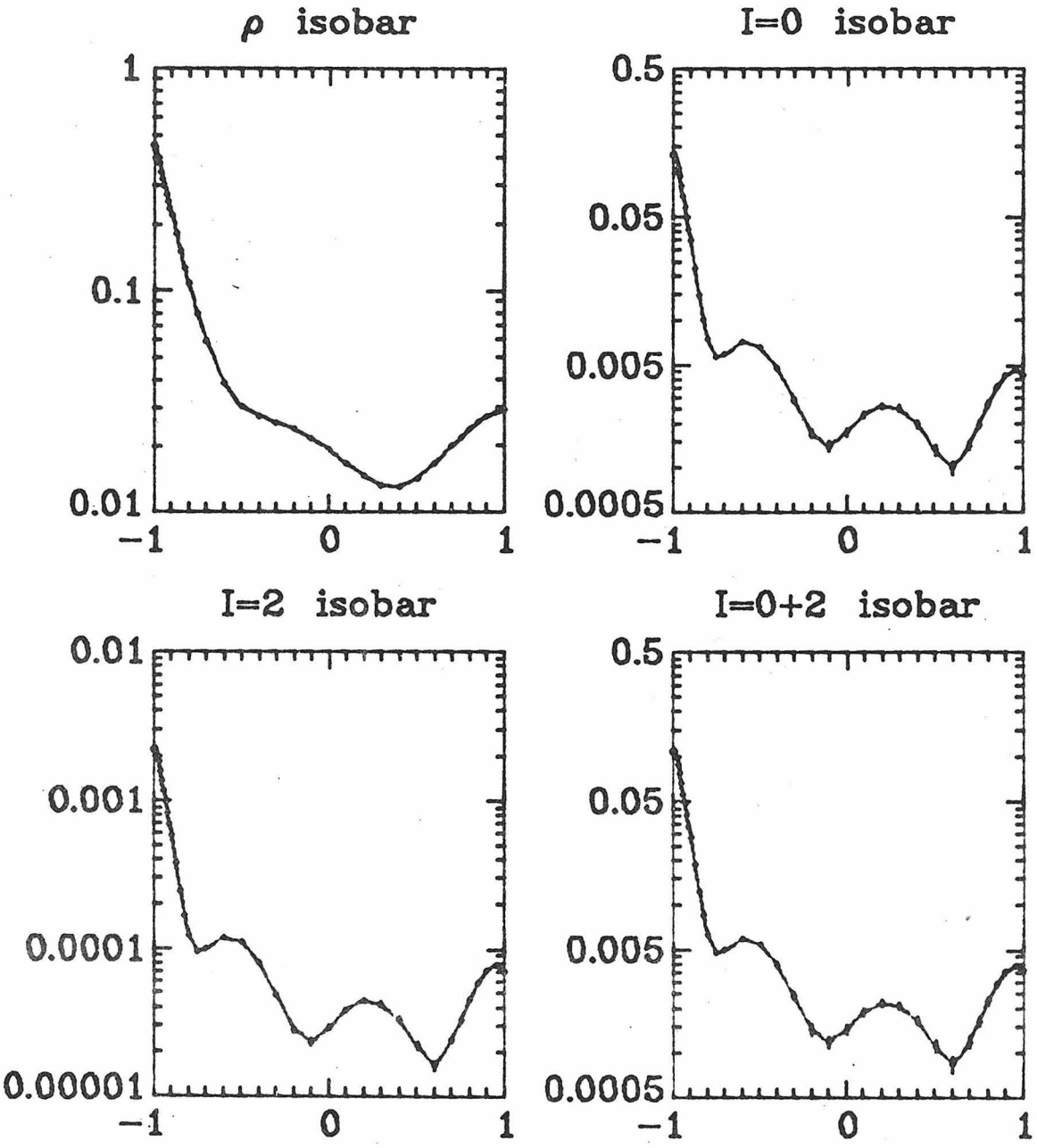
$$\frac{d\sigma^{(\text{all isobars})}}{d\cos\Theta_\pi} = \frac{d\sigma^{(\rho)}}{d\cos\Theta_\pi} + \frac{d\sigma^{(I=0+2)}}{d\cos\Theta_\pi} \quad .$$

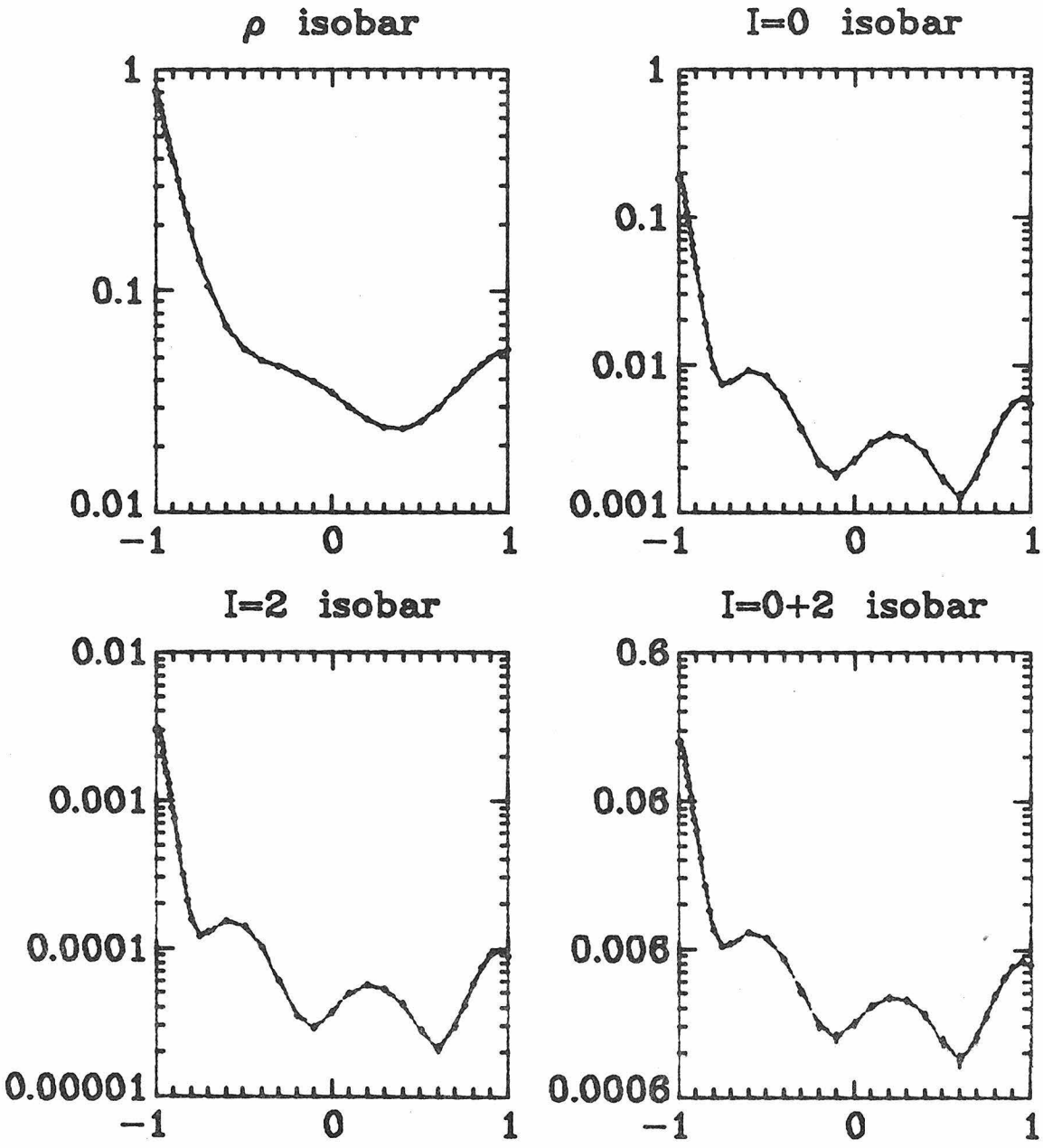
For the $\pi^\pm p \to p\pi^\pm\pi^o$ channels,

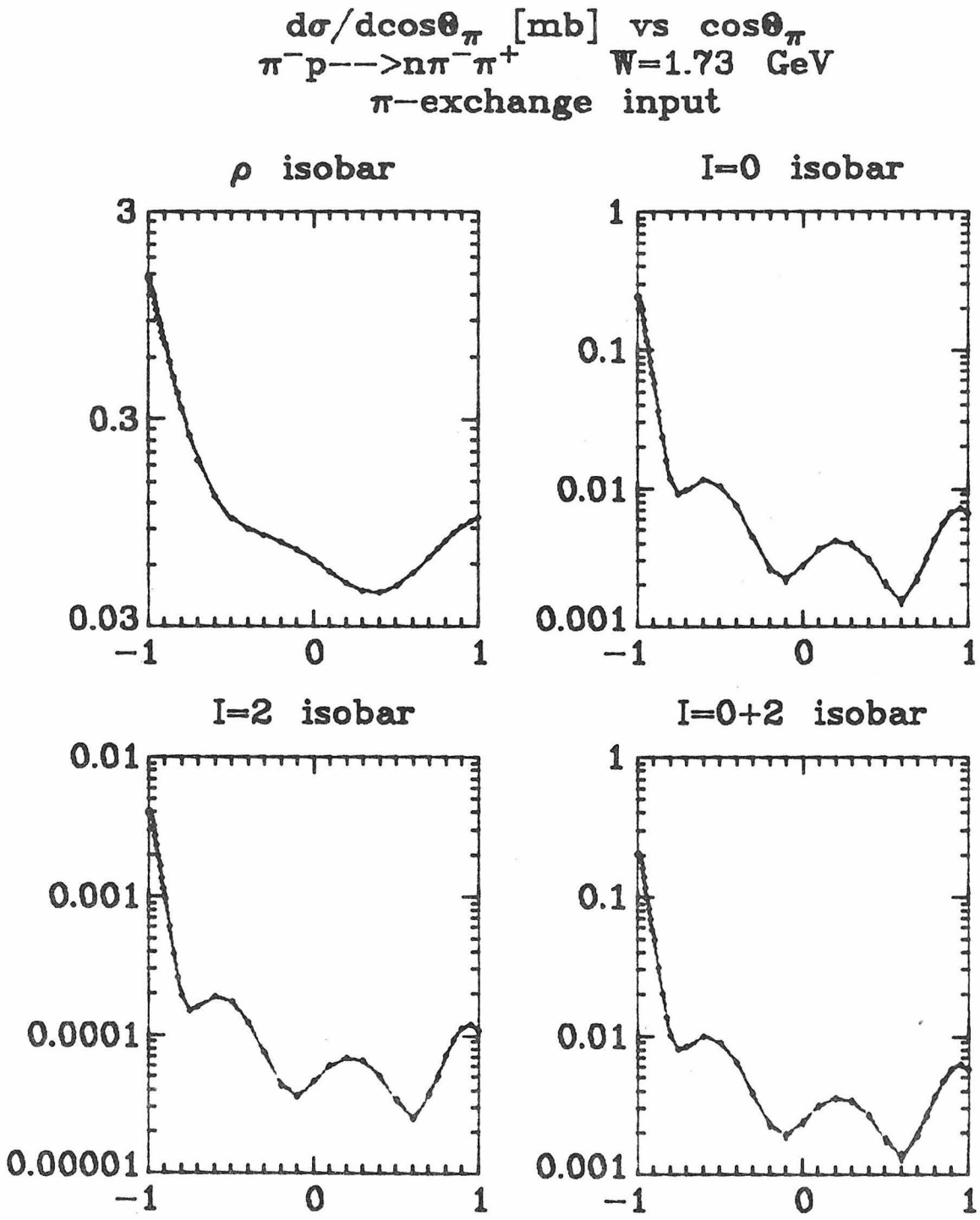
$$\frac{d\sigma^{(\text{all isobars})}}{d\cos\Theta_\pi} = \frac{1}{2}\frac{d\sigma^{(\rho)}}{d\cos\Theta_\pi} + \frac{9}{2}\frac{d\sigma^{(I=2)}}{d\cos\Theta_\pi} \quad .$$

Similar expressions hold for the invariant mass ($w_{\pi\pi}$) distributions.

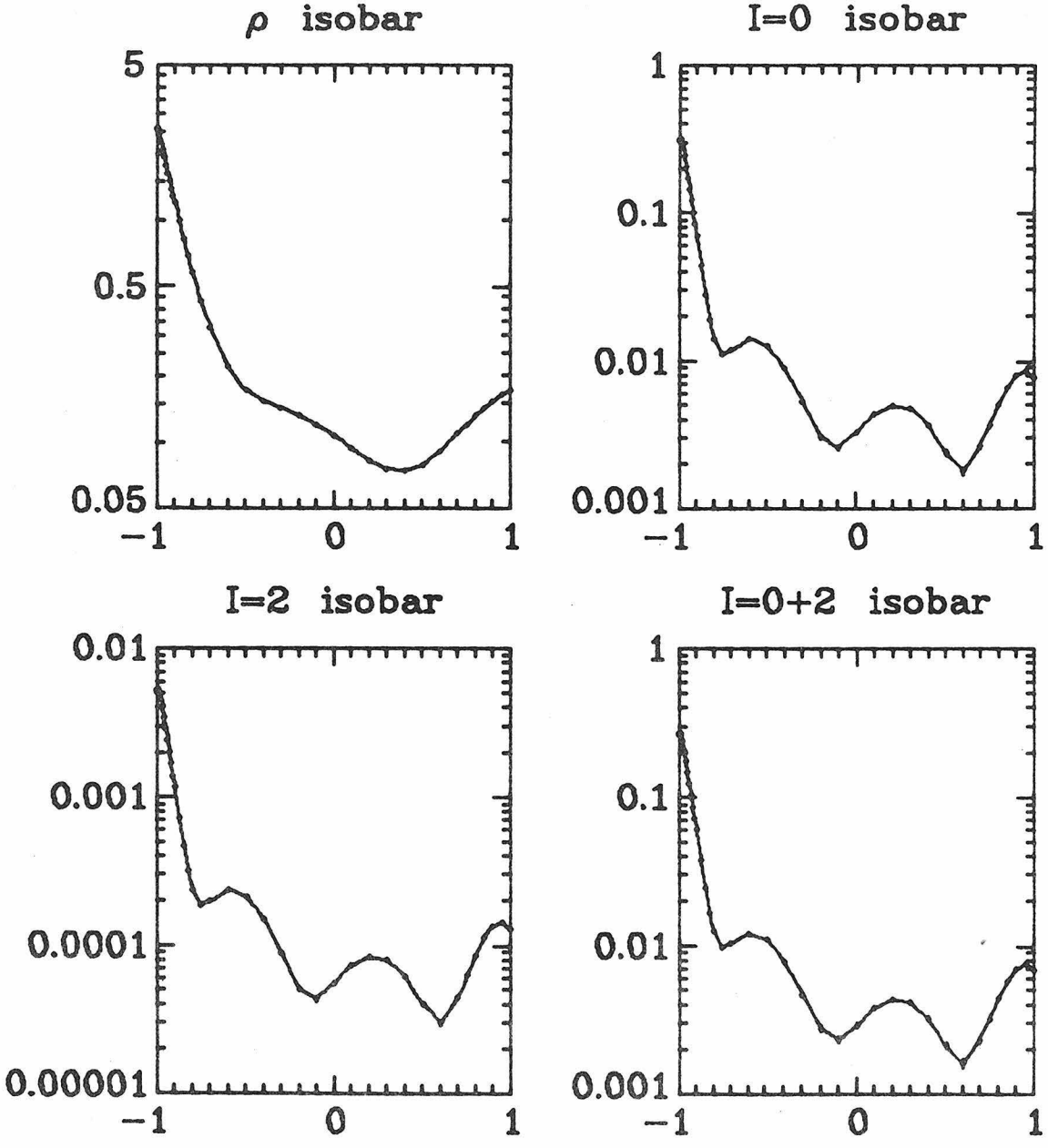
$d\sigma/d\cos\theta_\pi$ [mb] vs $\cos\theta_\pi$
$\pi^- p \rightarrow n\pi^-\pi^+$ W=1.65 GeV
π-exchange input



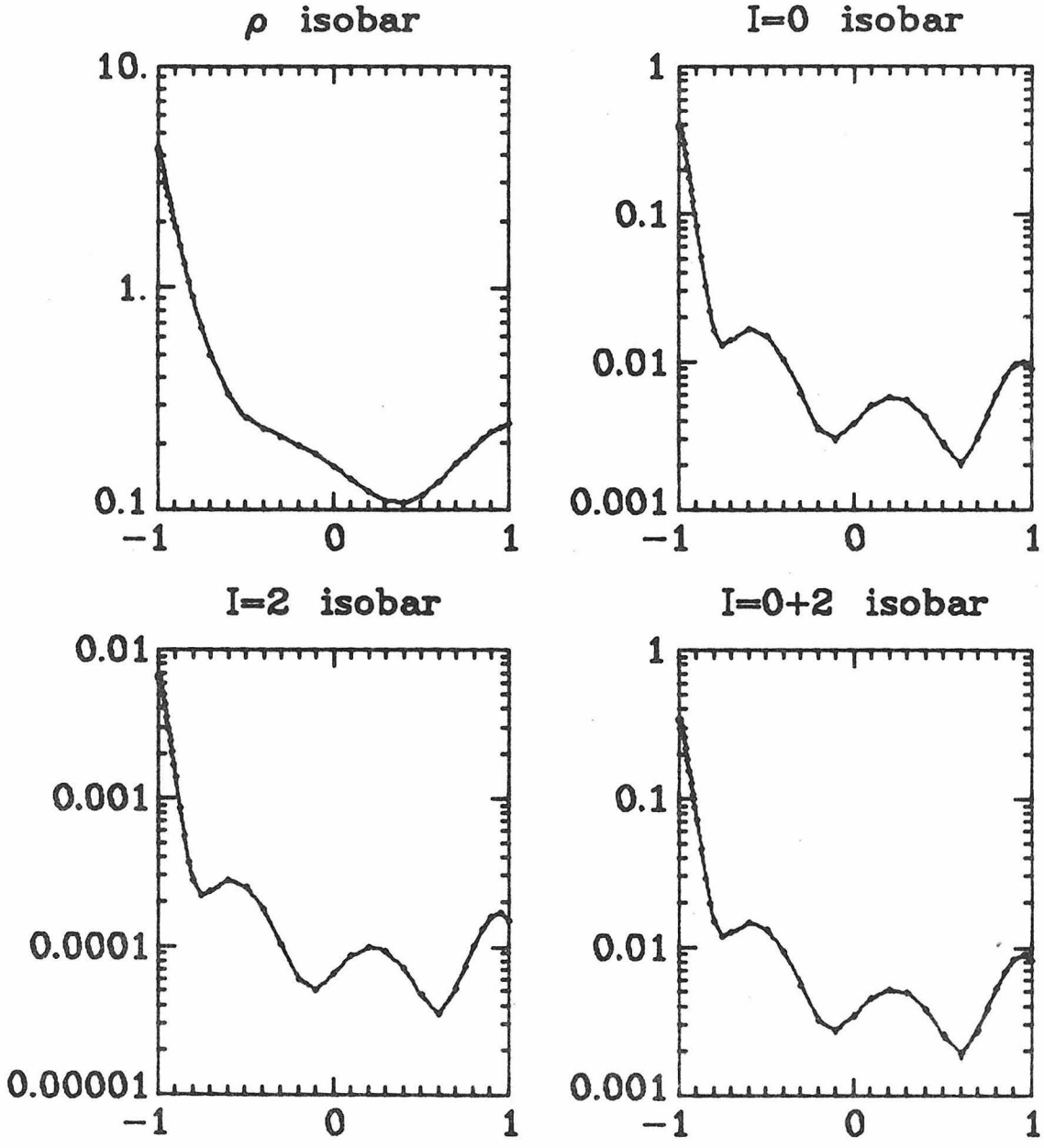

dσ/dcosθ$_\pi$ [mb] vs cosθ$_\pi$
π⁻p-->nπ⁻π⁺ W=1.69 GeV
π-exchange input
ρ isobar
I=0 isobar
I=2 isobar
I=0+2 isobar
1
0.1
0.01
0.001
0.0001
0.00001
0.6
0.06
0.006
0.0006
-1
0
1


dσ/dcosθ_π [mb] vs cosθ_π
π⁻p--->nπ⁻π⁺ W=1.73 GeV
π-exchange input
ρ isobar
I=0 isobar
I=2 isobar
I=0+2 isobar
3
0.3
0.03
1
0.1
0.01
0.001
0.01
0.001
0.0001
0.00001
1
0.1
0.01
0.001
-1
0
1

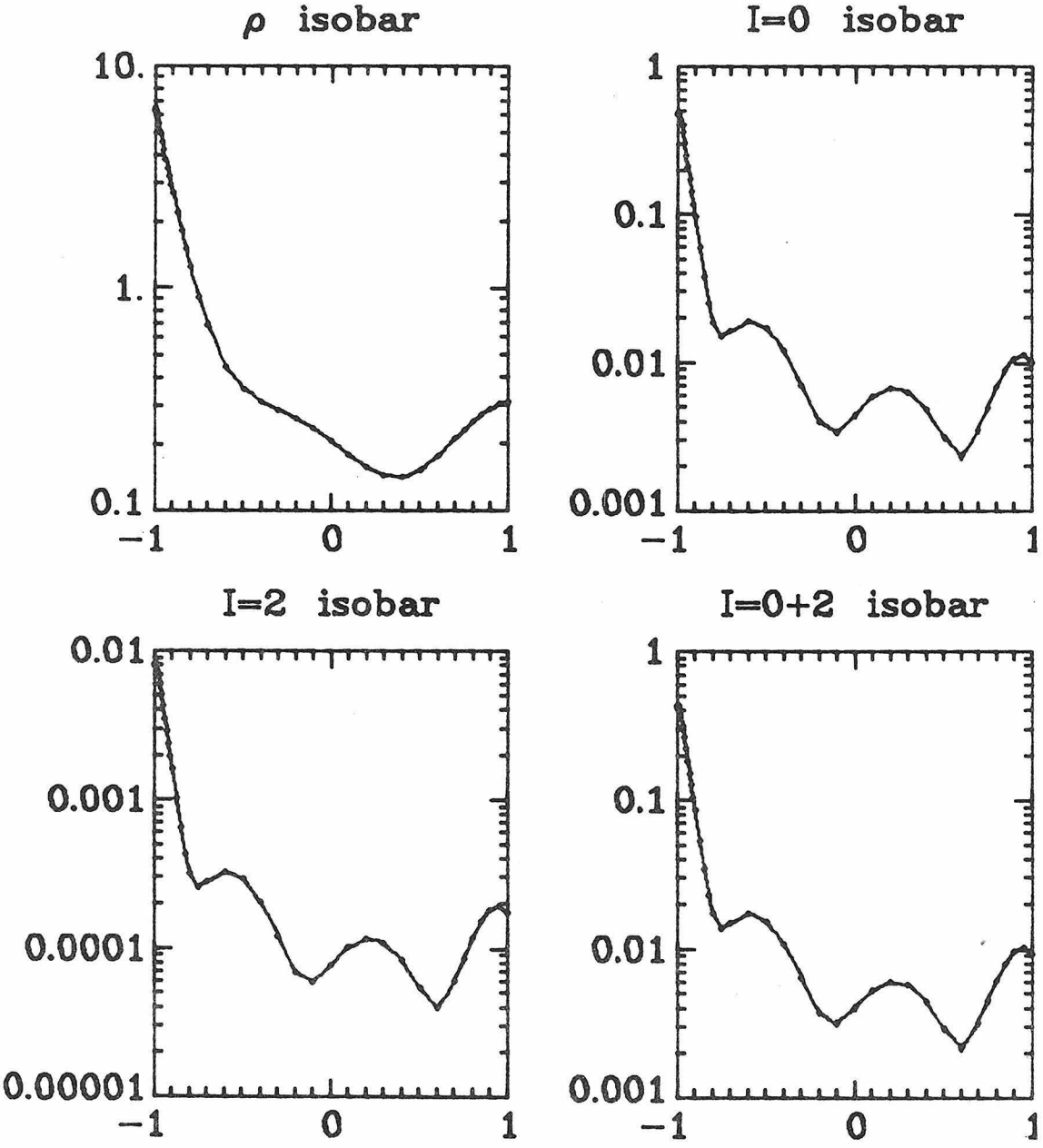
$d\sigma/d\cos\theta_\pi$ [mb] vs $\cos\theta_\pi$
$\pi^- p \to n\pi^-\pi^+$ W=1.77 GeV
π-exchange input

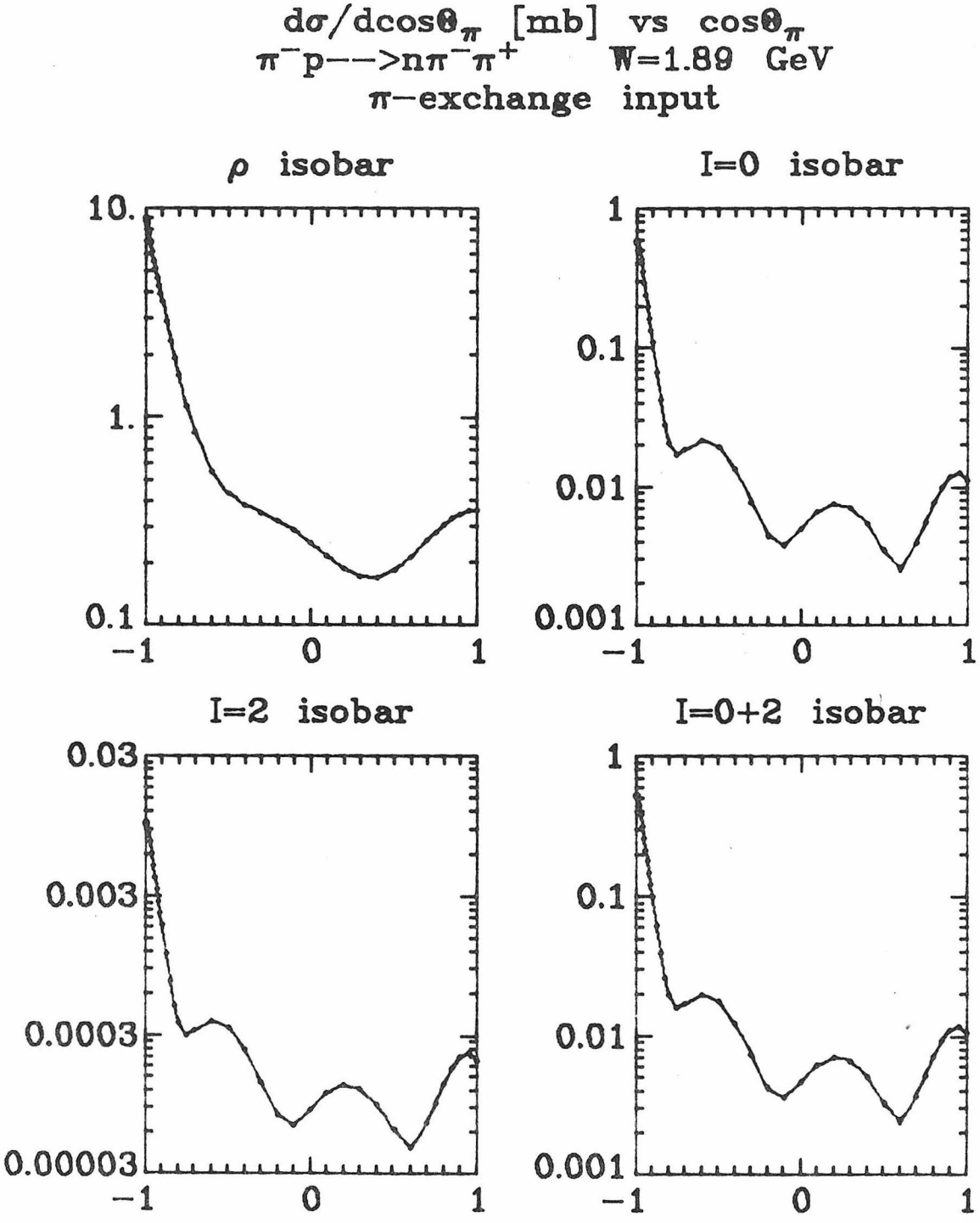


$d\sigma/d\cos\theta_\pi$ [mb] vs $\cos\theta_\pi$
$\pi^- p \rightarrow n\pi^-\pi^+$ W=1.81 GeV
π-exchange input

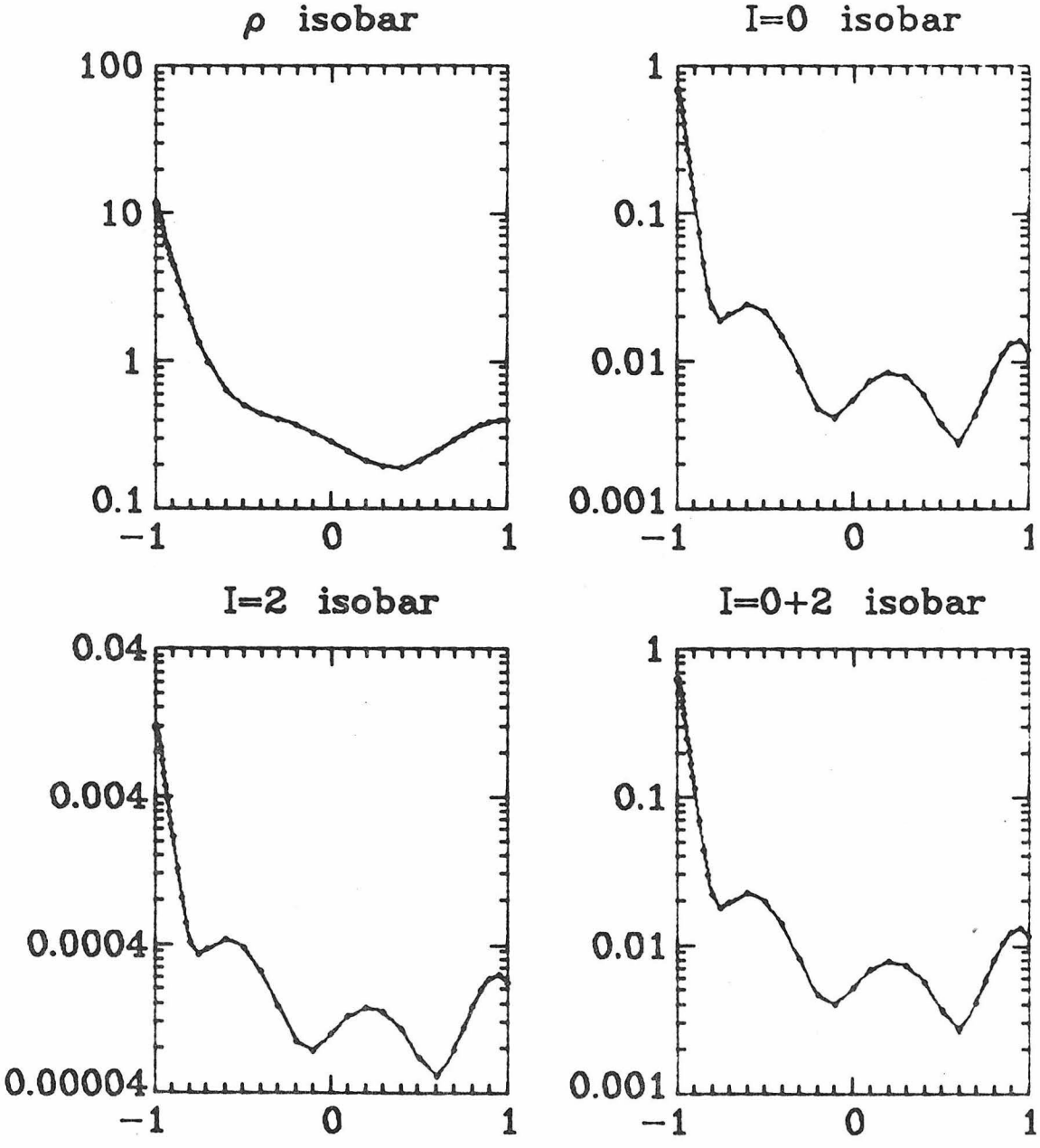


$d\sigma/d\cos\theta_\pi$ [mb] vs $\cos\theta_\pi$
$\pi^- p \rightarrow n\pi^-\pi^+$ W=1.85 GeV
π-exchange input

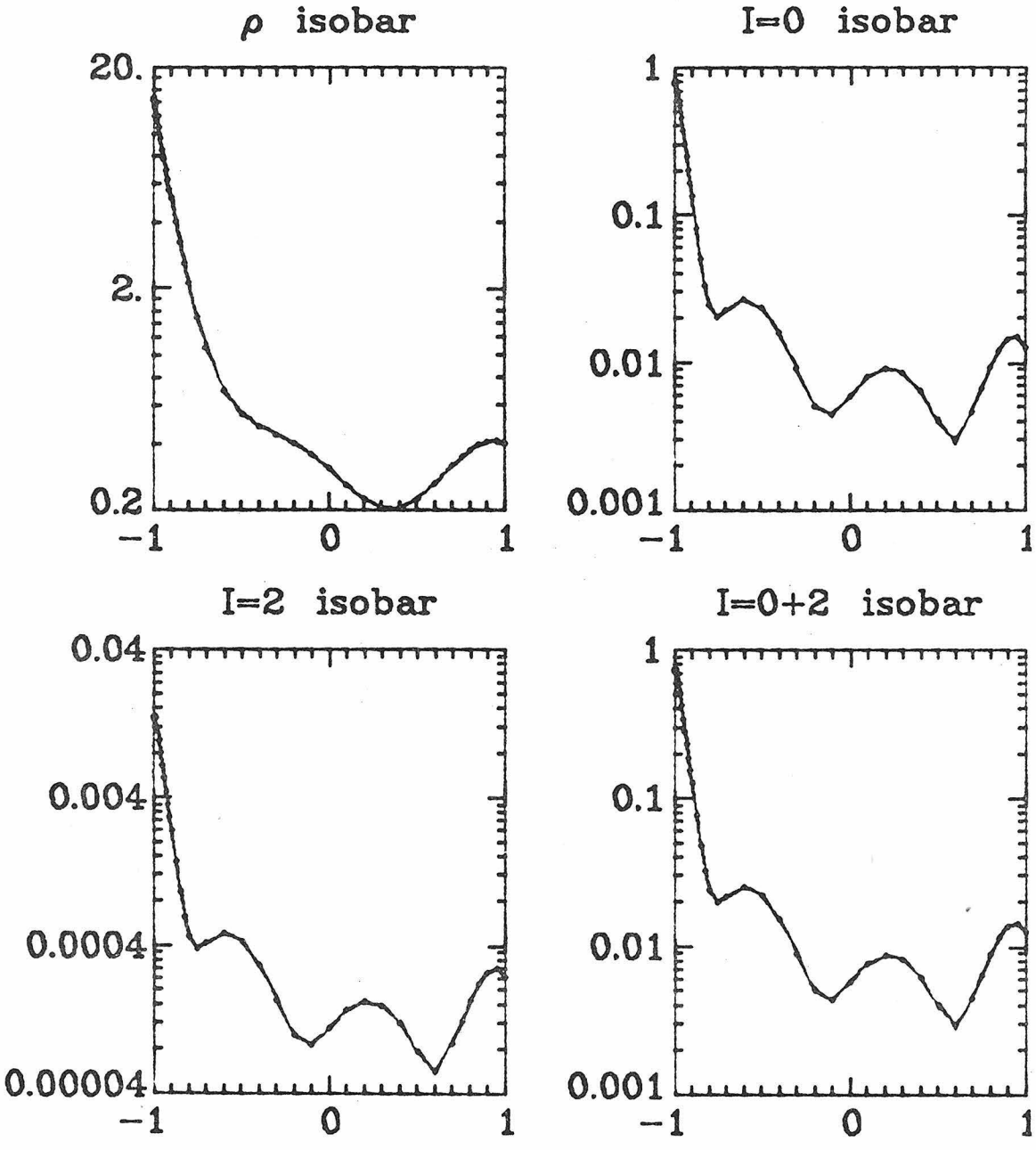



dσ/dcosθ_π [mb] vs cosθ_π
π⁻p−−>nπ⁻π⁺ W=1.89 GeV
π−exchange input
ρ isobar
I=0 isobar
I=2 isobar
I=0+2 isobar
10.
1.
0.1
1
0.1
0.01
0.001
0.03
0.003
0.0003
0.00003
−1
0
1

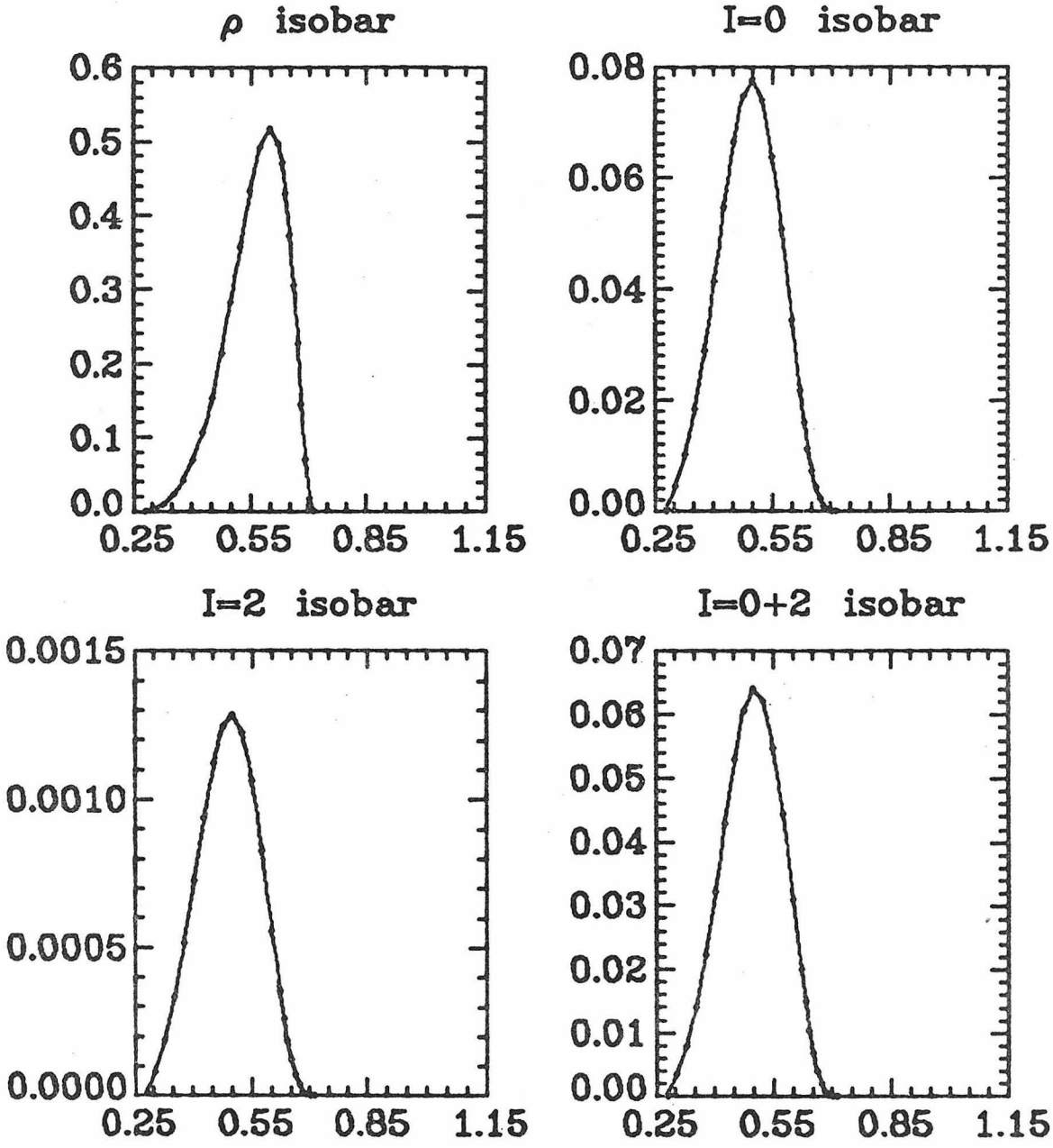
$d\sigma/d\cos\theta_\pi$ [mb] vs $\cos\theta_\pi$
$\pi^- p \to n\pi^-\pi^+$ W=1.93 GeV
π-exchange input

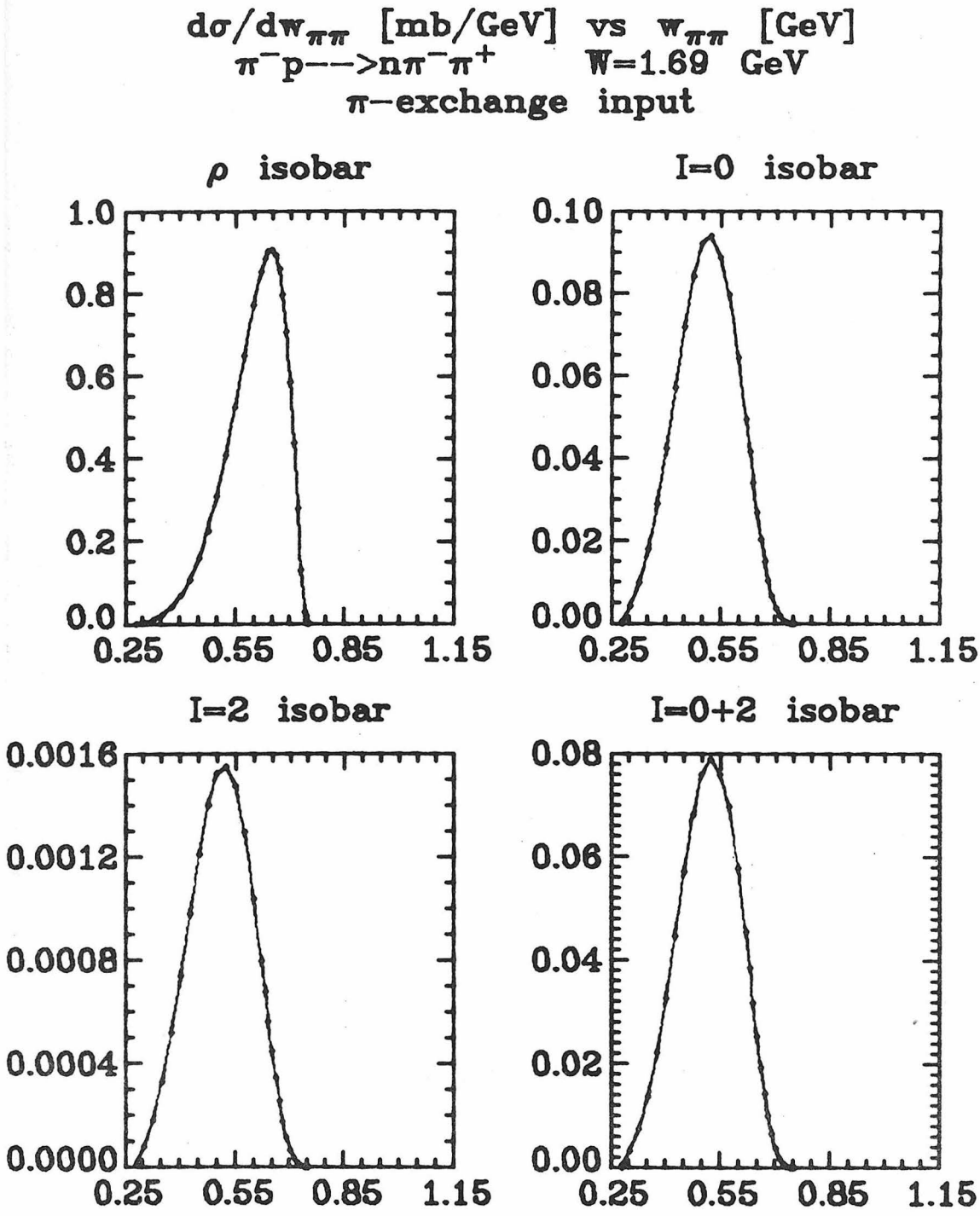


$d\sigma/d\cos\theta_\pi$ [mb] vs $\cos\theta_\pi$
$\pi^- p \to n\pi^-\pi^+$ W=1.97 GeV
π-exchange input

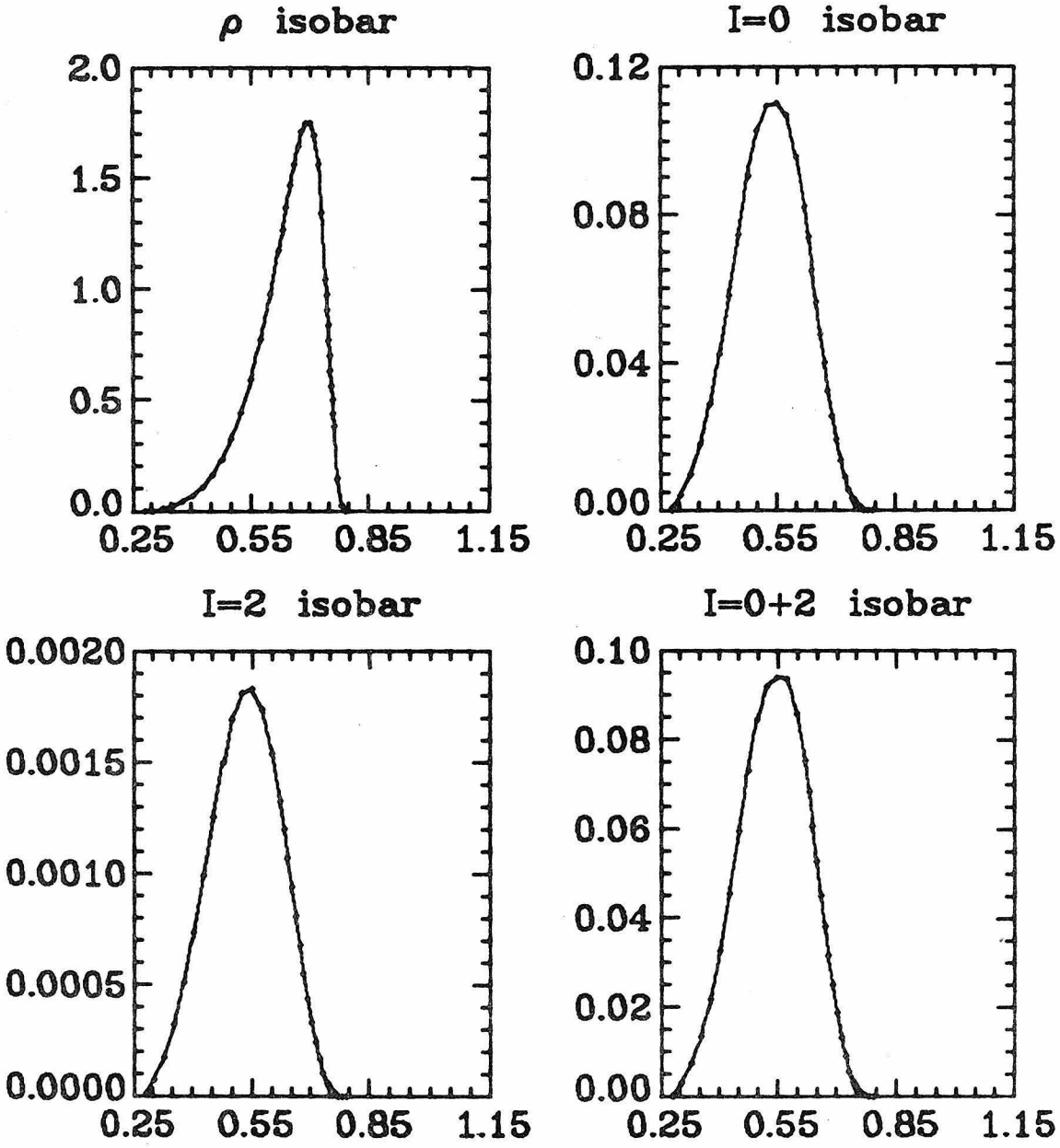


$d\sigma/dw_{\pi\pi}$ [mb/GeV] vs $w_{\pi\pi}$ [GeV]
$\pi^- p \rightarrow n\pi^-\pi^+$ W=1.65 GeV
π-exchange input

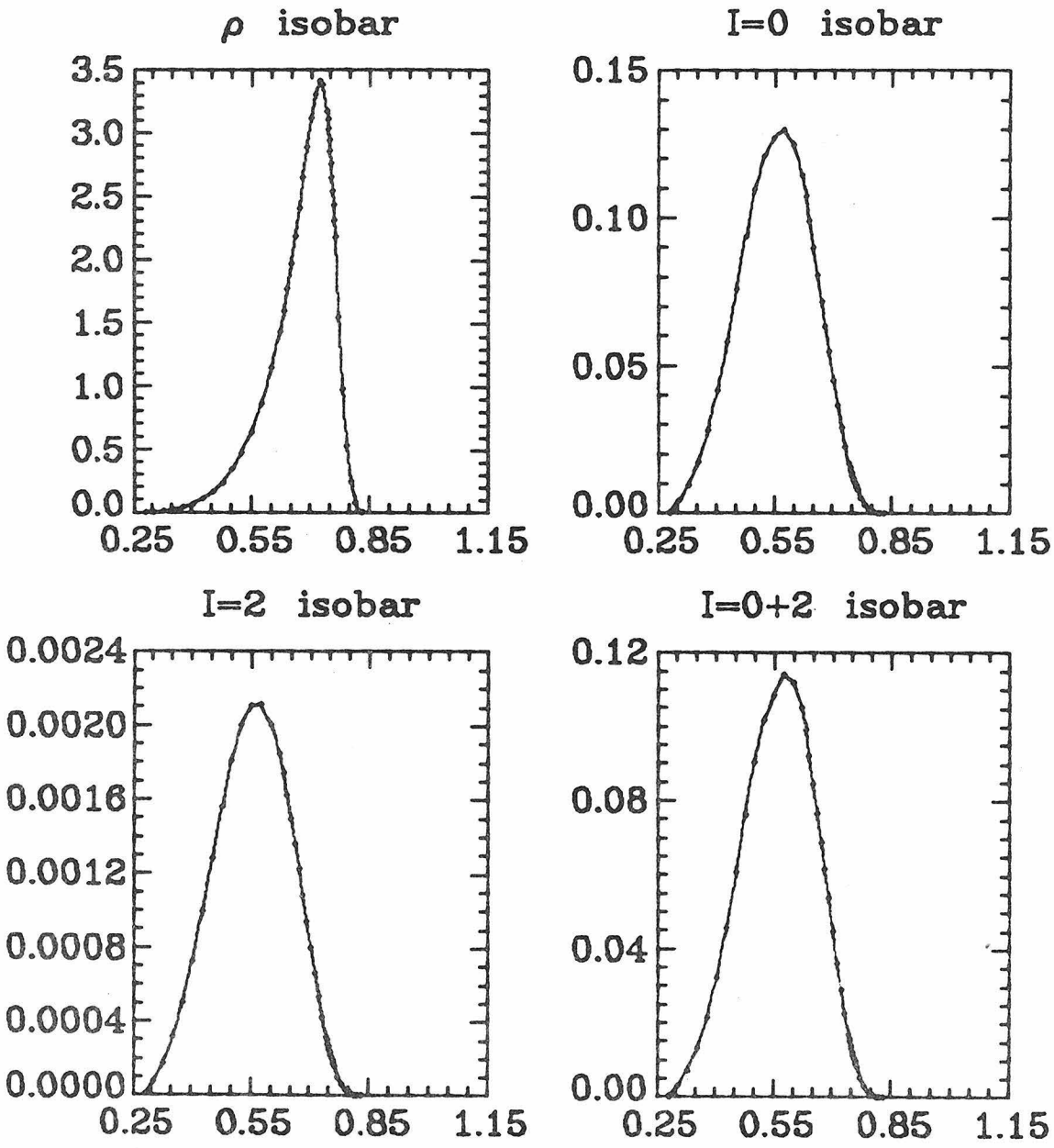



dσ/dw_ππ [mb/GeV] vs w_ππ [GeV]
π⁻p−−>nπ⁻π⁺ W=1.69 GeV
π−exchange input
ρ isobar
I=0 isobar
I=2 isobar
I=0+2 isobar
1.0
0.8
0.6
0.4
0.2
0.0
0.10
0.08
0.06
0.04
0.02
0.00
0.0016
0.0012
0.0008
0.0004
0.0000
0.08
0.06
0.04
0.02
0.00
0.25
0.55
0.85
1.15

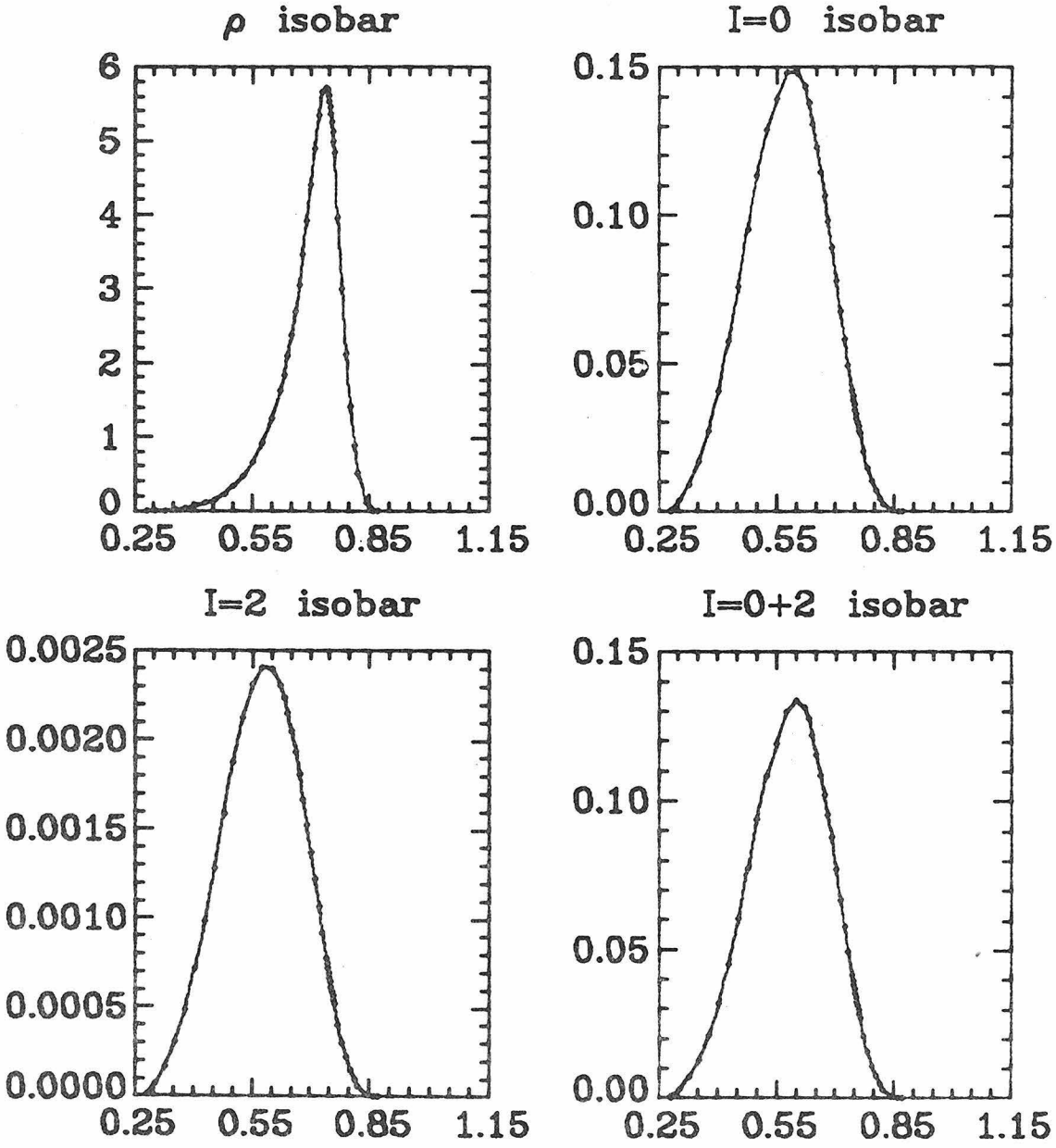
$d\sigma/dw_{\pi\pi}$ [mb/GeV] vs $w_{\pi\pi}$ [GeV]
$\pi^- p \rightarrow n\pi^-\pi^+$ W=1.73 GeV
π-exchange input

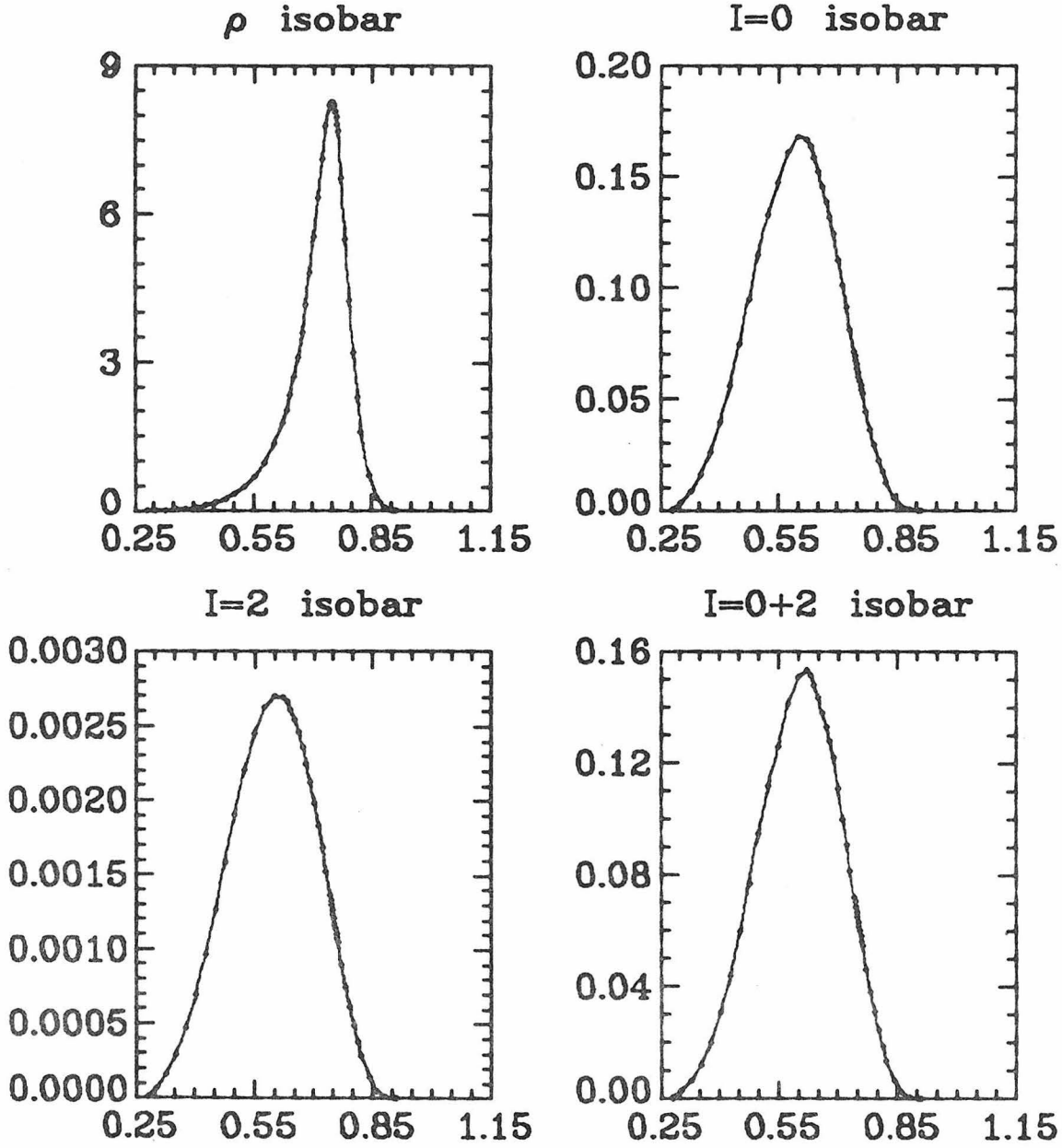


$d\sigma/dw_{\pi\pi}$ [mb/GeV] vs $w_{\pi\pi}$ [GeV]
$\pi^- p \rightarrow n\pi^-\pi^+$ W=1.77 GeV
π-exchange input

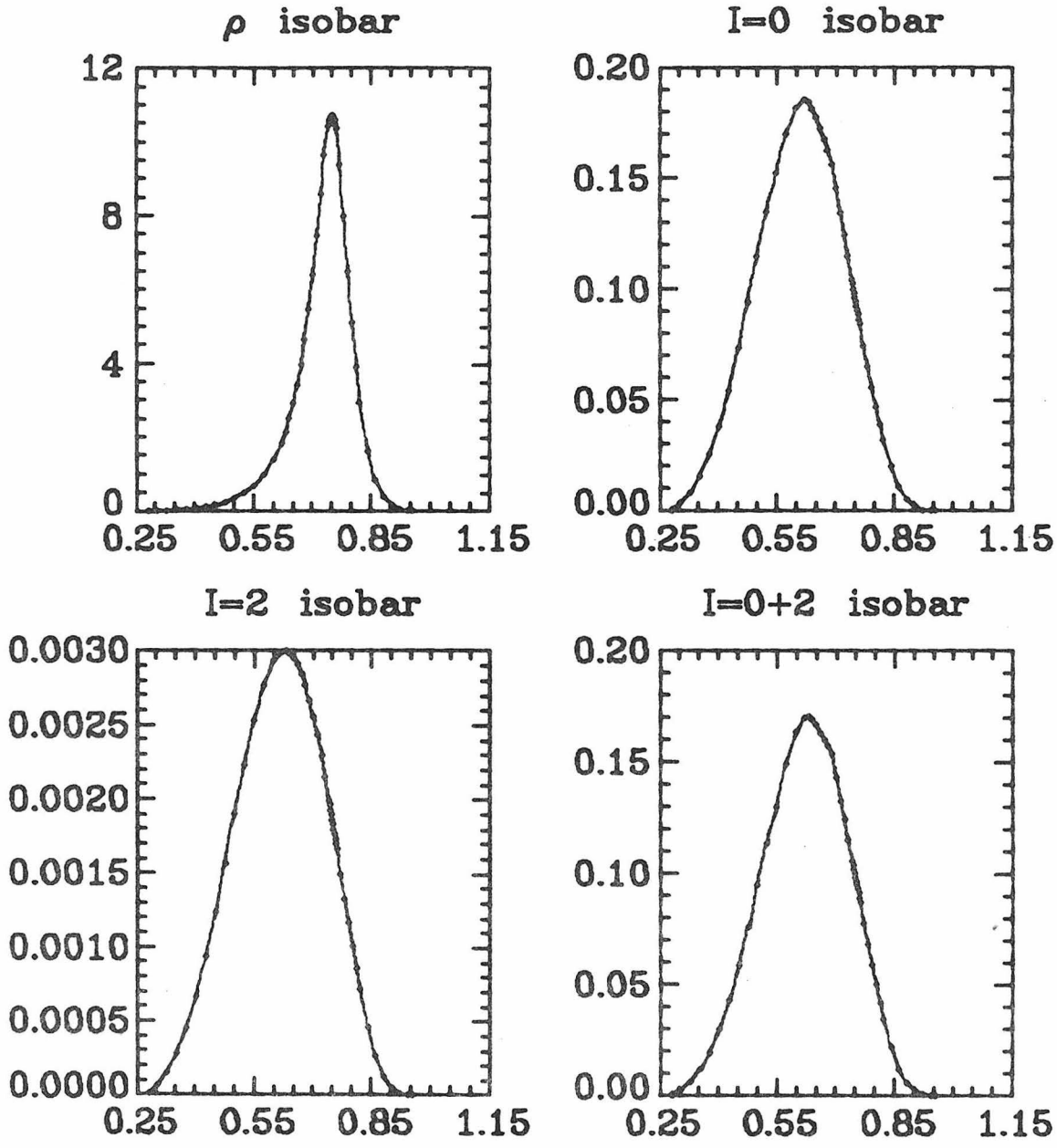


$d\sigma/dw_{\pi\pi}$ [mb/GeV] vs $w_{\pi\pi}$ [GeV]
$\pi^- p \rightarrow n\pi^-\pi^+$ W=1.81 GeV
π-exchange input

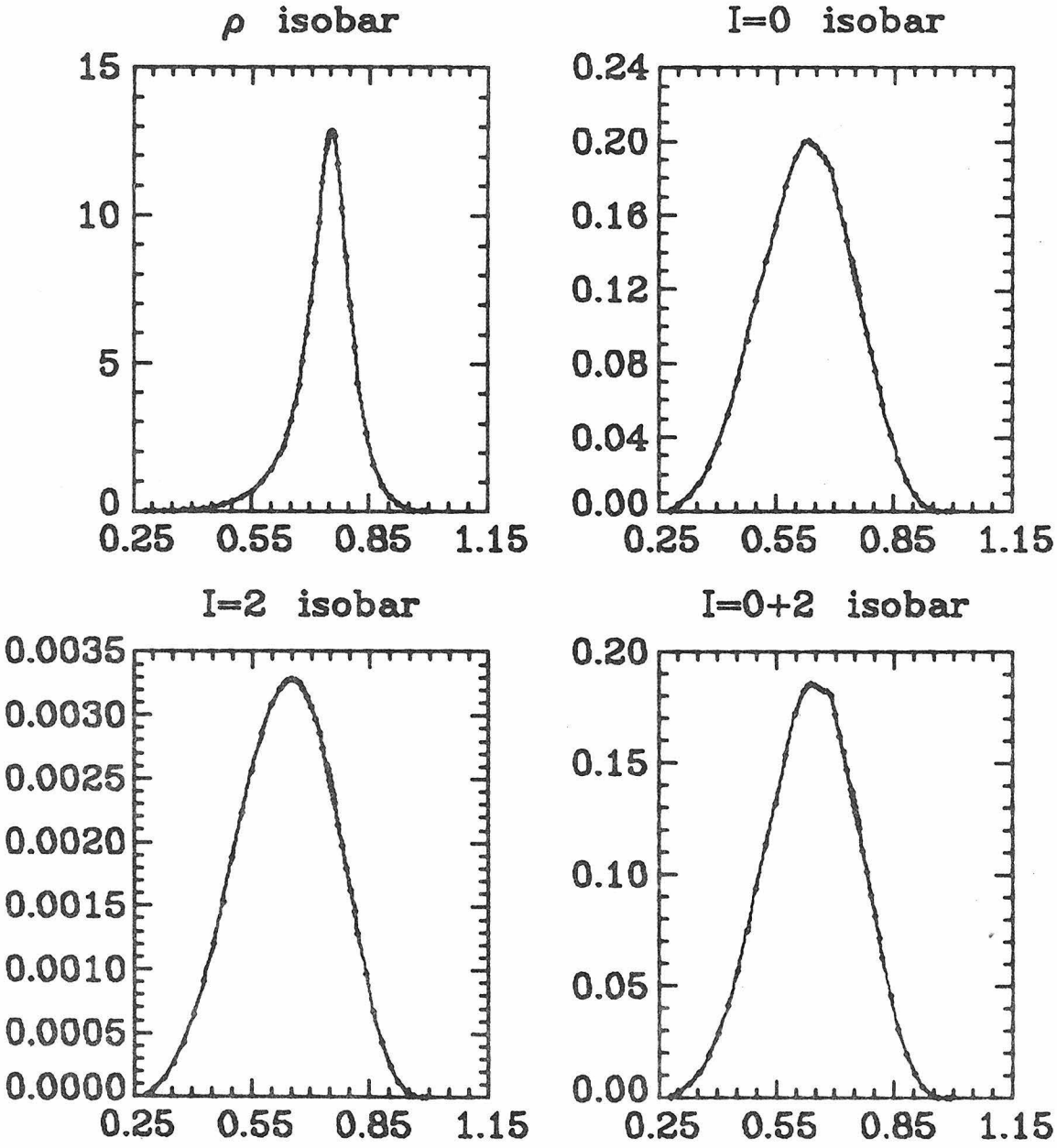



dσ/dw$_{\pi\pi}$ [mb/GeV] vs w$_{\pi\pi}$ [GeV]
$\pi^-p \rightarrow n\pi^-\pi^+$ W=1.85 GeV
π−exchange input
ρ isobar
I=0 isobar
I=2 isobar
I=0+2 isobar
0.25 0.55 0.85 1.15

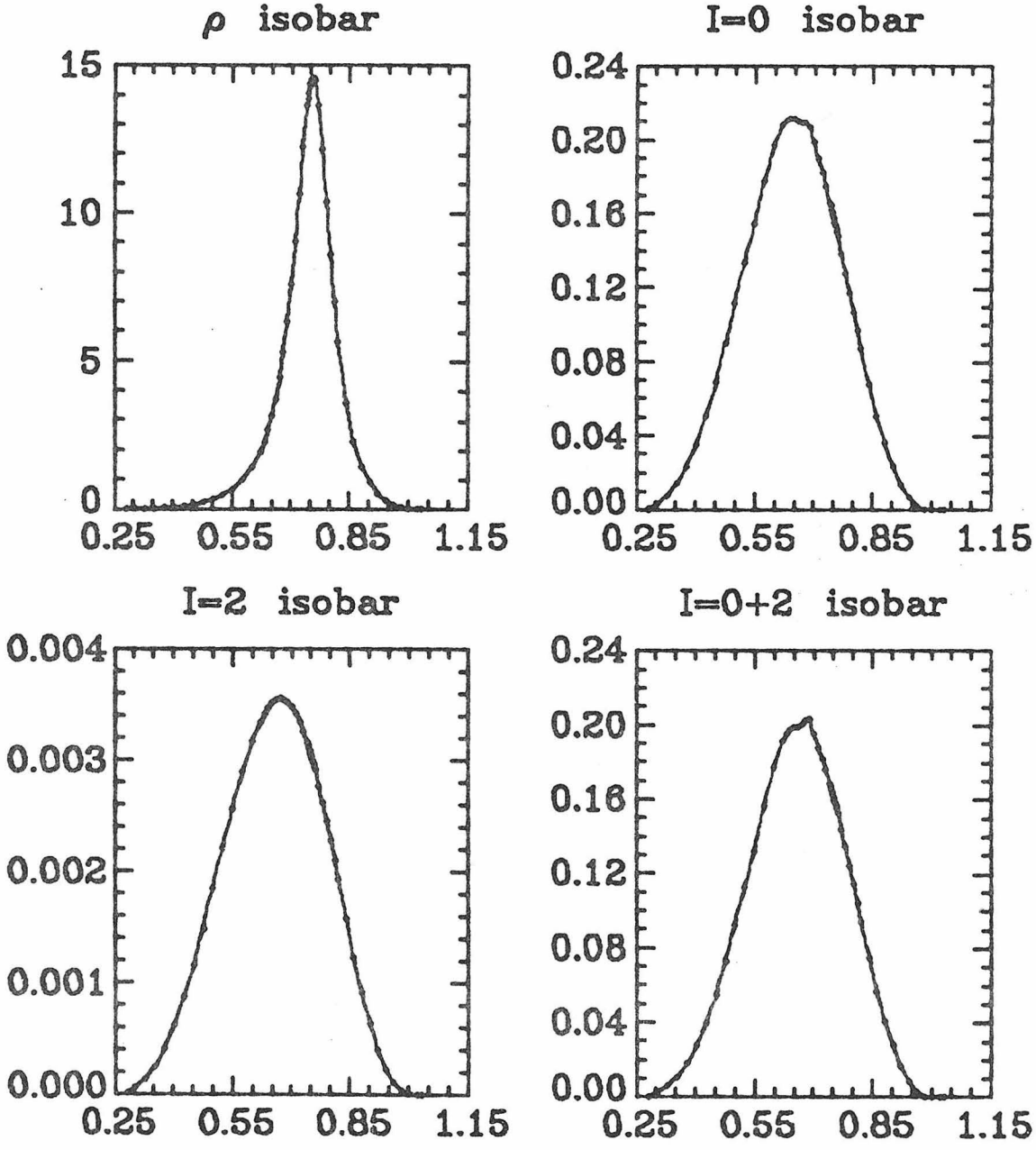
$d\sigma/dw_{\pi\pi}$ [mb/GeV] vs $w_{\pi\pi}$ [GeV]
$\pi^- p \rightarrow n\pi^-\pi^+$ W=1.89 GeV
π-exchange input



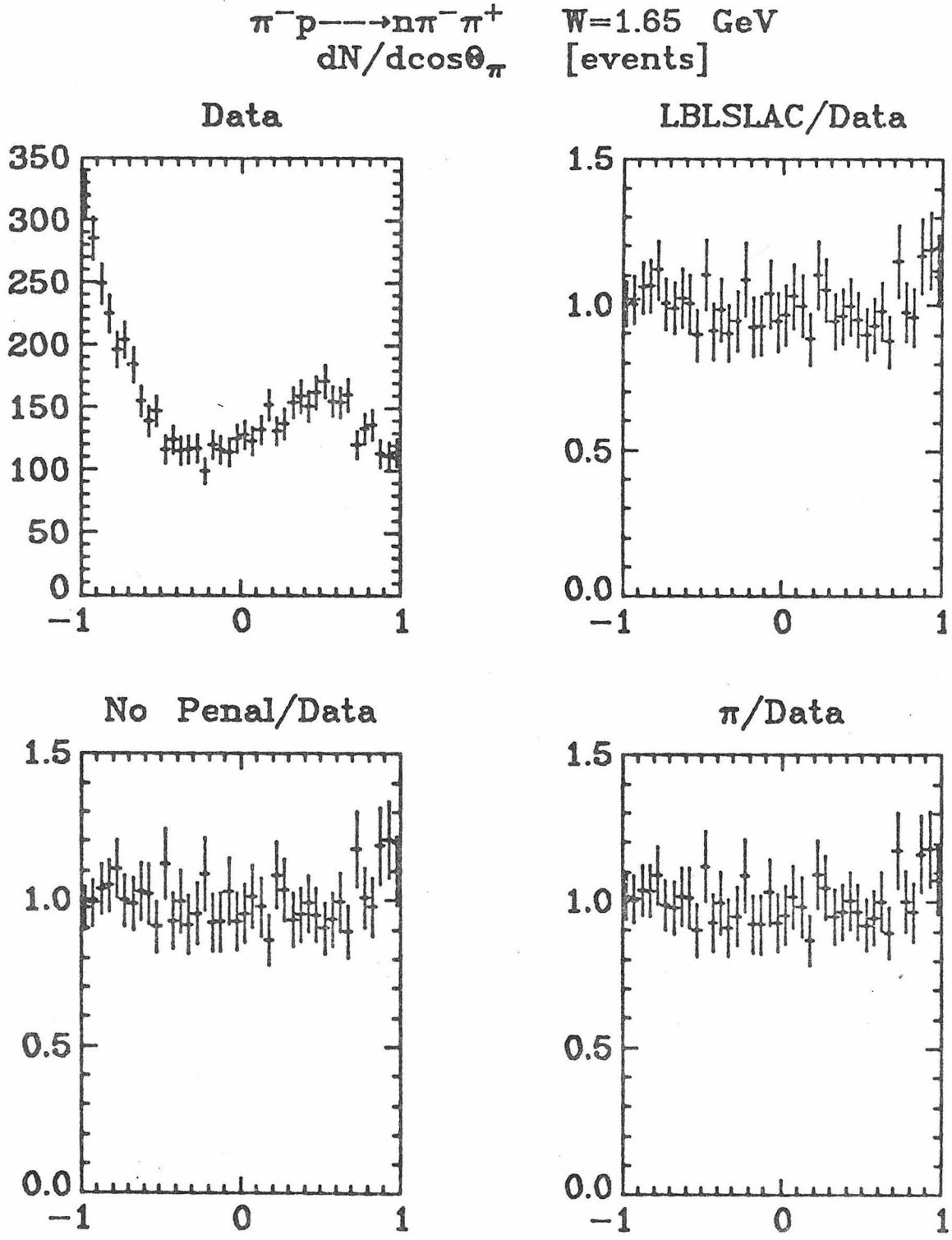
$d\sigma/dw_{\pi\pi}$ [mb/GeV] vs $w_{\pi\pi}$ [GeV]
$\pi^- p \rightarrow n\pi^-\pi^+$ W=1.93 GeV
π-exchange input

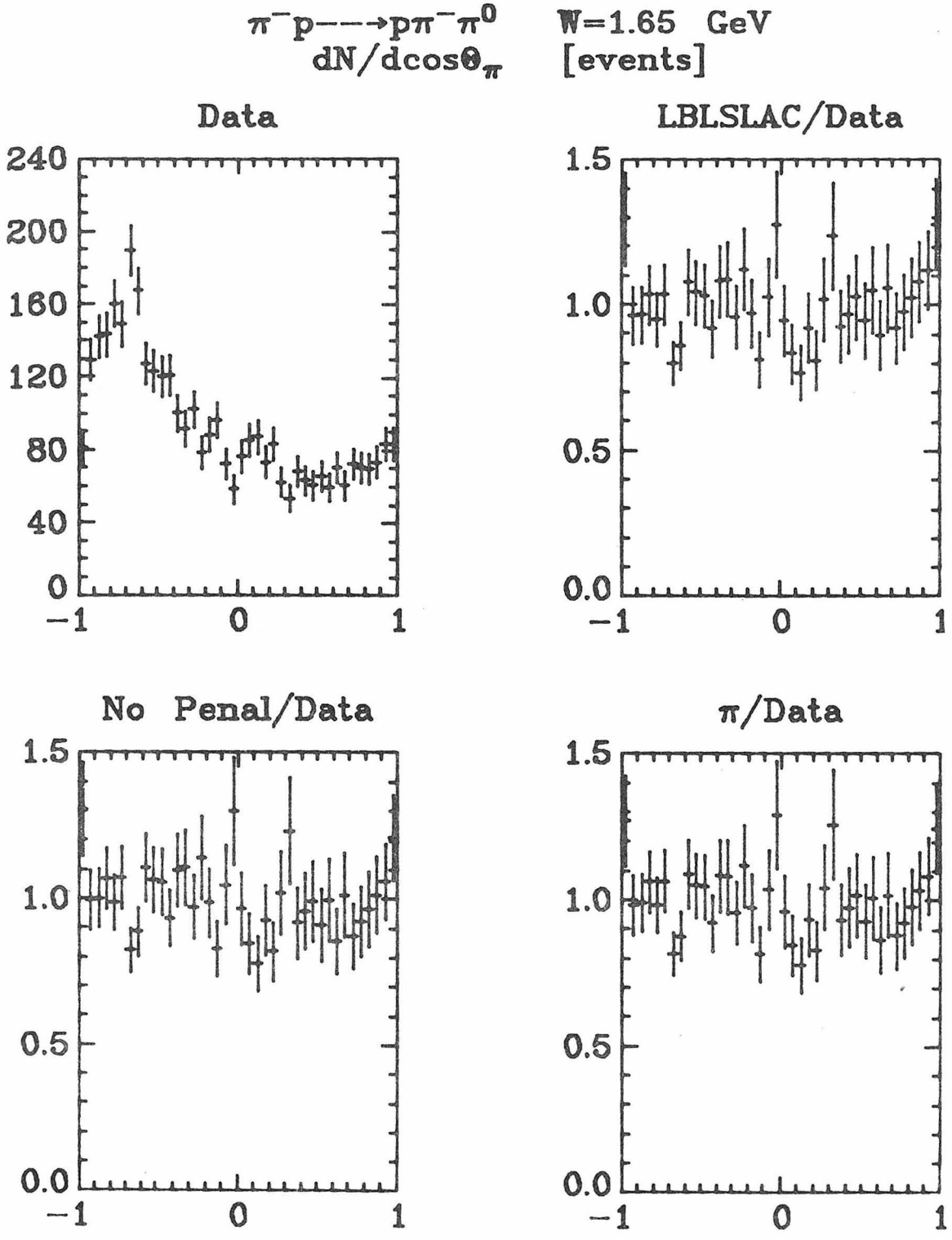


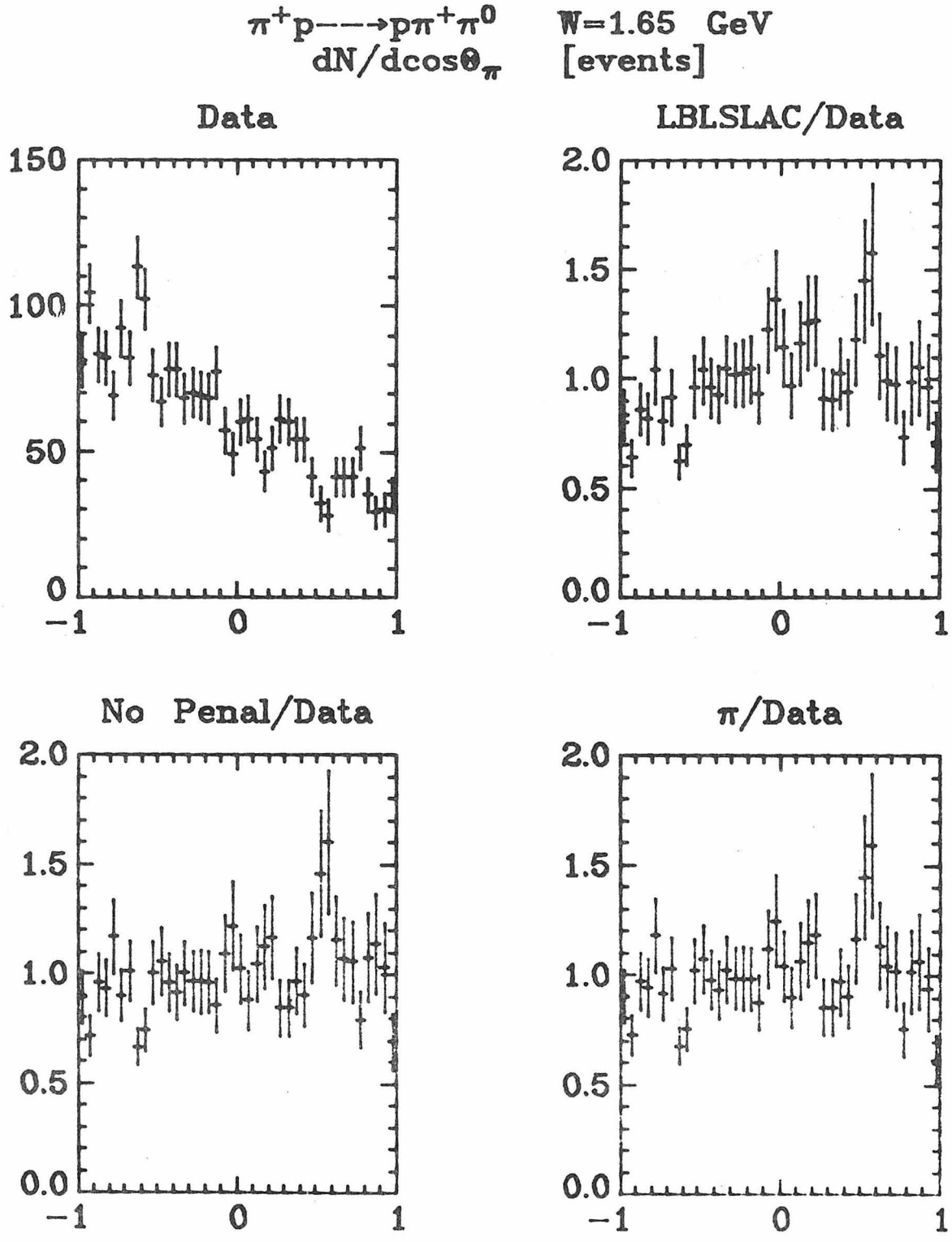
$d\sigma/dw_{\pi\pi}$ [mb/GeV] vs $w_{\pi\pi}$ [GeV]
$\pi^- p \rightarrow n\pi^-\pi^+$ W=1.97 GeV
π-exchange input

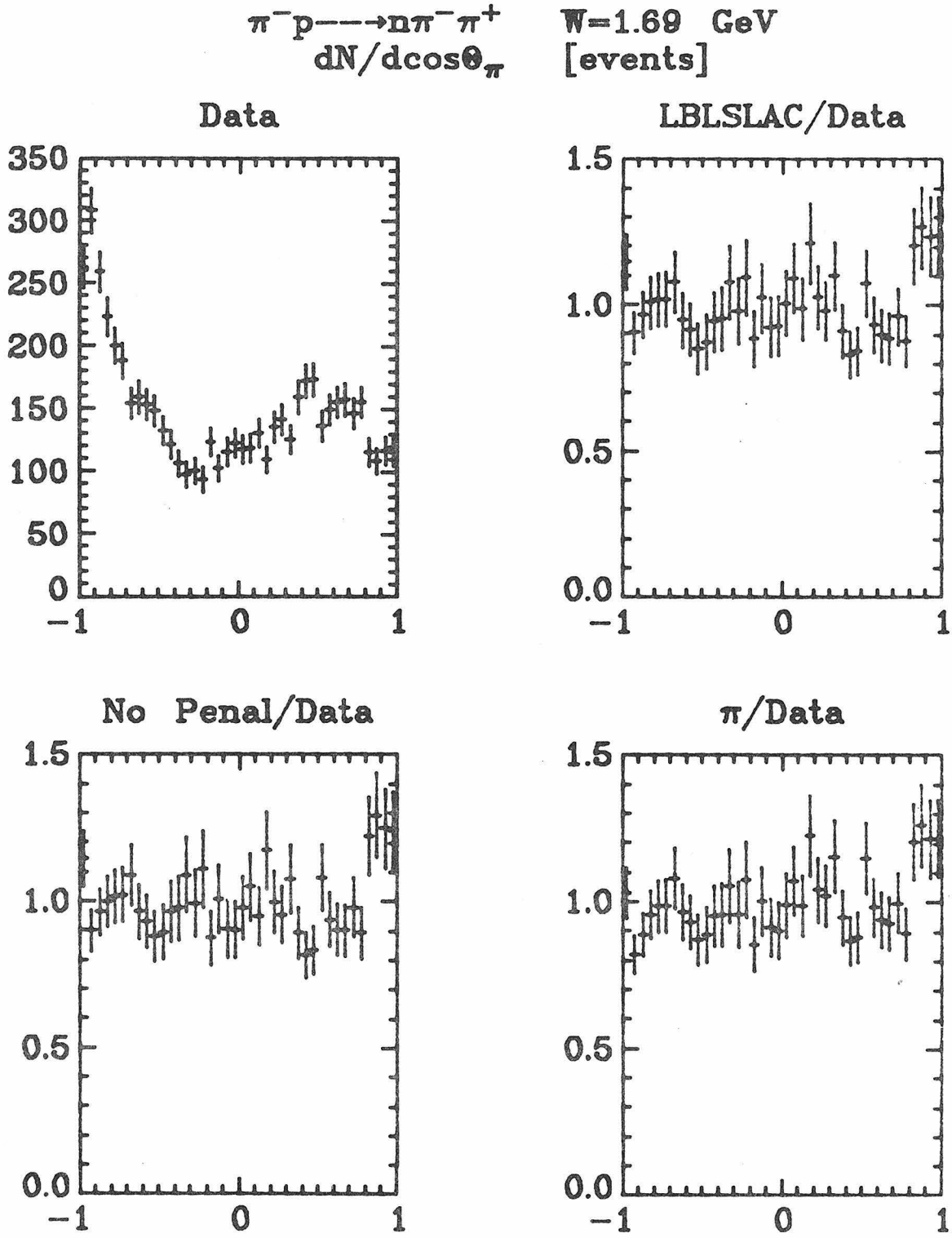


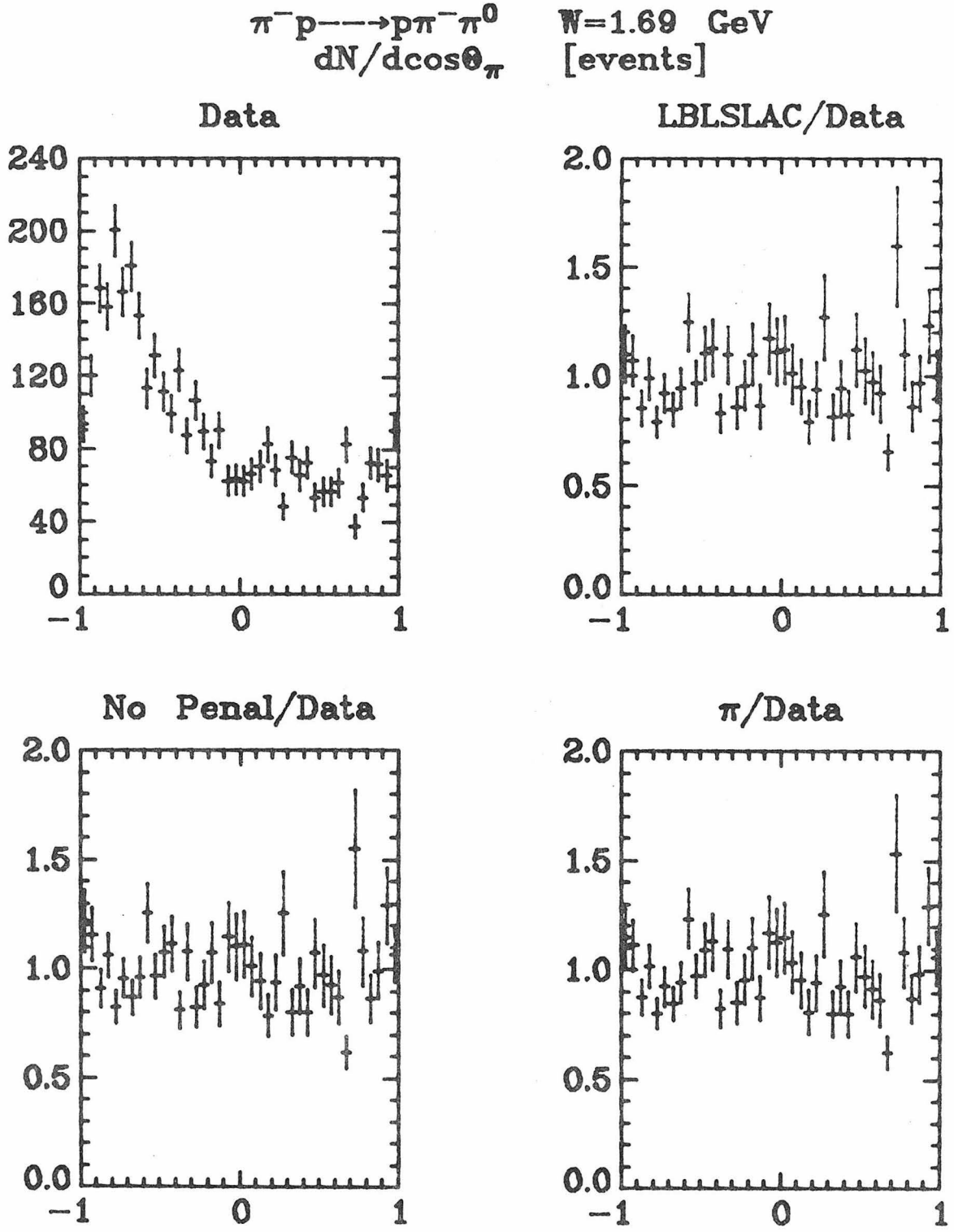
Appendix 2: $dN/d\cos\Theta_\pi$ vs. $\cos\Theta_\pi$ for all fits and all channels at all energies (1.65 GeV to 1.97 GeV) studied. A good fit would present a straight line in the plot of "Fit/Data".

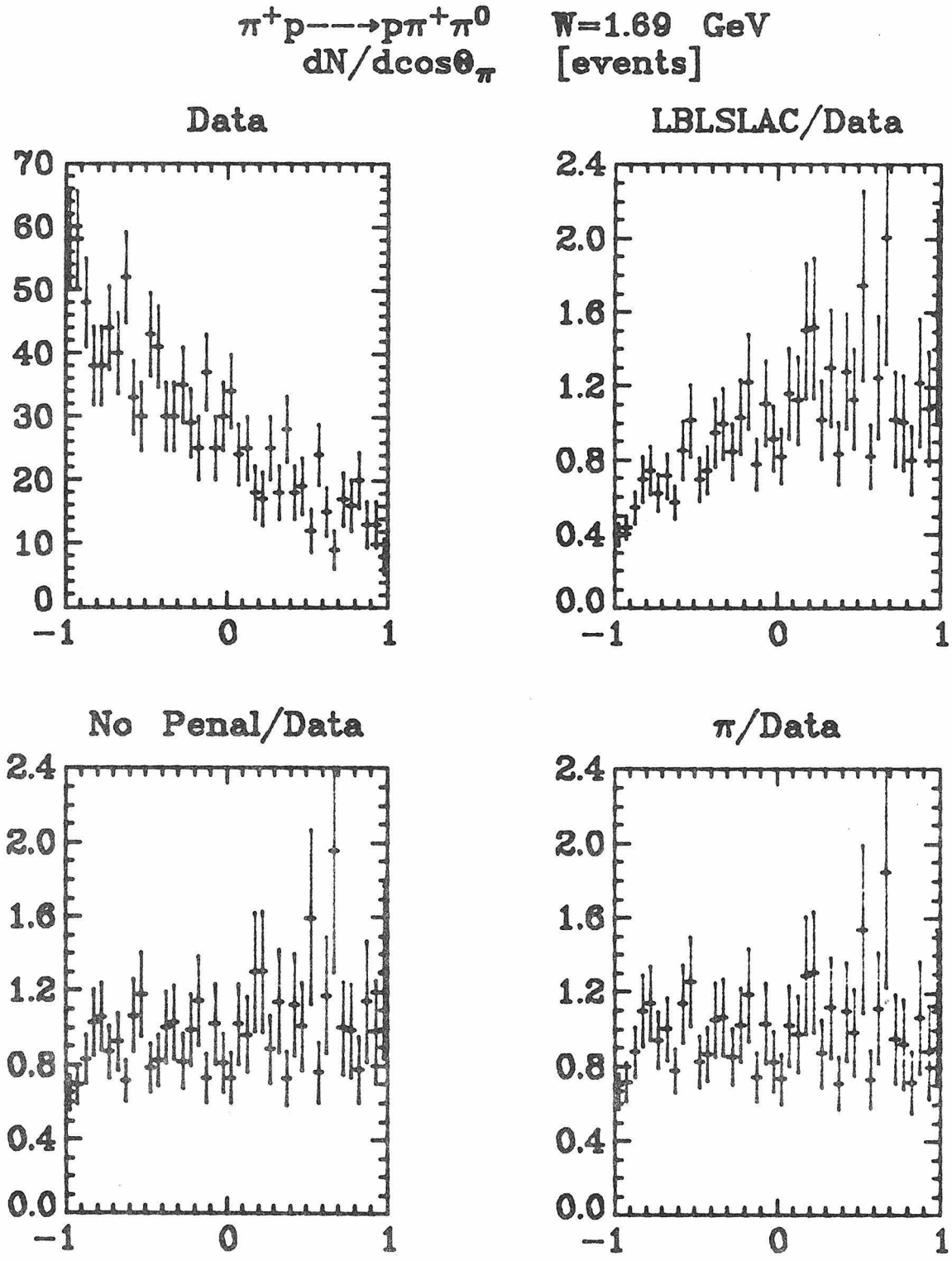

$\pi^- p \longrightarrow n\pi^-\pi^+$
$dN/d\cos\theta_\pi$
W=1.65 GeV
[events]
Data
LBLSLAC/Data
No Penal/Data
π/Data
350
300
250
200
150
100
50
0
1.5
1.0
0.5
0.0
−1
0
1

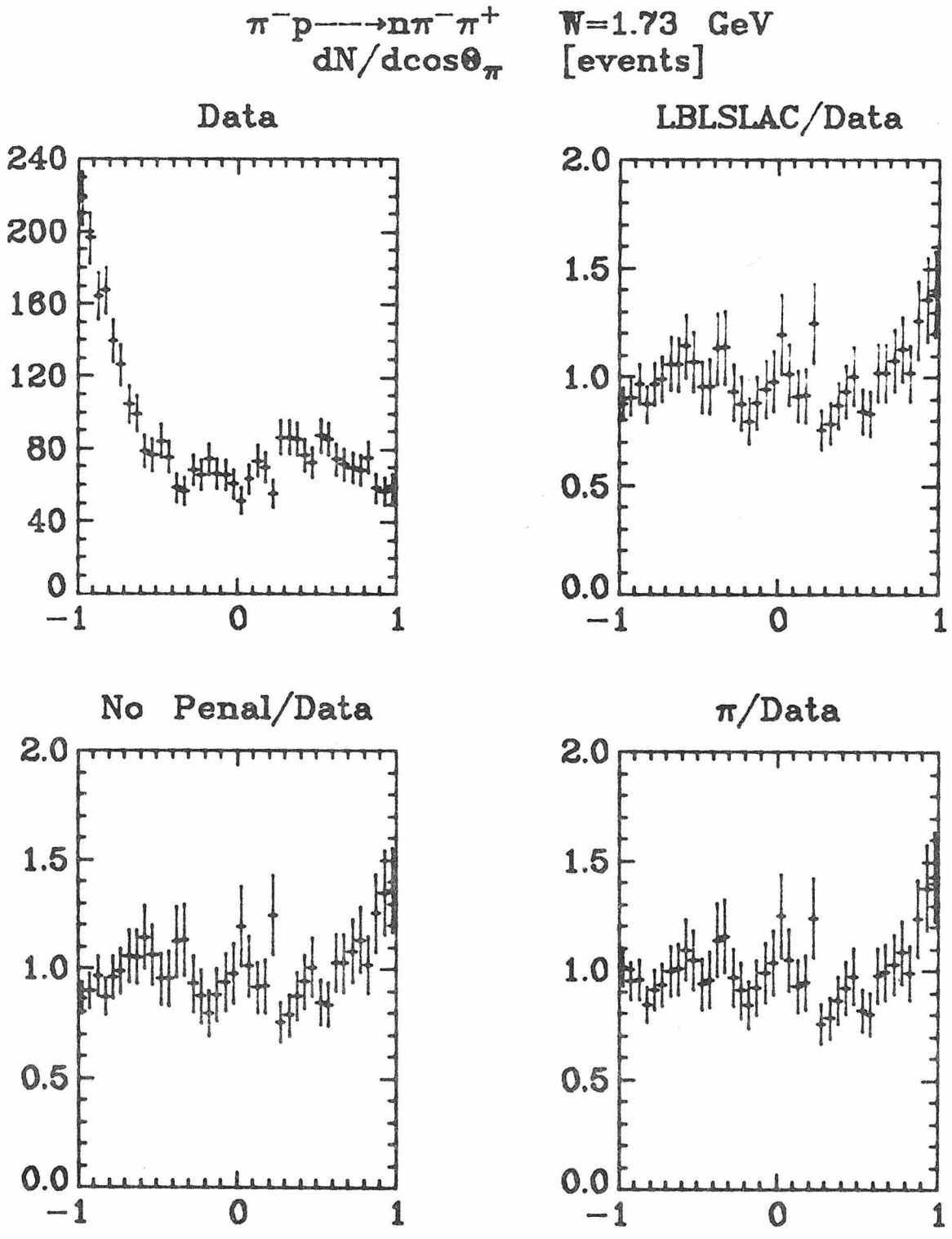

$\pi^- p \longrightarrow p\pi^-\pi^0$
$dN/d\cos\theta_\pi$
W=1.65 GeV
[events]
Data
LBLSLAC/Data
No Penal/Data
π/Data
240
200
160
120
80
40
0
1.5
1.0
0.5
0.0
−1
0
1

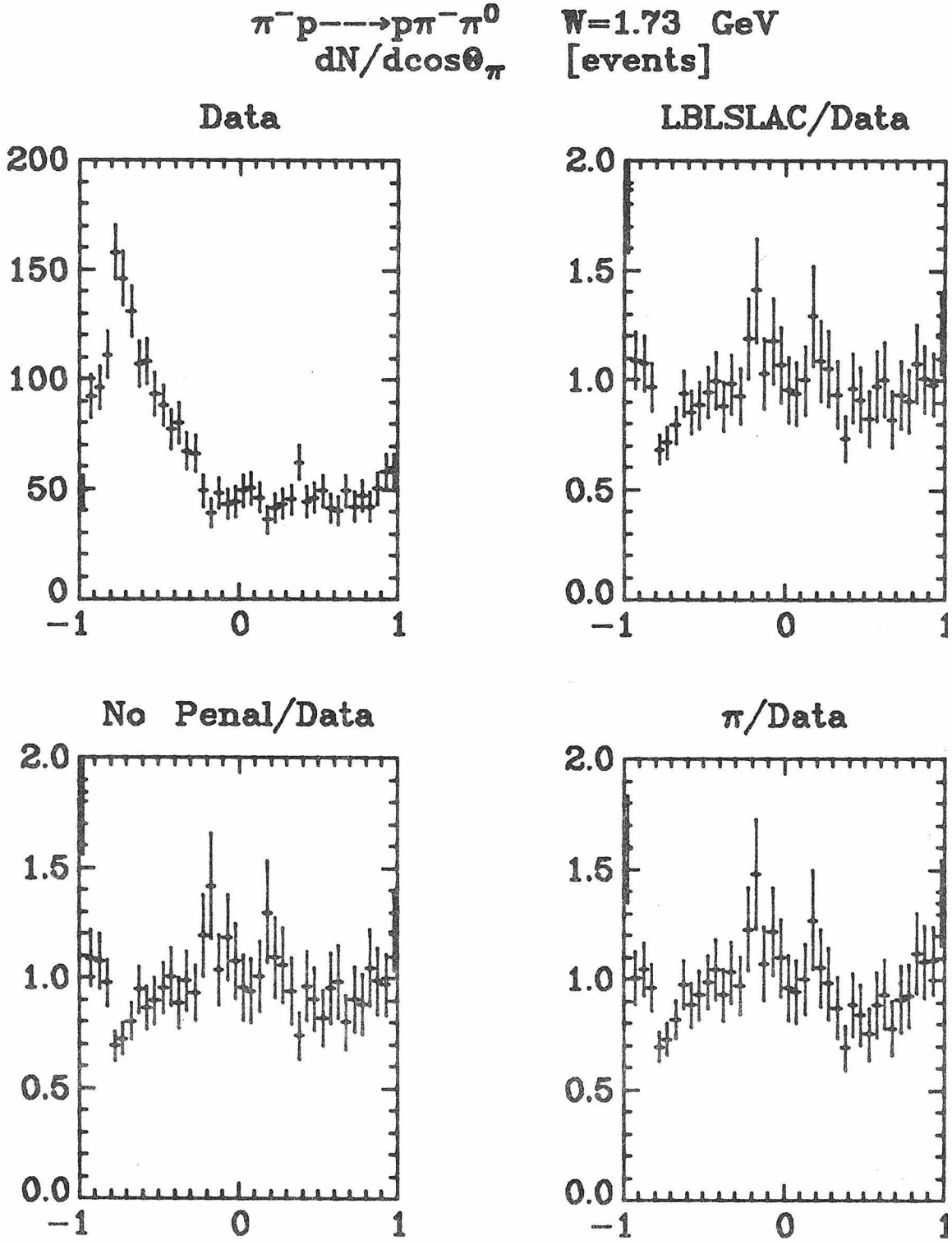

$\pi^+p \longrightarrow p\pi^+\pi^0$ W=1.65 GeV
$dN/d\cos\Theta_\pi$ [events]
Data
LBLSLAC/Data
No Penal/Data
π/Data
150
100
50
0
2.0
1.5
1.0
0.5
0.0
−1
0
1

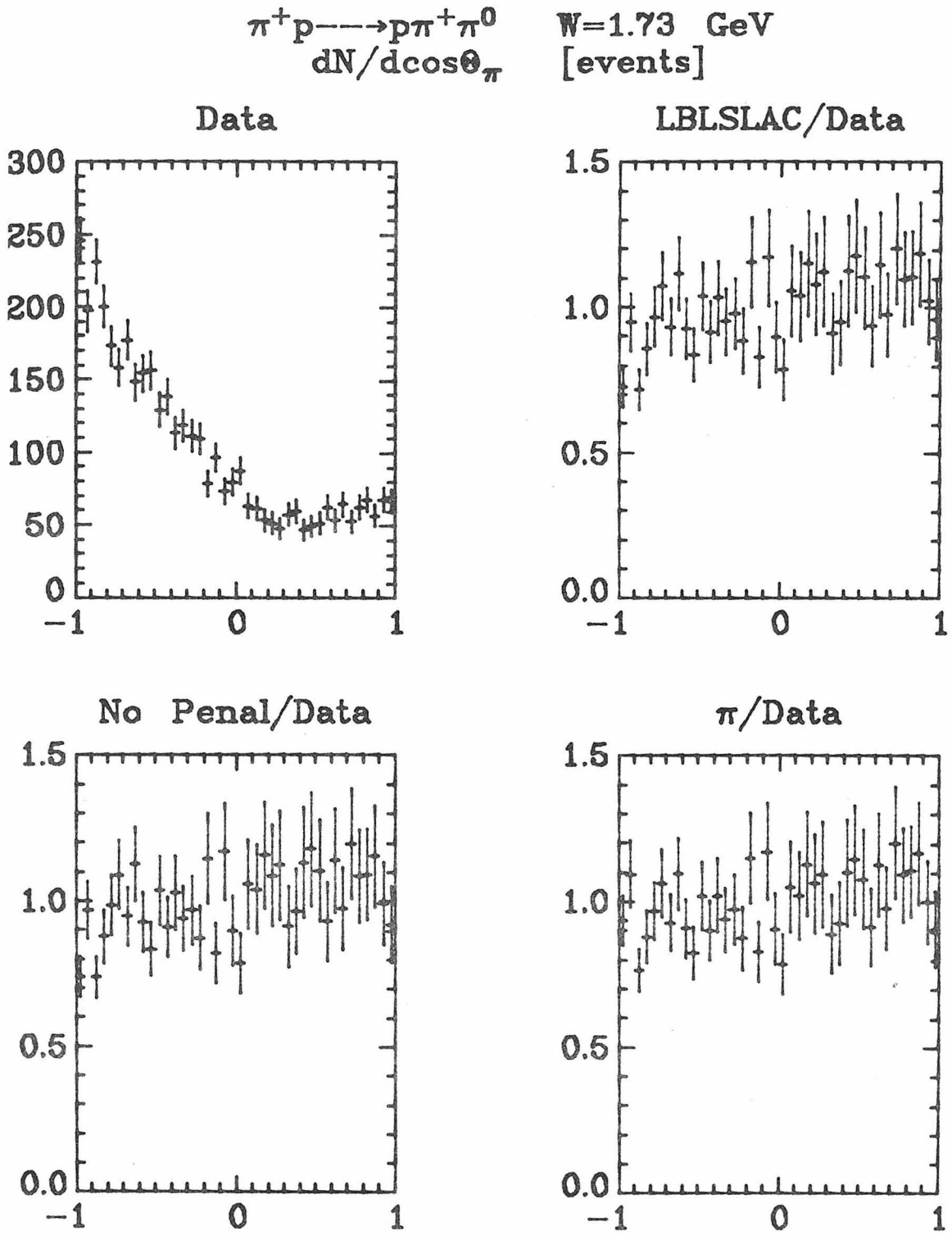

$\pi^- p \longrightarrow n\pi^-\pi^+$
W=1.69 GeV
$dN/d\cos\theta_\pi$
[events]
Data
LBLSLAC/Data
No Penal/Data
π/Data
350
300
250
200
150
100
50
0
1.5
1.0
0.5
0.0
−1
0
1

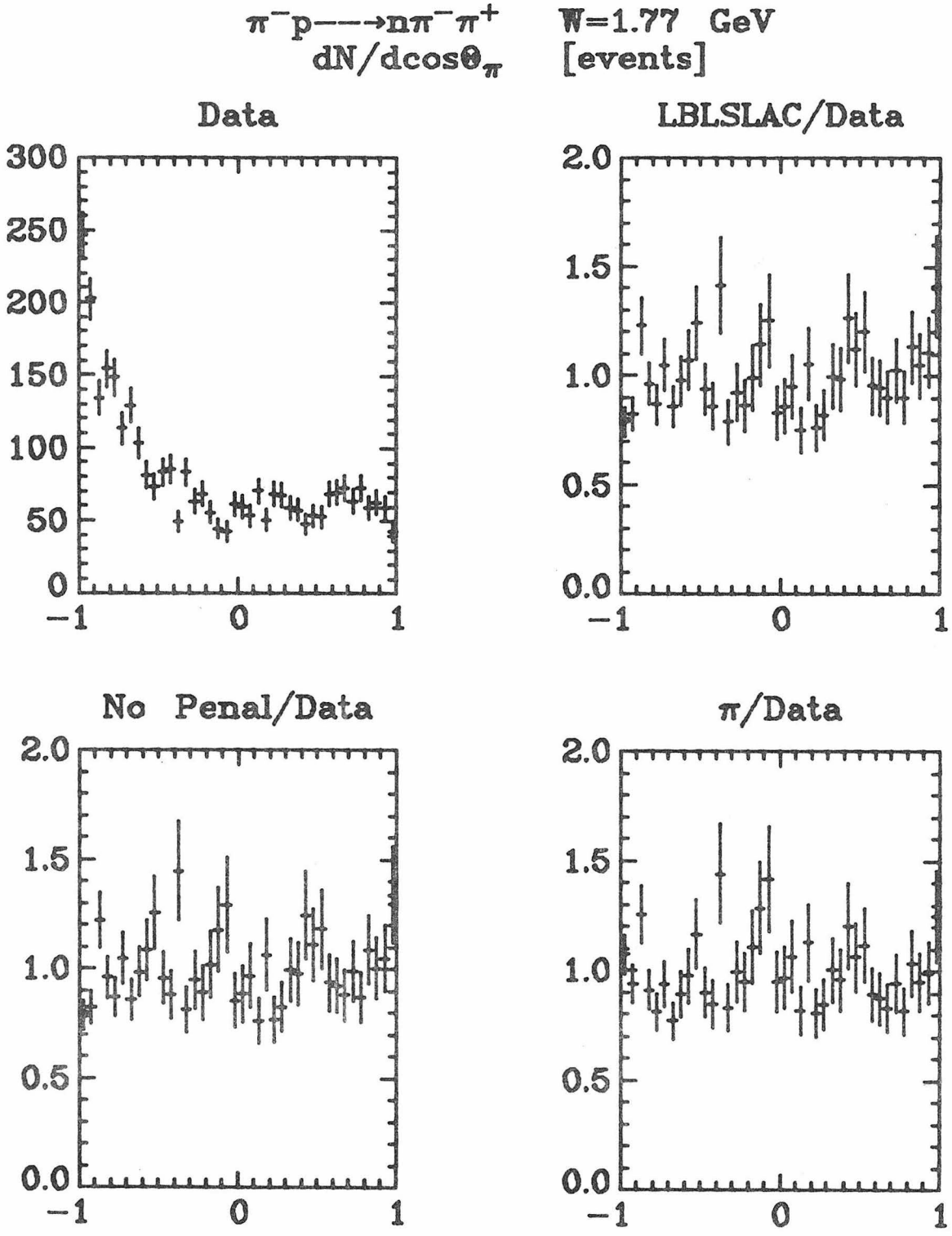

$\pi^- p \longrightarrow p\pi^- \pi^0$
W=1.69 GeV
$dN/d\cos\Theta_\pi$
[events]
Data
LBLSLAC/Data
No Penal/Data
π/Data
240
200
160
120
80
40
0
2.0
1.5
1.0
0.5
0.0
−1
0
1

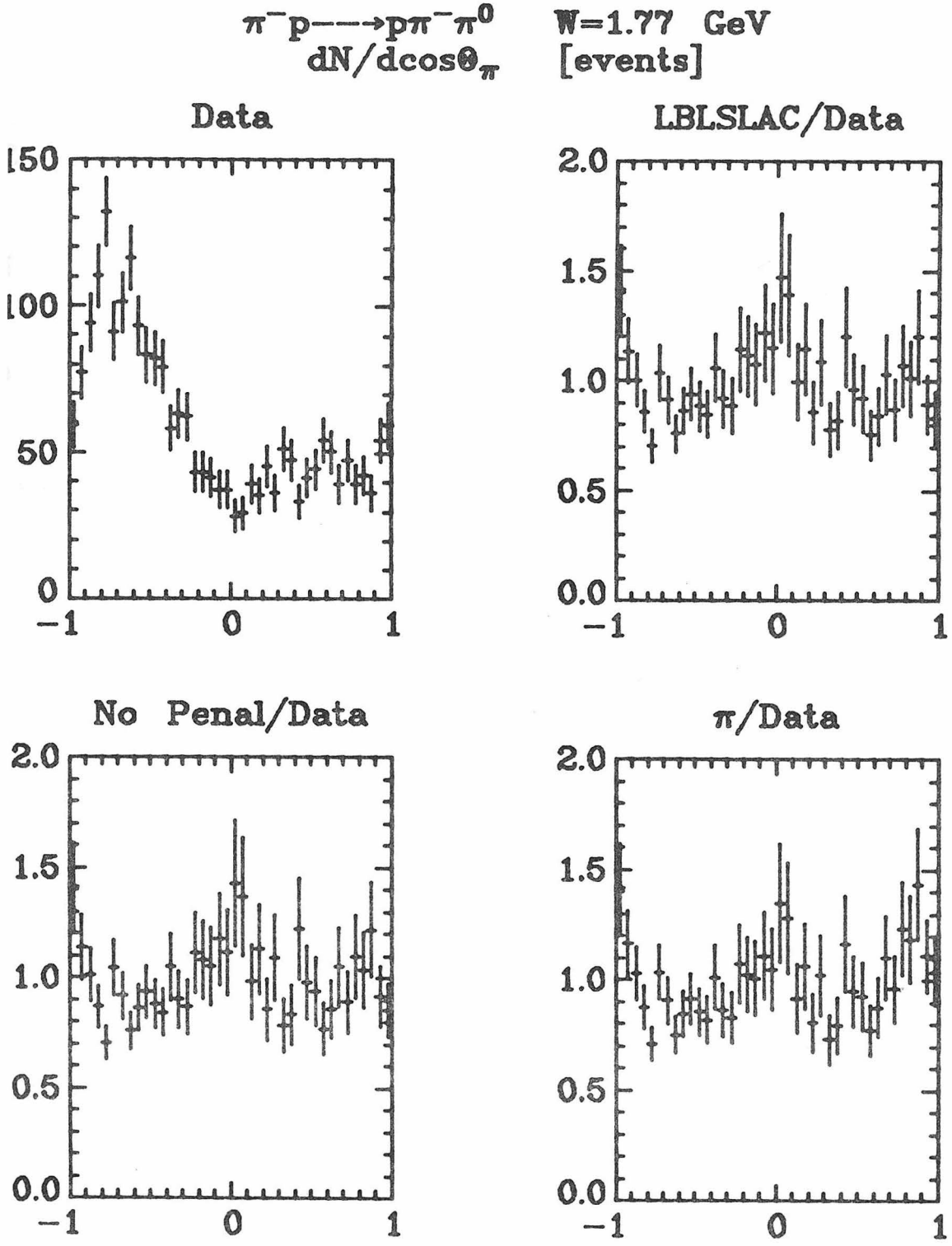

$\pi^+p \longrightarrow p\pi^+\pi^0$
$dN/d\cos\theta_\pi$
W=1.69 GeV
[events]
Data
LBLSLAC/Data
No Penal/Data
π/Data
70
60
50
40
30
20
10
0
2.4
2.0
1.6
1.2
0.8
0.4
0.0
−1
0
1

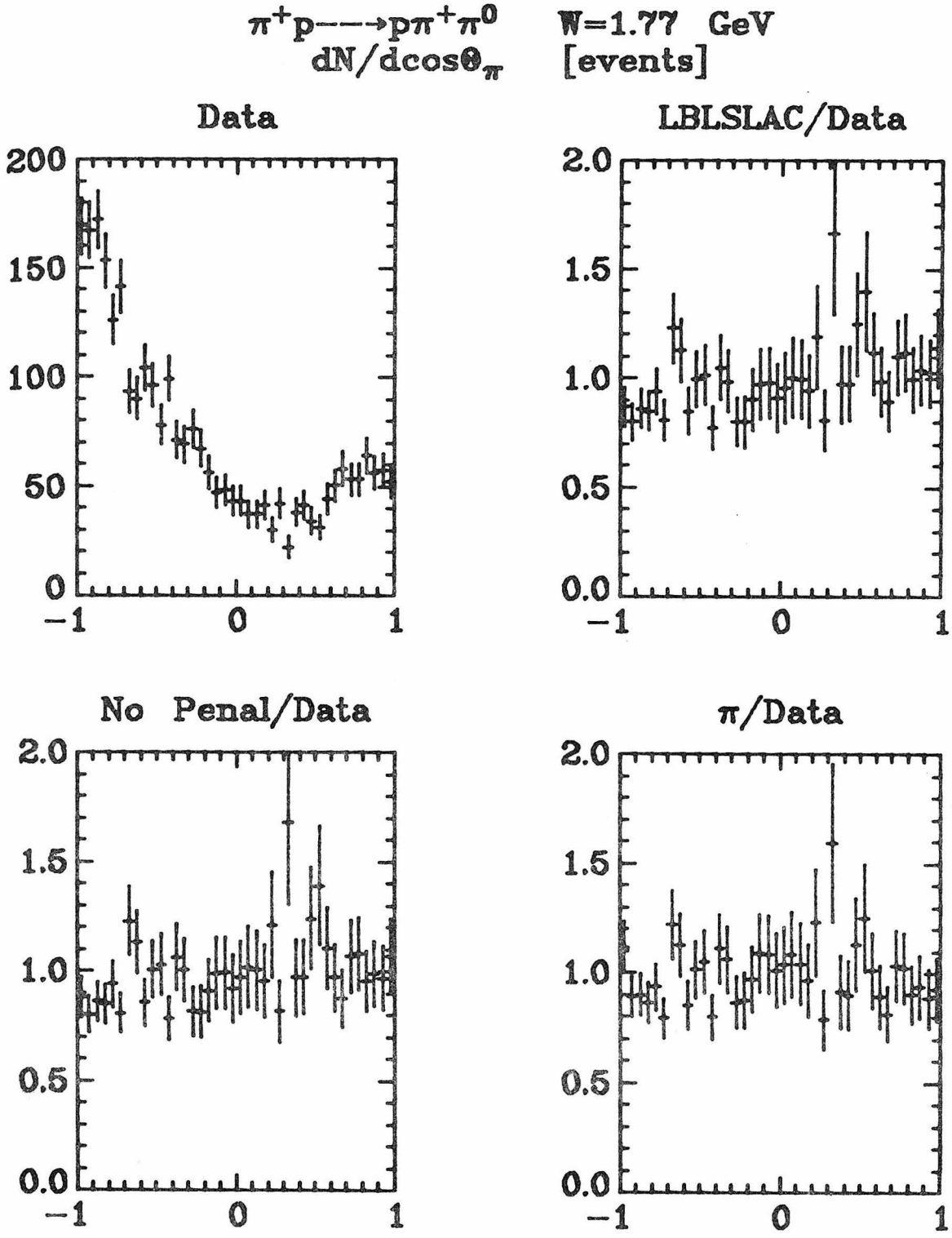

$\pi^- p \longrightarrow n\pi^-\pi^+$
W=1.73 GeV
$dN/d\cos\theta_\pi$
[events]
Data
LBLSLAC/Data
No Penal/Data
π/Data
240
200
160
120
80
40
0
2.0
1.5
1.0
0.5
0.0
−1
0
1

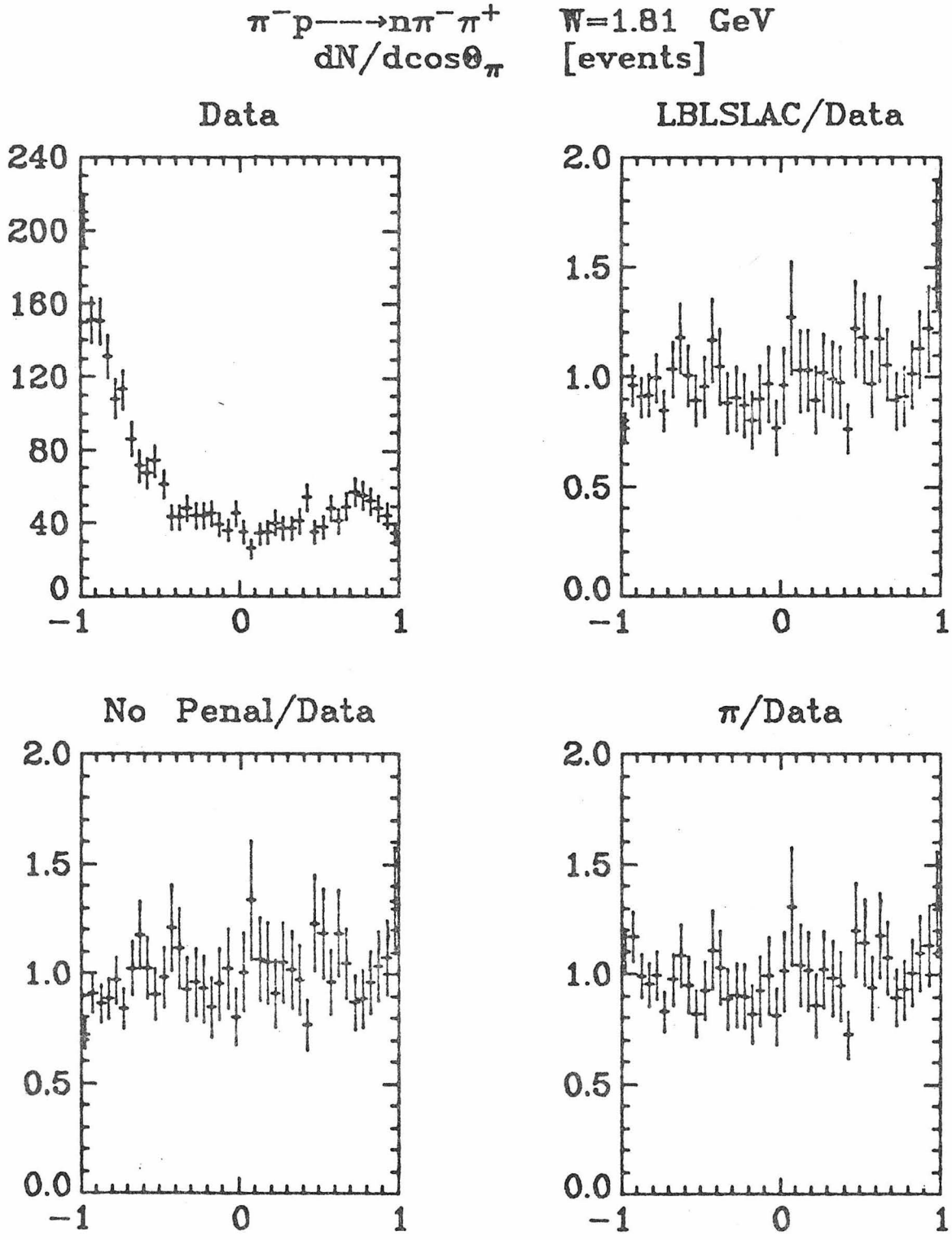

$\pi^- p \longrightarrow p\pi^- \pi^0$
W=1.73 GeV
$dN/d\cos\Theta_\pi$
[events]
Data
LBLSLAC/Data
No Penal/Data
π/Data
200
150
100
50
0
2.0
1.5
1.0
0.5
0.0
−1
0
1

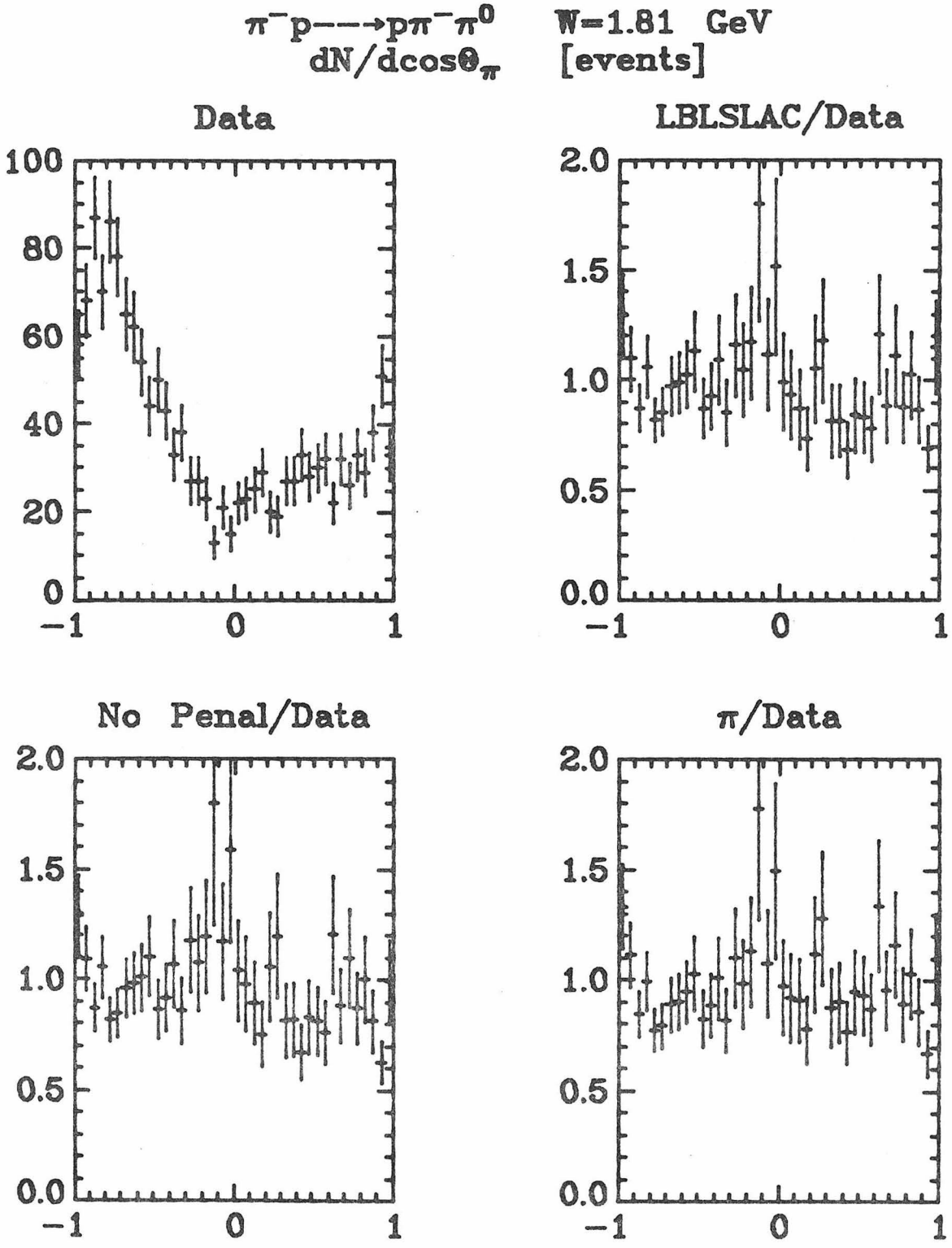

$\pi^+p\longrightarrow p\pi^+\pi^0$
W=1.73 GeV
$dN/d\cos\Theta_\pi$
[events]
Data
LBLSLAC/Data
No Penal/Data
π/Data
300
250
200
150
100
50
0
1.5
1.0
0.5
0.0
−1
0
1

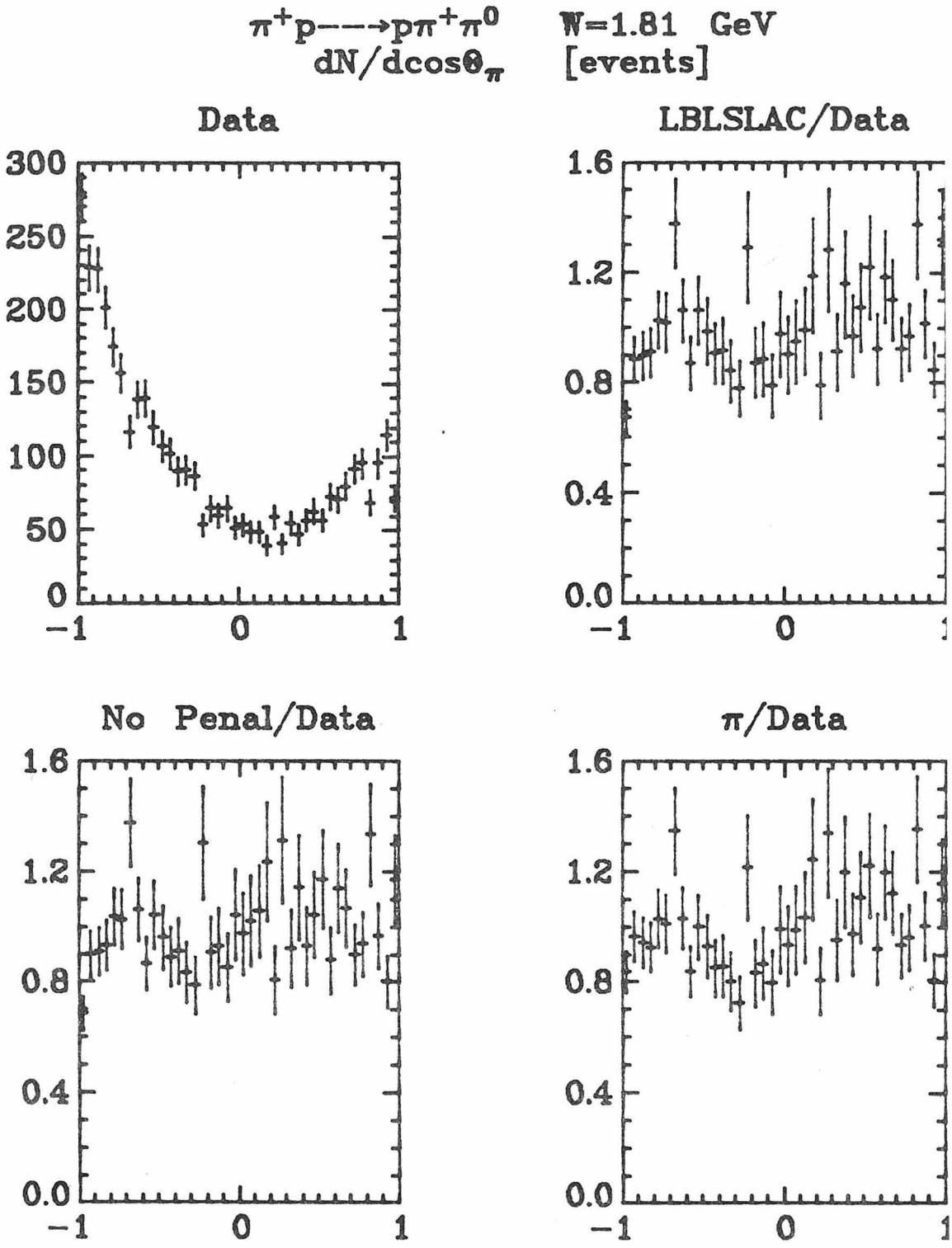

$\pi^- p \longrightarrow n\pi^-\pi^+$
W=1.77 GeV
$dN/d\cos\Theta_\pi$
[events]
Data
LBLSLAC/Data
No Penal/Data
π/Data
300
250
200
150
100
50
0
2.0
1.5
1.0
0.5
0.0
−1
0
1

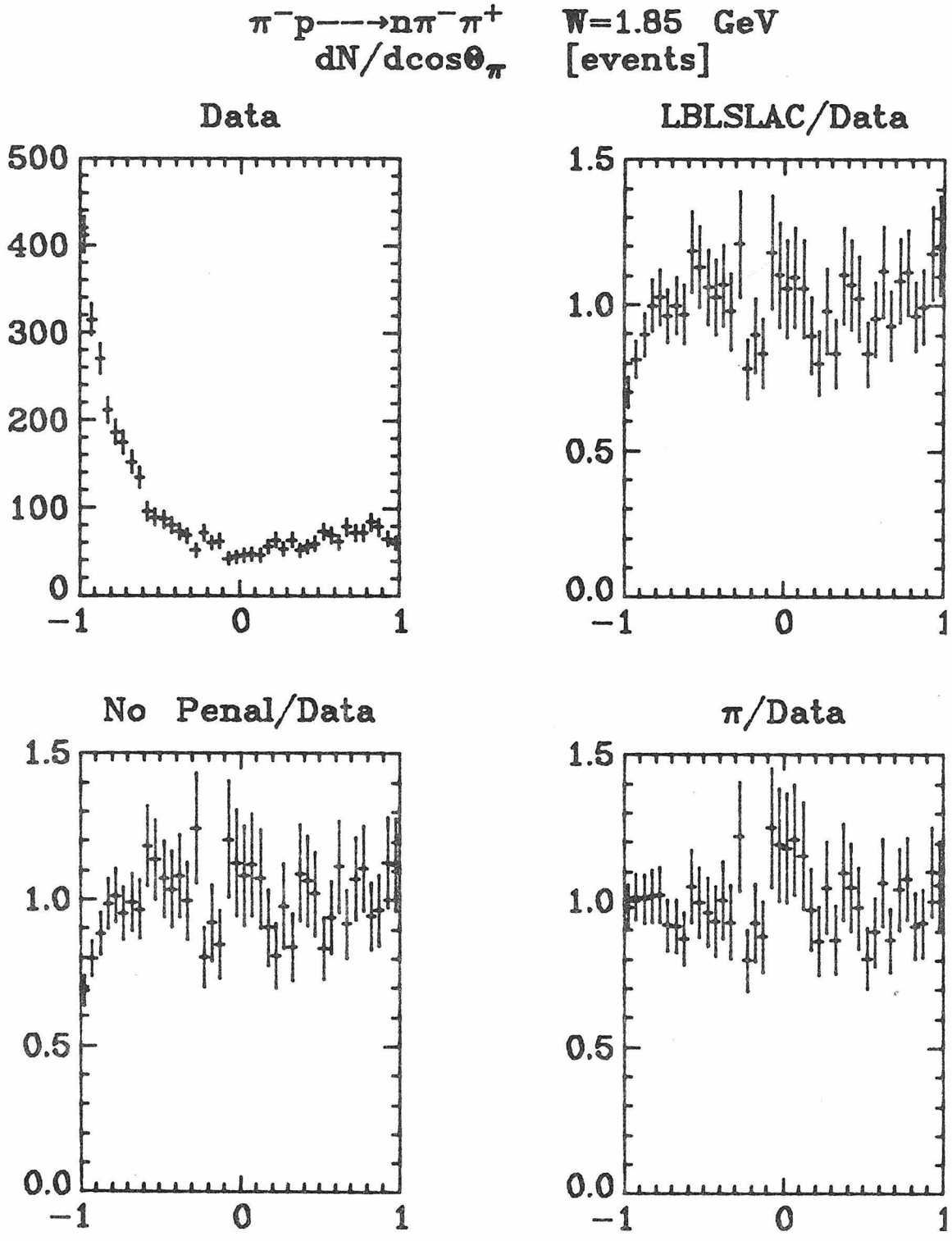

$\pi^- p \longrightarrow p\pi^-\pi^0$ W=1.77 GeV
$dN/d\cos\theta_\pi$ [events]
Data
LBLSLAC/Data
No Penal/Data
π/Data
150
100
50
0
2.0
1.5
1.0
0.5
0.0
−1
0
1

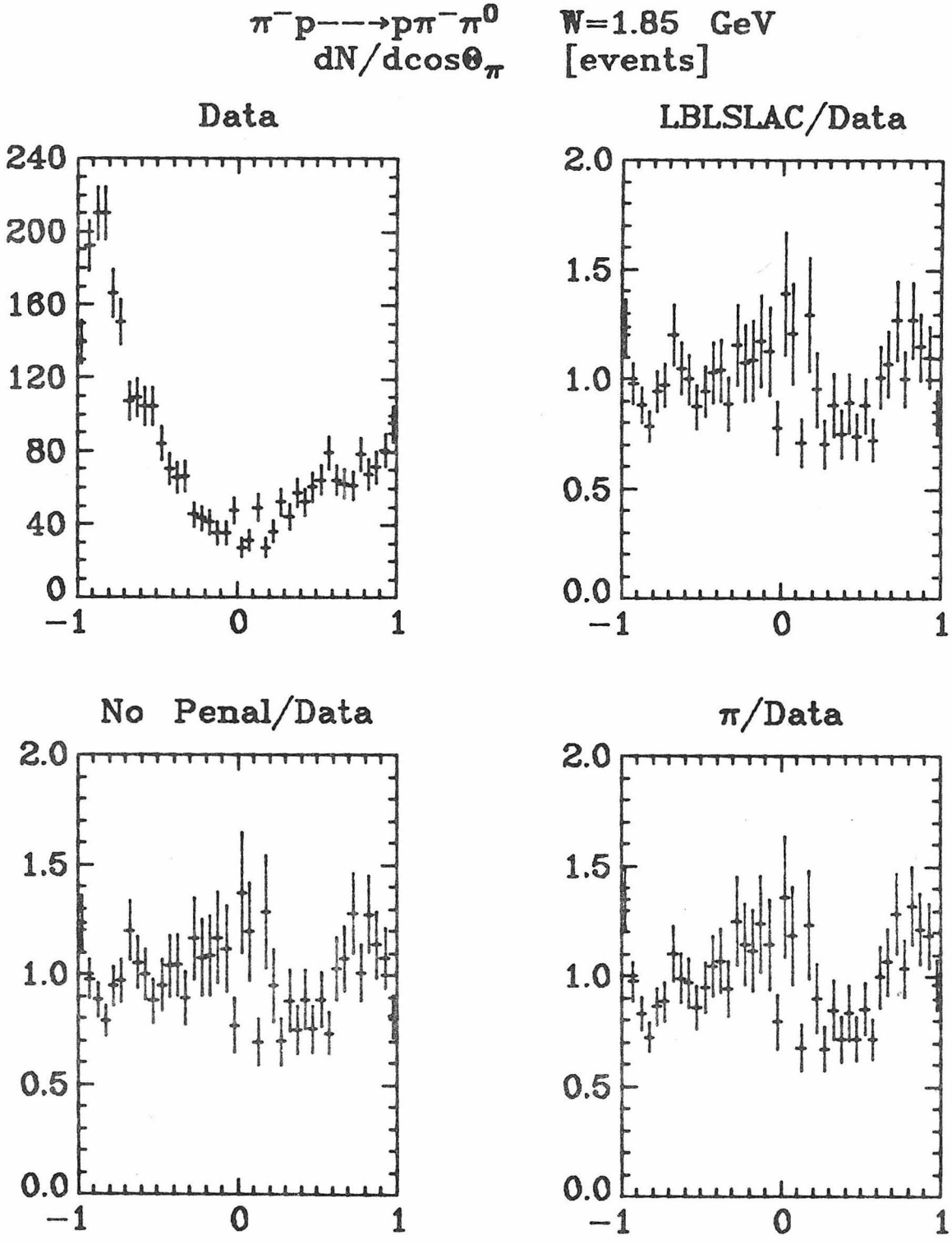

$\pi^+p \longrightarrow p\pi^+\pi^0$
W=1.77 GeV
$dN/d\cos\Theta_\pi$
[events]
Data
LBLSLAC/Data
No Penal/Data
π/Data
200
150
100
50
0
2.0
1.5
1.0
0.5
0.0
−1
0
1

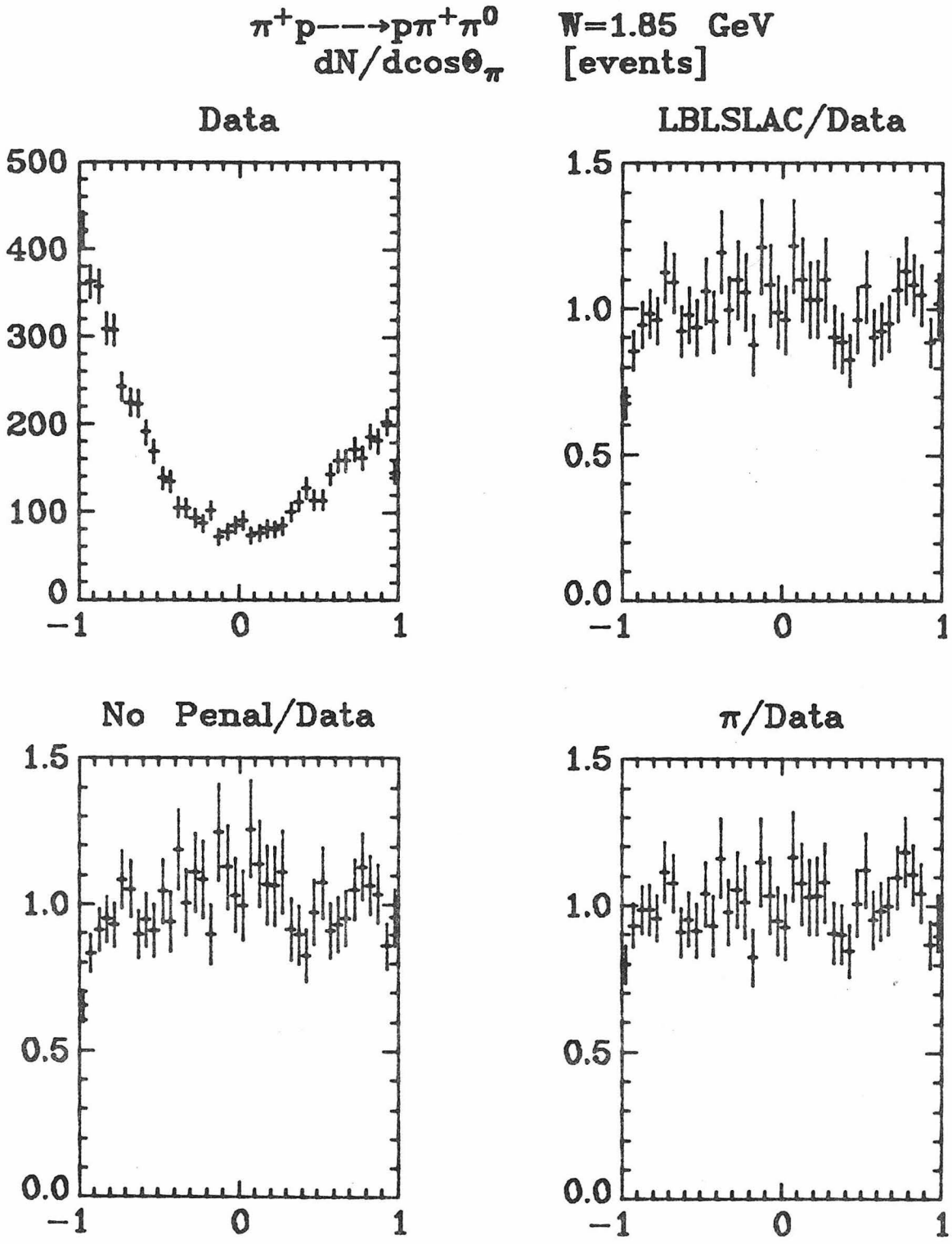

$\pi^- p \longrightarrow n\pi^-\pi^+$
$dN/d\cos\theta_\pi$
W=1.81 GeV
[events]
Data
LBLSLAC/Data
No Penal/Data
π/Data
240
200
160
120
80
40
0
2.0
1.5
1.0
0.5
0.0
−1
0
1

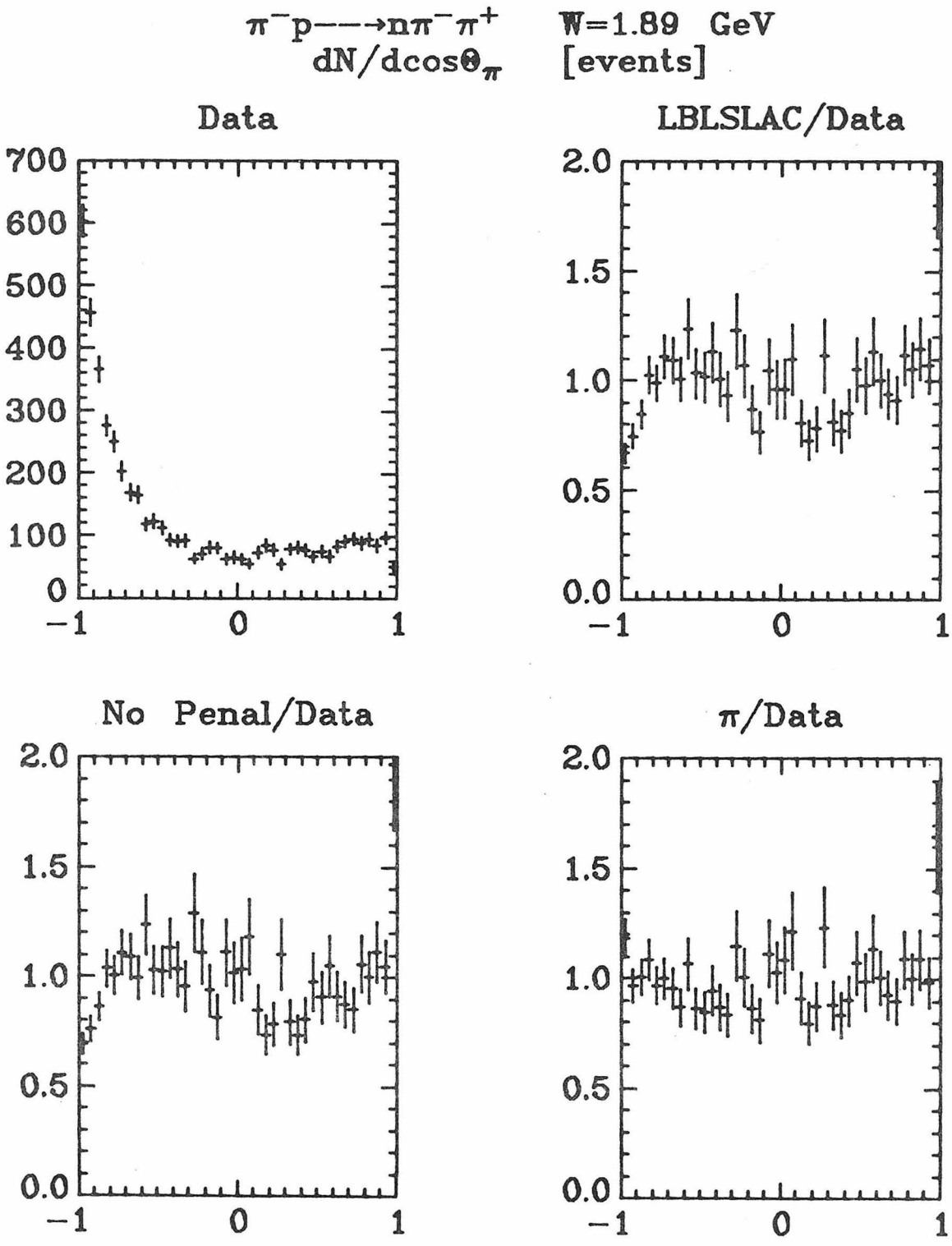

$\pi^- p \longrightarrow p\pi^- \pi^0$ W=1.81 GeV
$dN/d\cos\theta_\pi$ [events]
Data
LBLSLAC/Data
No Penal/Data
π/Data
100
80
60
40
20
0
2.0
1.5
1.0
0.5
0.0
−1
0
1

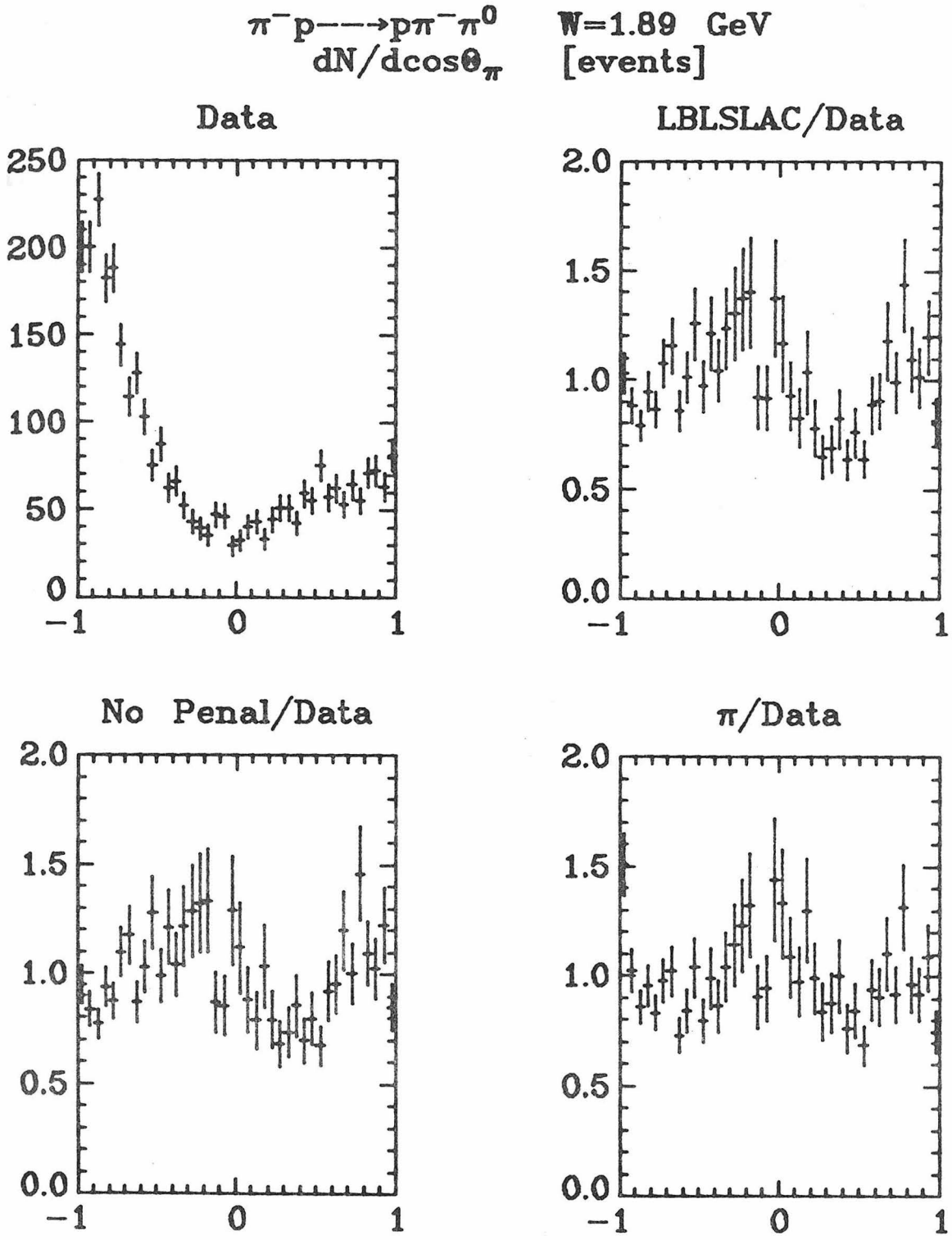

$\pi^+p \longrightarrow p\pi^+\pi^0$
W=1.81 GeV
$dN/d\cos\theta_\pi$
[events]
Data
LBLSLAC/Data
No Penal/Data
π/Data
300
250
200
150
100
50
0
1.6
1.2
0.8
0.4
0.0
−1
0
1

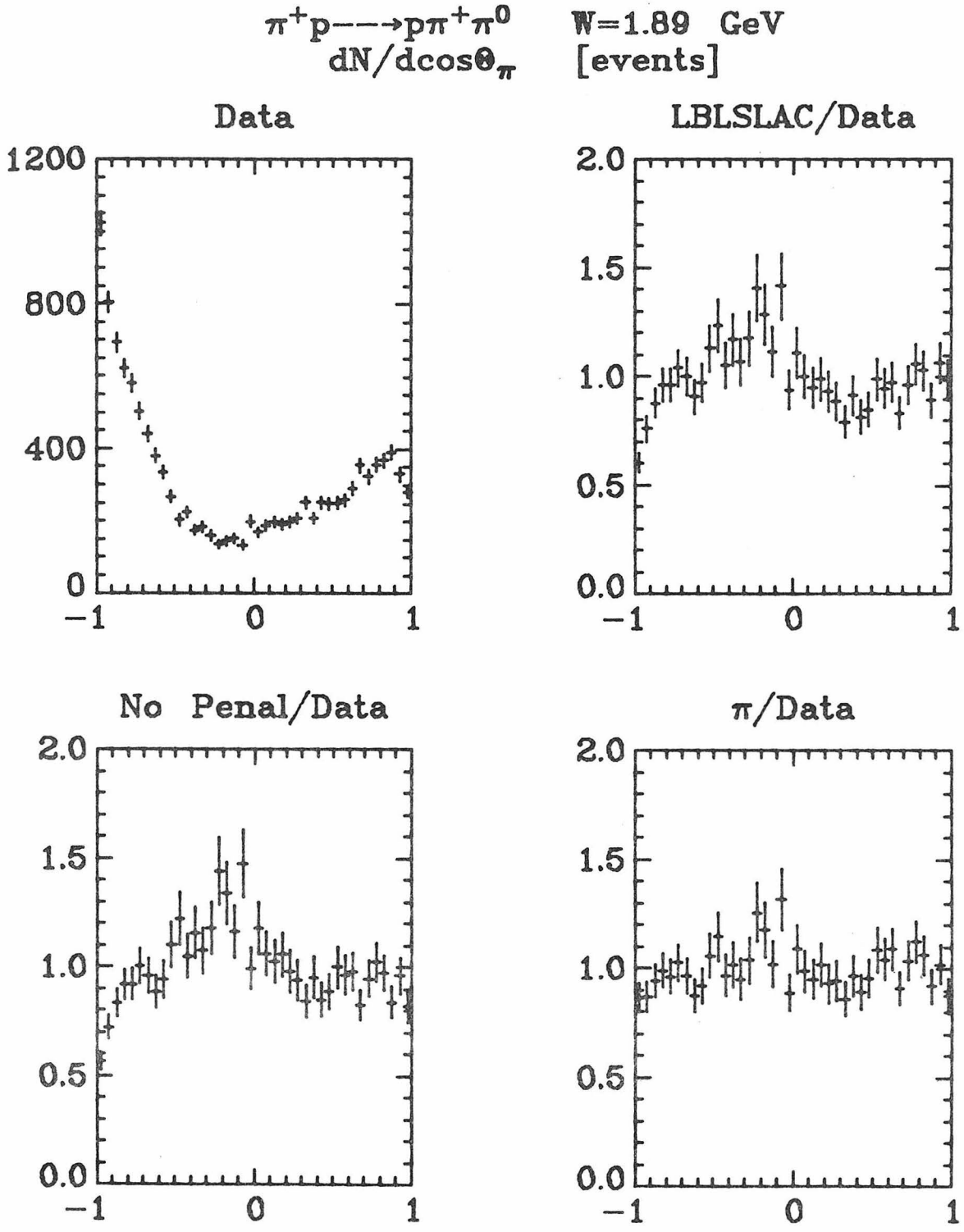

$\pi^-p\longrightarrow n\pi^-\pi^+$
$dN/d\cos\Theta_\pi$
W=1.85 GeV
[events]
Data
LBLSLAC/Data
No Penal/Data
π/Data
500
400
300
200
100
0
1.5
1.0
0.5
0.0
−1
0
1

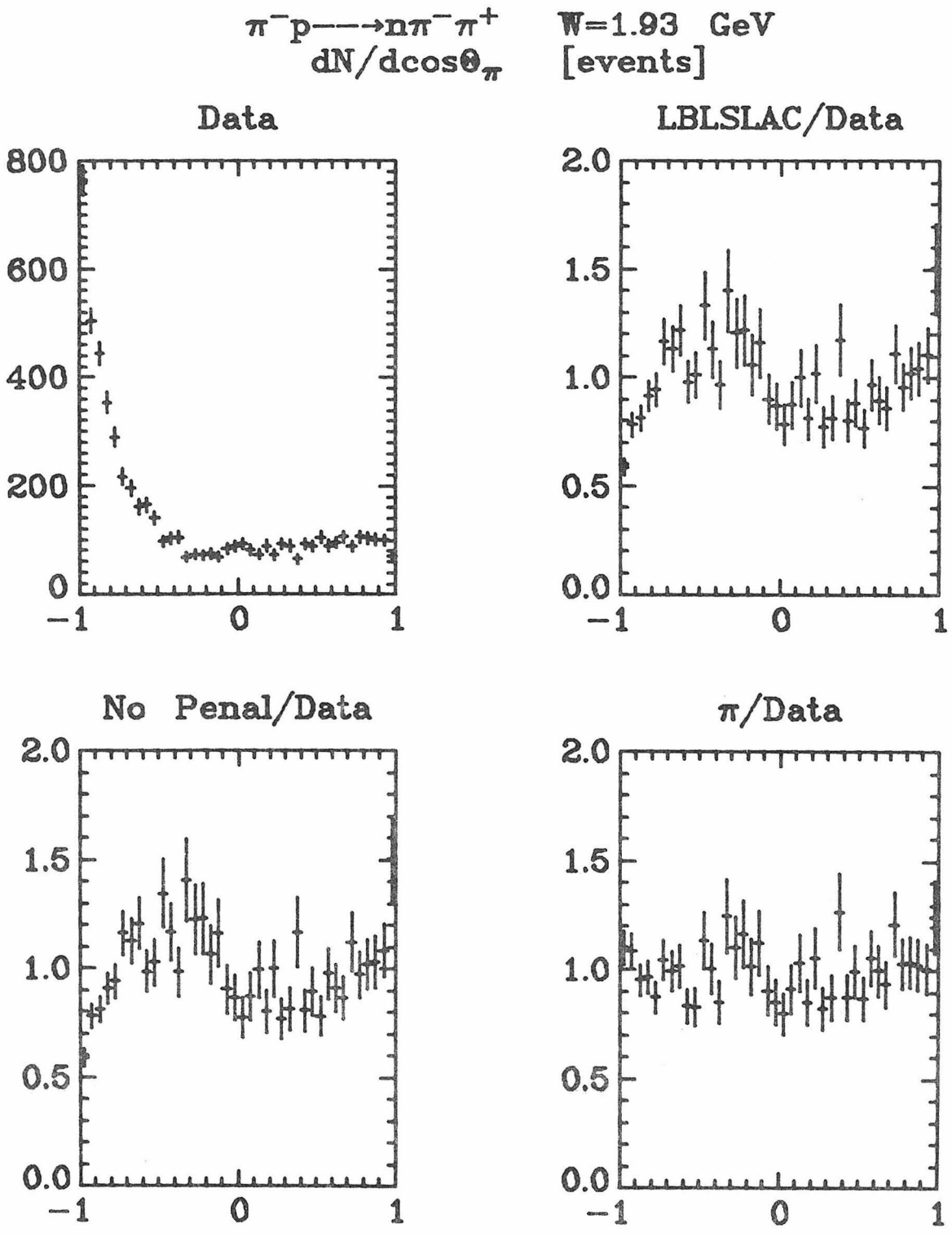

$\pi^- p \longrightarrow p\pi^-\pi^0$
W=1.85 GeV
$dN/d\cos\Theta_\pi$
[events]
Data
LBLSLAC/Data
No Penal/Data
π/Data
240
200
160
120
80
40
0
2.0
1.5
1.0
0.5
0.0
−1
0
1

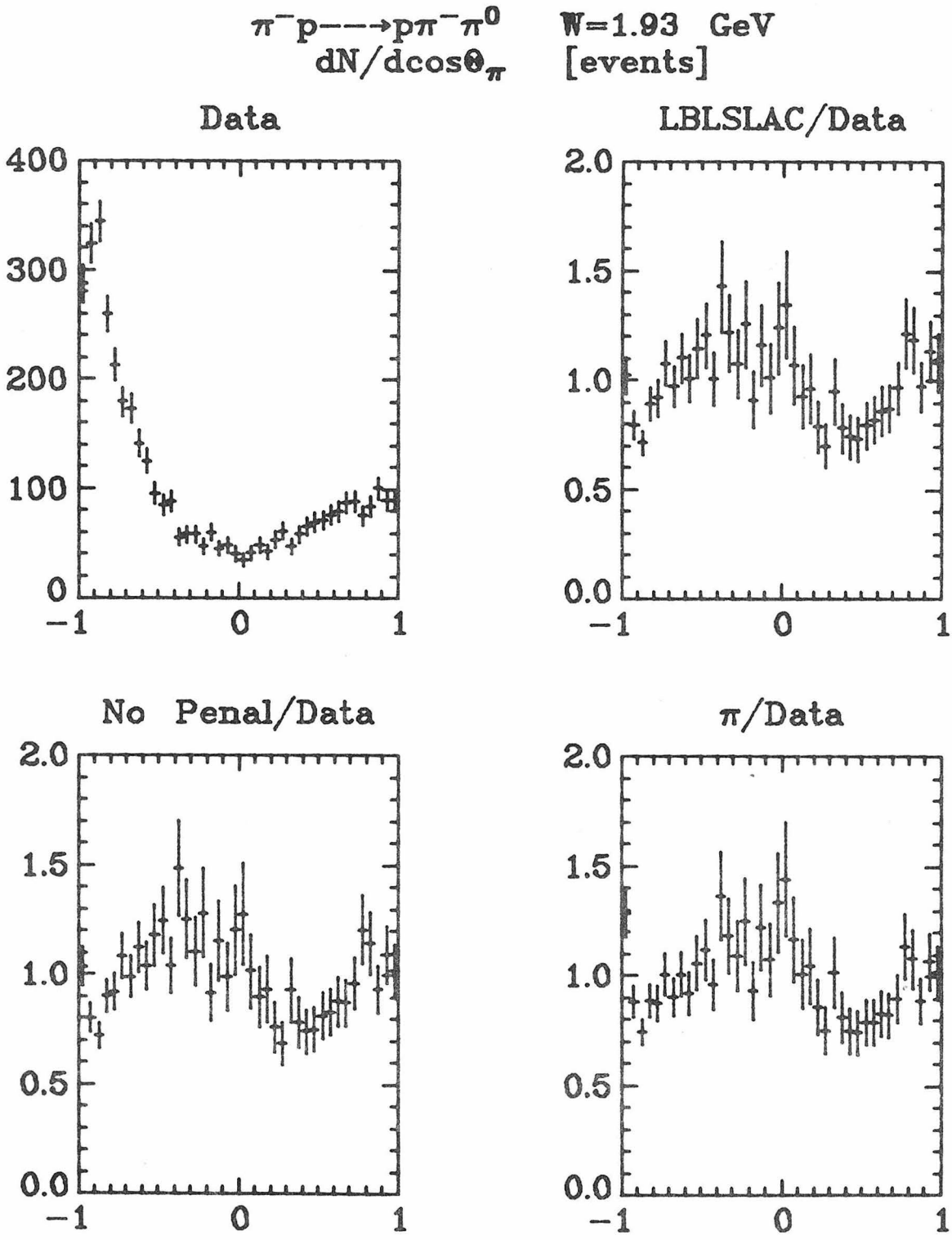

$\pi^+p \longrightarrow p\pi^+\pi^0$
W=1.85 GeV
$dN/d\cos\Theta_\pi$
[events]
Data
LBLSLAC/Data
No Penal/Data
π/Data
500
400
300
200
100
0
1.5
1.0
0.5
0.0
−1
0
1

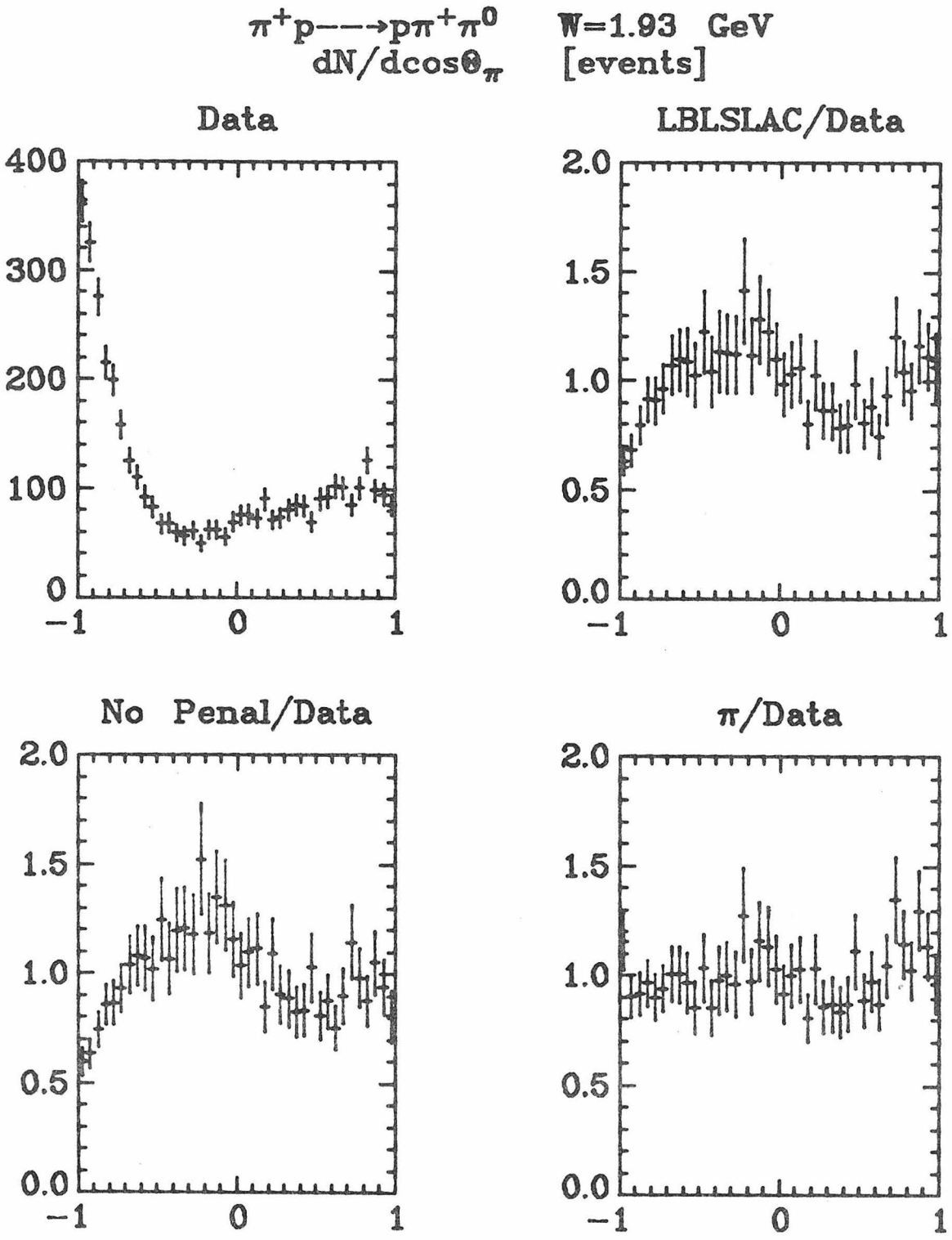

$\pi^- p \longrightarrow n\pi^-\pi^+$
$dN/d\cos\Theta_\pi$
W=1.89 GeV
[events]
Data
LBLSLAC/Data
No Penal/Data
π/Data
700
600
500
400
300
200
100
0
2.0
1.5
1.0
0.5
0.0
−1
0
1

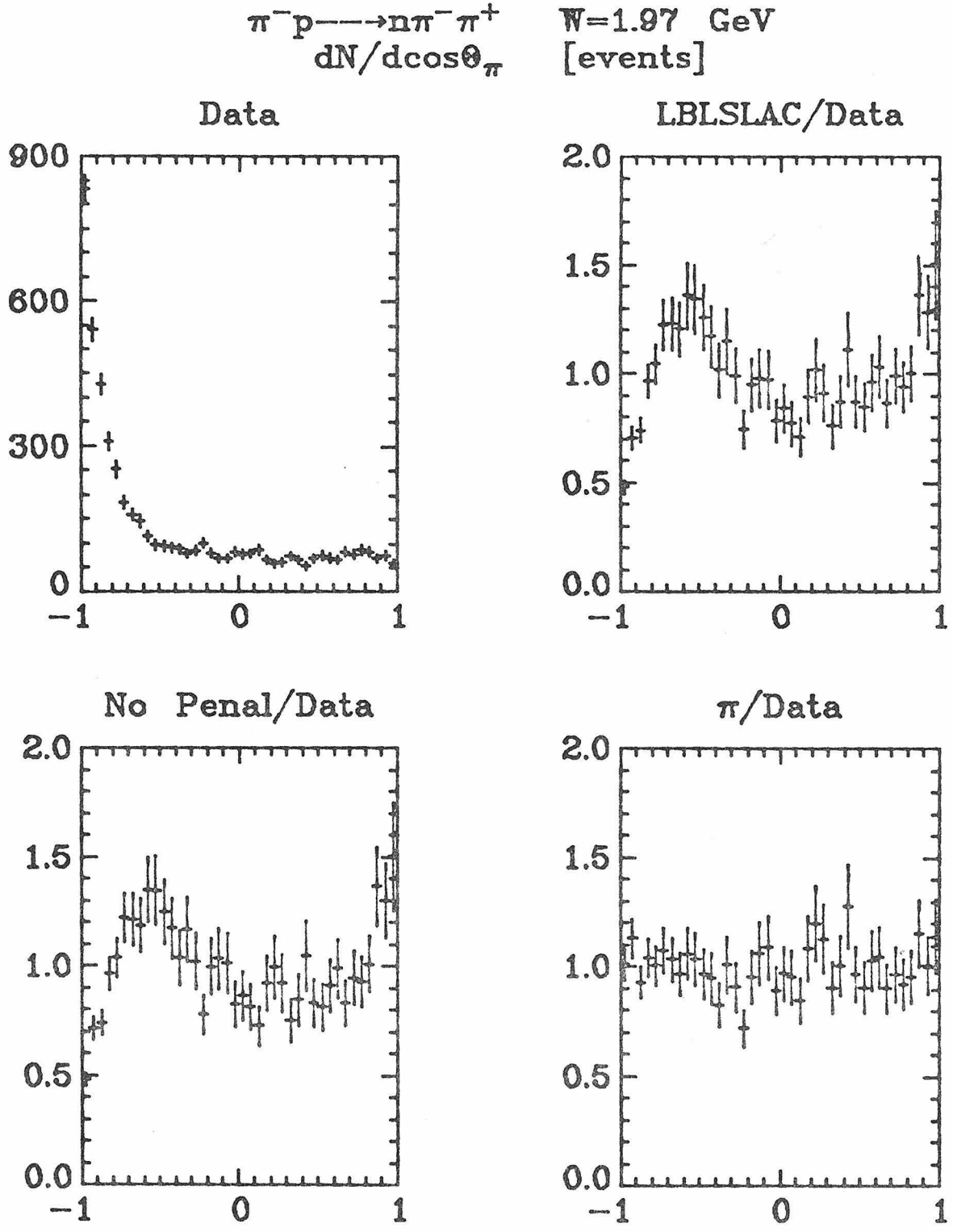

$\pi^- p \longrightarrow p\pi^- \pi^0$
$dN/d\cos\theta_\pi$
W=1.89 GeV
[events]
Data
LBLSLAC/Data
No Penal/Data
π/Data
250
200
150
100
50
0
2.0
1.5
1.0
0.5
0.0
−1
0
1

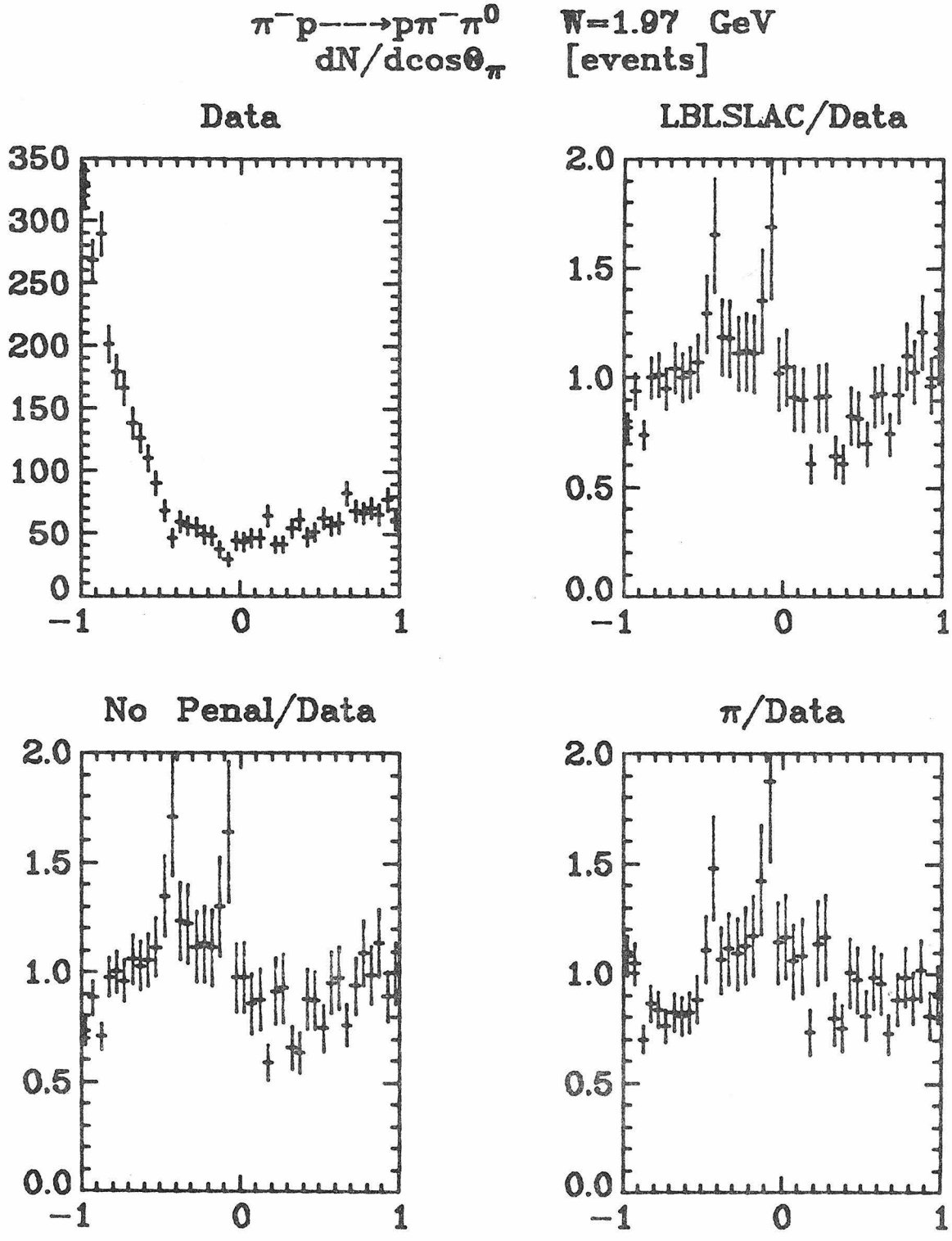

$\pi^+p \longrightarrow p\pi^+\pi^0$
W=1.89 GeV
$dN/d\cos\Theta_\pi$
[events]
Data
LBLSLAC/Data
No Penal/Data
π/Data
1200
800
400
0
2.0
1.5
1.0
0.5
0.0
−1
0
1

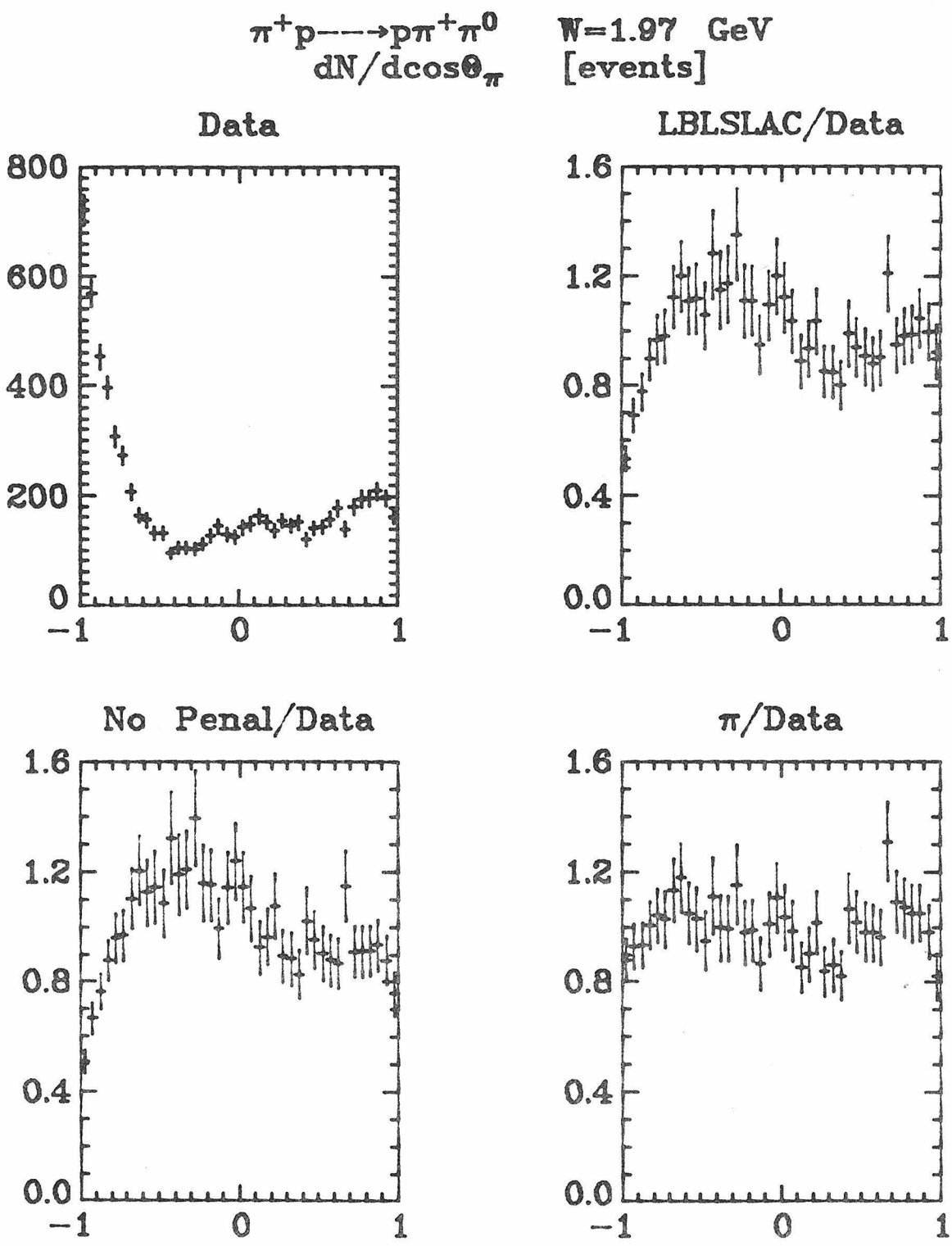

$\pi^- p \longrightarrow n\pi^-\pi^+$
W=1.93 GeV
$dN/d\cos\Theta_\pi$
[events]
Data
LBLSLAC/Data
No Penal/Data
π/Data
800
600
400
200
0
2.0
1.5
1.0
0.5
0.0
−1
0
1


$\pi^- p \longrightarrow p\pi^-\pi^0$
$dN/d\cos\Theta_\pi$
W=1.93 GeV
[events]
Data
LBLSLAC/Data
No Penal/Data
π/Data
400
300
200
100
0
2.0
1.5
1.0
0.5
0.0
−1
0
1


$\pi^+p \longrightarrow p\pi^+\pi^0$ W=1.93 GeV
$dN/d\cos\Theta_\pi$ [events]
Data
LBLSLAC/Data
No Penal/Data
π/Data
400
300
200
100
0
2.0
1.5
1.0
0.5
0.0
−1
0
1


$\pi^- p \longrightarrow n\pi^-\pi^+$
W=1.97 GeV
$dN/d\cos\Theta_\pi$
[events]
Data
LBLSLAC/Data
No Penal/Data
π/Data
900
600
300
0
2.0
1.5
1.0
0.5
0.0
−1
0
1


$\pi^- p \longrightarrow p\pi^-\pi^0$
$dN/d\cos\theta_\pi$
W=1.97 GeV
[events]
Data
LBLSLAC/Data
No Penal/Data
π/Data
350
300
250
200
150
100
50
0
2.0
1.5
1.0
0.5
0.0
−1
0
1


$\pi^+p \longrightarrow p\pi^+\pi^0$
$dN/d\cos\Theta_\pi$
W=1.97 GeV
[events]
Data
LBLSLAC/Data
No Penal/Data
π/Data
800
600
400
200
0
1.6
1.2
0.8
0.4
0.0
−1
0
1

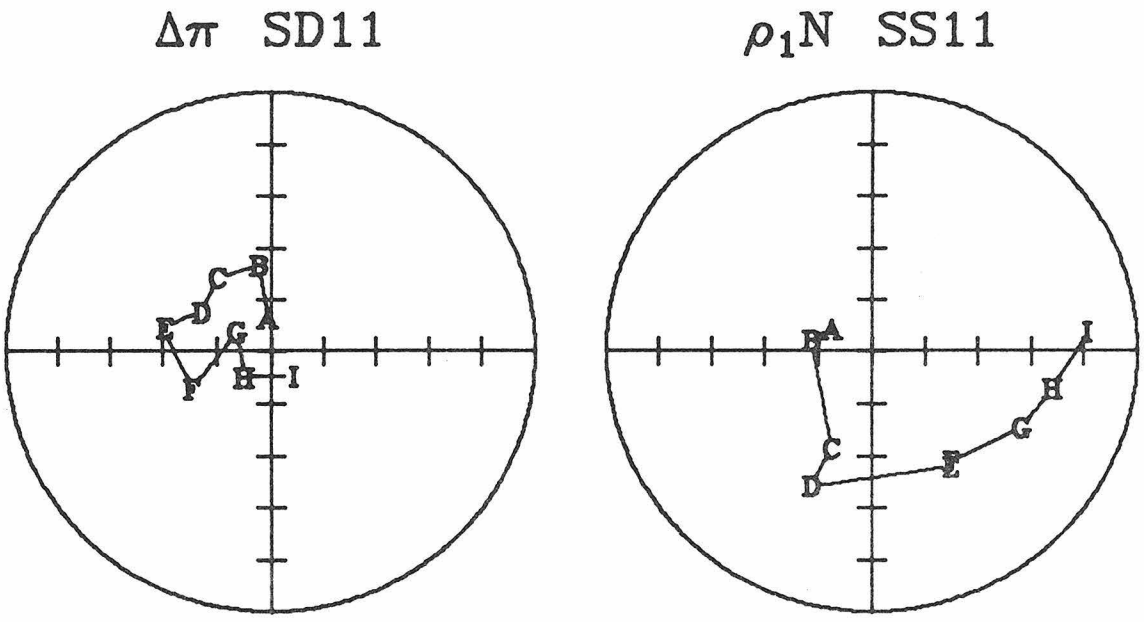
Appendix 3: Argand diagrams comparing the T-matrix elements for the LBL-SLAC and π-fits. The letters

A, B, C, D, E, F, G, H, I

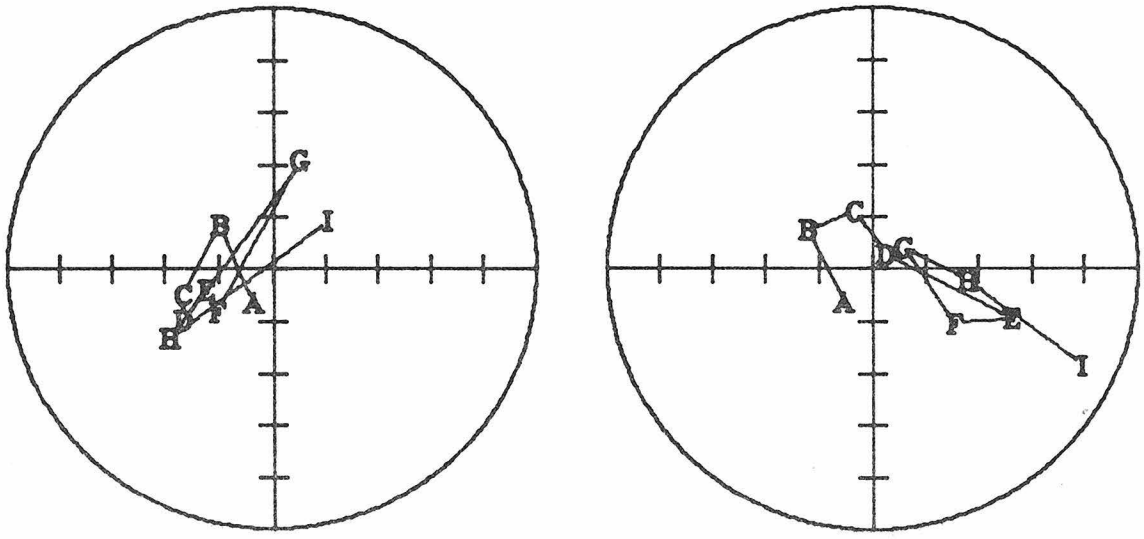
correspond to the c.m. energies

1.65,1.69,1.73,1.77,1.81,1.85,1.89,1.93,1.97

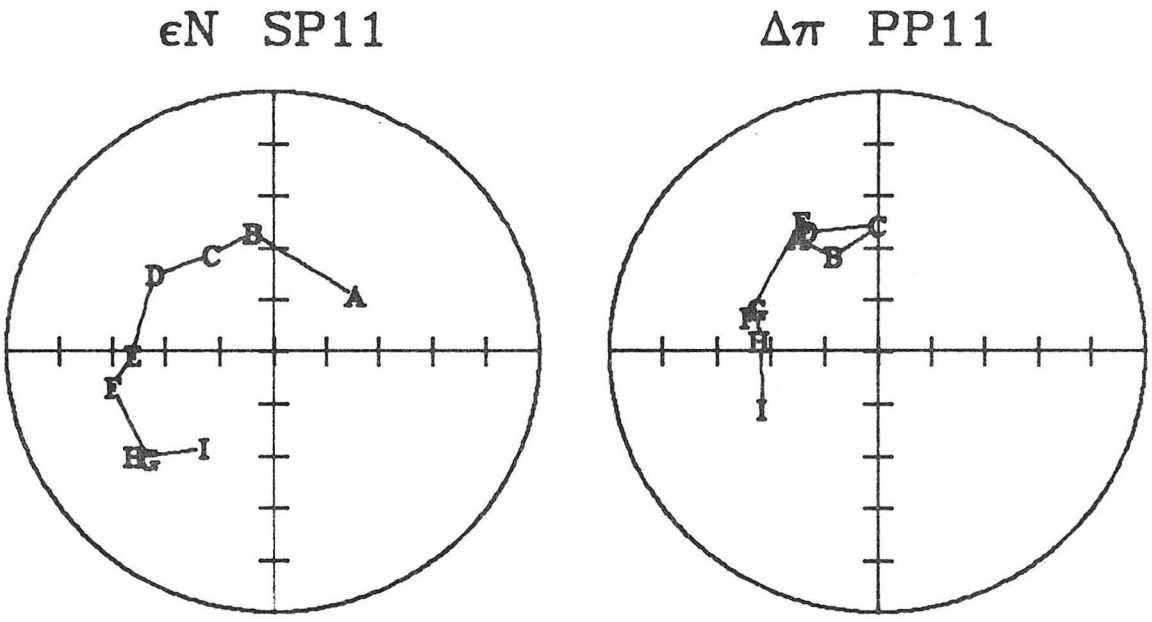
GeV respectively. Note that the overall phase of the π-fit is not well determined below 1.8 GeV, i.e. for points A,B,C and D, though the relative phases of the different waves are determined by the fit at all energies.



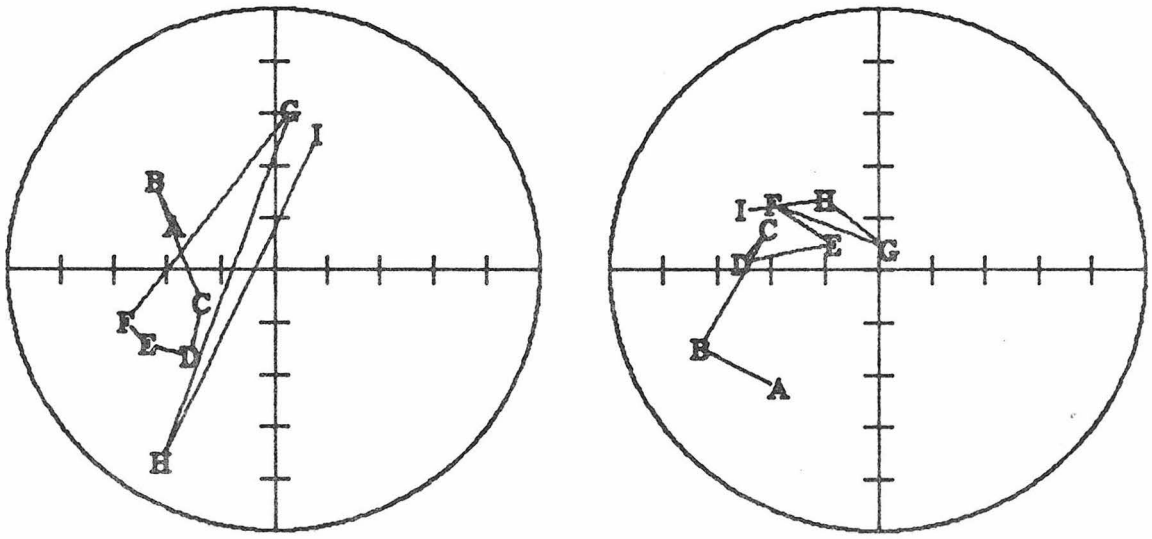
LBL–SLAC solution



π solution

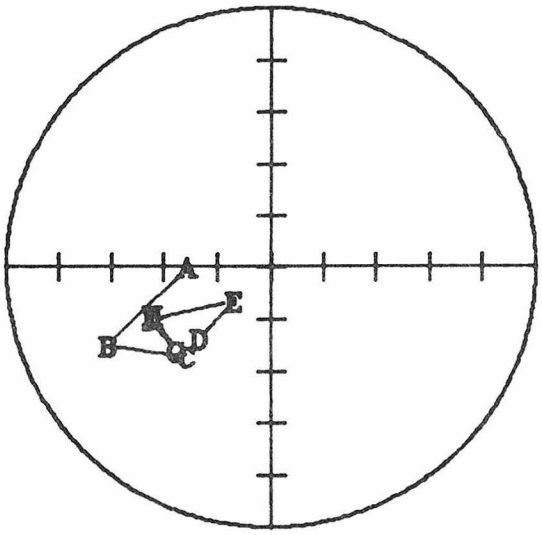


LBL–SLAC solution

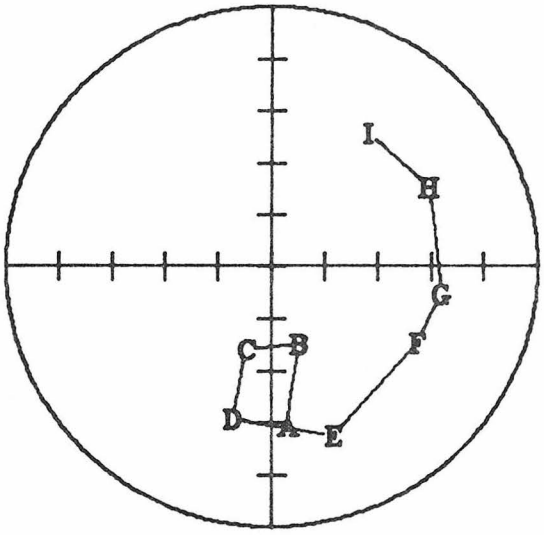


π solution

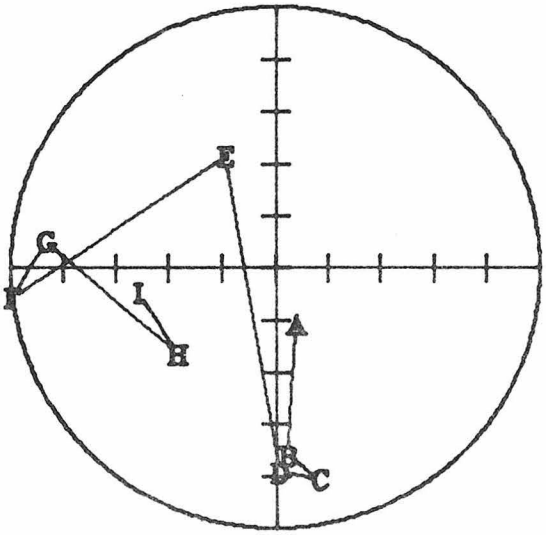
ρ_1N PP11

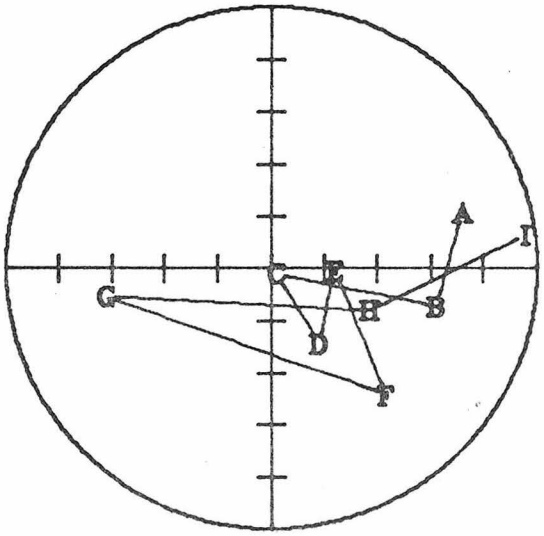


ϵN PS11

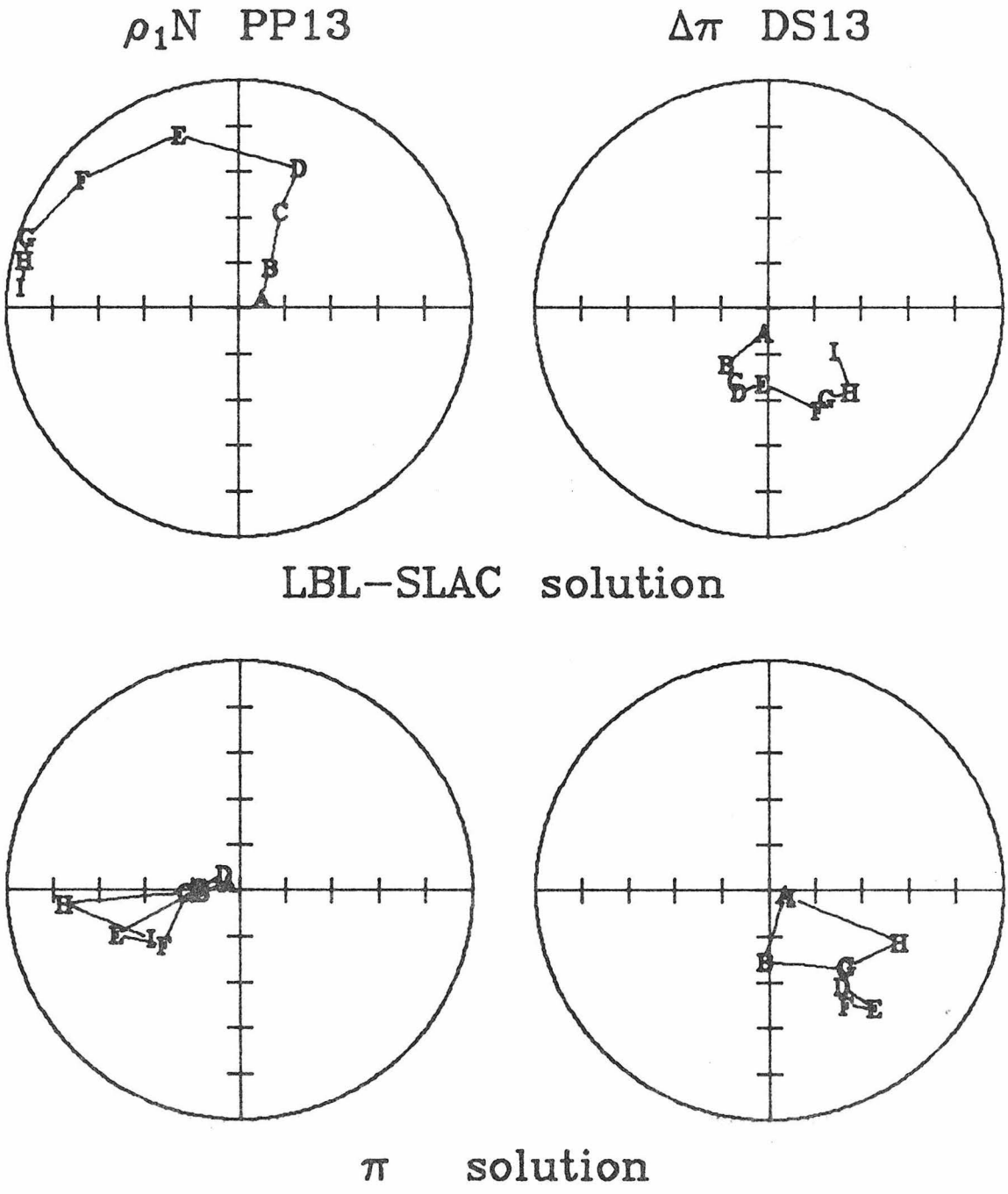


LBL–SLAC solution

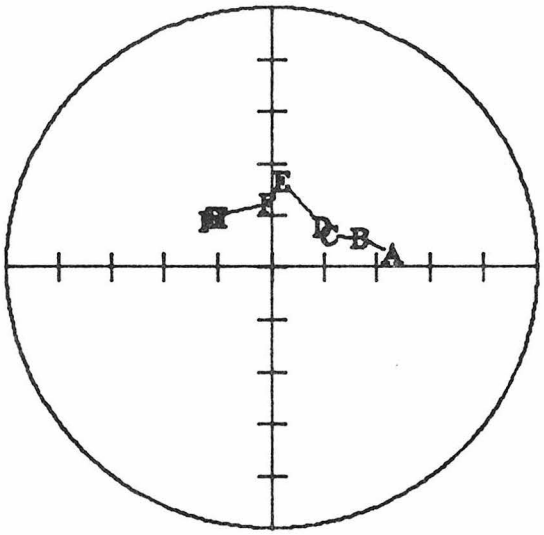




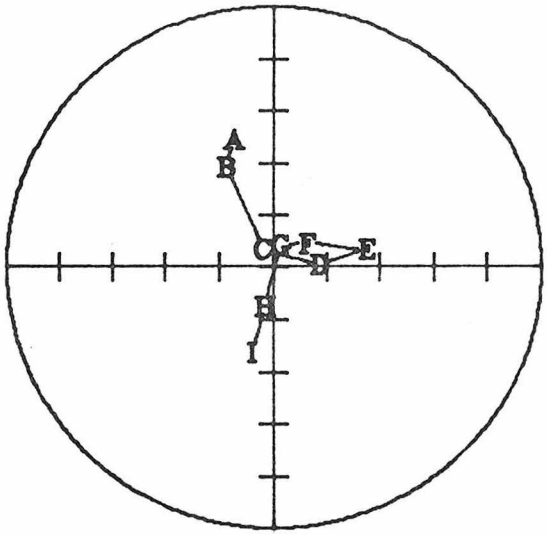
π solution


ρ_1N PP13
$\Delta\pi$ DS13
LBL–SLAC solution
π solution

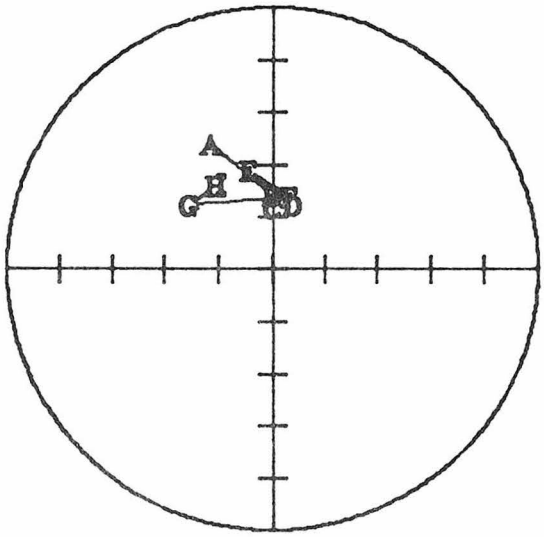
$\Delta\pi$ DD13

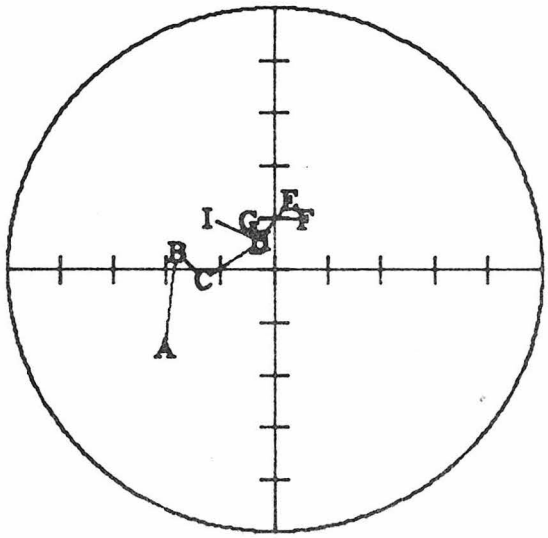


ρ_3N DS13

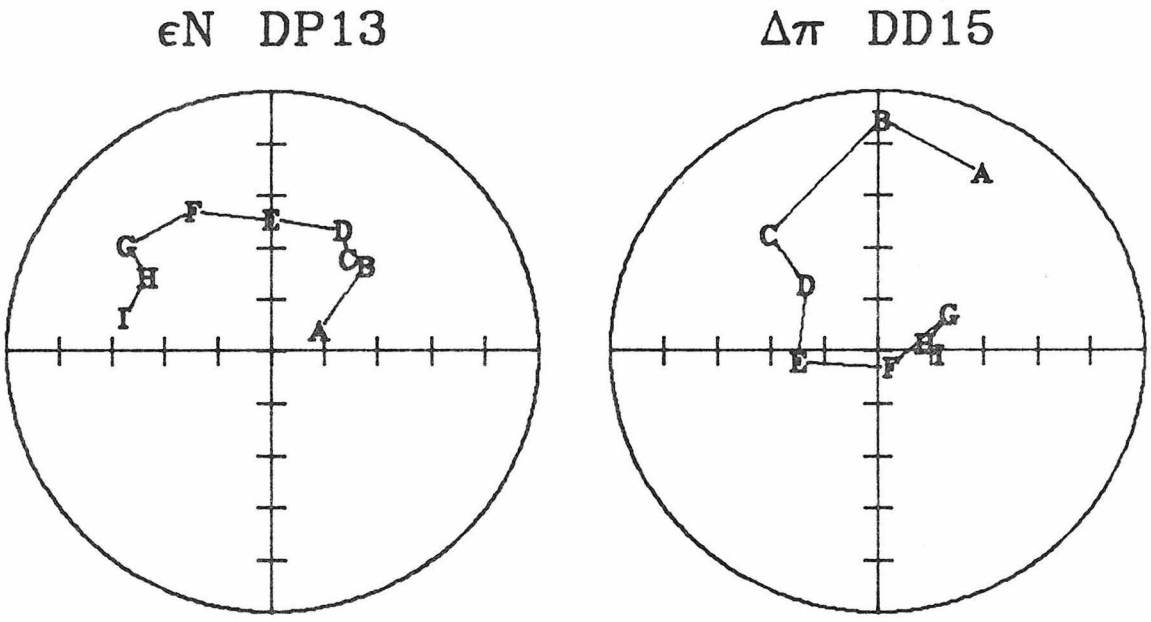


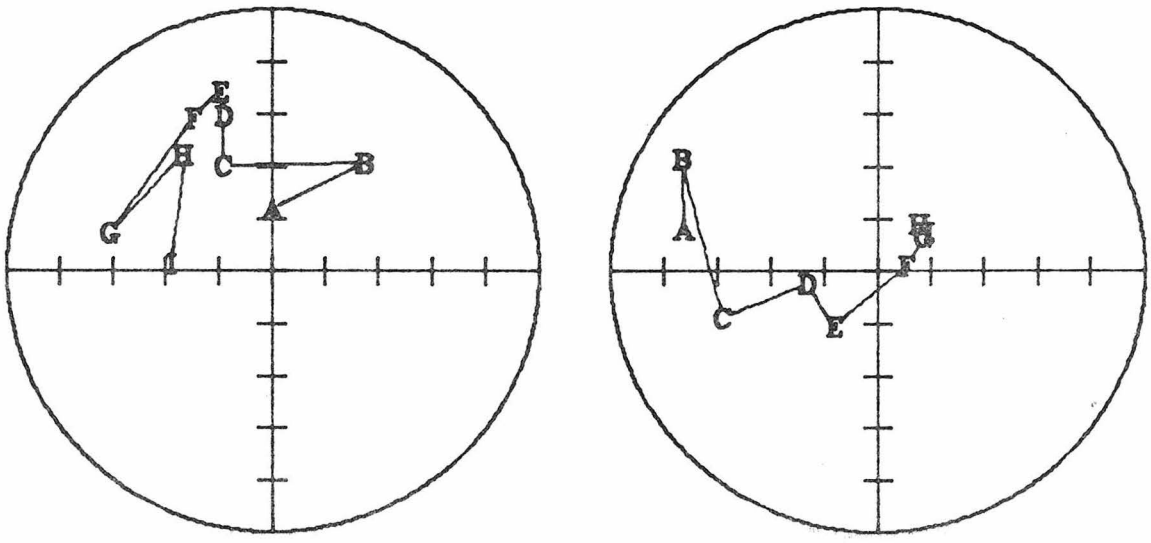
LBL–SLAC solution

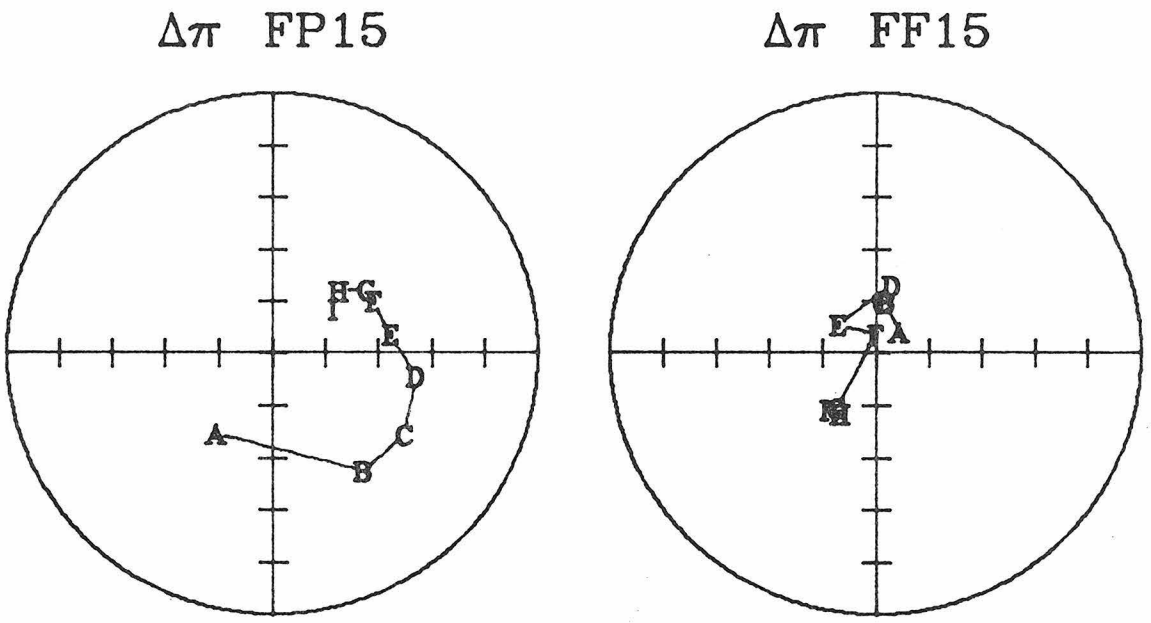


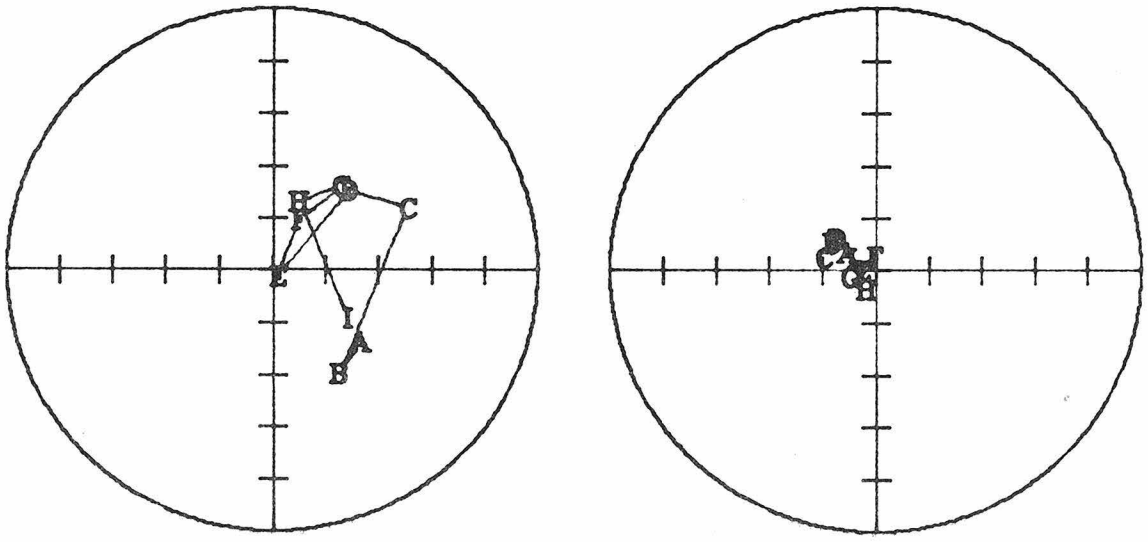


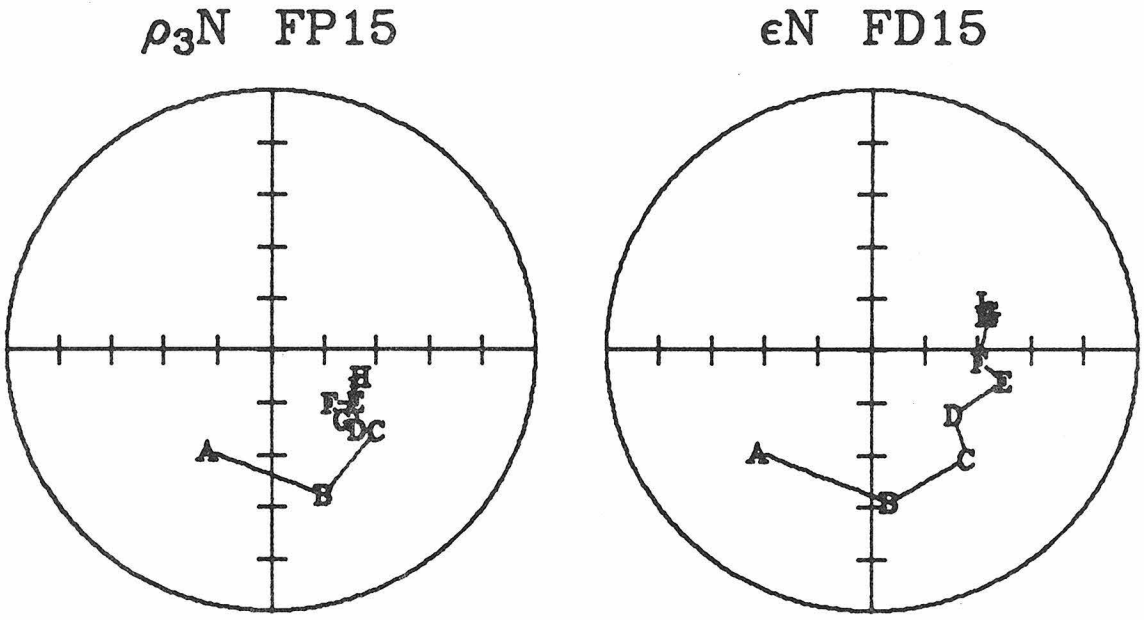
π solution


εN DP13
Δπ DD15
LBL–SLAC solution

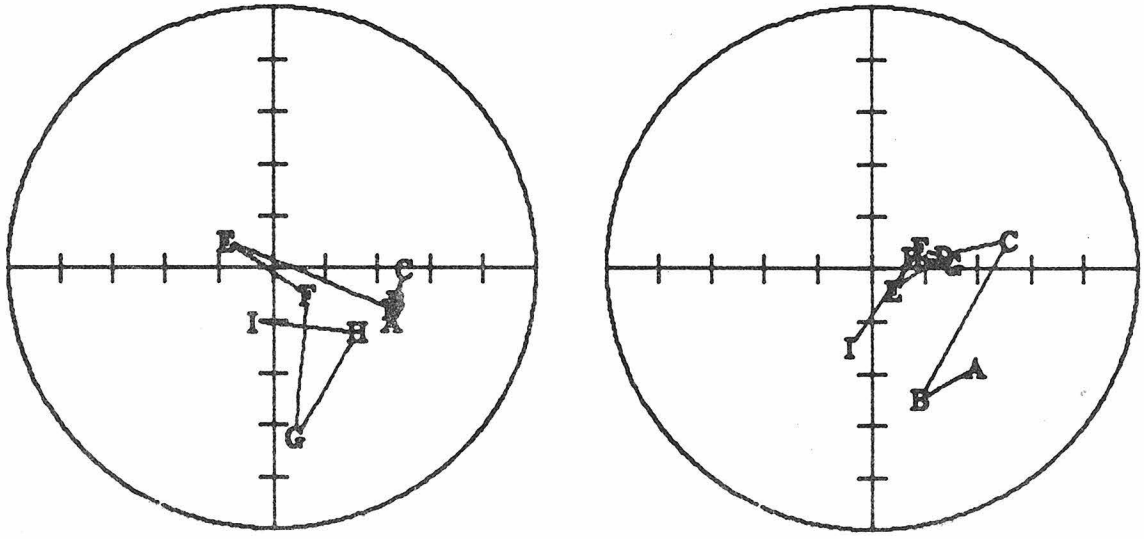

π solution


Δπ FP15
Δπ FF15
LBL–SLAC solution

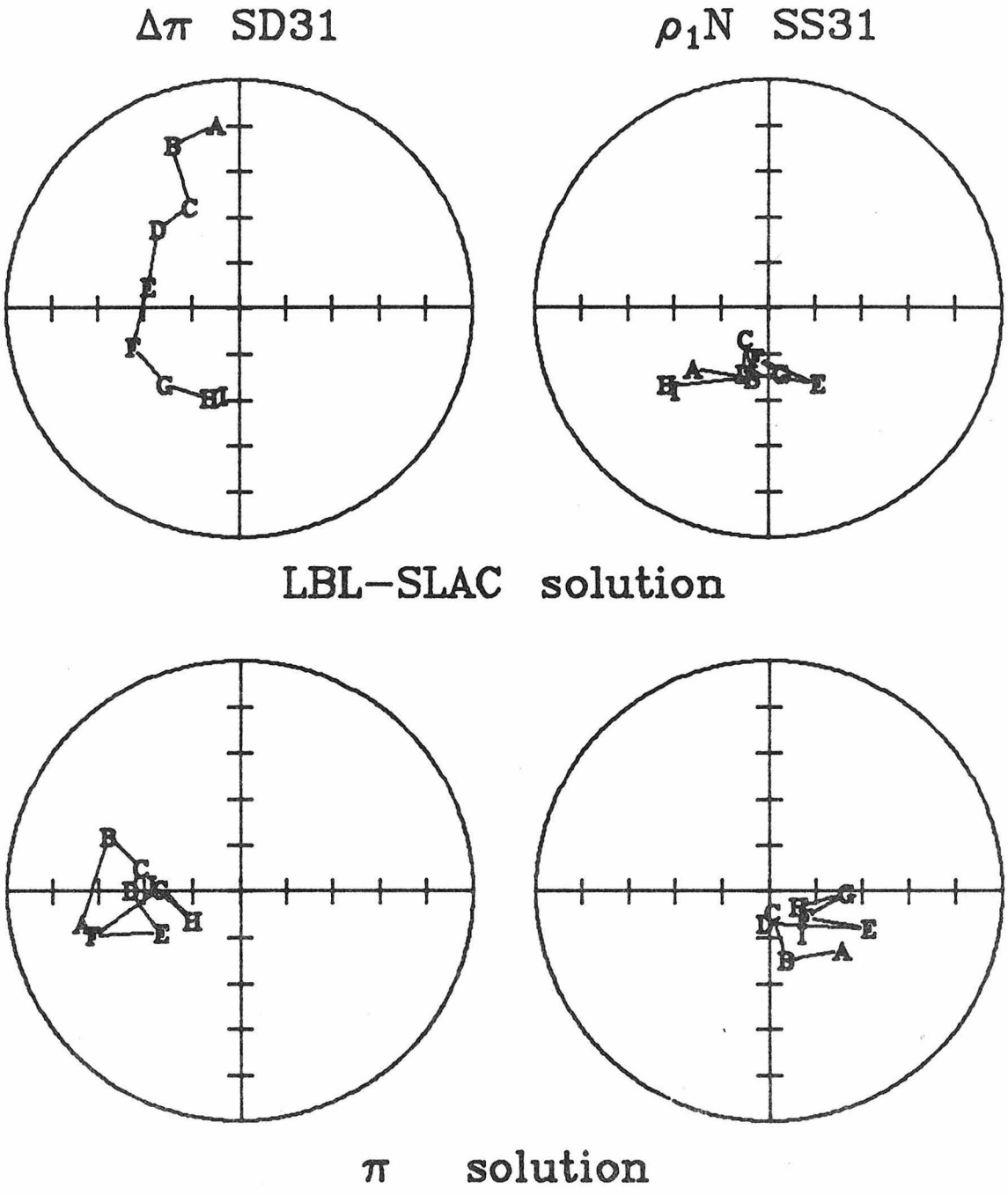

π solution



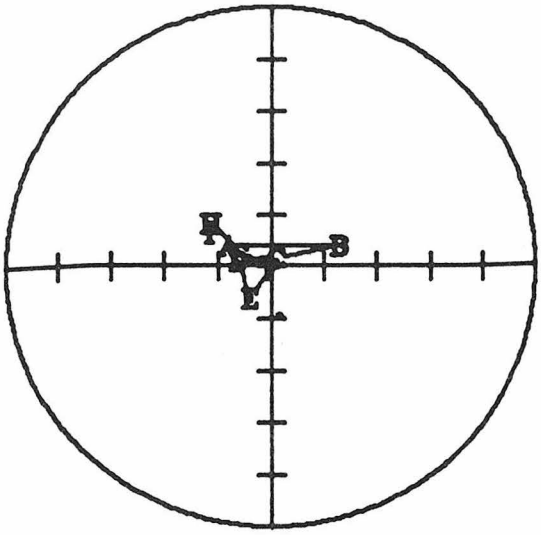
LBL–SLAC solution



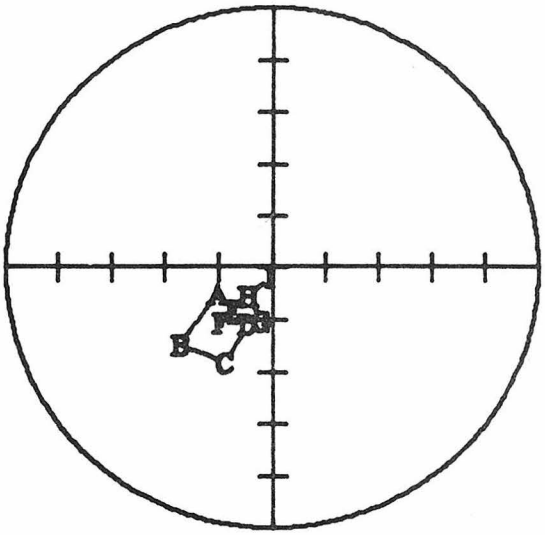
π solution


Δπ SD31
ρ1N SS31
A
B
C
D
E
F
G
H
I
LBL–SLAC solution
π solution

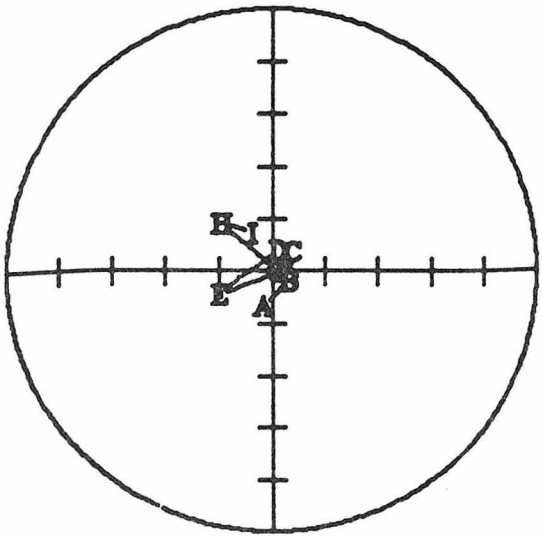
$\Delta\pi$ PP31

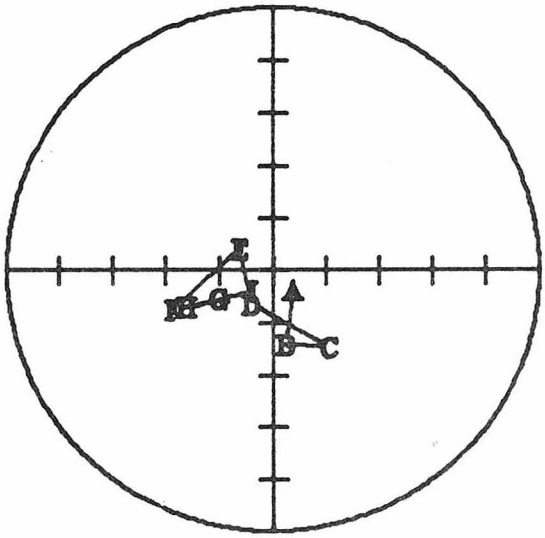


ρ_1N PP31

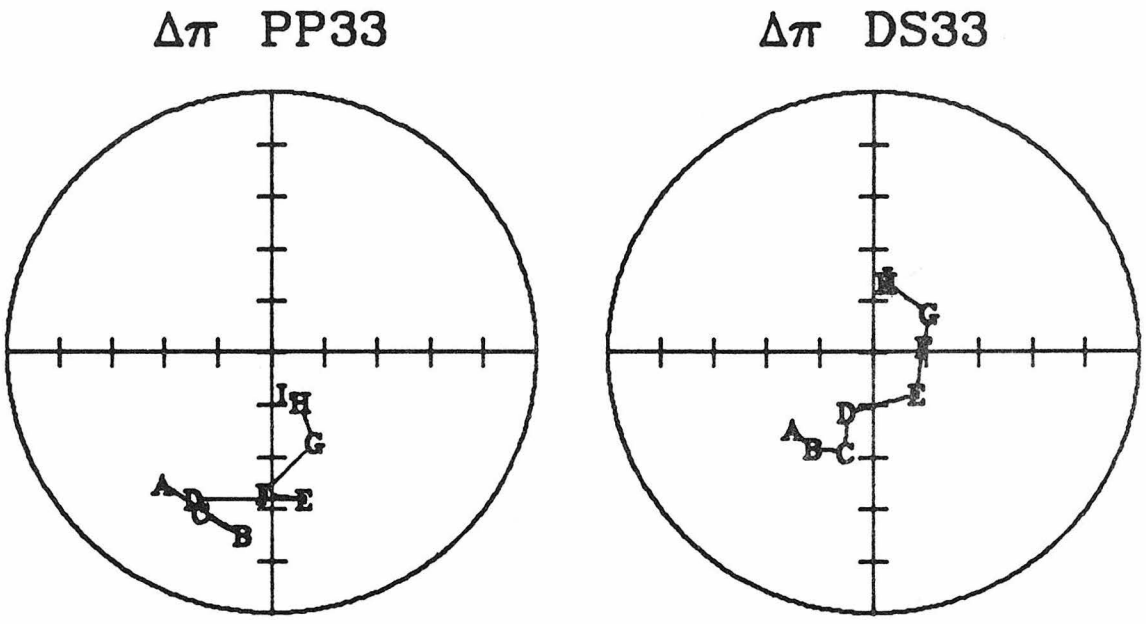


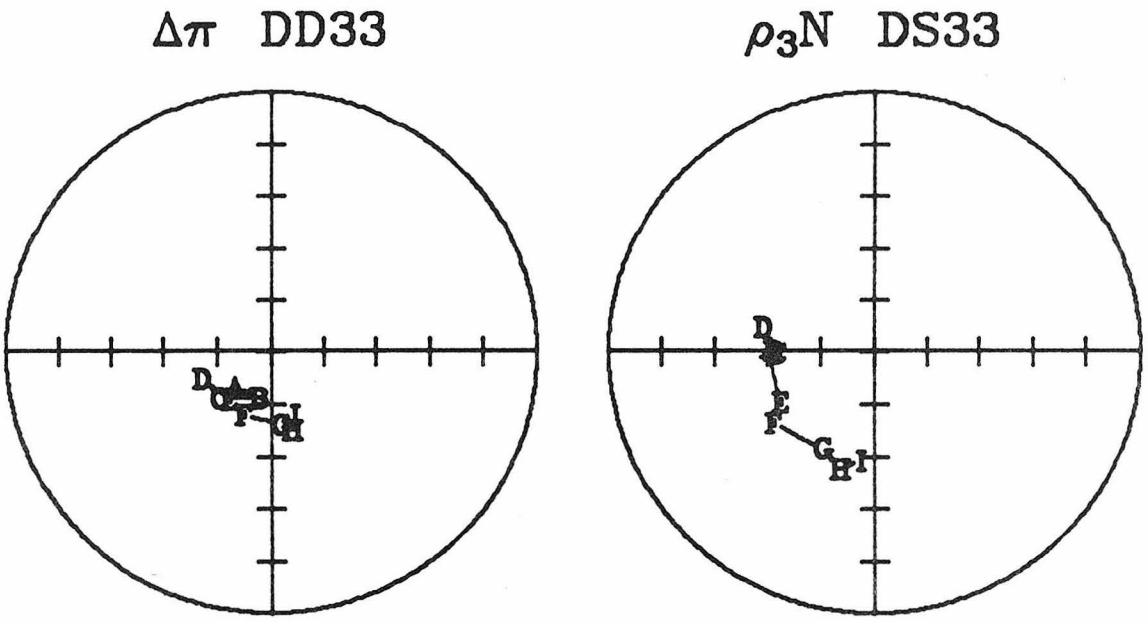
LBL–SLAC solution



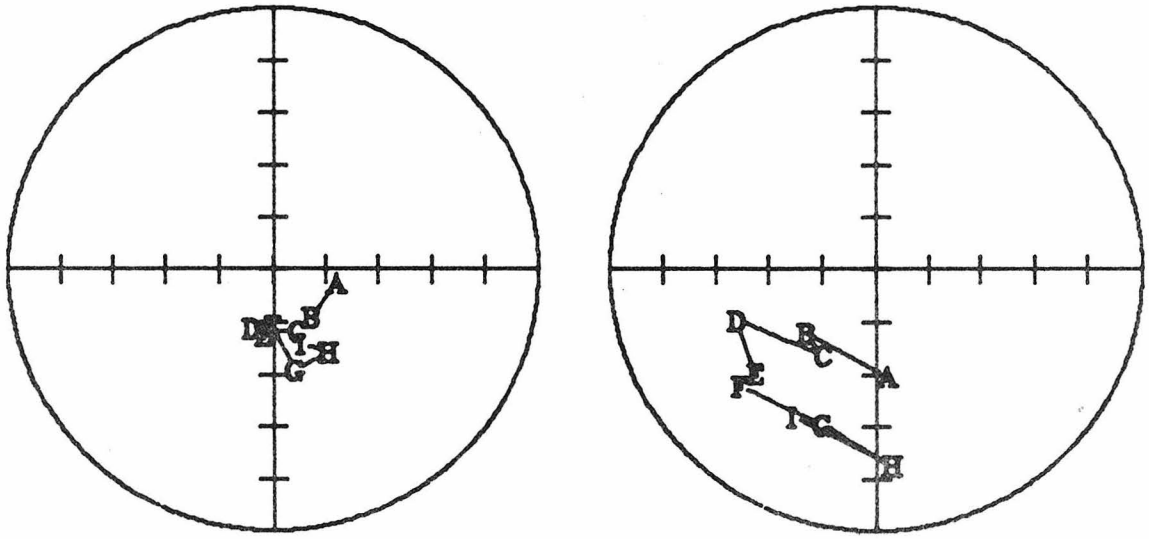


π solution

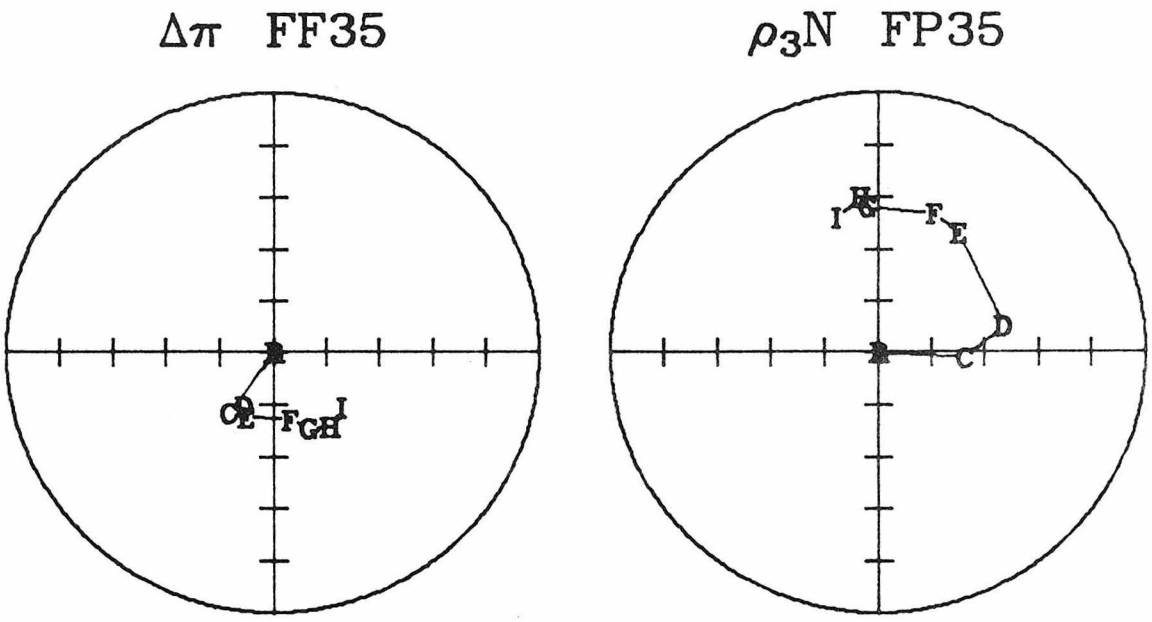

Δπ PP33
Δπ DS33
LBL–SLAC solution
π solution



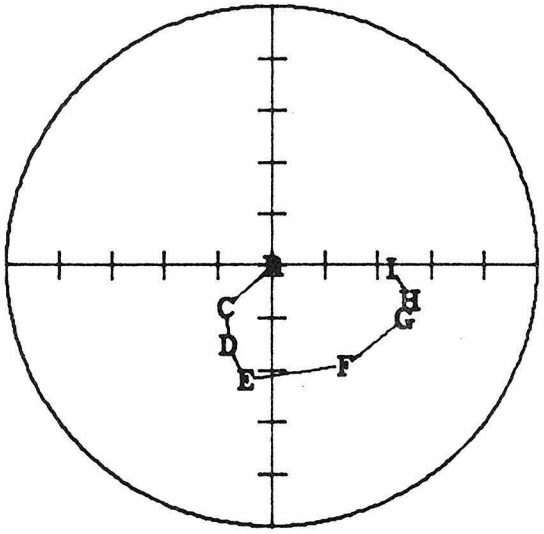
LBL–SLAC solution



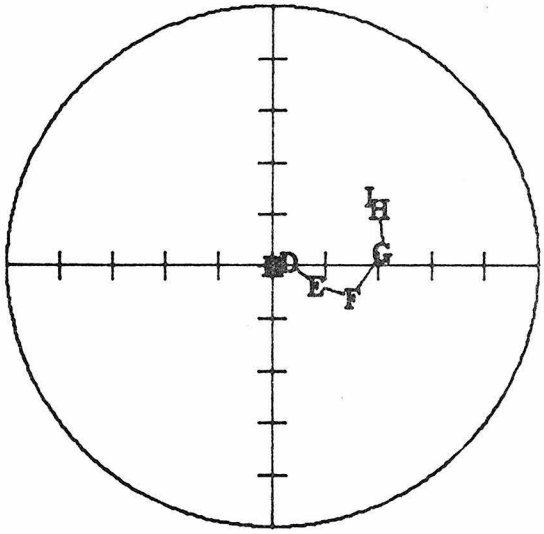
π solution


Δπ FF35
ρ3N FP35
LBL–SLAC solution
π solution

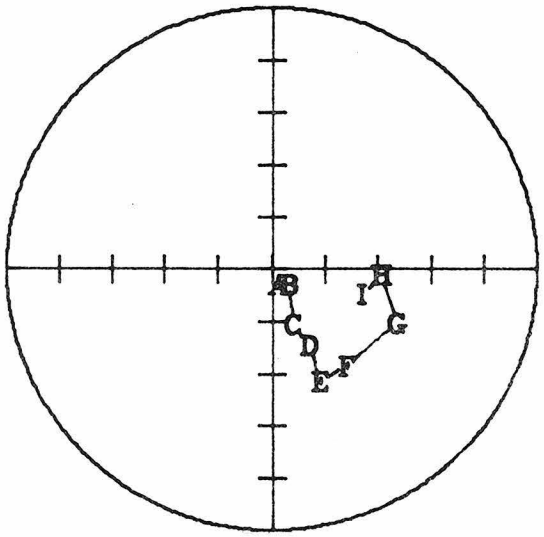
$\Delta\pi$ FF37

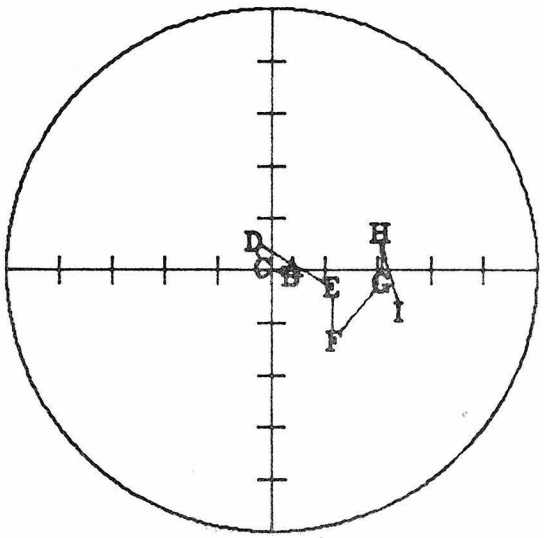


ρ_3N FF37



LBL–SLAC solution





π solution

Appendix 4: Table of all T-matrix elements from the π-fit. Errors are determined as in Part I of this thesis, Equation VI-8. The overall phase below 1.8 GeV is ill-determined, as described in Section VII.D.

ENERGY	REAL(T)	D(REAL(T))	IMAG(T)	D(IMAG(T))
Δπ SD11				
1.65	-.037102	.022979	-.064852	.027903
1.69	-.097428	.027947	.084165	.033730
1.73	-.166374	.026182	-.051755	.031874
1.77	-.165951	.028743	-.099496	.028743
1.81	-.123940	.034507	-.040638	.027005
1.85	-.102008	.025087	-.082809	.026759
1.89	.052812	.026161	.205759	.026161
1.93	-.190094	.022684	-.135802	.024747
1.97	.106622	.020359	.091504	.024883
ρ_1N SS11				
1.65	-.053486	.021217	-.063647	.025461
1.69	-.121416	.019824	.075173	.031719
1.73	-.033244	.026743	.110495	.023400
1.77	.026233	.024891	.028839	.024891
1.81	.260495	.025035	-.095236	.033380
1.85	.152283	.022016	-.104527	.024218
1.89	.059958	.020515	.041876	.020515
1.93	.180238	.016359	-.021752	.018696
1.97	.395857	.018995	-.186315	.018995
εN SP11				
1.65	-.187463	.032315	.083587	.031048
1.69	-.222843	.037711	.168690	.035514
1.73	-.137485	.026226	-.064544	.032148
1.77	-.157416	.037095	-.166236	.027584
1.81	-.238254	.047842	-.143665	.035616
1.85	-.279310	.036377	-.099199	.037550
1.89	.031109	.030779	.305139	.031420
1.93	-.212133	.037501	-.369853	.020140
1.97	.082363	.027655	.260090	.028402
Δπ PP11				
1.65	-.188526	.034133	-.226144	.034133
1.69	-.332083	.030013	-.150549	.042518
1.73	-.205988	.024365	.078389	.029779
1.77	-.258508	.026327	.012451	.029252
1.81	-.086456	.028163	.049576	.034421
1.85	-.199500	.023087	.125760	.026385
1.89	.019531	.020874	.039563	.020874
1.93	-.100890	.021957	.134204	.025616
1.97	-.258082	.019080	.114845	.026712

ENERGY	REAL(T)	D(REAL(T))	IMAG(T)	D(IMAG(T))
ρ_1N PP11				
1.65	.037877	.023971	-.109073	.023050
1.69	.021829	.042277	-.361326	.020755
1.73	.083094	.035042	-.407770	.022853
1.77	.007812	.033051	-.394091	.021825
1.81	-.093529	.035868	.214304	.025947
1.85	-.496754	.018585	-.056298	.029205
1.89	-.431836	.021076	.051692	.028101
1.93	-.183774	.022174	-.165534	.019957
1.97	-.258463	.024336	-.047919	.025552
εN PS11				
1.65	.359246	.031247	.107024	.044113
1.69	.308362	.034126	-.074553	.043159
1.73	.008507	.025814	-.010141	.034416
1.77	.090368	.032109	-.144710	.032109
1.81	.119524	.044603	-.003168	.040991
1.85	.215446	.030305	-.242721	.030305
1.89	-.311242	.022264	-.052927	.031431
1.93	.184493	.023023	-.079182	.025732
1.97	.478892	.022247	.065433	.030589
ρ_1N PP13				
1.65	-.024086	.012601	.017962	.012908
1.69	-.080161	.013446	-.003973	.016905
1.73	-.088720	.016768	.006553	.016768
1.77	-.032505	.017455	.036004	.014338
1.81	-.264587	.022126	-.098139	.022889
1.85	-.162109	.015054	-.121592	.017710
1.89	-.113254	.015077	-.003943	.014072
1.93	-.377918	.012184	-.030706	.015507
1.97	-.188694	.018270	-.105321	.014616
$\Delta\pi$ DS13				
1.65	.034239	.012757	-.007751	.019135
1.69	-.010455	.026233	-.156549	.019674
1.73	.160054	.019447	-.169623	.025930
1.77	.155903	.026315	-.208933	.019736
1.81	.223036	.026158	-.257905	.026158
1.85	.162864	.019598	-.251479	.019598
1.89	.167289	.019450	-.164731	.012967
1.93	.279195	.013030	-.112113	.019545
1.97	.047403	.012892	-.014705	.019339

ENERGY	REAL(T)	D(REAL(T))	IMAG(T)	D(IMAG(T))
$\Delta\pi$ DD13				
1.65	-.114961	.032202	.239251	.025597
1.69	-.001603	.022264	.140809	.021298
1.73	-.000431	.017194	.115207	.020611
1.77	.038435	.019668	.122086	.019669
1.81	-.046835	.025541	.188447	.022536
1.85	.029815	.018467	.137333	.020145
1.89	-.156923	.016865	.121809	.020612
1.93	-.106450	.016540	.158344	.018607
1.97	-.095988	.015825	.163694	.018086
ρ_3N DS13				
1.65	-.203317	.022320	-.148221	.027634
1.69	-.180529	.015871	.035059	.022483
1.73	-.130770	.015038	-.016110	.016709
1.77	-.028696	.015339	.051102	.017256
1.81	.027621	.018763	.133543	.018763
1.85	.058483	.013204	.098361	.017606
1.89	-.046156	.015936	.095586	.011383
1.93	-.025950	.014015	.057224	.011679
1.97	-.125203	.011871	.098988	.014245
ϵN DP13				
1.65	.000240	.023464	.117810	.023114
1.69	.173852	.030021	.206089	.029288
1.73	-.092149	.028768	.201902	.023691
1.77	-.090369	.031863	.298437	.018547
1.81	-.097450	.035066	.343327	.020189
1.85	-.148948	.024656	.292778	.019960
1.89	-.305806	.019890	.074089	.020531
1.93	-.165711	.019439	.223320	.016662
1.97	-.189196	.018687	.015402	.019435
$\Delta\pi$ DD15				
1.65	-.364020	.016478	.081800	.048610
1.69	-.367691	.027101	.215289	.042587
1.73	-.291572	.013727	-.088026	.026310
1.77	-.132853	.017063	-.023647	.018375
1.81	-.081932	.020981	-.105506	.017984
1.85	.055650	.016803	.011125	.015123
1.89	.087211	.013090	.068062	.014960
1.93	.078967	.012406	.091050	.014473
1.97	.096177	.013602	.075236	.015869

ENERGY	REAL(T)	D(REAL(T))	IMAG(T)	D(IMAG(T))
$\Delta\pi$ FP15				
1.65	.164401	.020763	-.138011	.025377
1.69	.124667	.027862	-.199505	.020263
1.73	.254564	.016396	.117647	.027327
1.77	.141804	.017676	.152985	.017676
1.81	.008839	.018843	-.012577	.018842
1.85	.049009	.016595	.096698	.013276
1.89	.131399	.013939	.162118	.013939
1.93	.049608	.014694	.132668	.011021
1.97	.142586	.011465	-.091742	.015287
$\Delta\pi$ FF15				
1.65	-.054110	.010742	.035558	.018108
1.69	-.084191	.013797	.053826	.018780
1.73	-.097847	.012306	.024666	.018706
1.77	-.074479	.015573	.061407	.016771
1.81	-.025292	.016817	.002244	.019739
1.85	-.001076	.014689	.027001	.016423
1.89	-.045569	.013256	-.011276	.014275
1.93	-.016372	.011784	-.035576	.016497
1.97	-.043910	.013564	.024968	.014921
ρ_3N FP15				
1.65	.224759	.017532	-.102132	.030144
1.69	.232920	.014217	-.063723	.025360
1.73	.250325	.012692	-.002065	.022344
1.77	.224367	.014339	-.077569	.018079
1.81	-.089704	.016040	.052462	.014513
1.85	.064256	.011511	-.052751	.012396
1.89	.042091	.017076	-.324521	.011049
1.93	.161725	.009962	-.122197	.013282
1.97	-.038476	.013391	-.101845	.012174
εN FD15				
1.65	.193394	.026649	-.189056	.027258
1.69	.089307	.031457	-.249254	.018696
1.73	.256451	.015992	.055374	.026102
1.77	.134437	.019324	.026336	.017804
1.81	.039180	.025727	-.041107	.019552
1.85	.090358	.017599	.041490	.017003
1.89	.154554	.015038	.009907	.016405
1.93	.076585	.013926	.022437	.012379
1.97	-.041774	.016513	-.151924	.013472

ENERGY	REAL(T)	D(REAL(T))	IMAG(T)	D(IMAG(T))
$\Delta\pi$ SD31				
1.65	-.336717	.016273	-.069744	.048007
1.69	-.278725	.025162	.119848	.042581
1.73	-.208864	.017215	.050309	.022953
1.77	-.231176	.019788	.001385	.022420
1.81	-.167190	.028667	-.092533	.022632
1.85	-.314578	.015116	-.097999	.023514
1.89	-.165954	.014991	.005274	.014991
1.93	-.099837	.020784	-.066276	.020784
1.97	-.185198	.015827	.014179	.018087
ρ_1N SS31				
1.65	.154785	.024711	-.128946	.028829
1.69	.035868	.031498	-.151882	.026248
1.73	.007458	.020154	-.045956	.016795
1.77	-.008479	.021115	-.070262	.023033
1.81	.211461	.025039	-.082538	.025039
1.85	.077922	.019809	-.056238	.019809
1.89	.167793	.015956	-.004114	.013675
1.93	.061390	.023120	-.033546	.016184
1.97	.071044	.019098	-.094924	.014323
$\Delta\pi$ PP31				
1.65	-.016621	.017713	-.066546	.024355
1.69	.032171	.021997	-.016920	.026885
1.73	.038026	.015940	.039665	.021253
1.77	.012255	.020056	.041615	.020057
1.81	-.099653	.021599	-.043482	.021599
1.85	.021040	.016290	.001222	.016293
1.89	.008308	.010332	.002164	.013777
1.93	-.095868	.018063	.092155	.018063
1.97	-.035196	.015189	.072728	.015189
ρ_1N PP31				
1.65	.034738	.021765	-.036249	.019976
1.69	.023098	.027840	-.143008	.023645
1.73	.105878	.020966	-.147303	.018921
1.77	-.040526	.022939	-.065822	.021665
1.81	-.062313	.025214	.041683	.023686
1.85	-.187800	.019492	-.076309	.019492
1.89	-.099793	.014045	-.055034	.014045
1.93	-.160204	.020107	-.071408	.017873
1.97	-.035704	.015747	-.039153	.015747

ENERGY	REAL(T)	D(REAL(T))	IMAG(T)	D(IMAG(T))
$\Delta\pi$ PP33				
1.65	.265131	.028025	-.173422	.039702
1.69	.210120	.033246	-.221189	.033246
1.73	.175364	.024782	-.228892	.019275
1.77	.087374	.026529	-.271208	.014738
1.81	.084728	.025226	-.240250	.018920
1.85	.022585	.016640	-.218486	.016640
1.89	.067590	.010482	-.085081	.010482
1.93	.020155	.011007	-.019779	.014676
1.97	-.041119	.011506	-.007969	.015340
$\Delta\pi$ DS33				
1.65	.199412	.019421	-.143257	.032369
1.69	.093416	.026283	-.205005	.019712
1.73	.145452	.019401	-.137220	.019401
1.77	.030116	.019555	-.134703	.013037
1.81	.181916	.013124	-.014832	.019686
1.85	.192331	.013119	-.002350	.013117
1.89	.201247	.013042	.169703	.013042
1.93	.073214	.012929	.249637	.012929
1.97	.165123	.013070	.200125	.013070
$\Delta\pi$ DD33				
1.65	.118551	.012117	-.024215	.022618
1.69	.070514	.021129	-.092052	.023050
1.73	.044439	.016001	-.119794	.014857
1.77	-.041860	.017080	-.113739	.013139
1.81	-.020002	.019507	-.127392	.015005
1.85	-.001381	.013406	-.108092	.013407
1.89	.041995	.011219	-.192024	.009349
1.93	.104598	.014533	-.159552	.014533
1.97	.051317	.011262	-.142427	.013514
ρ_3N DS33				
1.65	.020457	.030942	-.204544	.012377
1.69	-.131240	.019690	-.122358	.021002
1.73	-.099108	.018459	-.163632	.013425
1.77	-.262889	.013457	-.097151	.023070
1.81	-.227407	.018762	-.199431	.018762
1.85	-.256977	.013202	-.222377	.015402
1.89	-.099337	.015930	-.297558	.009103
1.93	.030502	.018456	-.374180	.009228
1.97	-.158250	.011934	-.280024	.009548

ENERGY	REAL(T)	D(REAL(T))	IMAG(T)	D(IMAG(T))
$\Delta\pi$ FF35				
1.65	.025302	.009858	-.039573	.015236
1.69	.031262	.014134	-.052998	.015662
1.73	.076675	.012392	-.116780	.012888
1.77	.060451	.015819	-.129652	.013385
1.81	.058101	.014666	-.063415	.013200
1.85	.075503	.009528	-.081732	.012127
1.89	.088425	.008151	-.091407	.010189
1.93	.147124	.010771	-.062961	.013164
1.97	.110813	.008073	-.069652	.010763
ρ_3N FP35				
1.65	.023190	.009844	.014243	.009546
1.69	.053555	.013718	.094190	.013337
1.73	.061665	.010732	.091684	.009199
1.77	.087359	.012737	.160509	.010826
1.81	-.023217	.013766	.164849	.011472
1.85	-.019813	.010639	.154679	.008866
1.89	-.070482	.008031	.070449	.006024
1.93	-.003265	.011135	.065215	.007795
1.97	-.025667	.008484	.100766	.007272
$\Delta\pi$ FF37				
1.65	.011640	.008937	-.026906	.012512
1.69	.032845	.012561	-.027234	.014845
1.73	.039298	.013858	-.105113	.008414
1.77	.070500	.015798	-.146306	.009722
1.81	.089275	.019069	-.215186	.011735
1.85	.139464	.012144	-.184764	.010409
1.89	.234933	.007120	-.102002	.012205
1.93	.205618	.008377	-.008797	.013163
1.97	.169861	.006732	-.047745	.010771
ρ_3N FF37				
1.65	.038359	.009452	.010286	.009207
1.69	.035995	.011560	-.008836	.011726
1.73	-.017898	.008899	.005381	.006595
1.77	-.034666	.011029	.057561	.007954
1.81	.111457	.007838	-.031345	.012876
1.85	.115290	.009081	-.134575	.008899
1.89	.205792	.004176	-.021791	.011367
1.93	.203911	.008628	.074191	.012496
1.97	.239941	.005928	-.078875	.011856